# Characterising the potential health risks associated with coal dust

## By: Conchita Kankindi Kamanzi

A thesis submitted to the University of Cape Town

in fulfilment of the requirements for the degree of

### Doctor of Philosophy

Date 30 March 2023

### Minerals to Metals

minerals to metals

### Department of Chemical Engineering

UNIVERSITY OF CAPE TOWN
IYUNIVESITHI YASEKAPA · UNIVERSITEIT VAN KAAPSTAD

# Abstract

Coal dust is inextricably linked to the development of dust diseases. To date, the role of mineral matter in coal has been investigated for its links to pulmonary damage; however, no consensus has been reached on which characteristics are relevant to pulmonary toxicity. This study hypothesises that the toxic potential of inhalable coal dust can be attributed to reactive mineralogy and the specific surface area for interaction between the particles and primary phagocytes such as macrophages. To test this hypothesis, the study developed an advanced understanding of the relationship between the physicochemical and mineralogical characteristics of coal particles and pulmonary toxicity.

Three objectives were constructed to achieve this aim. Objective 1 developed a detailed particle characterisation dataset on coal particle samples utilising both routine (X-ray diffraction and X-ray fluorescence) and advanced methods of coal analysis (automated scanning electron microscopy systems). Objective 2 elucidated multivariant relationships between the particle characteristics and the immunological responses from exposed macrophage cells *in vitro* using advanced statistical methods. Lastly, objective 3 developed a protocol to empirically characterise the relative risk of coal dust-related damage on a cellular level.

In developing a detailed characterisation dataset on the coal samples, both routine and automated analysis tools were used to define general, chemical, mineralogical, and mineral specific characteristics. An auto-SEM-EDS-XRD (Automated scanning electron microscope coupled with Energy Dispersive X-ray Spectroscopy and analyses generated by X-ray Diffraction) protocol was developed to obtain a broad spectrum of particle data by mineralogically mapping each particle. This protocol involved the rigorous analysis of uncertainty in the data using comparative datasets generated from XRD and XRF (X-ray Fluorescence) analyses. In summary, the study demonstrated that the combined use of both routine and advanced particle analysis tools allowed for the classification of chemical and mineralogical distributions as well as a discrimination between general and mineral-specific particle characteristics. Generally, these results suggested that features relating to general particle characteristics (size, shape, roughness, and surface area) are more strongly a function of mechanical breakage and deformation than compositional variation.

To assess the multivariant relationships between the numerous characteristics defined and response measures of cellular toxicity, a PLSR (partial least squares regression) was applied in a novel approach to attempt a single model comparison of such relationships. This model was chosen for its ability to relate response and explanatory variables based on a new set of variables which have undergone dimensionality reduction whilst maximising the covariance. The results from the relationship analysis showed that physical

characteristics (particle shape in particular) displayed a greater influence on cytotoxicity and lipid peroxidation over mineral and chemical-based characteristics. Relating this observation to previous research it was suggested that the influence of shape and roughness on phagocytosis may have strong implications for magnitude of direct and indirect cellular harm and the predominance of either intracellular or extracellular damage. The results also showed that, apart from the influence of particle shape, radical-induced stress and cytotoxicity displayed a strong dependency on (1) the chemical and mineralogical reactivity Ca hosted in gypsum, (2) the release/inhibition of Fe from pyrite and Fe-sulfates, and (3) the surface activity of quartz based on its crystallite size. However, the relationships defined in the context of cytotoxicity displayed a more nuanced dependency with the silicate mineral content and their associated properties compared to lipid peroxidation. From this it was suggested that non-radical related pathways to cytotoxicity could also occur from coal dust exposure. Ultimately, the study demonstrates the first analysis which assesses relative impact and magnitude of multiple particle characteristics on cytotoxicity and cellular stress.

Finally, to provide a more easily interpretable format for the analysis of the PLSR relationships, a protocol was developed to screen variables based on: (1) their level of importance to the defined relationship and (2) the rank of importance for each influential variable represented on a unified scale. Elements which explained the variability within the sample characteristics and the responses were clustered using the k-means algorithm to determine classes of samples which display similar characteristics or levels of toxicity. The comparison of the classes grouping samples with similar properties versus samples groups with similar toxicity levels showed that even though samples may share similar properties, their reported level of toxicity may differ. This confirms the observations from previous studies which have shown that the relative toxicity of coal dust cannot be explained on the basis of isolated properties. Rather the set of 'influential variables' showed that a combination of general, chemical, mineralogical and mineral specific data are needed to determine the differences between levels of toxicity. Ultimately, the application of this protocol on 17 different dust-sized coal samples demonstrated the key differences between samples and their influence on levels of cytotoxicity and lipid peroxidation, which until this study have not been demonstrated by a single regression. As an outcome of such results, this study provides a robust analysis strategy for elucidating particle cell relations which can further advance the understanding of coal dust induced disease pathology. Additionally, the protocol has demonstrated the usefulness of disseminating the complex data structures to more easily interpretable data formats such that a generalisable analysis of risk factors related to coal dust-based cellular damage can be utilised by stakeholders in data-based decision making. Ultimately, the results of this study propose that the toxic potential of coal dust is primarily a function of the reactive mineralogical

and chemical components within the particles, however, the magnitude of this intrinsic reactivity is subject to the mitigative factors which can either neutralise of supress the anticipated reactivity.

## Plagiarism declaration

I, Kankindi Conchita Kamanzi, declare that the work in this document is my own, save for that which has been properly acknowledged. The two papers incorporated in this thesis are all comprised of work that I have performed as part of the scope of my PhD. This was conducted under the supervision of A/Professor Jennifer Broadhurst, A/Professor Megan Becker, Dr Johanna von Holdt and Professor Muazzam Jacobs. All work that was conducted by others was cited or acknowledged appropriately and does not compromise the originality of this thesis. The contributions made by co-authors to the jointly authored works are subsequently listed in the sections to follow.

Signed     | Signed by candidate |                                    Date 30 /03 /2023

## Acknowledgement of author contributions to publications

I confirm that I have been granted permission by the University of Cape Town's Doctoral Degrees Board to include the following publication(s) in my PhD thesis, and where co-authorships are involved, my co-authors have agreed that I may include the publication(s):

## List of publications incorporated in this thesis

Kamanzi, C., Becker, M., Jacobs, M., Konečný, P., Von Holdt, J. and Broadhurst, J. 'The impact of coal mine dust characteristics on pathways to respiratory harm: investigating the pneumoconiotic potency of coals', Environmental Geochemistry and Health. Springer Nature 2023, p.1-26.https://doi.org/10.1007/s10653-023-01583-y

C. Kamanzi prepared, conceptualised, and edited the manuscript and all the associated graphics and material. The co-authors critically reviewed the manuscript prior to submission.

Kamanzi, C., Becker, M., Von Holdt, J. and Broadhurst, J. (2022) 'Development of a SEM-EDS-XRD Protocol for the Physicochemical and Automated Mineralogical Characterisation of Coal Dust Particles', Resources. Multidisciplinary Digital Publishing Institute, 11, p. 114. doi: 10.3390/RESOURCES11120114.

C. Kamanzi prepared, conceptualised, and edited the manuscript and all the associated graphics and data analysis presented. M. Becker and J. Broadhurst provided key feedback relating to the conceptualisation

and structure of the final manuscript respectively. The co-authors critically reviewed the manuscript prior to submission.

Kamanzi, C., Becker, Hsu, N., M., Jacobs, M., Konečný, P., Von Holdt, J. and Broadhurst, J. 'Multivariant analysis of the dependences between coal particle characteristics & coal-exposed macrophages in vitro', In preparation to be published post examination of this thesis.

C. Kamanzi prepared, conceptualised, and edited the manuscript and all the associated graphics and data analysis presented. P. Konečný and N. Hsu and M. Jacobs provided expertise and technical guidance in the planning of the experiments conducted for this manuscript. The co-authors provided critical review of the work as it stands in the thesis.

## List of conference presentations and workshops associated with this thesis

Kamanzi, C., Becker, M., Von Holdt, J. and Broadhurst, J. (2018) 'A review of methods to characterise the physiochemical attributes of inhalable coal dust' in 2nd International Symposium on Medical Geology in Africa.

C. Kamanzi prepared and delivered an oral presentation relating to the early conceptualisation of the project in the months leading up to the upgrade from MSc to PhD, with a specific focus on the suite of techniques used to analyse the particulates.

Kamanzi, C., Jacobs, M., Von Holdt, J., Becker, M., and Broadhurst, J. (2019) 'Incorporating potential harm into risk characterisation of inhalable coal dust' in 2019 NACA National Conference.

C. Kamanzi prepared and presented a poster which demonstrated the conceptual framework governing the research project. This further crystallised the key elements of the study and positioned them as a progressive effort to understand how particle characteristics affect cellular health.

Kamanzi, C., Jacobs, M., Von Holdt, J., Becker, M., and Broadhurst, J. (2019) 'The characterisation of coal dust particles for the assessment of inhalation risk' in SAIMM 2019 Minerals Research Showcase.

C. Kamanzi prepared and presented a poster which demonstrated the early data on the characterisation of the coal particulates using the QEMSCAN.

Kamanzi, C., Becker, M., Jacobs, M., Von Holdt, J. and Broadhurst, J. (2019) 'The incorporation of potential harm into risk characterisation of inhalable coal dust' in SMI Next Generation Resources 2019 Student Conference.

C. Kamanzi prepared and delivered a video presentation which demonstrated the key elements of the thesis to a generalised audience. Out of a larger pool of presentations, this presentation was chosen to be broadcast at the conference representing the group of the best student presentations.

# Acknowledgements

Here I would like to express my sincere and heartfelt gratitude to:

# Contents

# List of Figures

## List of Tables

# List of Abbreviations

Auto-SEM-EDS – Automated scanning electron microscope coupled with Energy Dispersive X-ray Spectroscopy

AM – Alveolar macrophage

BAI – Bioavailable iron

BET – Brunauer–Emmett–Teller surface area analysis method

BSE – Back scattered electrons

CM – Carbonaceous matter

CRY – Crystallite size

CV – Cross validation

CWP – Coal Workers' Pneumoconiosis

ECD – Equivalent circular diameter (2-D based)

Kln/K – Kaolinite

LDH – Lactate dehydrogenase

MDA – Malondialdehyde

PLSR – Partial Least Squares Regression

Py/P – Pyrite

QEMSCAN/QS – Quantitative Evaluation of Materials by Scanning Electron Microscopy

Qz/Q – Quartz

ROS – Reactive Oxygen Species

SEM – Scanning Electron Microscope

SSA – Specific Surface Area

VIP – Variable of importance

XRD – X-ray Diffraction

XRF – X-ray Fluorescence

## Glossary

**Apoptosis** – A form of cell death where a series of molecular pathways within a cell subsequently lead to its death.

**Auto-SEM-EDS** – An operational system that performs image and compositional analysis of materials using a combination of scanning electron microscopy (SEM) as the hardware and an integrated software platform to control the SEM routine and perform data extraction.

**Beneficiation** – This is the process of transforming the primary mined material to a high value product.

**Calcium signalling** – The use of $Ca^{2+}$ cations to regulate and drive intracellular processes such as cell death, proliferation, and inflammation, in the context of cellular harm.

**Chemokine and cytokine** – Cytokines are a large group of pro or anti-inflammatory factors which are involved in cell signalling. Chemokines are a group of non-structural secreted proteins within the cytokine family whose genetic function is to induce cell migration.

**Coal dust** – Explicitly refers to the dust produced from coal ore which may contain carbonaceous matter, minerals, and host rock contaminants.

**Coal mine dust** – The dust produced on site within a colliery, these particles may comprise coal dust and a wide array of additional and potentially site specific contaminants such as diesel particulates and processing chemicals.

**Coal Worker's pneumoconiosis** – An interstitial lung disease caused by the inhalation of coal mine dust and characterised by chronic inflammation and the formation of coal laden nodules in the lung which can lead to fibrosis, scarring and eventual death if prolonged.

**Crystallite size (Domain size)** – The smallest size of a domain of solid-state matter that has the same structure as a single crystal. For context a group of crystallites compose a grain of a solid-sate phase.

**Cytotoxicity** – The propensity of a substance to mediate cell death through direct or indirect reactivity.

**Dimensionality reduction** – A statistical technique used to reduce the number of random variables in a problem by computing a set of principal variables.

**Discriminant analysis** – A statistical technique that can determine groups of variables based on a collection of metric predictors that are independent variables.

**Dust-sized particles** – This refers to the size range of particles which are conventionally viewed as in the size range of dust particles (1 – 400 µm).

**Extracellular** – Processes/events occurring outside the cell.

**Fenton chemistry** – A type of chemical reaction which involves the conversion of peroxides (mostly hydrogen peroxide) into active oxygen species such as hydroxyl radical via a transition metal-based catalytic reaction.

**General characteristics** – This term refers to the characteristic shape, roughness, particle size, specific surface area.

**Geo-anthropogenic** – The process by which naturally sourced materials such as dust are modified or enhanced by human activities, e.g., the crushing of ore subsequently leading to the formation of potentially chemically reactive dust-sized particles.

**Intracellular** – Processes/events occurring within the cell.

**Inflammation** – A part of the body's immune response to harmful pathogens, damaged cells of irritants which involves the action of immune cells, blood vessels and molecular mediators.

**Inhalable particles** – In this study inhalable particles refers to a size range which implies that particles can both enter and be entrained in the lower respiratory tract (< 10 µm in size).

**Latent variables** – A non-observable variables which can only be inferred indirectly through a mathematical model derived from observable variables.

**Lipid peroxidation** – A process resulting from a chain of reactions resulting from the oxidative degradation of unsaturated fatty acids in a lipid membrane.

**Mineral association**– This is a form of mineral texture information and refers to the percentage grain boundary association between different minerals in a composite particle.

**Mineral liberation** – The percentage of area occupied by a mineral of interest in the total volume of a particle.

**Mineral specific characteristics** – This term refers to characteristics specifically related to a mineral of interest such as mineral liberation and crystallite size.

**Multivariant analysis** – This analysis is a subdivision of statistics which allows for the analysis of multiple sets of data for each individual. This is used to study more complex sets of data where univariant analysis is not applicable.

**Open cast mining** – A surface mining technique used to extract ore via an open-air pit.

**Oxidative stress** – A phenomena resulting from an imbalance between free radicals and antioxidant compounds in the body.

**Partial least squares regression** – A latent variable regression technique used to reduce many correlated and uncorrelated predictors to a smaller set of uncorrelated components upon which a least squares regression is performed on the components and not the original data.

**Phagocyte** – A type of immune cell capable of ingesting foreign substances in the blood stream or in tissue as well as secrete various pro and anti-inflammatory indicators in cases of infection or foreign particle overload.

**Reactive oxygen species** – Highly reactive chemicals derived from molecular oxygen and formed from redox reactions.

**Run of mine** – Unprocessed mined material which contains the ore mined as well as host rock.

**Textural information** – In the context of mineralogy this refers to the special relationship between minerals grains in a composite rock or particle which make up a fabric.

**Variable of importance** – This refers to a scale of how much a given statistical model utilises each variable to make accurate predictions.

**X and Y loadings** – An element of a latent variable model that describes the weighting and direction of each explanatory (X) or response (Y) variable when computing the components of the model.

**X and Y scores** – An element of a latent variable model that geometrically represents the re-projected data of each individual in a rotated coordinate system. This is calculated in the context of representing the maximum covariance of individuals with respect to X and Y simultaneously.

# Chapter 1

# INTRODUCTION

## 1.1. Background

Air pollution in its various forms has been identified as a severe public health concern by bodies such as the World Health Organization. As of 2019, air pollution has been classed as the fourth leading factor for mortality worldwide (HEI and IHME, 2020), where occupational airborne exposure has been highlighted as an important cause of mortality and morbidity (Driscoll et al, 2020; GBD 2016 Occupational Chronic Respiratory Risk Factors Collaborators, 2020; Minov, 2021). Regarding the contribution from the mining industry, epidemic levels of pneumoconiotic diseases such as asbestosis, silicosis, and coal workers' pneumoconiosis (CWP) have historically contributed to disease burden in certain countries (Attfield and Castellan, 1992; Heppleston, 1992; Driscoll et al, 2005; Petsonk et al, 2013; Blackley et al, 2018). While all the diseases described are incurable but preventable, the causes relating to CWP remain uncertain. Once it was established that pneumoconiotic diseases were caused by the inhalation and subsequent retention of the dust in the lung tissue, the management strategies employed focused on the reduction of dust in the mining setting. While such practices did lead to a reduction in the prevalence of CWP, resurgences in CWP – characterised by regional differences in prevalence – have been observed since the early 2000s, (Cohen, 2016; Blackley et al, 2018; Leonard et al, 2020).

Currently there is no robust understanding of the health risks associated with coal dust exposure based on the particle characteristics. Mechanistic studies have generally established that the physicochemical and mineralogical characteristics of coal dust play a role in eliciting both cytotoxic and pro-inflammatory pathways (Fubini and Otero Areán, 1999; Zhang et al, 2002; Schoonen et al, 2006; Fubini and Fenoglio, 2007). However, no single feature of the dust has been consistently identified as a causal agent. As variability in the dust generated at a mine can be due to changes in the ore characteristics as well as the activity which generated the dust (crushing, cutting, blasting etc.), studies have investigated the variability in coal dust generated on both an inter and intra-colliery scale to provide more information on the dust characteristics which may contribute to the toxicity of the particles (Johann-Essex et al, 2017a; Sarver et al, 2019; LaBranche et al, 2021, 2022). This investigation was prompted based on the suspected effect of numerous inter-related causal factors involved in cellular damage and cytotoxicity resulting from physical and composition-based characteristics of dust. Building on such work, a recent study by Cohen et al, (2022) ascribed an increase in the levels of crystalline silica particles as a result of cutting into the wall rock as a cause for the localised resurgence and intensity of progressive massive fibrosis (late-stage chronic

pneumoconiosis) within a single geographic region. While such a study only referred to a certain mining context and went to further ascribe the toxicity of the dust to crystalline silica, it is well understood that coal is a highly variable material comprised of varying amounts of organic and inorganic mineral matter (Finkelman, 1994; Ward, 2016; Finkelman et al, 2019). Considering such, it can be argued that not all coals may be considered equally toxic due to the inherent viability in both their mineralogy and chemistry. Hence, it cannot be assumed that conclusions relating to risk factors identified by one mine may be extendable across coalfields, particularly as inter-relationships between minerals have been found to impact the reactivity and toxicity experienced to lung cells (Huang et al, 1994; Wallace et al, 1994; Fubini, 1997).

While several studies have investigated the relationships between the toxicological and immunological responses related to disease development and the characteristics of coal dust, they tend to only include data on particle size, mineral abundance, and major/trace element chemistry (Trechera et al, 2020, 2021a, 2021b; Zosky et al, 2021; Song et al, 2022). Furthermore, such studies provide a limited understanding of the variation in the particle characteristics related to the context of the parental coal and the inter-relationships between a broad set of characteristics and measured toxicological/immunological responses. As a result, the conclusions drawn have been restricted to outlining potentially harmful components in the dust on a parameter-by-parameter basis by determining associations between pairwise or small groups of variables (considering 3 to 4 variables) – without considering the net contribution of the properties to the responses. Hence such methods make it difficult to screen extensive sets of variables to assess the relative magnitude, and net contribution of particle characteristics to such responses. Ultimately, it can be argued that without a robust understanding of the degree to which the dust may possess intrinsic toxicity as a function of its characteristics, the relative harm associated with coal dust cannot be assessed.

In terms of understanding the current burden of coal workers' pneumoconiosis, there is limited disease burden data for many countries. This has created great difficulties in establishing baselines for understanding disease prevalence for some coal producing countries, particularly in the Global South. Adding to this, studies based in Colombia and India have highlighted the contributions of coal dust to ambient dust levels, exposing both miners and individuals who live in proximity to collieries (Ghose and Majee, 2000b; Huertas et al, 2012a; Mishra et al, 2012). While the impact of coal dust on proximal communities has largely not been investigated, a study based in Brazil detected comparable levels of indicators for respiratory stress between surface workers at a colliery and local residents (Ávila Júnior et al, 2009). From this, it was suggested that individuals in proximity to the mining area may also be vulnerable to contracting coal dust related diseases.

Looking to the future, it has been suggested that the landscape of coal extraction and use is likely to change, due to pressures to phase out fossil fuels (Carley and Konisky, 2020; Chattopadhyay et al, 2021). While the transition is necessary from a climate change perspective, Carley and Konisky (2020) have

discussed that it is unlikely that one energy resource will be completely replaced by another considering historical cases. Even so, the transition to the low carbon economy will not necessarily eliminate the mining and processing of coal as metallurgical coal is still anticipated to be required for the foreseeable future. Additionally, the complex socioeconomic ties involved with the production and use of coal are anticipated to render miners and proximal communities vulnerable to the public health issues caused by coal dust exposure for some years to come (Hendryx et al, 2020). Thus, the need for risk characterisation protocols, rooted in prioritising the factors leading to disease development is essential for providing individuals with a safe and dignified livelihood.

## 1.2. Problem statement

The contraction of respiratory diseases has become synonymous with coal mining. Several respiratory diseases have been linked to coal dust exposure. Coal workers' pneumoconiosis is a preventable but incurable disease that is exclusively contracted from prolonged exposure to coal dust. While management strategies have been employed in an attempt to prevent coal workers' pneumoconiosis and other dust related diseases, they are based on the implicit assumption that all coal dust is equally toxic. Through the anomalous resurgence of coal workers' pneumoconiosis, studies have highlighted the potentially toxic nature of coal dust particulates derived from the presence of reactive minerals. While datasets which provide corresponding toxicological/immunological and particle characterisation are limited for coal dust, few studies have attempted to investigate the relationships between the particle characteristics and the expressed responses. While such studies have built on previous work suggesting that the reactive components are mineral derived, they mainly focus on defining associations or subsets of characteristics which are correlated. Thus, the nuances relating to how different particle characteristics may exacerbate or depress adverse responses is not well understood. As a result, no clear methods have been identified to holistically understand the particle-cell interactions through regression and discriminant analysis as primary information to aid in the decision-making process of future management strategies. In this context, it can be argued that the application of a protocol to characterise the relative health risk of coal dust based on an array of physicochemical and mineralogical characteristics will be useful in future efforts to determine pneumoconiotic potential.

## 1.3. Aim of study

To develop an advanced understanding of the relationships between the physicochemical and mineralogical characteristics of coal dust particles and pulmonary toxicity. Based on this advanced understanding, the study further aims to propose an empirical protocol for characterising the potential health risks associated with inhalable coal particles.

## 1.4. Scope and limitations

To achieve the study aim, a systematic approach was used. This involved (1) the generation of both explanatory and response variables, (2) relationship analysis between variables through regression modelling, and (3) utilisation of the model outputs to generate information that can aid in data driven decision making towards a risk characterisation protocol for coal dust. As the elements of risk involve the identification of hazardous properties of coal samples in the context of pulmonary toxicity, and do not quantify actual exposure, this study mostly focuses on hazard identification and characterisation, which can later be applied to future risk characterisation . In this context, the study was based on, and limited to, a sample size of 17 bituminous coal samples which represented a range of different source materials (geologically distinct versus operationally distinct). The nature of these samples ranged from beneficiation discards (coal waste products from the washing process) to run of mine coal (unprocessed coal), which is further described in chapter 3. While most comparable studies in literature have commonly used coal standards or parental coal from the mined seams, the choice of including coals that have undergone beneficiation processes was mainly to (1) increase the compositional variability among samples, and (2) prioritise the associated mineral matter to carbonaceous material in the coal. Since the predominant focus of the study was on the characterisation and potential relationships between the associated mineral matter in coal dust particles and their toxic responses produced in vitro, the inclusion of such samples was considered appropriate.

As the coal samples received were too coarse for what can be considered as dust ($< 100$ μm), crushing, and sieving steps were applied based on methodologies employed in literature to reduce the particle size to a range which is considered dust-sized (screened to a passing size $< 25$ μm with a $D_{50} \sim 10$ μm in size). While the particles generated maybe be considered dust-sized this study also acknowledges that the material has not physically become airborne and are not necessarily representative of the dust obtained on an actual mine site. Having said this, lab-based methods of dust generation and suspension are considered out of the scope of this study, as the intention is not to mimic a particular mine or operational scenario but to develop an understanding of the relationship between the coal particle characteristics and their resulting toxic responses. Furthermore, it should be noted that such practices are not uncommon for such studies, and this is further justified in chapter 3.

Concerning the methods of analysis, various microscopy, spectroscopy, and analytical tools were used to characterise the physicochemical and mineralogical properties of the coal particles (chapter 3 further substantiates these methods), the results of which represent the explanatory variables of the study. The experimental component of the study – whose results represented the response variables – included the exposure of a human macrophage cell line (THP-1) with the dust and subsequent assay for toxicological

and immunological indicators *in vitro*. The assay selection was based on their combined ability to highlight different points on the pathogenic pathway to disease development (further substantiated in chapter 3). In terms of tissue culture conditions, the cell lines were only tested as monocultures although it is known that complex interactions between cells occur in the body. Thus, the results presented are not fully translatable to what reactions cells would have in the body. Furthermore, after establishing the dose response nature of a subset of samples over 24h, 48h and 72h timepoints in the context of cell death, one time point was chosen – which represented the highest response signal – for the subsequent assay to ensure relatability across the two assays (the effect of time on the signal of the responses assayed as a sub study of the response kinetics was considered out of the scope of the work). Regarding the reproducibility of the experiments, monetary constraints rendered experimental repeats (inter-experiment variability) infeasible, however, all experimental wells were conducted in duplicate and the intra-experiment variance and standard deviation are all reported (discussed in chapter 3).

The observation and further interpretation of possible relationships between explanatory and response variables were assessed through multivariant regression analysis. While the sample number used in the analysis can be considered low, the results were able to highlight the statistical approach employed. However, a result of the low sample translated to some of the analyses being reflective of few or extreme samples. In this context it is acknowledged that the developed protocol does not provide an absolute measure of risk but rather a relative evaluation of risk in the context of the samples analysed and the general trends observed between them. Lastly, the protocol does not intend to preclude the need for a more rigorous assessment of the actual exposure, through site-specific dose-response studies as methods for risk or hazard definition. Similarly, this study does not intend to measure the risks associated with the exposure to mine dust.

## 1.5. Thesis layout

The structure of the thesis has been subdivided into seven chapters which are based on a literature review article and three research papers. Figure 1-1 graphically represents the overall structure of the thesis, highlighting briefly what is expected in each chapter. Following the introduction which has contextualised and outlined the overarching aim of the study, is the critical literature review from which the hypothesis and objectives have been derived. Each objective outlined depicts the premise for the technical chapters and their associated papers. At the onset of each technical chapter, an overview will be given on the objective and key questions to be answered in that specific chapter as well as an outline of how the research questions are addressed by the associated paper. The final discussion and integration of the findings, conclusions, and recommendations are presented in the final chapter. Here the hypothesis and overarching aim will be directly addressed for the project as a whole. All supplementary material and links to the datasets used in this study can be found in the Appendices Chapter.
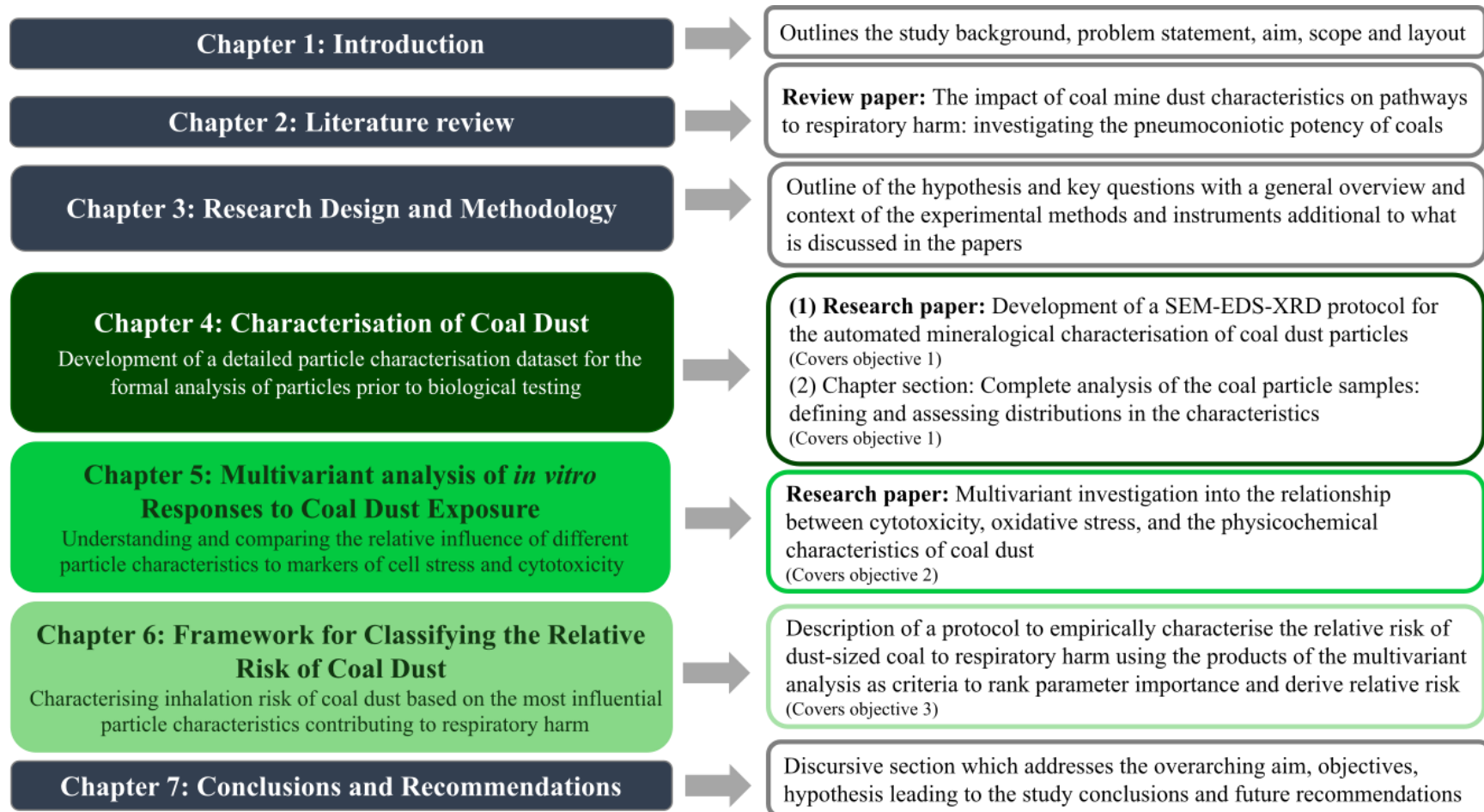
Figure 1-1 Thesis structure and outline of chapters with their main outputs

# Chapter 2

# LITERATURE REVIEW



| Coal dust exposure | Mitigation & Management | Anomalous current CWP resurgence |

1831          1970s          2000s

**Epidemic levels of morbidity**

**Reduction of exposure concentration**

**Assumption: all dust has equal toxicity**

**Defining the pneumoconiotic potency of coal dust**

Coal Mine Dust Related Diseases:
Coal Worker's Pneumoconiosis (CWP)

- Critical issue for countries whose CWP prevalence baseline is greatly underestimated

- Mines with equivalent exposure concentrations showed differing CWP prevalence rates

- Minerals in coal were found to elicit immune responses in pulmonary environment

- Definition of pathogenic pathways resulting in CWP yield new opportunities to assess relationships between material and immune responses

- Advancements in particle toxicity and particle characterisation highlight potential for cross disciplinary approaches to defining pneumoconiotic potency

This graphic describes the disease burden related to coal dust exposure over time. The shaded lungs refer to the severity of the disease in comparison to the exposure to dust (depicted by the particles).

## 2.1. Overview

In this chapter the mechanisms and potential actors involved in the development of coal workers' pneumoconiosis are discussed in a review article. Through this review, the relevant literature was critically analysed and synthesised to discuss (1) dust generating activities and their impact on particle characteristics, (2) the coal dust-induced biological pathways to cell-stress, inflammation, and cell death, (3) the mechanistic role that physicochemical and mineralogical characteristics have in coal dust-induced toxicity, and (4) the utilisation of particle characteristics in the understanding and prediction of coal dust-induced cellular damage.

Review paper: The impact of coal mine dust characteristics on pathways to respiratory harm: investigating the pneumoconiotic potency of coals

## Abstract

Exposure to dust from the mining environment has historically resulted in epidemic levels of mortality and morbidity from pneumoconiotic diseases such as silicosis, coal workers' pneumoconiosis (CWP), and asbestosis. Studies have shown that CWP remains a critical issue at collieries across the globe, with some countries facing resurgent patterns of the disease and additional pathologies from long-term exposure. Compliance measures to reduce dust exposure rely primarily on the assumption that all "fine" particles are equally toxic irrespective of source or chemical composition. For several ore types, but more specifically coal, such an assumption is not practical due to the complex and highly variable nature of the material. Additionally, several studies have identified possible mechanisms of pathogenesis from the minerals and deleterious metals in coal. The purpose of this review is to provide a reassessment of the perspectives and strategies used to evaluate the pneumoconiotic potency of coal mine dust. Emphasis is on the physicochemical characteristics of coal mine dust such as mineralogy/mineral chemistry, particle shape, size, specific surface area, and free surface area – all of which have been highlighted as contributing factors to the expression of proinflammatory responses in the lung. The review also highlights the potential opportunity for more holistic risk characterisation strategies for coal mine dust, which consider the mineralogical and physicochemical aspects of the dust as variables relevant to the current proposed mechanisms for CWP pathogenesis.

## 2.2. Introduction

Air pollution has been reported as the fourth leading risk factor for mortality worldwide, accounting for approximately 6.7 million deaths in 2019 (HEI and IHME, 2020). Of these deaths, approximately 20 % are accounted for by chronic respiratory diseases such as pneumoconiosis (caused by fugitive mineral dust exposure). Historically, epidemic levels of morbidity and mortality from such diseases have been recorded in mining settings, due to the associated chronic exposure of individuals to dust (Ross and Murray, 2004; Patra et al, 2016; Perret et al, 2017).

Mine dust has been linked to a range of pneumoconiotic diseases, where the most prominent examples of this class of dust-induced diseases are silicosis, coal workers' pneumoconiosis (CWP), and

asbestosis. In modern terms, these diseases are commonly thought to be relics of the past, based on the assumption that modern technologies and dust control strategies could manage dust concentrations to safe levels (Cohen, 2016). However, CWP remains a prevalent occupational dust disease across the globe, accounting for 25% of the total pneumoconiosis cases in 2017 (Shi et al, 2020).

Apart from occupational exposure, studies have demonstrated that coal mine dust can disperse to proximal communities (Huertas et al, 2012a, 2014; Mishra et al, 2012). As exposure limits for ambient areas are set at lower levels compared to occupational settings, irrespective of whether they are affected by the same source, mining communities may be vulnerable to a range of respiratory diseases. To date, studies have recorded cases of emphysema, chronic obstructive pulmonary disease, and bronchitis in individuals proximal to coal mines (Laney and Weissman, 2014; Yadav and Jamal, 2018). However, trends in the global prevalence of CWP suggest that cases of these diseases are greatly underreported for countries that fall into the middle SDI (sociodemographic index), due to disparities in clinical reporting schemes and surveillance programmes (Shi et al, 2020). Thus, apart from posing a serious occupational health hazard, coal mine dust may constitute a significant public health concern for coal-producing countries, particularly in the Global South where established mining communities are prevalent.

By definition, CWP is classified as an interstitial lung disease caused by the inhalation of coal mine dust and the subsequent damage of the lung tissue (Laney and Weissman, 2014). Apart from the well-established link between CWP and coal mine dust, no clear causal agent(s) have been consistently identified for the disease across different global contexts. As coal mine dust particles compose of varying amounts of carbonaceous (organic) and mineral matter (inorganic), studies have debated and demonstrated the role that minerals play in pathways leading to CWP development (Kuempel et al, 2003; Cohn et al, 2006a; Schoonen et al, 2010; Harrington et al, 2012; Zosky et al, 2021; Song et al, 2022; Sun et al, 2022). In addition to coal mine dust produced from the mined material, coal mine dust in the broader context potential dust sources can also contain diesel exhaust particle, which have been associated with acute pulmonary damage (Mauderly et al, 1987; Hiura et al, 1999; Maynard and Kuempel, 2005; Stoeger et al, 2006). Despite knowledge of these various pathways to pulmonary damage, mechanisms to screen the factors relating to the pneumoconiotic potency of coal mine dust remain underexplored. To begin to address these concerns, an understanding of the hypotheses/discoveries related to the management of CWP and coal mine dust diseases is needed to describe the shift in understanding that coal mine dust may possess inherent and variable pneumoconiotic potency.

2.2.1. Historical advancements in the management and mitigation of coal mine dust diseases

Research on the management of coal mine dust-related diseases has spanned over 60 years, involving stakeholders from various sectors. These include the government, industry parties, and research institutes – predominantly from both Europe and the USA. Some of the major events from this timeline include the first pathological description of what we now know as coal workers' pneumoconiosis (CWP) in 1831 (Donaldson et al, 2017) – (Figure 2-1 timepoint 1). For a considerable period between 1831 and the mid-1900s, CWP was thought to be a form of silicosis. This led to what Heppleston (1992) (Figure 2-1 timepoint 3) referred to as "decades of doubt", where it was unclear as to whether the coal mine dust disease observed in 1831 could be considered a clinically distinctive disease.

However, between 1936 and 1942 the Medical Research Council (MRC) in Britain conducted an epidemiological survey to understand the nature of the resurgence in coal mine dust disease among workers (Figure 2-1 timepoints 4-6). During this period, the disease was termed pneumoconiosis of coal workers, a clinically distinctive disease to silicosis (D'Arcy Hart and Tansey, 1998). As part of the research efforts, a report was produced by Hart and Aslett (1942) which formed the basis for the first strategy for reducing the cases of CWP (Figure 2-1 timepoint 6). They suggested that CWP would not progress if dust concentrations were under a certain level. Furthermore, it was proposed that a limit could be set based on a value of the mass concentration of dust in the air (mg of dust/$m^3$ of air). Apart from commenting on the management of CWP, it was suggested that the differing prevalence levels between mines could be related to the rank of the coal.

Following the results of the MRC survey, a second epidemiological survey termed the Pneumoconiosis Field Research (PFR) program was initialised in 1952. During this period, research was conducted to define safe dust limits for British collieries. Concurrent with this, the USA implemented legislation to curb the burden of CWP cases at American collieries. This resulted in the implementation of dust limits and the initiation of the national epidemiological survey to understand the state of CWP in the USA (Figure 2-1 timepoints 8,9).
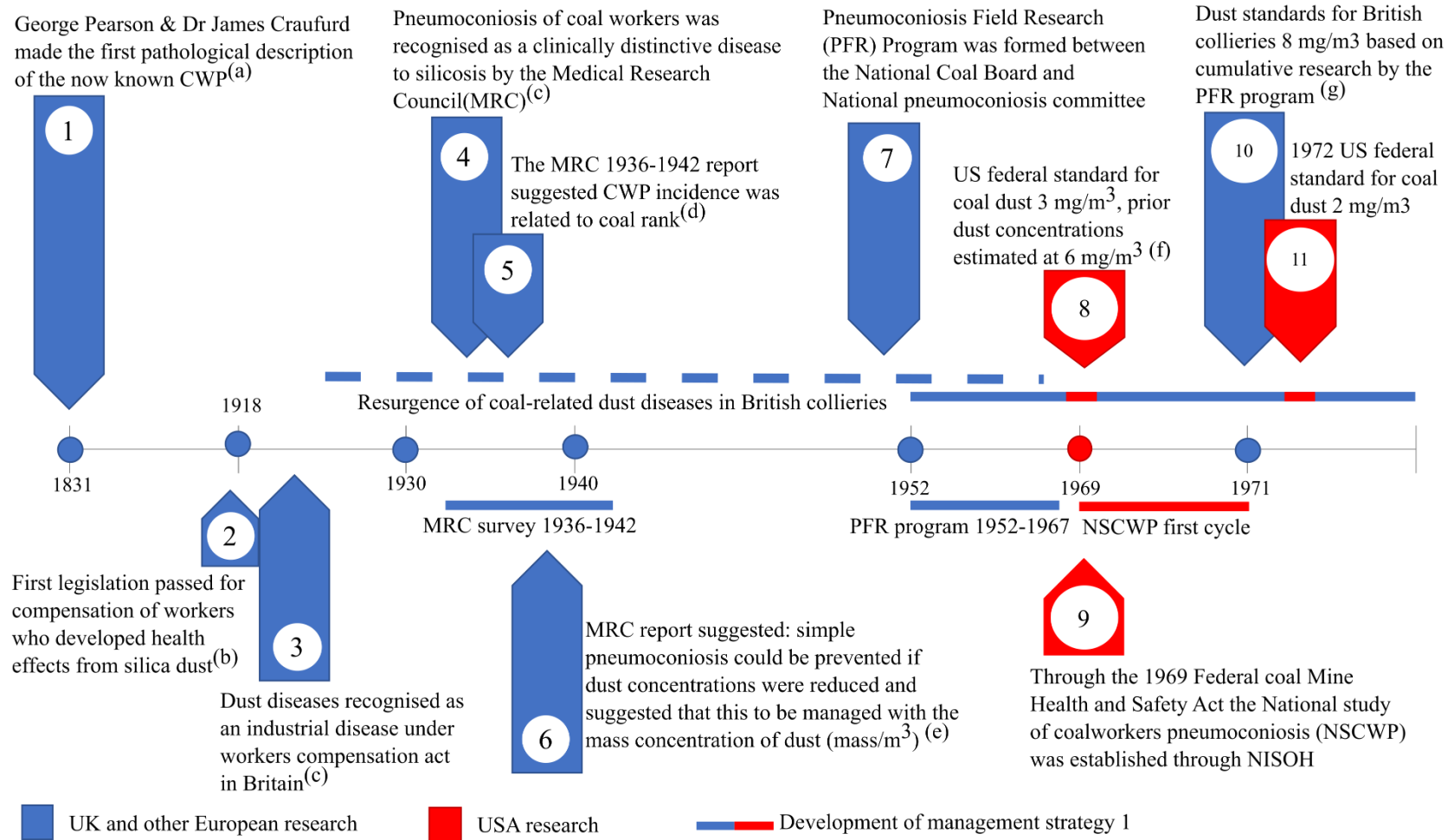
Figure 2-1 A timeline from 1831 to 1971 that covers the historical development of strategies for coal mine dust diseases. Primary references for the points mentioned are as follows: a. Donaldson et al (2017), b. Bufton and Melling (2005), c. Heppleston (1992), d. D'Arcy Hart and Tansey (1998), e. D'arcy Hart and Aslett (1942), f. Attfield and Morring (1992a), g. Jacobsen et al (1970).

As part of the research collated by the PFR program, a dust limit of 8 mg/m$^3$ was suggested for collieries in 1970 based on British mines (Jacobsen et al, 1970) – (Figure 2-1 timepoint 10). Upon implementation of the standards, which resulted in a dramatic reduction of dust, Britain further opted to remove miners with detected issues to "less risky" areas of the mine and limit the time of work shifts (D'Arcy Hart and Tansey, 1998). By contrast, the USA prioritised the refinement of dust limits which were further lowered to 2 mg/m$^3$ in 1972 (Figure 2-1 timepoint 11). For the period directly after the intervention, both approaches reduced the incidence of CWP over time and were widely implemented across the globe (Blackley et al, 2018). However, several European countries reported regional discrepancies in the prevalence of CWP despite comparable dust concentrations (Davis et al, 1982). Stemming from the unexplained discrepancies, several studies investigated potential links between epidemiological and experimental results to understand if a causal component in the coal could be identified (Bennett et al, 1979; Gormley et al, 1979; Reisner et al, 1982; Le Bouffant et al, 1988) – (Figure 2-2 timepoint 12).

In 1988 a hypothesis for the pathogenesis of CWP was proposed stating that coal particles have the potential to persistently generate reactive compounds which leads to a continuum of inflammatory responses and subsequent disease progression (Vallyathan et al, 1988a) – (Figure 2-2 timepoint 13). This hypothesis elicited several studies postulating the role of minerals in generating reactive compounds and subsequently led to the idea that certain dust may possess inherent toxicity based on their mineralogical and chemical properties (Huang et al, 1994, 1999, 2002; Vallyathan, 1994; Vallyathan et al, 1998) – (Figure 2-2 timepoints 13,15,18,19). A study in 2005 tested the application of predicting CWP prevalence with chemical compounds, namely bioavailable iron released from coals (Huang et al, 2005) – (Figure 2-2 timepoint 20). This provided what can be considered the first demonstration of an alternative strategy to identify the pneumoconiotic potency of coal prior to mining.
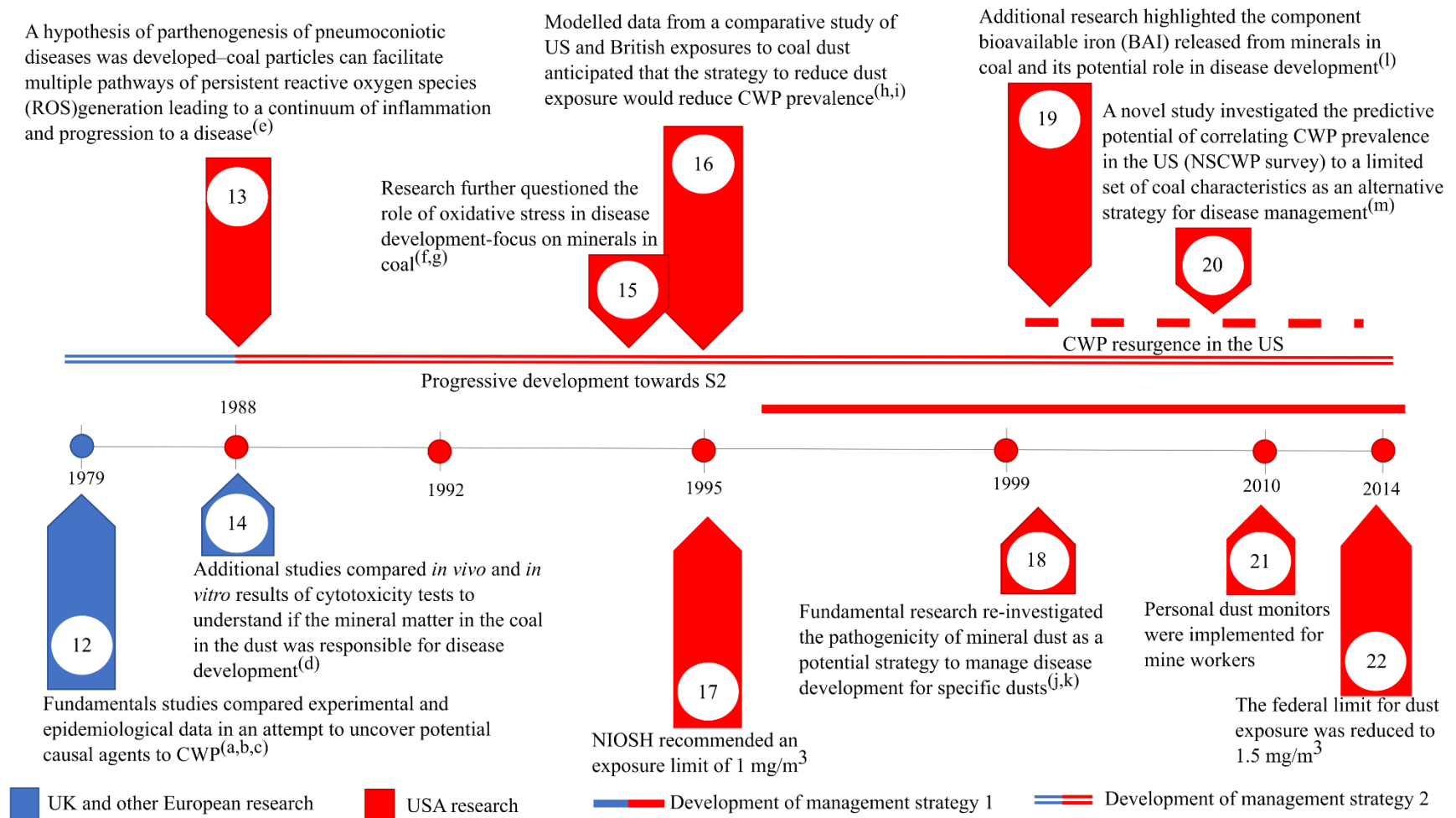
Figure 2-2 Timeline from 1979 to 2014 continuing the historical development of strategies for coal mine dust diseases from Figure 1. Primary references for points mentioned are as follows: a. Gormley et al (1979), b. Bennett et al (1979), c. Reisner et al (1982), d. Bouffant et al (1988), e. Vallyathan, Schwegler, et al (1988), f. Vallyathan (1994), g. Huang et al, (1994), h. Attfield and Morring (1992b), i. Attfield and Seixas (1995), j. Vallyathan et al (1998), k. Huang et al, (1999), l. C. Huang et al (2002), and m. Huang et al, (2005).

Despite dust concentration limits at collieries in the USA being reduced to 1.5 mg/m$^3$ in 2014 (Figure 2-2 timepoint 22), the prevalence of CWP was on an increasing trend, particularly in Appalachia (Blackley et al, 2018) – (Figure 2-3 timepoint 24). This led to research focused on understanding the physicochemical characteristics of the coal mine dust to shed light on the aspects of the dust which could potentially be linked to CWP and other health effects (Johann-Essex et al, 2017a; Sarver et al, 2019) – (Figure 2-3 timepoints 23, 25). From this work, it was established that the mineralogical and physical characteristics of coal mine dust could vary both between geographical locality and between point sources derived from primary processing streams (Johann-Essex et al, 2017a; LaBranche et al, 2021; Pan et al, 2021; Sarver et al, 2021) – (Figure 2-3 timepoints 23,29), suggesting that not all coal mine dust can be considered equivalent in terms of its characteristics. Additionally, studies suggested that exposure to silicate minerals derived from cutting into the wall rock may have an impact on the prevalence of coal mine dust diseases, based on an increase in silica-related pathologies in Appalachia (Hall et al, 2019; Cohen et al, 2022b) – (Figure 2-3 timepoints 31, 26). Later studies by Keles et al (2022) and Keles and Sarver (2022) provided additional characterisation data on the abundance and sources of quartz in coal mine dust within USA collieries. Their results demonstrated that coal mine dust resulting from activities which cut into the rock strata (such as roof boltering) produced elevated levels of quartz compared to the dust produced from run of mine coal. Furthermore, their results showed that, on a regional scale, mines which practise thin seam-mining tended to display elevated levels of quartz in the sampled coal mine dust.
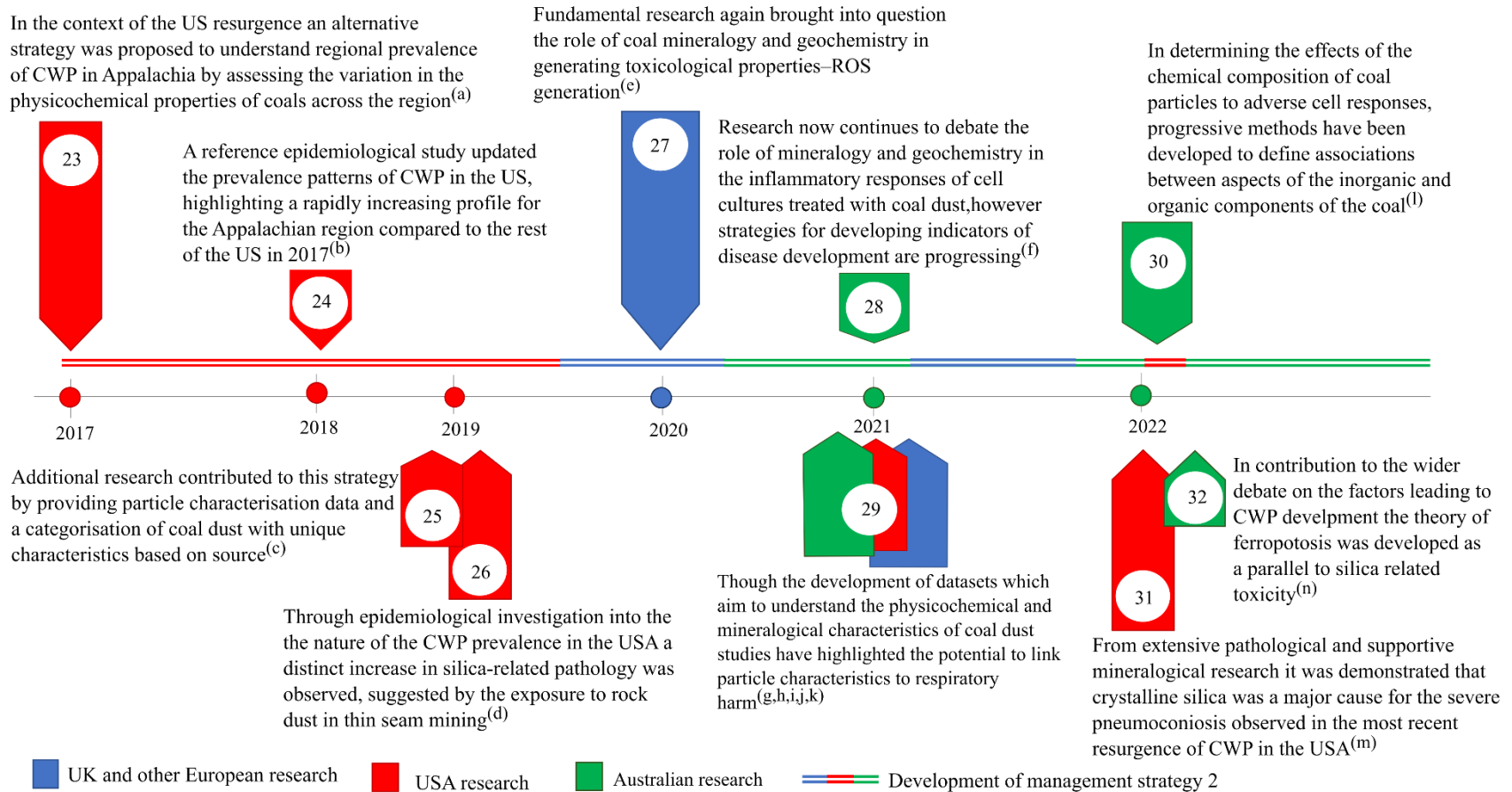
Figure 2-3 Timeline from 2017 to 2022 continuing the historical development of strategies for coal mine dust diseases from Figures 1and 2. Primary references for points mentioned are as follows: a. Johann-Essex et al (2017), b. Blackley et al (2018) ,c. Sarver et al (2019), d. Hall et al (2019), e. Trechera et al (2020), f. Zosky et al (2021), g. Trechera et al, (2021a), h. Trechera et al, (2021b), i. Pan et al (2021), j. Sarver et al (2021), k. Song et al (2022), l. LaBranche et al (2021),  m. Cohen et al (2022), and n. Sun et al (2022).

2.2.2. Modern perspectives on the mitigation of coal mine dust diseases

Following the progression of the resurgence of CWP in the USA, research addressing the health effects of coal mine dust shifted to elucidate the factors relating to the development of coal mine dust diseases (Huang and Finkelman, 2008; Harrington et al, 2013; Sun et al, 2021; Shangguan et al, 2022; Song et al, 2022). By investigating the resulting particle-cell effects, a strong focus has been placed on relating the physicochemical and mineralogical characteristics of coal mine dust to their potential for generating immune/toxic responses. As coal is a chemically complex material, several characteristics related to its composition have been shown to induce tissue damage and serve as potential predictors for CWP risk. In particular, the established mechanism for toxicity and inflammation induced from quartz and its prevalence in coal has commonly been drawn upon when discussing predictors for the harmfulness of coal mine dust (Fubini, 1998; Castranova, 2000). Studies such as Cohn et al (2006), Harrington et al (2012), and Schoonen et al (2010) have also demonstrated the role of pyrite and bioavailable iron as additional agents responsible for tissue damage via mechanisms independent to quartz. As a result, both pyrite and bioavailable iron have been debated as potential predictors for CWP development. However, the prevalence of silicosis-type CWP, observed by miners post resurgence in the USA, has brought into question the relevance of iron-bearing minerals over quartz in CWP development (Hall et al, 2019; Cohen et al, 2022b) – (Figure 2-3 timepoints 31,26).

Studies have compared the bulk mineralogy and geochemistry of sampled coal mine dust to chemical markers of toxicity to elucidate and demonstrate the mechanistic effects of coal mine dust composition on toxicity (Trechera et al, 2020, 2021a, 2021b) – (Figure 2-3 timepoints 27,29). Through such analyses, multiple sets of mineralogical and geochemical components were found to contribute to the expression of toxic responses. However, not all the components identified can be attributed to mechanistic pathways relevant to CWP development.  Correlations defined by Song et al (2022), Trechera et al (2021b), and Zazouli et al (2021) have demonstrated, in particular, that the pyrite and iron content in coal mine dust can be considered a strong determinant for oxidative potential (an indicator of cellular oxidative stress). Building on this body of work suggesting the relevance of pyrite and bioavailable iron as a significant predictor for CWP development, a pathogenic pathway termed "ferropotosis" was linked to the development of CWP (Sun et al, 2022) – (Figure 2-3 timepoint 32). In defining this pathway, *in vitro* tests confirmed the relevance of iron derived from pyrite, as well as additional iron-bearing minerals, as a strong explanatory factor for both cytotoxic and proinflammatory responses in lung cells, in the presence of quartz. Despite these recent advancements there is still no clear understanding or means to holistically compare the relative impact of the various characteristics on the toxic/inflammatory responses observed in mechanistic studies. Consequently, many studies consider the individual strength of characteristics as a potential

predictor, but do not address the potential for mechanisms to co-occur or progress at varying magnitudes based on the properties of the dust.

This review aims to provide a means of contextualising the debate on the potential causal factors relating to CWP development by synthesising and integrating the current understanding of coal mine dust as an inherently harmful material and defining the generalised pathways leading to cellular stress and damage post-exposure. Through establishing these concepts, the review further aims to critically assess the physicochemical characteristics of coal mine dust which should be considered as predictors for the development of CWP and other coal mine dust-related diseases based on an integrated understanding of particle toxicology and the geo-anthropogenic nature of the dust. Lastly, the review provides a synthesis of the approaches developed to define the pneumoconiotic potency of coal mine dust and further demonstrates the potential usefulness of coal mine dust characteristics as a tool to assess respiratory harm.

## 2.3. Coal as a geo-anthropogenic dust source

In the mining environment, unwanted dust is generated as a by-product of several anthropogenic operations. To understand the overall dust burden within collieries, several studies have applied geospatial methods such as satellite imagery to define the amount of dust generated from these sources (Ghose and Majee, 2000a; Mandal et al, 2012; Huertas et al, 2014). Collectively, the results from these studies highlighted operations such as ore excavation, transportation, and primary processing of the material as major contributors to the burden of dust within and around collieries. As each of these operations has the potential to impact the inherent characteristics of the dust, and thus their potential toxicity, studies have investigated the variability within intra- and/or inter-colliery settings for their potential to produce characteristically distinct particle populations (Johann-Essex et al 2017; LaBranche et al 2021; Trechera et al 2021b).

In the context of underground mines, studies by Johann-Essex et al (2017) and LaBranche et al (2021) have shown that the mineralogical composition of the coal mine dust can vary significantly based on the mine location and operation. Between the different mines investigated, these studies showed that the coal mine dust from cutting sites contained higher proportions of minerals relative to carbonaceous matter. Consistent with the previous observations of Johann-Essex et al (2017), Sarver et al (2021), and LaBranche et al (2021), a study by Trechera et al (2020) found that the proportion of mineral matter relative to carbonaceous matter varied between sampled coal mine dust. Moreover, some of the dust samples displayed compositional abundances similar to the parental coal whereas other sampled dust was enriched in mineral content compared to their parental coal. To account for this variation, these studies cited both geogenic variability (such as differences in the regional geology) and anthropogenic activities such as rock dusting and cutting into wall rock. Apart from composition, the results presented by Johann-Essex et al (2017) and

LaBranche et al (2021) showed that the particle size distributions across different point sources varied both within and between the underground mines investigated. Specifically, the dust collected near cutting zones and return airways (extractive ventilation near cutting) tended to yield higher proportions of finer particles than sites near the intake airways. Apart from coal and mineral dust, both studies in addition to studies by Pan et al (2021) and Sarver et al (2021) noted the presence of diesel exhaust particles in the submicron fraction of some mines. Such results highlight the heterogenous nature of coal mine dust. In assessing whether different cutting methods have an impact on particle size, a study by LaBranche et al (2021) found that the locality of the mine from where the dust was sampled had a stronger impact on the size distributions than the cutting method (longwall versus continuous miner). In expanding on reasons for this unexpected result, the study proposed that potential differences in geology and the mining conditions (cutting speed, deterioration of cutting pick and dust suppression) may influence the particle size distributions resulting from the different cutting methods.

To assess the impact of various mining operations in an open cast environment, the intra-colliery variability between the characteristics of coal mine dust sourced from several locations in a pit was compared (Trechera et al, 2021b). The results showed that each operation or activity produced distinctly different distributions of particle size and chemical compositions, similarly to the results obtained from the underground mines. Specifically, dust produced from tailings handling and by truck traffic tended to consist of more minerals than carbonaceous matter. This was compared to the dust produced at the coal work fronts, which was predominantly carbonaceous matter. Across the different sites, the particle size of the dust sampled at the coal work front was found to be coarser compared to the dust produced from tailings handling and by truck traffic. To explain this, studies by Amato et al (2010) and Colinet et al (2021) proposed that the frequent spraying of dust at the work front could have promoted agglomeration. This contrasts with the tailings handling zone which is not sprayed and is thus not affected by additional moisture.

Ultimately, these findings indicate that the physicochemical and mineralogical properties of coal mine dust are a function of both the anthropogenic activities on collieries which produce the particles and the geogenic properties of the parental coal. Apart from coal mine dust derived from extractive operations, little is known about the anthropogenic dust generated from the stored wastes of the coal beneficiation process. As coal beneficiation waste products are generally enriched in mineral matter (clays, quartz and sulfides) and subsequently deposited in tailings zones (Oliveira et al 2012a; Oliveira et al 2012b; Tambwe et al 2020), understanding and managing dust derived from these zones may be important to mitigate the health effects seen by individuals proximal to mines.

## 2.4. The relationship between coal mine dust, cellular stress, and inflammation

### 2.4.1. The fate of inhaled coal particles

Once a particle has been inhaled its ultimate deposition in the respiratory tract is understood to be based on the individual's breathing pattern (through either the nose or mouth) as well as the aerodynamic diameter of the particles (Yeh et al, 1976; McClellan, 2000; Schulz et al, 2000) – (see Figure 2-4). In addition to these factors, further studies have outlined the role of geometric size, shape and morphology in the sedimentation and entrainment of particles in lung tissue (Muhle and Mangelsdorf, 2003; Plumlee et al, 2006; Fubini and Fenoglio, 2007; Hassan and Lau, 2009). To further assess the translocation and potential dose of inhaled particles, the International Commission on Radiological Protection Human Respiratory Tract Model was developed (Bair, 1991, 2000). As part of the outputs of this dosiometric model, the probability of deposition for particles of a given size can be interpreted within various regions along the respiratory tract (as demonstrated in Figure 2-4). To account for differences in breathing patterns, normal nasal breathing and oral breathing after light exercise were examined as conditions to contextualise the deposition environment. While the model was developed for radionuclide particles, it has been widely cited as a tool to assess the deposition profiles of airborne particles along the respiratory tract (Oberdörster, 2000; Maynard and Kuempel, 2005; Plumlee et al, 2006; Haddrell et al, 2015; Kodros et al, 2018; Patel et al, 2020).

Depending on where the particles are deposited, a variety of mechanisms may be employed as a part of the body's protective strategies against foreign material (Lauweryns and Baert, 1977; Wanner et al, 1996; Plumlee et al, 2006). In the upper and lower respiratory tract (up to the bronchioles) particles are mostly cleared mechanically via the mucociliary escalator. By trapping the inhaled particles in a mucus coat, particles are then moved upward by ciliated epithelium where they are eventually swallowed. This process prevents most particles from encountering the sensitive alveolar region and potentially entering the bloodstream through the air-blood boundary. However, several studies have established that fine (< 10 µm) and ultrafine (<1 µm) particles – particularly particles which are poorly soluble in lung fluids – have the potential to penetrate deeper into the lung, particularly the alveolar region (Muhle et al, 1990; Oberdörster et al, 1994; Oberdörster, 2000; Donaldson et al, 2002; Nel et al, 2006; Kroll et al, 2011). In the context of coal mine dust, studies such as (Gonzalez et al, 2022a), LaBranche et al (2021), Pan et al (2021), and Sarver et al (2021), have generally found that respirable particulates range in size from 5 µm to 1 µm. In parallel with these findings, studies by Shangguan et al (2022) and Trechera et al (2021) measured the distribution of particle sizes from deposited coal mine dust to obtain the volume percentage of particles in different size classes. Collectively, their results showed that 10-30 % of deposited dust collected is < 10 µm, while 2-25 % of the dust reports < 4 µm. As the content of coal mine dust is poorly soluble but potentially biologically

reactive, such proportions of particles in these size classes highlights the necessity to understand how different physicochemical properties impact cellular activity and the general pulmonary environment.
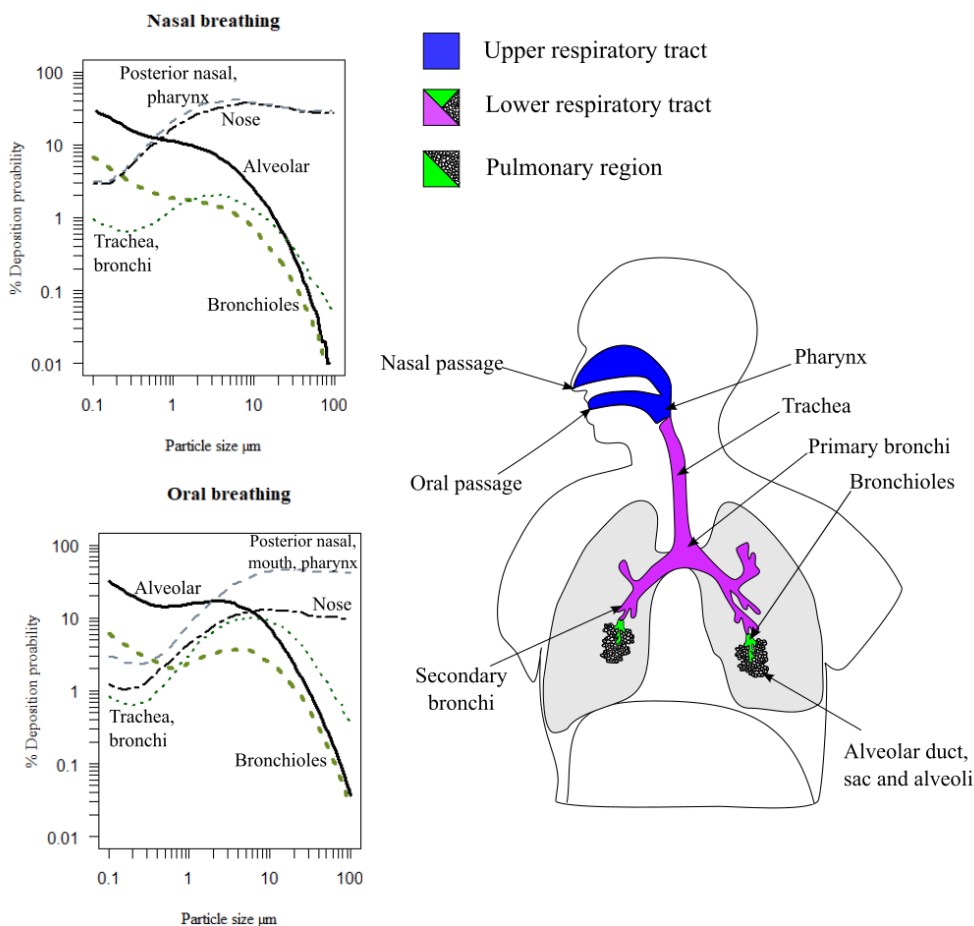


Figure 2-4 Deposition profiles particles of particles sized between 0.1-100 µm under conditions of normal nasal breathing and oral breathing after light exercise; graphs adapted from Bair (2000).

In the instance where foreign particles have made their way to the alveolar region, phagocytic cells (e.g., macrophages) are activated to remove the contaminant. At a high exposure, the phagocytes can become overwhelmed and secrete signals to mobilise additional cells of the immune system by inducing further pro-inflammatory responses (see Figure 2-5). In addition to deposition, the composition of the particles has also been found to impact the bio-geochemistry of the alveoli, triggering the macrophages and epithelial cells to release stress signals and pro-inflammatory mediators (Borda and Schoonen, 2001; Leung et al, 2012; Harrington et al, 2013; Orona et al, 2014; Sun et al, 2022). These mechanisms emphasise the need to develop an understanding of the cytotoxic and immunological implications of particle-cell interactions based on the inherent properties of inhalable particles to address this knowledge gap.
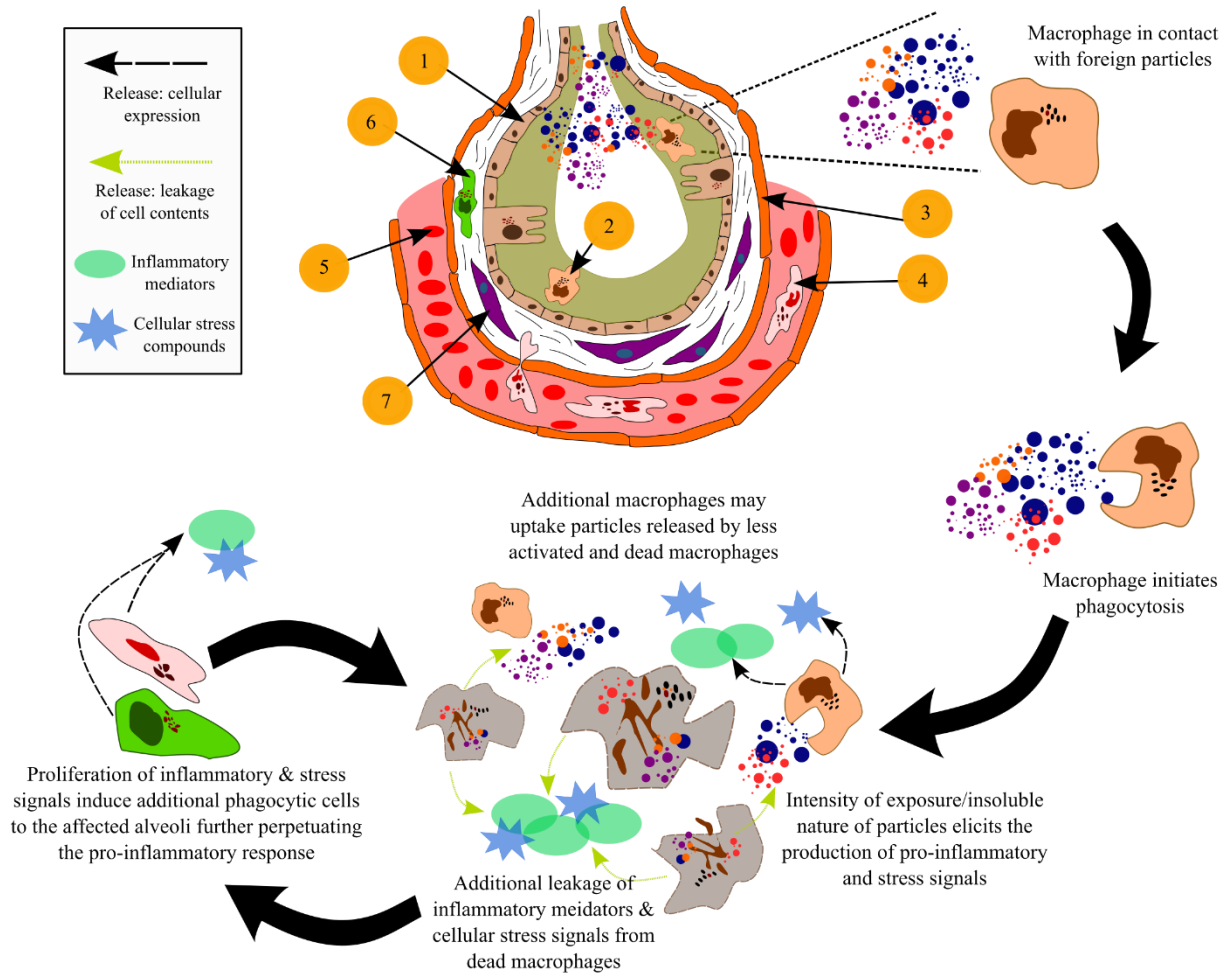
Figure 2-5 Structure of the alveoli and progressive cycle of inflammation derived from macrophages. Description of cells and tissue present 1. Alveolar epithelial cells lined by a surfactant –olive green. 2. Alveolar macrophage (phagocytic cell). 3. Endothelium –orange, and capillary – pink space containing red blood cells. 4. Neutrophil (type of white blood cell) present in an adjacent capillary. 5. Red blood cells present in the pulmonary capillary. 6. Additional macrophage cells present in the interstitium (collection of support tissue including the epithelial cells), 7. Fibroblasts (cells that synthesise collagen and produce connective tissue) present in the interstitium.

## 2.4.2. The role of oxidative stress and inflammation in the pathogenicity of coal mine dust

In outlining the pathogenicity of coal mine dust, markers of pulmonary damage have been characterised to follow a set of stages leading to the development of diseases such as CWP (Vallyathan et al, 1998; Schins and Borm, 1999; Castranova, 2000) – outlined in Figure 2-6. Starting from the initial deposition, particles settle into alveolar fluid secreted by epithelium cells (see Figure 2-4). Once in the fluid, the nature and chemistry of the particle surface have the potential to interact with compounds such as molecular oxygen, releasing highly reactive chemicals known as Reactive Oxygen Species (ROS) – Stage 1 in Figure 2-6. The presence of both the particles and these reactive compounds activates the alveolar macrophages, which travel to the sites of deposition to ingest the particles via phagocytosis. In cases where

the number of particles or chemical reactivity of the material has not overwhelmed the system, the abundance of ROS is counteracted by antioxidant compounds secreted by macrophages. These compounds ultimately mediate the potential for ROS to damage healthy cells and tissue. However, when the exposure is acute, severe damage may occur to both the macrophages and epithelial cells via direct and indirect means (Yang et al, 2009; Michael et al, 2013; Orona et al, 2014). As a result, pathways leading to the direct cytotoxicity and indirect damage of DNA (genotoxicity) can be enacted (Könczöl et al 2011; León-Mejía et al 2016; Roesslein et al 2013).
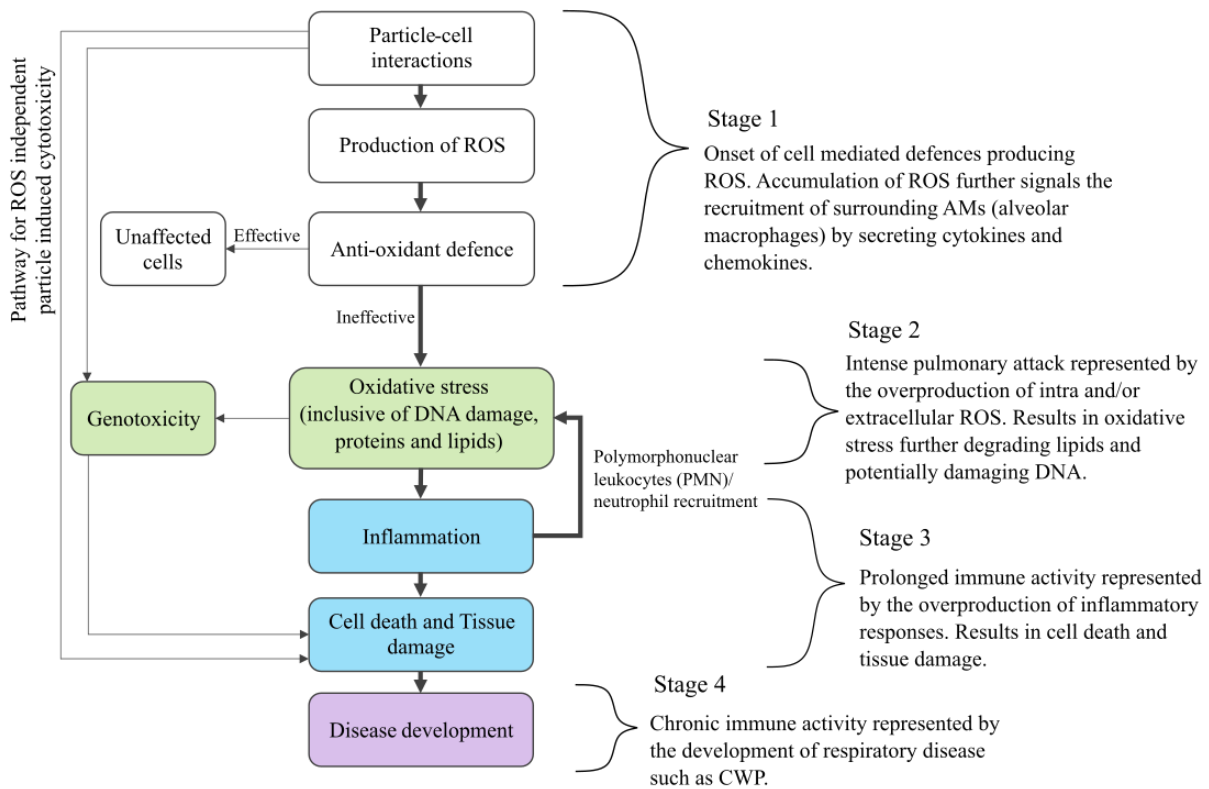


Figure 2-6 A generalised depiction of the disease induction pathways from particle exposure based on Roesslein et al (2013).

Although both direct and indirect cellular damage is understood to play a role in the physiological degradation of the lung, studies have shown that the overproduction of ROS and subsequent development of oxidative stress is most likely the dominant pathway involved in the development of pneumoconiosis and other coal mine dust related diseases (Vallyathan et al, 1998; Maanen et al, 1999; Schins and Borm, 1999; Castranova and Vallyathan, 2000; Zhang and Huang, 2002; Zhang et al, 2002; Pinho et al, 2004) – Stage 2 in Figure 2-6. In addition to ROS generated from alveolar cells, it has been demonstrated that redox reactions between transition metals (at the surface of minerals and from metal leaching) and minerals such as quartz can produce highly reactive hydroxyl radicals (Cohn et al 2006a; Cohn et al 2006b; Dalal et al

1990, 1995; Ghio and Quigley 1994; Schoonen et al 2010; Vallyathan et al 1998; Vallyathan, Schwegler et al 1988; Winterbourn 1995). In this context, the cause to tissue damage and eventual fibrosis is attributed to cycles of non-specific damage of cell membrane phospholipids via lipid peroxidation, consequently leading to the release of inflammatory mediators known as cytokines and chemokines and the recruitment of additional inflammatory cells (polymorphonuclear leucocytes (PMNs)/ neutrophils) (Rice-Evans, 1994; Borish and Steinke, 2003; Laskin, 2009; Hiraiwa and Van Eeden, 2013; Vanka et al, 2022) – Stage 3 in Figure 2-6.

## 2.5. Physical particle characteristics relevant to cellular stress and inflammation

### 2.5.1. Size

In addressing the importance of particle size relative to inflammation and lung injury, studies by Morrow (1988) and Muhle et al (1990) hypothesised that the volumetric loading of highly insoluble ultrafine particles could impair the ability of macrophages to further internalise particles and thus hinder the removal of particles in the alveoli. Under such circumstances Morrow (1988) proposed that this occurs when approximately 6 % of the normal macrophage volume is filled by phagocytized particles. As a result of impaired clearance, the build-up of particles may occur and can subsequently lead to direct and indirect damage to macrophage and epithelial cells depending on the chemical reactivity of the particles (Broug-Holub et al, 1997; Lison et al, 1997; Warheit et al, 1997; Donaldson et al, 2000). Furthermore, the particles may translocate into the bloodstream where they can potentially impact the cardiovascular system (Wallenborn et al, 2007; Decuzzi et al, 2010).

To assess the dependency of particle sizes on the entrainment of particles within the lung, as well as associated inflammatory damage *in vivo*, a study by Oberdörster et al (1994) exposed groups of rats to two size fractions (<250 nm and <20 nm) of highly insoluble $TiO_2$ particles under equivalent doses. To compare the effects of the different size fractions, a group of rats were only exposed to filtered air. The findings showed that, over the same period, the <250 nm particles were retained in the alveolar space for twice as long as the control (where the retained particles in the macrophages reached ~9 % of the macrophage volume). In comparison, the <20 nm particles were retained four times longer in the alveolar space relative to the control (where the retained particles in the macrophages reached ~2.6 % of the macrophage volume). Based on these results, Oberdörster et al (1994) challenged the cut-off phagocyte internalisation volume proposed by Morrow (1988), and further suggested that the size of particles can inhibit the internalisation of particles by macrophages to different degrees irrespective of the phagocytized volume of the cell. In this context, it was presumed that effective macrophage removal would result in the migration of cells to the upper respiratory tract via the mucociliary escalator – further described by Wanner et al (1996).

By investigating the dependency of particle size on inflammatory responses at a dose congruent with particle overload, the results from Oberdörster et al (1994) showed that the <20 nm particles displayed a greater influx of recruited monocytes and polymorphonuclear leucocytes (PMNs) and secreted more proteins (such as lactate dehydrogenase indicating cytotoxicity from cytosolic damage) than the <250 nm particles of the same dose. These results highlighted that the effective dose in alveoli is not a consistent predictor of impaired clearance or inflammation where there is a distribution in particle sizes. To complement these results, the inflammatory influx of PMNs was compared to the surface area of the retained particles. Through this relationship, both <20 and <250 nm particles could be explained by a common dose-response curve. This suggests that the surface area of retained particles may be a more useful determinant for impaired macrophage clearance and inflammation than retained dose. These observations were supported by similar studies on chemically non-reactive particles such as rutile, polystyrene, diesel, and carbon-based soot which showed a common dose-response relationship between the surface area/number of particles and the influx of PMN and other inflammatory indicators (Lison et al, 1997; Tran et al, 2000; Brown et al, 2001; Maynard and Kuempel, 2005; Oberdörster et al, 2005; Stoeger et al, 2006).

Regarding the effect of size of inflammation by more biologically reactive particles, a study by Mischler et al (2016) investigated the level of mitochondrial ROS and TNF-α (an inflammatory indication) expressed by murine macrophages across different size fractions of quartz. Their results showed that particles in their coarsest class (4 µm) displayed a consistent relationship between mitochondrial ROS generation and TNF-α release from acute exposures (2-,4-, and 8-hour timepoints). However, the results for finest fraction (0.3 µm) showed that the finer particles were able to be internalised by macrophages at a higher rate. This in turn translated to higher rates of mitochondrial ROS production and TNF-α release from the finer particles after 4 hours compared to the coarser particles. This could suggest that the activity of biologically reactive particles such as quartz could be exacerbated by their particle size.

## 2.5.2. Surface area and reactivity

From the perspective of particle reactivity, observations have shown that an increase in the specific surface area of particles allows for a greater proportion of atoms/molecules to bind and react at the surface (Oberdörster et al, 2005). However, such an outcome could arise either from a reduction in particle size or by a change in the aspect ratio, both of which have been shown to elicit independent pathways to the production of Reactive Oxygen Species (ROS) and inflammatory mediators (Oberdörster et al, 1994; O'Neill, 2008).

In the context of coal mine dust pathology, the surface reactivity of free minerals and coal-mineral composites have been observed to strongly influence the production of toxic hydroxyl radicals (Fubini et al, 1990; Schoonen et al, 2010; Zhang et al, 2018). This is based on *in situ* reactions between surface

functional groups and metal complexation sites enabling transition metal-based redox reactions. However, the contribution of these surface-based reactions to the overall ROS burden remains unclear. In addition to these reactions, defects at the surface of crystalline matter (induced by grinding) have been shown to serve as sites for free radical generation (Schoonen et al, 2006). In the context of mining and mineral processing, such observations may be occupationally relevant as a harmful geo-anthropogenic alteration to dust generated from mechanical crushing. By investigating the effect of grinding on poorly soluble minerals such as quartz, studies have found that these freshly fractured particles not only generate hydroxyl radicals, but also display higher rates of cytotoxicity at equivalent doses compared to aged particles (Fubini et al, 1987; Vallyathan et al, 1995; Lison et al, 1997).

In composite particles, the toxic effects resulting from surface reactivity, morphology and surface area exposure are known to occur simultaneously. Although studies have extensively outlined the individual toxic effects for each of these characteristics (in monomineralic systems), the degree to which these combined factors impact phagocytosis in composite particles is not yet understood.

## 2.5.3. Shape
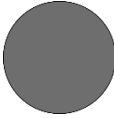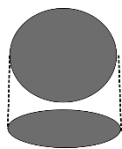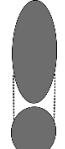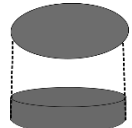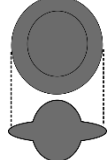
In the scope of physical characteristics related to particle toxicity, the potential impact of particle shape on toxicity and inflammation has been widely acknowledged through research conducted on fibrous minerals (Plumlee and Ziegler, 2003; Maynard and Kuempel, 2005; Fubini and Fenoglio, 2007). However, particle shape has rarely been examined by immunological studies investigating the pneumoconiotic potency of coal mine dust. Currently, it is generally understood that high aspect ratio particle shapes can disrupt the successful internalisation of particles during phagocytosis (Cannon and Swanson, 1992; Schins and Borm, 1999). In this process, termed "frustrated phagocytosis", affected macrophages generate ROS and inflammatory indicators in response to the failure to successfully internalise a given particle (O'Neill, 2008). As a result of this response, epithelial and fibroblast cells are triggered to produce secondary pro-inflammatory and fibrogenic mediators which may subsequently induce scarring if perpetuated.

Apart from the research conducted on fibrous particles, a study by Champion and Mitragotri (2006) determined that various non-spherical particle shapes can impact the functioning of macrophages, leading to frustrated phagocytosis. Based on their findings, it was determined that phagocytosis could be initiated for a range of particle shapes with equal size, surface area, and chemistry (see Table 2-1 for a description of the particle shapes). Their results further indicated that, depending on the initial contact point (flat versus a curved surface), complete phagocytosis may not occur, irrespective of the size of the particle relative to the cell volume. By defining the contact point as the angle between the macrophage membrane and the point of contact on the particle surface, they were able to generalise the relationship between shape and phagocytosis (displayed in Figure 2-7). Based on this relationship, the rate of phagocytosis was found to

decrease when the angle of the contact point was less than 45°. For a contact point with an angle greater than 45° (which represents a flat surface or concave contact point), no change in the rate of phagocytosis was observed. The results further demonstrated that, for particles with equivalent ratios of particle volume to macrophage volume, the angle of initial contact was found to determine whether complete internalisation or macrophage spreading would occur (see Figure 2-7). In this context, macrophage spreading was induced where the contact point was initiated at flat surfaces and concave points. In contrast to this observation, complete phagocytosis was found to occur when the macrophages encountered spheres, dome/ring-shaped particles, and the rounded edges of the ellipsoids.

Ultimately, the implications of incomplete phagocytosis amount to the persistence of particles in the lung, as discussed in the section on particle size. As a result of this, biogeochemical reactions between soluble particles and extracellular fluids can continue, further leading to the direct/indirect damage of tissues via radical attack. In this context, particle characteristics which have been demonstrated to impair phagocytic activities (such as particle shape) may serve as strong predictors for pneumoconiotic potency of both poorly and moderately soluble dust. However, in the case of coal mine dust, which has soluble and reactive components, it is unclear what contribution impaired phagocytosis makes to acute inflammatory responses relative to particle-cell biogeochemical reactions, as both processes are likely to occur simultaneously.

Table 2-1 Representation of the top and side view of the particle shapes represented in Champion and Mitragotri (2006).

| Sphere | Oblate ellipsoid | Prolate ellipsoid | Elliptical disk | Rectangular disk | UFO |
|---|---|---|---|---|---|
| Radius: (1.0-12.5 µm) | Major axis: (4 µm) Aspect ratio: (4) | Major axis: (2-6 µm) Aspect ratio: (1.3-3) | Major axis: (2-6 µm) Aspect ratio: (2-4) Thickness: (400-1000 nm) | Major axis: (4-8 µm) Aspect ratio: (1.5-4.5) | Sphere radius: (1.5 µm) Ring radius: (4 µm) |
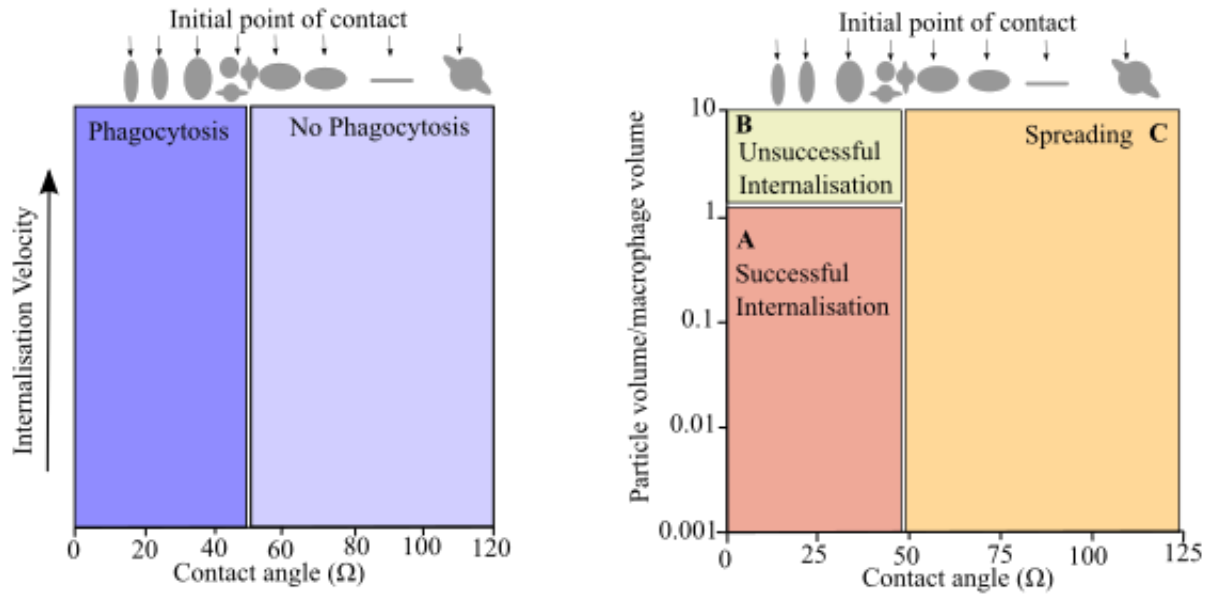
Figure 2-7 Left-hand side represents the ability of phagocytosis to occur depending on the shape of the particle and the initial contact point. The right-hand side displays a phase diagram highlighting the different responses macrophages display post initiation of phagocytosis, where area A represents a complete engulfment of the particle by the macrophage, area B represents the incomplete engulfment, and area C represents the spreading of the macrophages over the particle surface rather than engulfment – based on Champion and Mitragotri (2006).

## 2.6. The role of composition and geochemistry in cellular stress and inflammation

### 2.6.1. Carbonaceous material

In early epidemiological research on the prevalence of CWP, observations from several mine cohorts found that the prevalence of CWP differed depending on the geographic region (Morgan et al, 1973; Hurley et al, 1982; Le Bouffant et al, 1988; Attfield and Morring, 1992a). In explaining the possible reasons for this discrepancy, the regional differences in coal rank were found to show a limited level of explanatory power in accounting for disease prevalence. Based on this observation, a study by Dalal et al (1989) attempted to uncover an experimental link between coal rank and CWP. From their results, it was determined that freshly ground coal produces an increasing number of carbon-centred free radicals with increasing rank. By collating these results with the knowledge that free radicals are highly influential in progressing toxic pathways leading to CWP development, studies hypothesized that these carbon-centred radicals could be implicated in oxidative damage and serve as a potential predictor for the differential toxicity of coal mine dust (Dalal et al, 1990; Huang et al, 1999). However, further experimentation showed that these free radicals are highly sensitive to air and displayed low reactivity with oxidising agents, suggesting that these types of free radicals are inert (Huang et al, 1999).

To further assess the role of the carbonaceous matter in the production of hydroxyl radicals from coal mine dust samples, a study by Cohn et al (2006a) investigated the contribution of hydroxyl radicals

produced from mixtures of carbonaceous matter and pyrite (a mineral known to produce ROS through redox chemistry). The results showed that, upon adding consistent quantities of the coal (containing no pyrite) to a fixed quantity of pyrite, no significant change to the levels of hydroxyl radical was detected. This suggested that carbonaceous matter in coals does not play an active role in the generation of highly reactive oxygen radicals. However, studies have also shown that compounds derived from carbonaceous matter can play a supporting role in redox-based reactions by forming a complexation site with transition metals derived from mineral sources (Ghio et al, 1992; Ghio and Quigley, 1994; Dalal et al, 1995). Despite these studies, no definitive conclusion has been reached on the role of the carbonaceous matter in coal and its implication for disease development, with experimental studies to date indicating that it may not play a causative role in the definition of pneumoconiotic potency of coal mine dust.

## 2.6.2. Bioavailable iron

Since the discovery of iron concentrated in the lungs of miners with CWP, studies postulated the role of bioavailable iron in the pathology of coal mine dust (Ghio and Quigley, 1994; Dalal et al, 1995). In the context of biogeochemical reactions in the body, transition metals and iron especially, have been shown to react with extracellular hydrogen peroxide producing highly reactive hydroxyl radicals via Fenton chemistry (Eq.2-1) (Winterbourn, 1995; Meneghini, 1997). While this pathway may seem direct and further limited by the availability of ferrous iron, studies have shown that a large concentration of reducing agents, such as ascorbate, pyruvate and glutathione, have the potential to facilitate the reduction of ferric to ferrous iron by cycling the ferrous iron and perpetuating the Fenton mechanism (Eq. 2-2) (Slade et al, 1985; Cross et al, 1994; Pritchard et al, 1996; Sun et al, 2022). Additionally, studies have shown that ferrous iron can facilitate a feedback production of hydrogen peroxide in the presence of oxygen via the Haber-Weiss reaction, which further drives the Fenton mechanism (Eq. 2-3 and 2-4) (Ghio and Quigley, 1994; Winterbourn, 1995; Kehrer, 2000; Schoonen et al, 2010).

$$Fe^{2+}{}_{(aq)} + H_2O_2 \rightarrow \bullet OH + OH^- + Fe^{3+}{}_{(aq)} \qquad \text{Eq. 2-1}$$
$$Fe^{3+}{}_{(aq)} + Reductant \rightarrow Fe^{2+}{}_{(aq)} + Reductant^+ \qquad \text{Eq. 2-2}$$
$$Fe^{2+}{}_{(aq)} + O_2 \rightarrow Fe^{3+}{}_{(aq)} + (O_2{}^\bullet)^- \qquad \text{Eq. 2-3}$$
$$Fe^{2+}{}_{(aq)} + (O_2{}^\bullet)^- + 2H^+ \rightarrow Fe^{3+}{}_{(aq)} + H_2O_2 \qquad \text{Eq. 2-4}$$
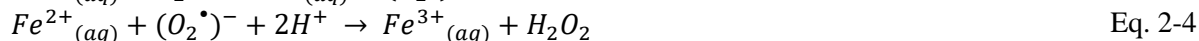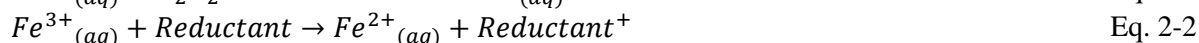
To date, research defining the mechanics of iron-mediated oxidative damage has predominantly focused on the complexation of aqueous iron as the main mode of iron availability (Cohn et al 2006a; Dalal et al 1995; Harrington et al 2012, 2015; Vallyathan 1994). Regarding the possible pathways for iron complexation, studies hypothesised that "humic-like substances" (HLS) derived from carbonaceous matter could form organometallic complexes with iron and serve as sites to catalyse the generation of ROS (Ghio et al, 1992; Ghio and Quigley, 1994; Pritchard et al, 1996). Under these conditions it was proposed that

continuous cycles of the Fenton mechanism could occur through the reduction of iron by natural reducing agents, perpetuating oxidative damage to lung tissues. Despite these results, the use of HLS as a potential predictor for iron-mediated oxidative damage has not been utilised in the context of coal mine dust toxicity. As studies aim to develop robust particle characterisation datasets of coal mine dust for the interpretation of health outcomes, the quantification of HLS may be a useful proxy for iron/transition metal-mediated damage.

## 2.7. Reactive mineralogy in coal and its implications for CWP

### 2.7.1. Quartz

The highly toxic nature of inhalable quartz particles has been well established in literature (Fubini et al, 1990; Fubini, 1998; Borm, 2002; Turci et al, 2016; Jelic et al, 2017). While the molecular mechanisms relating to its toxicity remain unclear, it is accepted that the silanol functional groups, formed on the surface of hydrated quartz particles, can readily produce hydroxyl radicals (Castranova and Vallyathan, 2000). Based on the unique properties of silanol groups and their propensity to produce hydroxyl radicals, quartz was thought to be the primary propagator of radical-related cytotoxicity and inflammation (Fubini et al, 1990; Castranova, 2000).

Although the presence of quartz in coal mine dust has been considered a causal agent in characteristic ROS-dominated pathways leading to CWP, workers exposed to coal mine dust with little to no quartz were still found to develop CWP (Collis and Gilchrist, 1928; Reisner et al, 1982; Heppleston, 1992; Finkelman et al, 2002). Mechanistically, studies found no consistent relationship between quartz content and toxicity when investigating the pulmonary potency of coal-quartz mixtures *in vitro* and *in vivo* (Ross et al, 1962; Davis et al, 1982). To account for such results, a study by Le Bouffant et al (1988) suggested that the presence of clay surface coatings on the quartz was a reason for the lack of a clear relationship between toxicity and quartz in coal mine dust. Subsequent experimentation confirmed this phenomenon and further suggested that quartz particles may exhibit surface aluminosilicate contamination in dusty work environments (Wallace et al, 1994; Harrison et al, 1997). In continuation of the findings by Harrison et al (1997) and Wallace et al (1994), studies by Gonzalez et al, (2022b) and Keles and Sarver (2022) have observed the surface coating of quartz in coal mine dust with aluminosilicate clays using SEM-EDS (scanning electron microscopy and electron dispersive X-ray spectroscopy). In this study, they further categorise the different textural associations between quartz and the clays as: clay-occluded quartz, micro-agglomerates containing quartz, and particles embedded with quartz grains. Such results demonstrate the complex textural relationships between minerals in coal mine dust and their potential to impact the level of mineral-related reactivity within the body.

While it is understood that the chemical reactivity of quartz may be variable, studies have found that freshly fractured surfaces of crystalline quartz particles can produce additional free radicals, further adding to the burden of ROS and oxidant-related damage (Fubini et al 1987; Vallyathan et al 1995; Vallyathan, Shi et al 1988). In the context of collieries which mine thin coal seams, the cutting of quartz-rich wall rock, and the concomitant generation of mine dust with a high abundance of fractured quartz particles, was found to induce the development of silica-related r-type opacities within the lungs of miners (Hall et al, 2019; Cohen et al, 2022b). Through an investigation into the mechanisms of fractured quartz toxicity, a study determined that the active fracturing of quartz leads to the disorganisation of surface functional groups (Turci et al, 2016; Leinardi et al, 2020). This was suggested to result in the development of reactive silanol patches and surface radicals.

Ultimately, it can be argued that the reactivity of quartz in composite coal mine dust particles (expressed by the abundance of quartz) may not serve as a consistent predictor of oxidative damage or CWP prevalence. This is in part due to the unresolved variability in surface chemistry and potential surface coating of quartz particles by association with clays or though dusting in the environment. However, parameters which can capture the impact of quartz surface fractures, such as specific surface area and surface reactivity, have been suggested as more representative of quartz-related damage than the abundance of quartz (Leinardi et al, 2020; Pavan et al, 2020).

## 2.7.2. Pyrite

For several years the abundance of pyrite in coal mine dust has been suggested as a potential predictor for oxidative damage and subsequent CWP development (Schins and Borm, 1999; Zhang et al, 2002; Huang and Finkelman, 2008). Through extensive experimentation, studies have established that hydrated pyrite particles in the presence of molecular oxygen can spontaneously generate hydrogen peroxide (Haber-Weiss reaction Eq. 2-3 and 2-4) and hydroxyl radicals (Fenton mechanism Eq. 2-1) (Borda and Schoonen 2001; Cohn et al 2005; Q. Zhang et al 2002; Zhang and Huang 2002). Based on these mechanisms, a study by Huang et al (2005) attempted to map and predict the prevalence of CWP across the USA through correlations with (1) bioavailable iron (BAI) content calculated from pyrite in coal, (2) pyritic sulfur, (3) total iron, (4) quartz content, and (5) coal rank. The data used included CWP prevalence rates from the national epidemiological survey reported by Morgan et al (1973) and coal quality data from twenty-four mines across seven states, obtained from the USGS (United States Geological Survey). To determine the quantitative values for BAI it was assumed that all BAI was derived from the oxidation of pyrite in water (displayed by Eq. 2-5), although it was acknowledged that additional sources of iron could come from both iron-containing carbonates and silicates. As the available data was limited to pyritic sulfur, sulfate, CaO and $Fe_2O_3$, an assumption was made that 1 mol pyritic sulfur would equate to 0.5 mol BAI

(represented in Eq. 2-6). Based on the geographical comparison of these characteristics, it was observed that, while the coal rank, quartz and calcite content showed little variation, the pyritic sulfur, total iron, arsenic, and nickel were found to vary from the eastern coal regions to the west. This observed pattern matched the disparities in prevalence records for CWP reported across the regions of the national epidemiological survey following 1973 (Attfield and Morring, 1992a).

$$2FeS_2 + 7O_2 + 2H_2O \rightarrow 2FeSO_4 + 2H_2SO_4 \qquad \text{Eq. 2-5}$$
$$BAI = [0.5 \times S_{py}] \qquad \text{Eq. 2-6}$$
$$Adujusted\ BAI = [0.5 \times S_{py} + SO_4 - CaO] \qquad \text{Eq.2-7}$$

By correlating the prevalence of CWP with the physicochemical characteristics of coals across the USA, strong positive relationships were found between BAI and pyritic sulfur; more so than total iron (see Table 2-2). Similar results were subsequently reported in mechanistic studies, which found that pyritic sulfur in the examined coals showed a positive correlation with the concentration of hydroxyl radicals and the degradation of nucleic acids (Cohn et al, 2006b). This further suggests that pyrite may serve as a good predictor for CWP development across coal regions. In addition to the correlations described, the study by Huang et al (2005) further assessed the effect of pH on BAI by adjusting the BAI content to account for the buffering capacity of coals (see Eq. 7). It was expected that the pH of the hydrated pyrite system would need to be lower than 4.5 after oxidation of the pyrite surface to stabilize the production of soluble iron sulfate, based on an earlier hypothesis by Huang et al (1994). In contrast to the lower pH system, the hypothesis further outlined that under systems with a pH higher than 4.5, the pyrite surface will be oxidised forming a non-reactive goethite alteration product. The resulting correlations between the adjusted BAI and CWP prevalence showed that the presence of acid-consuming species lowers the predictability of the BAI mechanism, which can further be supported by the hypothesis of Huang et al (1994) – refer to Table 2-2.

While the study by Huang et al (2005) indicated that BAI derived from pyrite could potentially be used as a consistent predictor of CWP prevalence, it was highlighted that the correlations observed did not necessarily represent causation. Additionally, it should be acknowledged that the context used in this analysis predated the current cases of CWP in this region which have been observed by Cohen et al (2022) and Hall et al (2019) to be more related to quartz related CWP. Despite these considerations, subsequent mechanistic studies further concurred on the toxic nature of pyrite based on the Fenton mechanism, the modality of this reaction was mostly discussed in the context of iron leached from pyrite (Cohn, et al 2006a; Harrington et al 2012, 2013; Sherekar et al 2022; Sun et al 2022). At the same time, it is known that these reactions can occur at the surface of pyrite particles (Borda and Schoonen, 2001; Schoonen et al, 2006; Zhang et al, 2018). Currently, there is a limited understanding of the relative contribution of Fenton

reactions at the pyrite surface compared to leached Fe in solution. As pyrite-containing coal particles may be deposited on epithelial cells, it is reasonable to assume that the production of hydroxyl radicals from surface-based Fenton mechanisms may cause direct damage to the cells. As a result, the epithelial cells may secrete pro-inflammatory signals leading to the mobilisation of macrophages. Based on this, it can be argued that research on the different modalities of direct and indirect pyrite-induced damage may be beneficial in determining additional predictors for inflammation and tissue damage. Ultimately, studies conducted to date have shown that pyrite in coal mine dust has the potential to both directly and indirectly produce highly reactive hydroxyl radicals. However, it remains unclear what relative impact Fenton related damage has on a cellular level in relation to other composition or morphological-based mechanisms of toxicity. By finding ways to elucidate its relative impact, the relevance of pyrite and bioavailable iron as a toxic agent in coal mine dust can be understood more holistically.

Table 2-2 Data on the statistical strength of the correlations between the physicochemical aspects of the coal (data from the USGS) and the CWP prevalence rates obtained from the NSCWP 1970 survey presented in Huang et al (2005).

| Physicochemical aspect | Correlation coefficient (r) | 95% confidence interval | P-value |
|---|---|---|---|
| **BAI** | **0.94** | 0.66-0.999 | **0.0015** |
| **$S_{py}$** | **0.91** | 0.35-0.99 | **0.0048** |
| **$Fe_T$** | **0.85** | 0.20-0.97 | **0.016** |
| Coal rank | 0.59 | 0.26-0.91 | 0.16 |
| Quartz | 0.28 | 0.55-0.82 | 0.54 |
| Calcite | -0.18 | -0.78-0.60 | 0.69 |
| **\*BAI Low pH** | **0.90** | 0.40-0.99 | **0.006** |
| **\*BAI Buffered pH** | **0.87** | 0.25-0.98 | **0.01** |

$S_{py}$-pyritic sulfur, $Fe_T$-total iron
All significant relationships are indicated in bold (p-value < 0.05)
*Low pH – assuming no neutralisation by calcite, high pH – accounting for acid neutralised by calcite

### 2.7.3. Miscellaneous minerals

Apart from pyrite, a study by Sun et al (2021) showed that other iron-bearing minerals such as siderite (an iron carbonate) may also play a role in Fenton-related inflammation and cytotoxicity. Whilst pyrite is often found to be the dominant iron-bearing mineral, its reactivity with water and carbonate minerals can lead to the formation of additional non-sulfate minerals, such as iron-bearing sulfides and iron oxyhydroxides under basic conditions. By understanding the different iron-bearing assemblages present in coals this may assist in determining whether iron may be present in a biologically active form or not.

In the context of quartz related toxicity, aluminosilicate clays (such as kaolinite) have been found to play a depressive role in the bio-reactivity of quartz surfaces (Tourmann and Kaufmann, 1994; Wallace et al, 1994). However, pure kaolinite has been shown by Davies (1983), Davies et al (1984), and Wastiaux and Daniel (1990) to induce cytotoxicity in macrophages, although its mechanisms are currently not completely understood. Considering that clays make a substantial proportion of the mineral content in coal

mine dust, apart from quartz and pyrite, the potential cytotoxic and depressive effects of kaolinite should be considered in discussions around the pneumoconiotic potency of coals.

## 2.8. The utilisation of coal particle characteristics to assess potential respiratory harm

The complex reactivity resulting from particle-cell interactions has been well documented for coal mine dust, particularly in relation to composition-driven reactions in the lung. While there is still uncertainty on the relative impact of composition and particle morphology on oxidative stress and inflammation, studies have sought to develop comprehensive datasets on coal mine dust characteristics to quantify known predictors of cellular damage (Johann-Essex et al, 2017a; Moreno et al, 2019; Trechera et al, 2020; LaBranche et al, 2021). Although methods exist for the quantification of physicochemical and mineralogical characteristics of coal, no systematic protocol has been developed for the robust characterisation of the physicochemical and mineralogical characteristics of coal mine dust particles.

Despite the lack of a systematic characterisation protocol, studies have attempted to define relationships between coal mine dust characteristics and the potential for oxidative damage using mineral abundances and element distributions (Trechera et al, 2021a, 2021b; Shangguan et al, 2022). Across all these studies, the authors constructed multilinear models to assess relationships between oxidative potential and the two composition-based datasets. While their modelled relationships were found to be consistent with earlier studies that showed the ROS generation potential of pyrite, sulfates, elemental iron, and, to a lesser extent, quartz, the issue of collinearity between characteristics was not addressed. As coal mine dust may contain primary and secondary minerals as well as multiple mineral hosts for a given element, the correlation between composite-based characteristics may confound the results of certain models. Despite not considering the effect of collinearity, the studies by Trechera et al (2021a) and Shangguan et al (2022) further described a positive correlation between siderite (iron-bearing carbonate) and oxidative potential, further affirming the contribution of iron-bearing minerals to the iron available for reaction (shown by Sun et al (2021)). In a study by Song et al (2022) the issue of collinearity, when relating composition-based data to inflammatory and cytotoxic responses, was mitigated using principal component analysis. By resolving multiple indicators of toxicity into principal components, a correlation matrix could be constructed using the composition data and the principal components for macrophages, epithelial and fibroblasts cells. While this approach does not allow for the relative weighting of the characteristics that could be achieved in a multilinear model, it does allow for a preliminary screening of potential predictors and the interrelationships between them.

In both modelling applications, the analysis conducted only looked at associations between few characteristics and not the synergistic and antagonistic relationships between the marker of toxicity/inflammation and physicochemical and mineralogical characteristics of the dust. As a result, whilst

additional chemical components were highlighted through correlation (such as potassium and titanium), no causative mechanism was linked to these components. Furthermore, these studies have not considered physical characteristics such as surface and shape when defining the pneumoconiotic potency of their coal mine dust samples, despite these parameters having been shown to greatly influence the functioning of phagocytes. Based on these limitations it can be argued that a deeper investigation into statistical methods is needed to find ways of holistically defining the pneumoconiotic potency of sampled coal mine dust.

## 2.9. Conclusions

Currently, CWP remains a prevalent occupational dust disease across the globe. Apart from the occupational setting, coal mine dust-related diseases have been documented in communities proximal to collieries (Laney and Weissman 2014; Yadav and Jamal 2018). Although extensive epidemiological surveys have been conducted to manage the burden of CWP and coal mine dust related diseases in high income countries, the latency of disease presents a challenge when attempting to connect current exposures and the future health outcomes. This implies that future migration strategies cannot solely rely on epidemiology, especially considering the advancements in tools used to understand the sources and characteristics of coal mine dust. Even so, with decades of research dedicated to understanding the pathology of CWP and the elucidation of causal factors related to its development, little consensus has been reached on the characteristics of coal which are responsible for disease development. Thus, it remains unclear which factor(s) should be taken forward in considering the pneumoconiotic potency of coals and, by extension, what actions need to be taken to mitigate the health effects caused from chronic coal mine dust exposure.

Generally, research efforts which have attempted to characterise coal mine dust and determine its source have identified that geo-anthropogenic alterations, resulting from crushing and wall rock contamination, may potentially impact the physicochemical properties of coal mine dust. By extension it has been shown that these alterations may further impact the ROS generation potential of dust produced from different activities. As numerous studies have shown that pathologies resulting from coal mine dust are strongly mediated by cycles of ROS production and inflammation, characterising, and understanding the anthropogenic alterations caused by mining and beneficiation processes may be important to mitigate the health effects. This is exemplified by the identification of silica-related r-type opacities within the lungs of miners who were exposed to dust contaminated by wall rock cutting.

Particle characteristics such as surface area/reactivity, particle shape, composition, and geochemistry have all been linked to the direct and/or indirect production of ROS. However, in the context of coal mine dust, mechanistic studies correlating particle characteristics to cytotoxicity and inflammation have mainly focused on composition-based data and have neglected the potential impact of surface

area/reactivity and particle shape on macrophage functioning. In the context of pulmonary damage, both composition-related damage and morphology-driven macrophage impairment/stress are anticipated to occur simultaneously. Thus, research which can systematically define the relative contribution and magnitude of the coal particles' physical, chemical, and mineralogical aspects to markers of respiratory harm could potentially assist in representing the pneumoconiotic potency of coal mine dust. Moreover, the development of screening methodologies for these various parameters would additionally assist in the evolution of targeted strategies to mitigate the variable pneumoconiotic potency of coal mine dust produced from different sources.

## 2.10. References

Amato, F., Querol, X., Johansson, C., Nagl, C. and Alastuey, A. (2010) 'A review on the effectiveness of street sweeping, washing and dust suppressants as urban PM control methods', *Science of the Total Environment*. Elsevier, 408(16), pp. 3070–3084. doi: 10.1016/j.scitotenv.2010.04.025.

Attfield, M. D. and Morring, K. (1992a) 'An investigation into the relationship between coal workers' pneumoconiosis and dust exposure in U.S. coal miners', *American Industrial Hygiene Association Journal*, 53(8), pp. 486–492. doi: 10.1080/15298669291360012.

Attfield, M. D. and Morring, K. (1992b) 'The derivation of estimated dust exposures for U.S. coal miners working before 1970', *American Industrial Hygiene Association Journal*, 53(4), pp. 248–255. doi: 10.1080/15298669291359609.

Attfield, M. D. and Seixas, N. S. (1995) 'Prevalence of pneumoconiosis and its relationship to dust exposure in a cohort of U.S. Bituminous coal miners and ex-miners', *American Journal of Industrial Medicine*. John Wiley & Sons, 27(1), pp. 137–151. doi: 10.1002/ajim.4700270113.

Bair, W. (1991) 'Overview of ICRP Respiratory Tract Model', *Radiation Protection Dosimetry*, 38(1–3), pp. 147–152. doi: 10.1093/RPD/38.1-3.147.

Bair, W. (2000) 'The ICRP Human Respiratory Tract Model for Radiological Protection', *Radiation Protection Dosimetry*, 60(4), pp. 307–310.

Bennett, J. G., Dick, J. A., Kaplan, Y. S., Shand, P. A., Shennan, D. H., Thomas, D. J. and Washington, J. S. (1979) 'The relationship between coal rank and the prevalence of pneumoconiosis', *British Journal of Industrial Medicine*, 36, pp. 206–210. doi: 10.1136/oem.36.3.206.

Blackley, D. J., Halldin, C. N. and Laney, A. S. (2018) 'Continued Increase in Prevalence of Coal Workers' Pneumoconiosis in the United States, 1970-2017', *American journal of public health*, 108, pp. 1220–1222. doi: 10.2105/AJPH.2018.304517.

Borda, M. J. and Schoonen, M. A. (2001) 'Pyrite-Induced Hydrogen Peroxide Formation as a Driving Force in the Evolution of Photosynthetic Organisms on an Early Earth Chemistry of surfaces and nanoparticles View project'. doi: 10.1089/15311070152757474.

Borish, L. C. and Steinke, J. W. (2003) 'Cytokines and chemokines', *Journal of Allergy and Clinical Immunology*, 111, pp. 460–475. doi: 10.1067/mai.2003.108.

Borm, P. J. A. (2002) 'Particle Toxicology: From Coal Mining To Nanotechnology', *Inhalation Toxicology*, 14(3), pp. 311–324. doi: 10.1080/08958370252809086.

Bouffant, L. Le, Bruyet, B., Daniel, H., Demarez, J., Kovacs, P., Martin, J. C., Addison, J., Bolton, R. E., et al (1988) 'Compared in vitro and in vivo toxicity of coalmine dusts. relationship with mineralogical composition', *Annals of Occupational Hygiene*, 32(1), pp. 611–620. doi: 10.1093/annhyg/32.inhaled_particles_VI.611.

Broug-Holub, E., Toews, G. B., Van Iwaarden, J. F., Strieter, R. M., Kunkel, S. L., Paine, R. and Standiford, T. J. (1997) 'Alveolar macrophages are required for protective pulmonary defenses in murine Klebsiella pneumonia: elimination of alveolar macrophages increases neutrophil recruitment but decreases bacterial clearance and survival', *Infection and Immunity*. American Society for Microbiology, 65(4), pp. 1139–1146. doi: 10.1128/IAI.65.4.1139-1146.1997.

Brown, D. M., Wilson, M. R., MacNee, W., Stone, V. and Donaldson, K. (2001) 'Size-dependent proinflammatory effects of ultrafine polystyrene particles: A role for surface area and oxidative stress in the enhanced activity of ultrafines', *Toxicology and Applied Pharmacology*, 175(3), pp. 191–199. doi: 10.1006/taap.2001.9240.

Bufton, M. W. and Melling, J. (2005) 'Coming up for air: Experts, employers, and workers in campaigns to compensate silicosis sufferers in Britain, 1918-1939', *Social History of Medicine*, 18(1), pp. 63–86. doi: 10.1093/sochis/hki007.

Cannon, G. J. and Swanson, J. A. (1992) 'The macrophage capacity of phagocytosis', *Journal of Cell Science*, 101, pp. 907–913. doi: 10.4135/9781452218991.n13.

Castranova, V. (2000) 'From Coal Mine Dust To Quartz: Mechanisms of Pulmonary Pathogenicity', *Inhalation Toxicology*, 12(3), pp. 7–14. doi: 10.1080/08958378.2000.11463226.

Castranova, V. and Vallyathan, V. (2000) 'Silicosis and Coal Workers' Pneumoconiosis', *Environmental Health Perspectives*, 108, pp. 675–684. Available at: https://ehp.niehs.nih.gov/doi/pdf/10.1289/ehp.00108s4675.

Champion, J. A. and Mitragotri, S. (2006) 'Role of target geometry in phagocytosis', *Proceedings of the National Academy of Sciences of the United States of America*, 103(13), pp. 4930–4934. doi: doi.org/10.1073/pnas.0600997103.

Cohen, R. A. (2016) 'Resurgent coal mine dust lung disease: Wave of the future or a relic of the past?', *Occupational and Environmental Medicine*, 73(11), pp. 715–717. doi: 10.1136/oemed-2016-103737.

Cohen, R. A., Rose, C. S., Go, L. H. T., Zell-Baran, L. M., Almberg, K. S., Sarver, E. A., Lowers, H. A., Iwaniuk, C., et al (2022) 'Pathology and Mineralogy Demonstrate Respirable Crystalline Silica Is a Major Cause of Severe Pneumoconiosis in U.S. Coal Miners', *Annals of the American Thoracic Society*, 19(9), pp. 1469–1478. doi: 10.1513/annalsats.202109-1064oc.

Cohn, C. A., Laffers, R., Simon, S. R., O'Riordan, T. and Schoonen, M. A. (2006a) 'Role of pyrite in formation of hydroxyl radicals in coal: Possible implications for human health', *Particle and Fibre Toxicology*, 3, pp. 1–10. doi: 10.1186/1743-8977-3-16.

Cohn, C. A., Mueller, S., Wimmer, E., Leifer, N., Greenbaum, S., Strongin, D. R. and Schoonen, M. A. (2006b) 'Pyrite-induced hydroxyl radical formation and its effect on nucleic acids', *Geochemical Transactions*. Springer International Publishing, 7(1), p. 3. doi: 10.1186/1467-4866-7-3.

Cohn, C. A., Pak, A., Strongin, D. and Schoonen, M. A. (2005) 'Quantifying hydrogen peroxide in iron-containing solutions using leuco crystal violet', *Geochemical Transactions*, 6(3), pp. 47–51. doi: 10.1063/1.1935449.

Colinet, J. F., Rider, J. P., Listak, J. M., Organiscak, J. A. and Wolfe, A. L. (2021) *Best Practices for Dust Control in Coal Mining*, *NIOSH*. Available at: http://www.cdc.gov/niosh/mining/UserFiles/works/pdfs/2010-110.pdf.

Collis, E. L. and Gilchrist, J. C. (1928) 'Effects of Dust upon Coal Trimmers.', *Journal of Industrial Hygiene*, 10, pp. 101–10.

Cross, C. E., Van Der Vliet, A., O'neill, C. A., Louie, S. and Halliwell2, B. (1994) 'Oxidants, Antioxidants, and Respiratory Tract Lining Fluids', *Environmental Health Perspectives*, 102, pp. 185–191.

D'arcy Hart, P. and Aslett, E. A. (1942) *Chronic Pulmonary Disease in South Wales Coalminers. I. Medical Studies. A.-Report by the Committee on Industrial Pulmonary Disease.*

D'Arcy Hart, P. and Tansey, E. M. (1998) 'Chronic Pulmonary Disease in South Wales Coal Mines: An Eye-Witness Account of the MRC Surveys (1937-1942)', *Social History of Medicine*, 11(3), pp. 459–468. doi: 10.1093/shm/11.3.459.

Dalal, N., Newman, J., Pack, D., Leonard, S. and Vallyathan, V. (1995) 'Hydroxyl Radical Generation by Coal Mine Dust: Possible Implication to Coal Workers' Pneumoconiosis (CWP)', *Free Radical Biology and Medicine*, 18(I), pp. 11–20.

Dalal, N., Shi, X. and Vallyathan, V. (1990) 'Role of free radicals in the mechanisms of hemolysis and lipid peroxidation by silica: Comparative esr and cytotoxicity studies', *Journal of Toxicology and Environmental Health*, 29(3), pp. 307–316. doi: 10.1080/15287399009531393.

Dalal, N., Suryan, M., Vallyathan, V., Green, F., Jafari, B. and Wheeler, R. (1989) 'Detection of Reactive Free Radicals In Fresh Coal Mine Dust and Their Implication for Pulmonary Injury', *The Annals of Occupational Hygiene*, 33(1), pp. 79–84. doi: 10.1093/annhyg/33.1.79.

Davies, R. (1983) 'Factors Involved in the Cytotoxicity of Kaolinite towards Macrophages in Vitro', *Environmental Health Perspectives*, 51, pp. 249–274.

Davies, R., Griffiths, D. M., Johnson, N. F., Preece, A. W. and Livingston, D. C. (1984) 'The cytotoxicity of kaolin towards macrophages in vitro', *British Journal of Experimental Pathology*, 65, pp. 453–466.

Davis, J. M. G., Addison, J., Bruch, J., Bruyere, S., Daniel, H., Degueldre, G., Dodgson, J., Gade, M., et al (1982) 'Variations in cytotoxicity and mineral content between respirable mine dusts from the Belgian , British , French and German coalfields', *Annals of Occupational Hygiene*, 26(541), pp. 541–549.

Decuzzi, P., Godin, B., Tanaka, T., Lee, S. Y., Chiappini, C., Liu, X. and Ferrari, M. (2010) 'Size and shape effects in the biodistribution of intravascularly injected particles', *Journal of Controlled Release*. Elsevier, 141(3), pp. 320–327. doi: 10.1016/j.jconrel.2009.10.014.

Donaldson, K., Brown, D., Clouter, A., Duffin, R., MacNee, W., Renwick, L., Tran, L. and Stone, V. (2002) 'The pulmonary toxicology of ultrafine particles', *Journal of Aerosol Medicine*, 15(2), pp. 213–220. doi: 10.1089/089426802320282338.

Donaldson, K., Stone, V., Gilmour, P. S., Brown, D. M. and MacNee, W. (2000) 'Ultrafine particles: mechanisms of lung injury', *Philosophical Transactions of the Royal Society A*, 358, pp. 2741–2749. doi: 10.1098/rsta.2000.0681.

Donaldson, K., Wallace, W. A., Elliott, T. and Henry, C. (2017) 'James Craufurd Gregory, 19th century Scottish physicians, and the link between occupation as a coal miner and lung disease', *Journal of the Royal College of Physicians of Edinburgh*, 47(3), pp. 296–302. doi: 10.4997/JRCPE.2017.317.

Finkelman, R. B., Orem, W., Castranova, V., Tatu, C. A., Belkin, H. E., Zheng, B., Lerch, H. E., Maharaj, S. V. et al (2002) 'Health impacts of coal and coal use: Possible solutions', *International Journal of Coal Geology*. Elsevier, 50(1–4), pp. 425–443. doi: 10.1016/S0166-5162(02)00125-8.

Fubini, B. (1998) 'Surface Chemistry and Quartz Hazard', *Annals of occupational hygiene*, 42(8), pp. 521–530. Available at: https://academic.oup.com/annweh/article/42/8/521/148104.

Fubini, B., Bolis, V. and Giamello, E. (1987) 'The surface chemistry of crushed quartz dust in relation to its pathogenicity', *Inorganica Chimica Acta*, 138, pp. 193–197.

Fubini, B., Giamello, E., Volante, M. and Bolis, V. (1990) 'Chemical functionalities at the silica surface determining its reactivity when inhaled. Formation and reactivity of surface radicals', *Toxicology and Industrial Health*, 6(6), pp. 571–598. Available at: https://pubmed.ncbi.nlm.nih.gov/1965871/.

Fubini, B. and Ivana, F. (2007) 'Toxic Potential of Mineral Dusts', *Elements*, 3(6), pp. 407–414. doi: 10.2113/GSELEMENTS.3.6.407.

Ghio, A. J., Kennedy, T. P., Whorton, A. R., Crumbliss, A. L., Hatch, G. E. and Hoidal, J. R. (1992) 'Role of surface complexed iron in oxidant generation and lung inflammation induced by silicates', *American Journal of Physiology*, 263, pp. 511–518. doi: 10.1152/ajplung.1992.263.5.l511.

Ghio, A. J. and Quigley, D. R. (1994) 'Complexation of iron by humic-like substances in lung tissue: role in coal workers' pneumoconiosis', *American Journal of Physiology*, 267(2), pp. L173–L179. doi: 10.1152/ajplung.1994.267.2.l173.

Ghose, M. K. and Majee, S. R. (2000) 'Assessment of dust generation due to opencast coal mining - An Indian case study', *Environmental Monitoring and Assessment*, 61(2), pp. 255–263. doi: 10.1023/A:1006127407401.

Gonzalez, J., Keles, C. and Sarver, E. (2022a) 'On the Occurrence and Persistence of Coal-Mineral Microagglomerates in Respirable Coal Mine Dust', *Mining, Metallurgy and Exploration*, 39(2), pp. 271–282. doi: 10.1007/s42461-022-00555-7.

Gonzalez, J., Keles, C., Pokhrel, N., Jaramillo, L. and Sarver, E. (2022b), 'Respirable dust constituents and particle size: a case study in a thin-seam coal mine', *Mining, Metallurgy and Exploration*, 1, pp. 1007–1015. doi: 10.1007/s42461-022-00611-2.

Gormley, I. P., Collings, P., Davis, J. M. G. and Ottery, J. (1979) 'An Investigation into the Cytotoxicity of Respirable Dusts from British Collieries', *British Journal of Experimental Pathology*, 60, pp. 526–536.

Haddrell, A. E., Davies, J. F. and Reid, J. P. (2015) 'Dynamics of Particle Size on Inhalation of Environmental Aerosol and Impact on Deposition Fraction', *Environmental Science and Technology*, 49(24), pp. 14512–14521. doi: 10.1021/acs.est.5b01930.

Hall, N. B., Blackley, D. J., Halldin, C. N. and Laney, A. S. (2019) 'Continued increase in prevalence of r-type opacities among underground coal miners in the USA', *Occupational and Environmental Medicine*, 76(7), pp. 479–481. doi: 10.1136/oemed-2019-105691.

Harrington, A. D., Hylton, S. and Schoonen, M. A. (2012) 'Pyrite-driven reactive oxygen species formation in simulated lung fluid: implications for coal workers' pneumoconiosis', *Environmental Geochemistry and Health*. Springer, 34(4), pp. 527–538. doi: 10.1007/s10653-011-9438-7.

Harrington, A. D., Smirnov, A., Tsirka, S. E. and Schoonen, M. A. (2015) 'Metal-sulfide mineral ores, Fenton chemistry and disease – Particle induced inflammatory stress response in lung cells', *International Journal of Hygiene and Environmental Health*. Elsevier, 218(1), pp. 19–27. doi: 10.1016/J.IJHEH.2014.07.002.

Harrington, A. D., Tsirka, S. E. and Schoonen, M. A. A. (2013) 'Inflammatory stress response in A549 cells as a result of exposure to coal: Evidence for the role of pyrite in coal workers' pneumoconiosis pathogenesis', *Chemosphere*, 93(6), pp. 1216–1221. doi: 10.1016/j.chemosphere.2013.06.082.

Harrison, J. C., Brower, P. S., Attfield, M. D., Doak, C. B., Keane, M. J., Grayson, R. L. and Wallace, W. E. (1997) 'Surface composition of respirable silica particles in a set of U.S. anthracite and bituminous coal mine dusts', *Journal of Aerosol Science*, 28(4), pp. 689–696. doi: 10.1016/S0021-8502(96)00033-X.

Hassan, M. S. and Lau, R. W. M. (2009) 'Effect of Particle Shape on Dry Particle Inhalation: Study of Flowability, Aerosolization, and Deposition Properties', *AAPS PharmSciTech*, 10(4), pp. 1252–1262. doi: 10.1208/s12249-009-9313-3.

HEI, Health Effects Institute. and IHME, Institute for Health Metrics and Evaluation. (2020) *State of Global Air 2020.Special Report*. Boston.

Heppleston, A. G. (1992) 'Coal workers' pneumoconiosis: a historical perspective on its pathogenesis.', *American Journal Of Industrial Medicine*, 22(6), pp. 905–923.

Hiraiwa, K. and Van Eeden, S. F. (2013) 'Contribution of Lung Macrophages to the Inflammatory Responses Induced by Exposure to Air Pollutants', *Mediators of Inflammation*, pp. 1-10. doi: 10.1155/2013/619523.

Hiura, T. S., Kaszubowski, M. P., Li, N. and Nel, A. E. (1999) 'Induce Apoptosis in Macrophages Generate Reactive Oxygen Radicals and Chemicals in Diesel Exhaust Particles', *The Journal of Immunology*, 163, pp. 5582–5591.

Huang, C., Li, J., Zhang, Q. and Huang, X. (2002) 'Role of Bioavailable Iron in Coal Dust-Induced Activation of Activator Protein-1 and Nuclear Factor of Activated T Cells Difference between Pennsylvania and Utah Coal Dusts scale mining', *American Journal of Respiratory Cell and Molecular Biology*, 27, pp. 568–574. doi: 10.1165/rcmb.4821.

Huang, X. and Finkelman, R. B. (2008) 'Understanding the Chemical Properties of Macerals and Minerals in Coal and its Potential Application for Occupational Lung Disease Prevention', *Journal of Toxicology and Environmental Health, Part B*, 11(1), pp. 45–67. doi: 10.1080/10937400701600552.

Huang, X., Li, W., Attfield, M. D., Nádas, A., Frenkel, K. and Finkelman, R. B. (2005) 'Mapping and prediction of coal workers' pneumoconiosis with bioavailable iron content in the bituminous coals.', *Environmental health perspectives*, 113(8), pp. 964–8. doi: 10.1289/ehp.7679.

Huang, X., Zalma, R. and Pezerat, H. (1999) 'Chemical reactivity of the carbon-centered free radicals and ferrous iron in coals: Role of bioavailable Fe2+ in coal workers' pneumoconiosis', *Free Radical Research*, 30(6), pp. 439–451. doi: 10.1080/10715769900300481.

Huang, X., Zalma, R., Pezerat, H. and Huang, X. (1994) 'Factors That Influence the Formation and Stability of Hydrated Ferrous Sulfate in Coal Dusts. Possible Relation to the Emphysema of Coal Miners', *Chemical Research in Toxicology*, 7(3), pp. 451–457. doi: 10.1021/tx00039a025.

Huertas, J. I., Huertas, M. E., Cervantes, G. and Di´az, J. (2014) 'Assessment of the natural sources of particulate matter on the opencast mines air quality', *Science of the Total Environment*. Elsevier, 493(2000), pp. 1047–1055. doi: 10.1016/j.scitotenv.2014.05.111.

Huertas, J. I., Huertas, M. E., Izquierdo, S. and Gonzalez, E. D. (2012) 'Air quality impact assessment of multiple open pit coal mines in northern Colombia', *Journal of Environmental Management*. Elsevier, 93(1), pp. 121–129. doi: 10.1016/j.jenvman.2011.08.007.

Hurley, J. F., Burns, J., Copland, L., Dodgson, J. and Jacobsen, M. (1982) 'Coal workers' simple pneumoconiosis and exposure to dust at 10 British coalmines', *British Journal of Industrial Medicine*, 39, pp. 120–127. doi: 10.1136/oem.39.2.120.

Jacobsen, M., Rae, S., Walton, W. H. and Rogan, J. M. (1970) 'New dust standards for British coal mines', *Nature*, 227(5257), pp. 445–447. doi: 10.1038/227445a0.

Jelic, T. M., Estalilla, O. C., Sawyer-Kaplan, P. R., Plata, M. J., Powers, J. T., Emmett, M. and Kuenstner, J. T. (2017), 'Coal Mine Dust Desquamative Chronic Interstitial Pneumonia: A Precursor of Dust-Related Diffuse Fibrosis and of Emphysema', *The International Journal of Occupational and Environmental Medicine*, 8, pp. 153–165. doi: 10.15171/IJOEM.2017.1066.

Johann-Essex, V., Keles, C., Rezaee, M., Scaggs-Witte, M. and Sarver, E. (2017) 'Respirable coal mine dust characteristics in samples collected in central and northern Appalachia', *International Journal of Coal Geology*. Elsevier, 182, pp. 85–93. doi: 10.1016/j.coal.2017.09.010.

Kehrer, J. P. (2000) *The Haber-Weiss reaction and mechanisms of toxicity*, *Toxicology*. Available at: www.elsevier.com/locate/toxicol.

Keles, C., Pokhrel, N. and Sarver, E. (2022), 'A Study of Respirable Silica in Underground Coal Mines: Sources', *Minerals*, 12, pp. 1115. doi: 10.3390/min12121555.

Keles, C. and Sarver, E. (2022), 'A Study of Respirable Silica in Underground Coal Mines: Particle Characteristics', *Minerals*, 12, pp. 1555. doi: 10.3390/MIN12121555/S1.

Kodros, J. K., Volckens, J., Jathar, S. H. and Pierce, J. R. (2018) 'Ambient Particulate Matter Size Distributions Drive Regional and Global Variability in Particle Deposition in the Respiratory Tract', *GeoHealth*, 1(10), pp. 298–312. doi: 10.1029/2018GH000145.

Könczöl, M., Ebeling, S., Goldenberg, E., Treude, F., Gminski, R., Gier, R., Grob, B., Rothen-Rutishauser, B., Merfort, I. and Mersch-Sundermann, V. (2011) 'Cytotoxicity and Genotoxicity of Size-Fractionated Iron Oxide (Magnetite) in A549 Human Lung Epithelial Cells: Role of ROS, JNK, and NF-κB', *Chemical Research in Toxicology*, 24(9), pp. 1460–1475. Available at: http://doc.rero.ch.

Kroll, A., Dierker, C., Rommel, C., Hahn, D., Wohlleben, W., Schulze-Isfort, C., Göbbert, C., Voetz, M., Hardinghaus, F. and Schnekenburger, J. (2011) 'Cytotoxicity screening of 23 engineered nanomaterials using a test matrix of ten cell lines and three different assays', *Particle and Fibre Toxicology*, 8(9), pp. 1–19. doi: 10.1186/1743-8977-8-9.

Kuempel, E. D., Attfield, M. D., Vallyathan, V., Lapp, N. L., Hale, J. M., Smith, R. J. and Castranova, V. (2003), 'Pulmonary inflammation and crystalline silica in respirable coal mine dust: dose-response', *Journal of Biosciences*, 1, pp. 61-69.

LaBranche, N., Keles, C., Sarver, E., Johnstone, K. and Cliff, D. (2021) 'Characterization of particulates from Australian underground coal mines', *Minerals*, 11(5), pp. 1–10. doi: 10.3390/min11050447.

Laney, A. S. and Weissman, D. N. (2014) 'Respiratory Diseases Caused by Coal Mine Dust', *Journal of Occupational and Environmental Medicine*, 56, pp. 18–22. doi: 10.1097/JOM.0000000000000260.

Laskin, D. L. (2009) 'Macrophages and inflammatory mediators in chemical toxicity: A battle of forces', *Chemical Research in Toxicology*, 22(8), pp. 1376–1385. doi: 10.1021/tx900086v.

Lauweryns, J. and Baert, J. (1977) 'Alveolar Clearance and the Role of the Pulmonary Lymphatics', *American Review of Respiratory Disease*, 115(4), pp. 625–683. Available at: https://www.atsjournals.org/doi/abs/10.1164/arrd.1977.115.4.625?journalCode=arrd.

Leinardi, R., Pavan, C., Yedavally, H., Tomatis, M., Salvati, A. and Turci, F. (2020) 'Cytotoxicity of fractured quartz on THP-1 human macrophages: role of the membranolytic activity of quartz and phagolysosome destabilization', *Archives of Toxicology*. Springer, 94(9), pp. 2981–2995. doi: 10.1007/s00204-020-02819-x.

León-Mejía, G., Silva, L. F. O., Civeira, M. S., Oliveira, M. L. S., Machado, M., Villela, I. V., Hartmann, A., Premoli, S., et al (2016) 'Cytotoxicity and genotoxicity induced by coal and coal fly ash particles samples in V79 cells', *Environmental Science and Pollution Research*, 23(23), pp. 24019–24031. doi: 10.1007/s11356-016-7623-z.

Lison, D., Cile Lardot, C., Ois Huaux, F., Zanetti, G. and Fubini, B. (1997) 'Influence of particle surface area on the toxicity of insoluble manganese dioxide dusts', *Archives of toxicology*, 71, pp. 725–729. Available at: https://link.springer.com/content/pdf/10.1007/s002040050453.pdf.

Maanen, J. M. S. Van, Borm, P. J. A., Knaapen, A., Herwijnen, M. Van, Schilderman, P. A. E. L., Smith, K. R., Aust, A. E. and Tomatis, M. (1999) 'In vitro effects of coal fly ashes: Hydroxyl Radical Generation, Iron Release , and DNA Damage and Toxicity in Rat Lung Epithelial Cells', *Inhalation Toxicology*, 11, pp. 1123–1141.

Mandal, K., Kumar, A., Tripathi, N., Singh, R. S., Chaulya, S. K., Mishra, P. K. and Bandyopadhyay, L. K. (2012) 'Characterization of different road dusts in opencast coal mining areas of India', *Environmental Monitoring and Assessment*, 184, pp. 3427–3441. doi: 10.1007/s10661-011-2197-1.

Mauderly, J. L., Jones, R. K., Griffith, W. C., Henderson, R. F. and Mcclellan, R. O. (1987) 'Diesel exhaust is a pulmonary carcinogen in rats exposed chronically by inhalation', *Toxicological Sciences*, 9(2), pp. 208–221. doi: 10.1093/toxsci/9.2.208.

Maynard, A. D. and Kuempel, E. D. (2005) 'Airborne nanostructured particles and occupational health', *Journal of Nanoparticle Research*, 7(6), pp. 587–614. doi: 10.1007/s11051-005-6770-9.

McClellan, R. O. (2000) 'Particle Interactions with the respiratory Tract', *Lung Biology in Health and Disease*, 143, pp. 3–56.

Meneghini, R. (1997) 'Iron Homeostasis, Oxidative Stress, and DNA Damage', *Free Radical Biology and Medicine*, 23(5), pp. 783–792. doi: 10.1016/S0891-5849(97)00016-6.

Michael, S., Montag, M. and Dott, W. (2013) 'Pro-inflammatory effects and oxidative stress in lung macrophages and epithelial cells induced by ambient particulate matter', *Environmental Pollution*, 183, pp. 19–29. doi: 10.1016/j.envpol.2013.01.026.

Mishra, R. K., Pandey, J., Chaudhary, S. K., Khalkho, A. and Singh, V. K. (2012) 'Estimation of air pollution concentration over Jharia coalfield based on satellite imagery of atmospheric aerosol', *International Journal of Geomatics and Geosciences*, 2(3), pp. 723–729.

Mischler, S. E., Cauda, E. G., Di Giuseppe, M., McWilliams, L. J., St. Croix, C., Sun, M., Franks, J. and Ortiz, L. A. (2016). Differential activation of RAW 264.7 macrophages by size-segregated crystalline silica. *Journal of Occupational Medicine and Toxicology, 11*(57), 1–14. doi: 10.1186/S12995-016-0145-2/FIGURES/9.

Mischler, S. E., Cauda, E. G., Di Giuseppe, M., McWilliams, L. J., St. Croix, C., Sun, M., Franks, J. and Ortiz, L. A. (2016), 'Differential activation of RAW 264.7 macrophages by size-segregated crystalline silica', *Journal of Occupational Medicine and Toxicology*, 11(57), pp. 1–14. doi: 10.1186/S12995-016-0145-2/FIGURES/9.

Moreno, T., Trechera, P., Querol, X., Lah, R., Johnson, D., Wrana, A. and Williamson, B. (2019) 'Trace element fractionation between PM10 and PM2.5 in coal mine dust: Implications for occupational respiratory health', *International Journal of Coal Geology*, 203, pp. 52–59. doi: 10.1016/j.coal.2019.01.006.

Morgan, W., C., K., Burgess, D. B., Jacobson, G., O'Brien, R. J., Pendergrass, E. P., Reger, R. B. and Shoub, E. P. (1973) 'The Prevalence of Coal Workers' Pneumoconiosis in US Coal Miners', *Archives of Environmental Health: An International Journal*. Taylor & Francis Group, 27(4), pp. 221–226. doi: 10.1080/00039896.1973.10666356.

Morrow, P. E. (1988) 'Possible Mechanisms to Explain Dust Overloading of the Lungs', *Fundamental and aplied Toxicology*, 10, pp. 369–384.

Muhle, H., Creutzenberg, O., Bellmann, B., Heinrich, U. and Mermelstein, R. (1990) 'Dust Overloading of Lungs: Investigations of Various Materials, Species Differences, and Irreversibility of Effects', *Journal of Aerosol Medicine*, 3(s1), p. S-111-S-128. doi: 10.1089/jam.1990.3.suppl_1.s-111.

Muhle, H. and Mangelsdorf, I. (2003) 'Inhalation toxicity of mineral particles: Critical appraisal of endpoints and study design', *Toxicology Letters*, 140–141, pp. 223–228. doi: 10.1016/S0378-4274(02)00514-3.

Nel, A., Xia, T., Mädler, L. and Li, N. (2006) 'Toxic Potential of Materials at the Nanolevel', *Science*, 311, pp. 622–627. doi: DOI: 10.1126/science.1114397.

O'Neill, L. A. J. (2008) 'How frustration leads to inflammation', *Science*, 320(5876), pp. 619–620. doi: 10.1126/science.1158398.

Oberdörster, G. (2000) 'Pulmonary effects of inhaled ultrafine particles', *International Archives of Occupational and Environmental Health*, 74(1), pp. 1–8. doi: 10.1007/s004200000185.

Oberdörster, G., Ferin, J. and Lehnert, B. (1994) 'Correlation between Particle Size, In Vivo Particle Persistence, and Lung Injury', *Environmental Health Perspectives*, 102, pp. 173–179. doi: 10.1016/B978-0-12-386454-3.00341-9.

Oberdörster, G., Oberdörster, E. and Oberdörster, J. (2005) 'Nanotoxicology: An emerging discipline evolving from studies of ultrafine particles', *Environmental Health Perspectives*, 113(7), pp. 823–839. doi: 10.1289/ehp.7339.

Oliveira, M. L. S., Ward, C. R., French, D., Hower, J. C., Querol, X. and Silva, L. F. O. (2012a) 'Mineralogy and leaching characteristics of beneficiated coal products from Santa Catarina, Brazil', *International Journal of Coal Geology*, 94, pp. 314–325. doi: 10.1016/j.coal.2011.10.004.

Oliveira, M. L. S., Ward, C. R., Izquierdo, M., Sampaio, C. H., de Brum, I. A. S., Kautzmann, R. M., Sabedot, S., Querol, X. and Silva, L. F. O. (2012b) 'Chemical composition and minerals in pyrite ash of an abandoned sulphuric acid production plant', *Science of the Total Environment*. Elsevier, 430, pp. 34–47. doi: 10.1016/j.scitotenv.2012.04.046.

Orona, N. S., Astort, F., Maglione, G. A., Saldiva, P. H. N., Yakisich, J. S. and Tasat, D. R. (2014) 'Direct and indirect air particle cytotoxicity in human alveolar epithelial cells', *Toxicology in Vitro*, 28, pp. 796–802. doi: 10.1016/j.tiv.2014.02.011.

Pan, L., Golden, S., Assemi, S., Sime, M. F., Wang, X., Gao, Y. and Miller, J. (2021) 'Characterization of particle size and composition of respirable coal mine dust', *Minerals*, 11(3), pp. 1–12. doi: 10.3390/min11030276.

Patel, S., Sankhyan, S., Boedicker, E. K., Decarlo, P. F., Farmer, D. K., Goldstein, A. H., Katz, E. F., Nazaroff, W. W., et al (2020) 'Indoor Particulate Matter during HOMEChem: Concentrations, Size Distributions, and Exposures', *Environmental Science and Technology*, 54(12), pp. 7107–7116. doi: 10.1021/acs.est.0c00740.

Patra, A. K., Gautam, S. and Kumar, P. (2016) 'Emissions and human health impact of particulate matter from surface mining operation-A review', *Environmental Technology and Innovation*. Elsevier, 5, pp. 233–249. doi: 10.1016/j.eti.2016.04.002.

Pavan, C., Santalucia, R., Leinardi, R., Fabbiani, M., Yakoub, Y., Uwambayinema, F., Ugliengo, P., Tomatis, et al (2020) 'Nearly free surface silanols are the critical molecular moieties that initiate the toxicity of silica particles', *Proceedings of the National Academy of Sciences*. National Academy of Sciences, 117(45), pp. 27836–27846. doi: 10.1073/PNAS.2008006117/SUPPL_FILE/PNAS.2008006117.SAPP.PDF.

Perret, J. L., Plush, B., Lachapelle, P., Hinks, T. S. C., Walter, C., Clarke, P., Irving, L., Brady, P., et al (2017) 'Coal mine dust lung disease in the modern era', *Respirology*, 22(4), pp. 662–670. doi: 10.1111/resp.13034.

Pinho, R. A., Bonatto, F., Andrades, M., Ma´rio, M., Frota, L. C., Ritter, C., Klamt, F. F., Dal-Pizzol, F., et al (2004) 'Lung oxidative response after acute coal dust exposure', *Environmental Research*, 96, pp. 290–297. doi: 10.1016/j.envres.2003.10.006.

Plumlee, G. S., Morman, S. and Ziegler, T. (2006) 'The Toxicological Geochemistry of Earth Materials: An Overview of Processes and the Interdisciplinary Methods Used to Understand Them', *Reviews in Mineralogy and Geochemistry*, 64(1), pp. 5–57. doi: 10.2138/rmg.2006.64.2.

Plumlee, G. S. and Ziegler, T. L. (2003) *The Medical Geochemistry of Dusts, Soils, and Other Earth Materials*. 9th edn, *Environmental geochemistry*. 9th edn. Elsevier. doi: 10.1016/B0-08-043751-6/09050-2.

Pritchard, R. J., Ghio, A. J., Lehmann, J. R., Winsett, D. W., Tepper, J. S., Park, P., Gilmour, M. I., Dreher, et al (1996) 'Oxidant Generation and Lung Injury after Particulate Air Pollutant Exposure Increase with the Concentrations of Associated Metals', *Inhalation Toxicology*. Taylor & Francis, 8(5), pp. 457–477. doi: 10.3109/08958379609005440.

Reisner, M. T. R., Bruch, J., Hilscher, W., Kriegseis, W., Prajsnar, D., Robock, K., Rosmanith, J., Scharmann, et al (1982) 'Specific harmfulness of respirable dusts from west German coal mines VI: Comparison of experimental and epidemiological results', *Annals of Occupational Hygiene*, 26(4), pp. 527–539. doi: 10.1093/annhyg/26.4.527.

Rice-Evans, C. A. (1994) 'Formation of free radicals and mechanisms of action in normal biochemical processes and pathological states', in Burdon, R. . and Rice-Evans, C. A. (eds) *Free Radical Damage and its Control*, pp. 131–153. doi: 10.1016/S0167-7306(08)60441-X.

Roesslein, M., Hirsch, C., Kaiser, J.-P., Krug, H. F. and Wick, P. (2013) 'Comparability of in Vitro Tests for Bioactive Nanoparticles: A Common Assay to Detect Reactive Oxygen Species as an Example', *International Journal of Molecular Sciences*, 14, pp. 24320–24337. doi: 10.3390/ijms141224320.

Ross, H. F., King, E. J., Yoganathan, M. and Nagelschmidt, G. (1962) 'Inhalation experiments with coal dust containing 5 per cent, 10 per cent, 20 per cent and 40 per cent quartz: Tissue reactions in the lungs of rats', *Annals of Occupational Hygiene*, 5(3), pp. 149–161. doi: 10.1093/annhyg/5.3.149.

Ross, M. H. and Murray, J. (2004) 'Occupational respiratory disease in mining', *Occupational Medicine*, 54(5), pp. 304–310. doi: 10.1093/occmed/kqh073.

Sarver, E., Keles, C. and Rezaee, M. (2019) 'Beyond conventional metrics: Comprehensive characterization of respirable coal mine dust', *International Journal of Coal Geology*. Elsevier, 207, pp. 84–95. doi: 10.1016/j.coal.2019.03.015.

Sarver, E., Keleş, Ç. and Afrouz, S. G. (2021), 'Particle size and mineralogy distributions in respirable dust samples from 25 US underground coal mines', *International Journal of Coal Geology*, 247, pp. 103851. doi: 10.1016/j.coal.2021.103851.

Schins, R. P. F. and Borm, P. J. A. (1999) *Mechanisms and Mediators in Coal Dust Induced Toxicity: A Review*, *Annals of Occupational Hygiene*. Available at: https://academic.oup.com/annweh/article-abstract/43/1/7/162163.

Schoonen, M. A., Harrington, A. D., Laffers, R. and Strongin, D. R. (2010) 'Role of hydrogen peroxide and hydroxyl radical in pyrite oxidation by molecular oxygen', *Geochimica et Cosmochimica Acta*, 74, pp. 4971–4987. doi: 10.1016/j.gca.2010.05.028.

Schoonen, M. A., Roemer, E. J. and Simon, S. (2006) 'Mineral-Induced Formation of Reactive Oxygen Species', *Reviews in Mineralogy and Geochemistry*, 64, pp. 179–222. doi: 10.2138/rmg.2006.64.7.

Schulz, H., Brand, P. and Heyder, J. (2000) 'Particle Deposition in the Respiratory Tract', in Gehr, P. and Heyder, J. (eds) *Particle-Lung Interactions*. New York, pp. 229–290.

Shangguan, Y., Zhuang, X., Querol, X., Li, B., Moreno, N., Trechera, P., Sola, P. C., Uzu, G., et al (2022) 'Characterization of deposited dust and its respirable fractions in underground coal mines: Implications for oxidative potential-driving species and source apportionment', *International Journal of Coal Geology*, 258(December 2021). doi: 10.1016/j.coal.2022.104017.

Sherekar, P., Jain, R., Pingle, S. and Suke, S. (2022) 'Role of Pyrite in Aggravating Coal Worker's Pneumoconiosis', in Randive, K., Pingle, S., and Agnihotri, A. (eds) *Medical Geology in Mining*. Springer G. Springer, pp. 15–47. doi: 10.1007/978-3-030-99495-2_2/COVER.

Shi, P., Xing, X., Xi, S., Jing, H., Yuan, J., Fu, Z. and Zhao, H. (2020) 'Trends in global, regional and national incidence of pneumoconiosis caused by different aetiologies: An analysis from the Global Burden of Disease Study 2017', *Occupational and Environmental Medicine*, 77(6), pp. 407–414. doi: 10.1136/oemed-2019-106321.

Slade, R., Stead, A. G., Graham, J. A. and Hatch, G. E. (1985) 'Comparison of lung antioxidant levels in humans and laboratory animals', *The American review of respiratory disease*, 131, pp. 742–746. doi: 10.1164/arrd.1985.131.5.742.

Song, Y., Southam, K., Basil, B., Zosky, G. R., Graeme Zosky, C. R., Bardin, P. and Reynolds, P. (2022) 'Effects of chemical composition on the lung cell response to coal particles: Implications for coal workers' pneumoconiosis', *Respirology*, 12, pp. 447–454. doi: 10.1111/resp.14246.

Stoeger, T., Reinhard, C., Takenaka, S., Schroeppel, A., Karg, E., Ritter, B., Heyder, J. and Schulz, H. (2006) 'Instillation of six different ultrafine carbon particles indicates a surface area threshold dose for acute lung inflammation in mice', *Environmental Health Perspectives*, 114(3), pp. 328–333. doi: 10.1289/ehp.8266.

Sun, Y., Kinsela, A. S., Cen, X., Sun, S., Collins, R. N., Cliff, D. I., Wu, Y. and Waite, T. D. (2021) 'Impact of reactive iron in coal mine dust on oxidant generation and epithelial lung cell viability', *Science of the Total Environment*. Elsevier B.V., 810, p. 152277. doi: 10.1016/j.scitotenv.2021.152277.

Sun, Y., Kinsela, A. S. and Waite, T. D. (2022) 'Elucidation of alveolar macrophage cell response to coal dusts: Role of ferroptosis in pathogenesis of coal workers' pneumoconiosis', *Science of the Total Environment*. Elsevier B.V., 823, p. 153727. doi: 10.1016/j.scitotenv.2022.153727.

Tambwe, O., Kotsiopoulos, A. and Harrison, S. T. L. (2020) 'Desulphurising high sulphur coal discards using an accelerated heap leach approach', *Hydrometallurgy*. Elsevier, 197(May), p. 105472. doi: 10.1016/j.hydromet.2020.105472.

Tourmann, J.-L. and Kaufmann, R. (1994) 'Laser Microprobe Mass Spectrometric (LAMMS) Study of Quartz-Related and Non-Quartz-Related Factors of the Specific Harmfulness of Coal Mine Dusts', *The Annals of Occupational Hygiene*, 38, pp. 455–467. doi: 10.1093/ANNHYG/38.INHALED_PARTICLES_VII.455.

Tran, C. L., Buchanan, D., Cullen, R. T., Searl, A., Jones, A. D. and Donaldson, K. (2000) 'Inhalation of poorly soluble particles. Influence of particle surface area on Inflammation and Clearance', *Inhalation Toxicology*, 12, pp. 1113–1126.

Trechera, P., Moreno, T., Córdoba, P., Moreno, N., Amato, F., Cortés, J., Zhuang, X., Li, B., et al (2021a) 'Geochemistry and oxidative potential of the respirable fraction of powdered mined Chinese coals', *Science of The Total Environment*. Elsevier, 800, p. 149486. doi: 10.1016/J.SCITOTENV.2021.149486.

Trechera, P., Moreno, T., Córdoba, P., Moreno, N., Zhuang, X., Li, B., Li, J., Shangguan, Y., et al (2021b) 'Comprehensive evaluation of potential coal mine dust emissions in an open-pit coal mine in Northwest China', *International Journal of Coal Geology*. Elsevier, 235, p. 103677. doi: 10.1016/J.COAL.2021.103677.

Trechera, P., Moreno, T., Córdoba, P., Moreno, N., Zhuang, X., Li, B., Li, J., Shangguan, Y., et al (2020) 'Mineralogy, geochemistry and toxicity of size-segregated respirable deposited dust in underground coal mines', *Journal of Hazardous Materials*. Elsevier, 399, p. 122935. doi: 10.1016/j.jhazmat.2020.122935.

Turci, F., Pavan, C., Leinardi, R., Tomatis, M., Pastero, L., Garry, D., Anguissola, S., Lison, D., et al (2016) 'Revisiting the paradigm of silica pathogenicity with synthetic quartz crystals: the role of crystallinity and surface disorder'. doi: 10.1186/s12989-016-0136-6.

Vallyathan, V. (1994) 'Generation of Oxygen Radicals by Minerals and Its Correlation to Cytotoxicity', *Environmental Health Perspectives*, 102, pp. 111–115.

Vallyathan, V., Castranova, V., Pack, D., Leonard, S., Shumaker, J., Hubbs, A. F., Shoemaker, D. A., Ramsey, D. M., et al (1995) 'Freshly fractured quartz inhalation leads to enhanced lung injury and inflammation: Potential role of free radicals', *American Journal of Respiratory and Critical Care Medicine*, 152(3), pp. 1003–1009. doi: 10.1164/ajrccm.152.3.7663775.

Vallyathan, V., Schwegler, D., Reasor, M., Stettler, L., Clere, J. and Green, F. H. Y. (1988a) 'Comparative in vitro cytotoxicity and relative pathogenicity of mineral dusts', *Annals of Occupational Hygiene*, 32(inhaled_particles_VI), pp. 279–289. doi: 10.1093/annhyg/32.inhaled_particles_VI.279.

Vallyathan, V., Shi, X. and Castranova, V. (1998) 'Reactive Oxygen Species: Their Relation to Pneumoconiosis and Carcinogenesis', *Environmental Health Perspectives*, 106, pp. 1151–1155.

Vallyathan, V., Shi, X., Dalal, N. S., Irr, W. and Castranova, V. (1988b) 'Generation of free radicals from freshly fractured silica dust. Potential role in acute silica-induced lung injury', *American Review of Respiratory Disease*, 138(5), pp. 1213–1219. doi: 10.1164/ajrccm/138.5.1213.

Vanka, K. S., Shukla, S., Gomez, H. M., James, C., Palanisami, T., Williams, K., Chambers, D. C., Britton, et al (2022) 'Understanding the pathogenesis of occupational coal and silica dust-associated lung disease', *European Respiratory Review*, 31(165). doi: 10.1183/16000617.0250-2021.

Wallace, W. E., Harrison, J. C., Grayson, R. L., Keane, M. J., Bolsaitis, P., Kennedy, R. D., Wearden, A. Q. and Attfield, M. D. (1994) 'Aluminosilicate surface contamination of respirable quartz particles from coal mines dust and from clay works dusts', *Annals of Occupational Hygiene*, 38, pp. 439–445.

Wallenborn, J. G., Mcgee, J. K., Schladweiler, M. C., Ledbetter, A. D. and Kodavanti, U. P. (2007) 'Systemic Translocation of Particulate Matter-Associated Metals Following a Single Intratracheal Instillation in Rats', *Toxicological science*, 98(1), pp. 231–239. doi: 10.1093/toxsci/kfm088.

Wanner, A., Salathe, M. and O'Riordan, T. G. (1996) 'Mucociliary clearance in the airways.', *American journal of respiratory and critical care medicine*, 154(6), pp. 1868–1902. doi: 10.1164/AJRCCM.154.6.8970383.

Warheit, D. B., Hansen, J. F., Yuen, I. S., Kelly, D. P., Snajdr, S. I. and Hartsky, M. A. (1997) 'Inhalation of High Concentrations of Low Toxicity Dusts in Rats Results in Impaired Pulmonary Clearance Mechanisms and Persistent Inflammation', *Toxicology and Applied Pharmacology*, 145(1), pp. 10–22. doi: 10.1006/TAAP.1997.8102.

Wastiaux, A. and Daniel, H. (1990) 'Pulmonary Toxicity of Kaolin in Rats Exposed by Inhalation', *Health Related Effects of Phyllosilicates*. Springer, pp. 405–414. doi: 10.1007/978-3-642-75124-0_36.

Winterbourn, C. C. (1995) 'Toxicity of iron and hydrogen peroxide: the Fenton reaction', *Toxicology Letters*, 82–83(C), pp. 969–974. doi: 10.1016/0378-4274(95)03532-X.

Yadav, A. K. and Jamal, A. (2018) 'Impact of mining on human health in and around mines', *Environmental Quality Management*, 28(1), pp. 83–87. doi: 10.1002/tqem.21568.

Yang, H., Liu, C., Yang, D., Zhang, H. and Xi, Z. (2009) 'Comparative study of cytotoxicity, oxidative stress and genotoxicity induced by four typical nanomaterials: the role of particle size, shape and composition Comparative study of cytotoxicity, oxidative stress and genotoxicity', *Journal of Applied Toxicology*, 29, pp. 69–78. doi: 10.1002/jat.1385.

Yeh, H. C., Phalen, R. F. and Raabe, O. G. (1976) 'Factors influencing the deposition of inhaled particles', *Environmental Health Perspectives*, Vol.15(June), pp. 147–156. doi: 10.1289/ehp.7615147.

Zazouli, M. A., Dehbandi, R., Mohammadyan, M., Aarabi, M., Dominguez, A. O., Kelly, F. J., Khodabakhshloo, N., Rahman, M. M., et al (2021) 'Physico-chemical properties and reactive oxygen species generation by respirable coal dust : Implication for human health risk assessment', *Journal of Hazardous Materials*. Elsevier B.V., 405, p. 124185. doi: 10.1016/j.jhazmat.2020.124185.

Zhang, P., Huang, W., Ji, Z., Zhou, C. and Yuan, S. (2018) 'Mechanisms of hydroxyl radicals production from pyrite oxidation by hydrogen peroxide: Surface versus aqueous reactions', *Geochimica et Cosmochimica Acta*, 238, pp. 394–410. doi: 10.1016/j.gca.2018.07.018.

Zhang, Q., Dai, J., Ali, A., Chen, L. and Huang, X. (2002) 'Roles of bioavailable iron and calcium in coal dust-induced oxidative stress: Possible implications in coal workers lung disease', *Free Radical Research*, 36(3), pp. 285–294. doi: 10.1080/10715760290019309.

Zhang, Q. and Huang, X. (2002) 'Induction of Ferritin and Lipid Peroxidation by Coal Samples With Different Prevalence of Coal Workers' Pneumoconiosis: Role of Iron in the Coals', *American Journal of Industrial Medicine*, 42, pp. 171–179. doi: 10.1002/ajim.10101.

Zosky, G. R., Bennett, E. J., Pavez, M. and Beamish, B. B. (2021) 'No association between pyrite content and lung cell responses to coal particles', *Scientific Reports*, 11(1), p. 8193. doi: 10.1038/s41598-021-87517-z.

# Chapter 3

# RESEARCH DESIGN AND METHODOLOGY
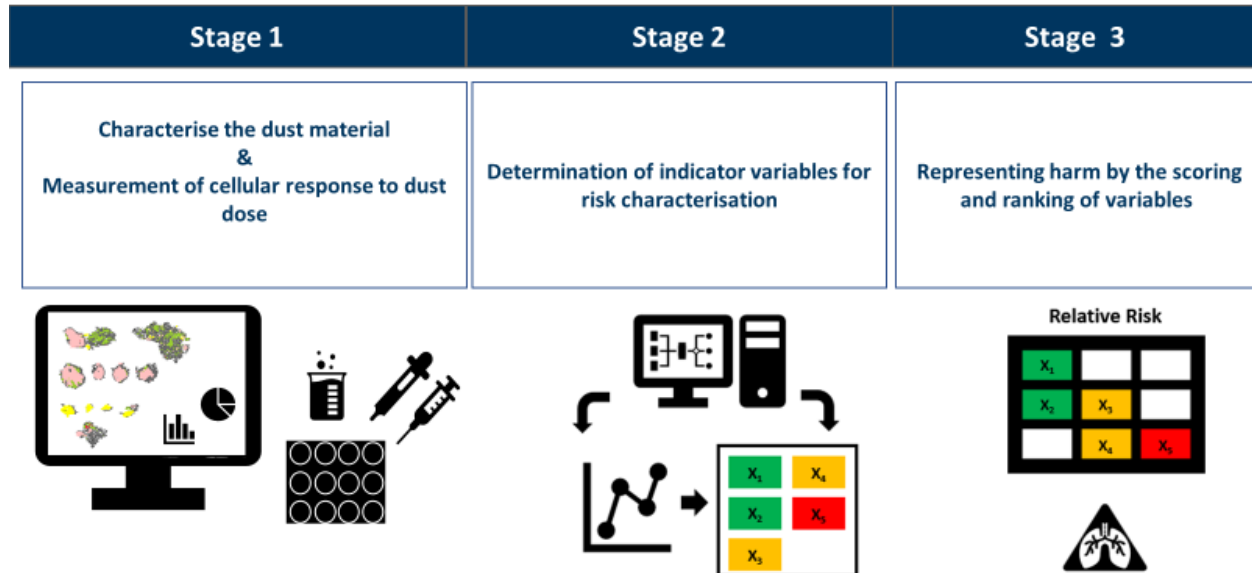


This graphic describes the staged block of experimental, analytical, and data analysis performed for this study.

## 3.1. Overview

This chapter will serve as a description of the hypothesis and objectives leading to the research undertaken. Details pertaining to the specific methodologies employed for each section of the study will be expanded in the subsequent chapters (presented within each paper). This chapter emphasises the description and preparation of the samples in the context of the project as this forms the basis on which the statistical conclusions will be drawn. A brief explanation of the analytical, experimental, and statistical approaches is also given. Considerations on the sources of variability in both the experimental and statistical approaches are discussed alongside the overall sources of uncertainty with respect to the preparation of the samples. It should be noted that all the particle analysis, tissue culture experimentation and statistical analysis were conducted by the candidate. This was except for the Measurement of the XRD and XRF spectral information.

## 3.2. Hypothesis, Objectives and Key Questions

The subsequent sections outline the study hypothesis as well as the research objectives and key questions used to scope and define the research approach of the study.

### 3.2.1. Hypothesis

The direct and indirect effects that coal dust has on pulmonary cells and tissue have been extensively investigated experimentally by numerous studies. Despite this body of work there is currently uncertainty on which characteristics act as catalysts for immunological responses and which properties have depressive or even benign effects on cellular harm. As a result of this uncertainty there has been little development in determining the relative risk of coal dust generated from different sources, from the perspective of hazard identification.

Based on comprehensive review of the relevant literature, it is hypothesised that the reactive mineralogy present in coal dust particles, as well as their physicochemical properties such as surface area, geometry, and size, collectively contribute to the accumulation of ROS and the subsequent perpetuation of oxidative stress leading to inflammation. As a result, it can be expected that these characteristics should provide an indication of pulmonary risk based on the defined interactions reported between the composite particles and primary phagocytes such as macrophages. More specifically, pyrite particles present in the coal with high surface area for reaction are expected to be key parameters which define the potential of a source material to yield an inflammatory/toxic response in macrophages. This is due to the high surface exposure for oxidation and the release of soluble iron via Fenton chemistry.

### 3.2.2. Objective 1:

To develop a detailed and quantitative particle characterisation dataset for coal dust in preparation for biological testing, using a combination of QEMSCAN (quantitative evaluation of minerals by scanning electron microscopy), XRD (X-ray Powder Diffraction) and XRF (X-ray fluorescence) and complementary physical analysis methods for the analysis of physical, compositional, mineral specific characteristics.

Key questions:

i. *Considering that the QEMSCAN is conceived to be the main tool, how should the coal sample be prepared before analysis and what operational requirements need to be made to successfully analyse the coal particles?*

ii. *How will the characteristics of the coal particles be quantified and furthermore, how can supporting techniques be used to build confidence in the accuracy of the dataset?*

iii.   *Do the characteristics defined by the various techniques allow for trends to be identified in the nature of the particles generated, considering that they have been mechanically broken down and can different source characteristics be identified among samples?*

## 3.2.3. Objective 2:

To investigate the multivariant relationships between the coal particle characteristics and immunological responses (cytotoxicity and oxidative stress) generated from exposed macrophage cells.

Key questions:

i.   *What is the relative significance of the various physicochemical characteristics in relation to their effect on the cells and on what basis can this be determined?*

ii.   *Is there a difference between the characteristics linked to cytotoxicity compared to those related to oxidative stress?*

iii.   *Does the addition of detailed particle characteristics (the quantification of mineralogical, chemical, and physical characteristics) aid in interpreting the measures of toxicity compared to more generalised particle characteristics (quantitative phase identification and physical characteristics)?*

## 3.2.4. Objective 3:

To empirically characterise the relative risk of coal dust related damage on a cellular level based on the ranking of the most influential particle characteristics contributing to the harm of pulmonary cells and determining if there are distinct classes of harm.

Key questions:

i.   *From the understanding developed in objective 2, on what basis will the empirical ranking criteria be determined?*

ii.   *Through the understanding developed under objective 1 and 2, how can the various data classes be combined to provide relevant information to decision makers and other stakeholders?*

## 3.3. Sample description

This section provides a detailed description of the samples used in the study and the methods applied to prepare them for subsequent analysis and experimentation.

## 3.3.1. Samples

Within the bituminous coal samples acquired for this study, the sample set has been defined by country of coal origin (South Africa, Brazil, Mozambique, and United States-Pennsylvania state), coalfield (for the South African coals) and sample type. These represent a wide range of different potential dust types

that may stem from dumpsites and stockpiles. For the description of the individual samples tested in this study, refer to Table 3-1.

Table 3-1 Description of the sample names and their origins.

| Sample name | Waste stream | Country | Coal field |
|---|---|---|---|
| SA-Dis1 | Discard | South African | Mine G Waterberg coal field |
| SA-UF1 | Ultrafine thickener underflow | South African | Mine G Waterberg coal field |
| SA-MDT | Medium dense wash waste | South African | Mine L Witbank coal field |
| SA-Dis2 | Discard | South African | Mine G Witbank coal field |
| SA-UF2 | Ultrafine thickener underflow | South African | Mine L Witbank coal field |
| SA-UF3 | Ultrafine coal | South African | Mine G Witbank coal field |
| SA-UF4 | Ultrafine coal | South African | Mine P Witbank coal field |
| SA-ROM3 | Run of mine | South African | Sasolburg coal field |
| SA-ROM2 | Run of mine | South African | Witbank coal field |
| Br-MDT | Medium dense wash waste | Brazilian | Santa Catarina coal field |
| Br-DSulf | Desulfurised coal | Brazilian | Santa Catarina coal field |
| Br-PyC | High pyrite concentrate waste | Brazilian | Santa Catarina coal field |
| Br-Tail | Coal from Dump | Brazilian | Santa Catarina coal field |
| Br-Dis | Discard | Brazilian | Santa Catarina coal field |
| Mz-ROM1 | Run of mine | Mozambican | |
| Mz-ROM2 | Run of mine | Mozambican | |
| US-ROM | Run of mine | USA | Pittsburgh coal field, Pennsylvania |

## 3.3.2. Sample generation

For this project, all the coal types described in section 3.3.1 were prepared into artificial 'dust sized' samples which, in the case of this project, refers to fine material below 25 µm in size – particles must be less than 20 µm for phagocytosis to occur (Cannon and Swanson, 1992). Figure 3-1 describes the process undertaken to mill the coals as received to the sub-25 µm fraction. This methodology takes reference to the process followed by Kaya et al (1996), which demonstrates a methodology of the generation of a dust sample for biological testing in a laboratory setting. To validate the size fractions classified from the sieve methodology, the size distributions were assessed using the Malvern Mastersizer (refer to section 3.4.4. for more detail). In this project, the choice of dry screening the sample and not classifying the sample through a cyclone was intentional as high volumes of the sample were needed for the various analytical techniques. Wet screening was not considered as this method would dissolve and remove soluble minerals such as the secondary sulfate phases. This decision was further justified by the coal dust preparation methods of several studies which opted to size segregate particles via dry mesh sieve for the assessment of cytotoxicity and genotoxicity induced by coal samples *in vitro* (Dalal et al, 1989; Lee et al, 1996; León-Mejía et al, 2016). As a result, the particles are classified by geometric particle size and not aerodynamic diameter.
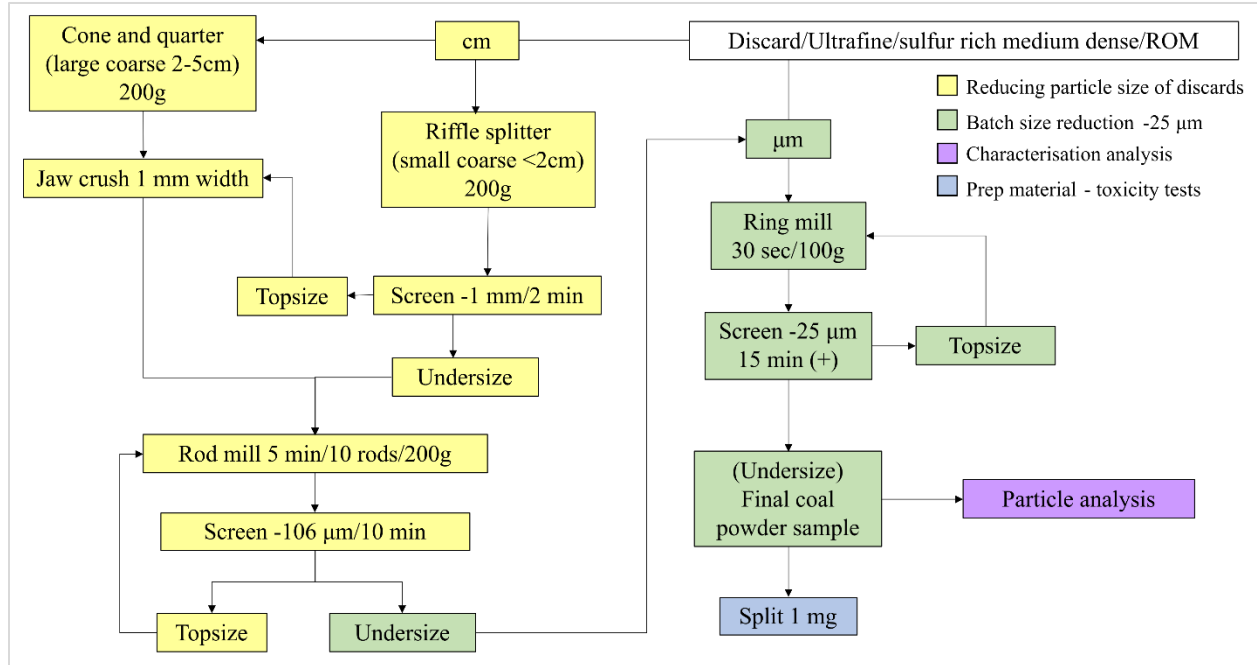
Figure 3-1 Flow diagram of the milling process for coal material both as coarse and fine samples (as received).

## 3.4. Analytical methods: description of analysis principles

In this study several analytical techniques were used to provide either complementary or individualised particle information. This integration of information was done to develop a detailed and comprehensive particle dataset which captures the physicochemical and mineralogical characteristics of coal dust relevant to toxicity. A summary of the main analytical methods used to characterise the coal samples, along with the purpose of analysis in the context of the project is listed in Table 3-2. Although each analytical technique applied machine-specific software to extract the data, the statistical language R and the R environment – version 4.0.3 (RStudio Team, 2020) – were used to visualise the resulting information. The following sections will address the analytical methods used in the study and how the generated data were utilised in developing a detailed particle characterisation dataset.

Table 3-2 Summary of analytical methods used to characterise the various physicochemical aspects of the milled coal particles and the specific purpose of each technique in the context of the project.

| Analytical method | Measurement | Reference to details |
|---|---|---|
| QXRD (Quantitative X-ray Powder Diffraction)<br><br>(Malvern Panalytical Aeris diffractometer<br>with a PiXcel detector XRD, conducted at Analytical and Consulting) | Quantitative measure of mineral distributions and their abundance | Chapter 4 |
| XRF (X-ray fluorescence)<br><br>(Malvern Panalytical Axios Wavelength Dispersive spectrometer, conducted at Central Analytical Facilities, Stellenbosch University) | Assay-based measure of chemical abundance (major element oxides) | Chapter 4, Appendix A3 |
| BET (Brunauer–Emmett–Teller)<br><br>(Micromeritics Tristar II 3020, conducted at the Analytical Laboratory, Department of Chemical Engineering, University of Cape Town) | Specific surface area | Chapter 3 |
| Malvern Panalytical Mastersizer 2000<br><br>(Conducted at the Department of Environmental and Geographical Sciences, University of Cape Town) | Projection-based measure of particle shape and size | Chapter 3 |
| QEMSCAN (Quantitative Evaluation of Minerals by Scanning Electron Microscopy)<br><br>(QEMSCAN 650F with a field emission gun-scanning electron microscope (FEG-SEM) from FEI, a high-resolution BSE (Backscattered electron) imaging, two Bruker Energy Dispersive Spectrometers (EDS) and a Spectral Analysis Engine (SAE) to analyse phases, housed in the New Engineering Building at the University of Cape Town) | 2D Physical characteristics: shape, size, roughness<br><br>Mineral specific characteristics: liberation<br><br>Mineral & chemical abundance | Chapter 4 |

### 3.4.1. Automated scanning electron microscope imaging analysis: QEMSCAN

The QEMSCAN is one of many automated scanning electron microscopy instruments. In principle, the instrument combines high-resolution backscattered electron images of microstructures with characteristic X-ray information from the sample to generate mineral maps of geological materials. From these maps various quantitative reports on the physicochemical, mineralogical, and textural characteristics of the material can be determined. For this study a FEI QEMSCAN 650F was used to understand both the general and mineral-specific characteristics of coal dust particles (further discussed in Table 3-2 and paper 1 Chapter 4). To operate the automated measurement functions of the instrument and process the results, the software packages iMeasure (for operational setting) and iDiscover (to process the scans offline) were used. For additional details on the sample preparation and instrument operation refer to paper 1 in Chapter 4. Here the protocol developed specifically for the analysis of coal dust particulates is discussed.

### 3.4.2. QXRD: Quantitative identification of crystalline material

QXRD is a technique used for the identification and quantification of crystalline phases in a sample and has been routinely used to determine the nature and quantity of mineral matter in coal (Ward, 2016). The principle of the technique involves the bombardment of a powdered sample with X-rays which then releases characteristic X-rays. To produce the diffractogram, XRD analysis follows Bragg's law. Here it states that when the X-rays are incident on the crystal surface, the angle between the incident ray and the surface will reflect back with the same angle of scattering and undergo constructive interference. This phenomenon results in a pattern with high-intensity peaks characteristic of the crystalline material being analysed. The resulting pattern is then captured and compared against reference powder diffraction patterns. As geological samples contain more than one mineral, and thus more than one spectrum, refinement algorithms are applied to best fit the reference pattern to the whole scan. For reference, the specific XRD machine used in this study is described in Table 3-2. A full description of the instrument operation methodology used to quantitatively derive the mineral abundances for each sample is given in Chapter 4 (paper 1). In this study, this technique was used to positively identify and provide a quantitative estimate of the minerals present in each coal sample. As the method can only quantify the crystalline material in the sample, the mineral matter reported had to be normalised relative to estimates of the carbonaceous content in the coal (further discussed in paper 1, Chapter 4). These mineral abundances were also used as an independent method to compare the mineral abundances measured by the QEMSCAN.

### 3.4.3. XRF: Major element chemistry

XRF is a standard analytical method used to determine the major element chemistry from materials. Similarly to QXRD, the principle of XRF involves the bombardment of the sample with X-rays and the subsequent collection of the spectra for post-identification and refinement. In this study, XRF was used to

measure the major element chemistry of the coal particles. For this, the material was further milled and prepared into glass fusion disks for homogeneous analysis. The specific machine used for this is described in Table 3-2. For additional details on the sample preparation and instrument operation refer to Appendix section A3. In the context of the work, the element distributions were used to validate the mineralogical analyses through relating the mineral chemistry to the main elements measured by the XRF analysis. The elemental distribution was also used as reliable and accurate bulk chemical information on each sample (further discussed in Chapter 4).

### 3.4.4. Malvern Mastersizer: Measurement of particle size by laser diffraction

The Malvern Mastersizer is a widely used tool for particle size analysis of spherical and non-spherical particles (described by geometric size). This tool uses the principle of laser diffraction to project a sphere that has the same area as the particle analysed. From this, the diameter of the projected sphere is used as the measurement of particle size. For this study, a Malvern Mastersizer 2000 coupled with the instrument associated software was used to conduct the analysis (see Table 3-2 for details). To perform the standard operating procedure, water was chosen as the medium to disperse the particles prior to analysis. Between runs the machine was flushed and cleaned to prevent any contamination between samples. For reference the measured distribution was reported as the volume percentage of particles measured.

In this study it is acknowledged that geometric size alone does not dictate the deposition of the particle to pulmonary cells. It is noted that an indication of size-related deposition aerodynamic diameter would be more appropriate as this measure considers the density of the particle in combination with its size. However, based on the consensus of several studies which looked at the definition of size in the context of *in vitro* experimentation, geometric size can be considered a justifiable substitute for, but not a replacement of, aerodynamic diameter (De Boer et al, 2002; Pilcer et al, 2008; Marsalek and Sassikova, 2016; Liu and Liu, 2020). Hence, the choice of reporting geometric size as opposed to aerodynamic diameter was considered justified based on the context of the project and the focus on providing a better understanding of how the particle characteristics such as particle size impact cells *in vitro*.

### 3.4.5. BET: Physisorption analysis of specific surface area

BET surface area analysis measures the specific surface area (SSA) of a powder substance. To perform this analysis a Micromeritics Tristar II 3020 machine was used to measure the amount of adsorbed nitrogen gas corresponding to a monomolecular layer on the surface of the sample (see Table 3-2 for details). To ensure that no absorbed gasses or vapours are present on the sample through handling, preparations are made by "outgassing" before the measurement. This maintains the sample at a specific pressure and temperature for a fixed duration before analysis. For this study, the outgassing conditions were set at 120°C for 12 hours.

## 3.5. Experimental assays: description of *in vitro* test principles

For this study, the ability of various coal particle samples to damage and induce stress to macrophage cells were investigated *in vitro*. All tests were conducted on monocyte THP-1 macrophage cell-line (details on their culture conditions are discussed in Chapter 5). The following subsections will discuss each assay performed, their respective test principle, and the relevance of the measured agent as an indicator of cytotoxicity or oxidative stress.

### 3.5.1. Cytotoxicity: Lactate dehydrogenase (LDH) assay

The use of assays that measure the cytoplasmic enzyme release of *Lactate dehydrogenase (LDH)* from damaged cells has been widely used as an index for cytotoxicity in coal toxicity literature (Adamis and Timar, 1978; Gormley et al, 1979; Vallyathan et al, 1988a; Vallyathan, 1994; Lee et al, 1996). The advantage of using LDH for this study was due to its stability, presence in all cells, and rapid release of the enzyme into the cell culture supernatant upon membrane damage. The assay specifically used in this study was the Roche Cytotoxicity Detection Kit (LDH) and was conducted on the THP-1 cells. The analysis of the sample was done by a spectrophotometric microplate reader (ELISA reader). This allowed for the simultaneous measurement of several samples, which proved beneficial for the number of coals which needed to be tested individually. The test principle of the assay revolves around the collection and incubation of cell-free supernatant containing LDH (proportional to the amount of dead or plasma membrane damaged cells) with tetrazolium salt. A two-stage enzymatic reaction oxidises LDH to pyruvate which then facilitates the transformation of tetrazolium salt (yellow) to formazan salt (red) with LDH as the limiting factor (explained in Figure 3-2). Since the amount of formazan depends on the LDH activity it is understood that the intensity of the colour formed is proportional to the number of cells lysed. In the context of oxidative stress, cytotoxicity represents the failure of antioxidant defences and the damage/death of cells, which may either be due to the material or by the reaction products of the material with the cell. Thus, for this project, the measure of cytotoxicity is regarded as an indication of the antioxidant performance.
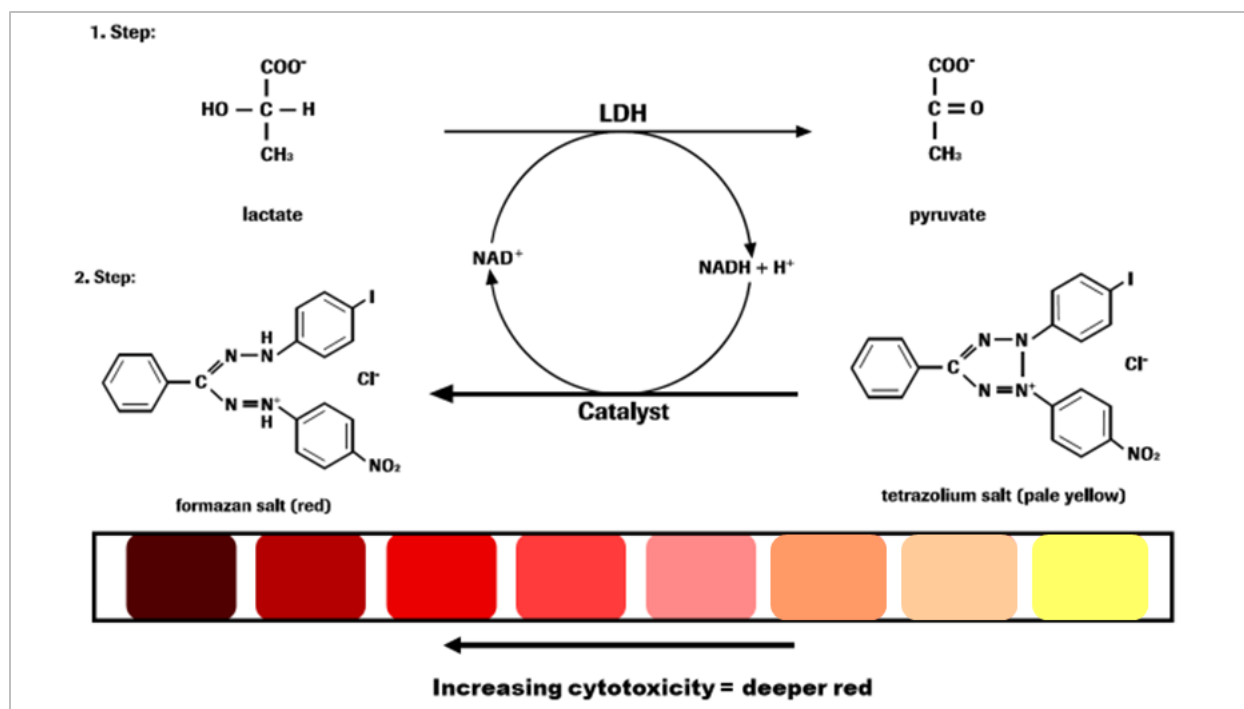
Figure 3-2 Summary of the enzymatic reactions which result in LDH activity. The first enzymatic reaction involves the release of LDH which then reduces NAD+ to NADH+H+ through the oxidation of lactate to pyruvate. The second reaction involves the transfer of 2H+ from NADH+H+ to the yellow tetrazolium salt INT (2-[4-iodophe-nyl]-3-[4-nitrophenyl]-5-phenyltetrazolium chloride) by the catalyst Diaphorase/NAD+. The plate below the reaction diagram shows the principle of the change in the intensity of red as cytotoxicity from cytosol or cell damage increases. Part of this figure is based on content from the Roche LDH assay protocol.

### 3.5.2. Lipid peroxidation: TBARS assay

Assays for lipid peroxidation are most widely used as an indication of free radical formation. The process itself involves the decomposition of phospholipids or polyunsaturated fatty acids (PUFAs) by free radicals. This is known to result in a series of defined chemical markers (aldehydes, alkanes, ketones, etc.) that are highly reactive with other cellular components and serve both as biomarkers for lipid peroxidation and onset signals for tissue damage. Of the known chemical markers, malondialdehyde (MDA) is a stable and widely assayed indicator of lipid peroxidation. In this project, a commercial assay from Sigma-Aldrich was used to measure lipid peroxidation via the MDA-TBA adduct. The principle of the assay is based on the reaction of MDA with thiobarbituric acid (TBA) to produce a colourimetric product, where MDA is the limiting factor. The absorbance of the colourimetric product is then measured using a spectrophotometric microplate reader and is regarded as an indication of the free radical formation. In the context of this project, the measurement of free radical formation is taken as a proxy indicator of the potential oxidative damage of each coal type tested on the THP-1 cells.

## 3.6. Experimental controls and sources of variability

This section aims to provide a rationale for the decisions taken concerning sample preparation and the immunological tests described in section 3.5.

### 3.6.1. Potential sample losses

During the processes of crushing, screening, and, splitting, sample losses were noted. Table 3-3 represents a summary of the loss scenarios for each preparation step and the mitigation strategy employed. To ensure consistency of the sample for analysis and experimental testing, batches of coal dust were prepared to accommodate the sample mass requirements of both the analytical and *in vitro* tests.

Table 3-3 Description of the potential sources of sample losses in sample preparation and the mitigation strategies employed.

| Sample preparation step | | Potential sample losses | | | Minimisation strategy |
|---|---|---|---|---|---|
| | | Airborne fines | Dust trapped in cleaning brush | Fines remaining on the surface | |
| Crushing | Jaw crusher | X | | X | Reduction of drop height when decanting milled material. |
| | Rod mill | X | X | X | |
| | Ring mill | X | X | X | |
| Screening | Shaker | | X | X | Tapping of the screen to remove dust trapped within the screen. |
| Splitting | Large rotary splitter | X | X | X | Reduced drop height of the sample to the machine and the rate at which the sample enters the machine. |
| | Benchtop rotary splitter | X | X | X | Cone and quarter smaller fractions on glossy paper to reduce the entrainment of fine on surfaces. |

### 3.6.2. Sources of contamination

As an additional source of variability, contamination of the sample by other ore bodies in the laboratory environment was minimised by ensuring that all equipment and surfaces were clean. A routine of vacuuming the workspace and equipment was carried out to remove residual dust. In addition to this, work surfaces and equipment were wiped with acetone to remove any residual material between the preparation of different samples.

For the immunological tests, bacterial contamination on the surface of the coal particles was eliminated by exposing the coal stock solutions to ultraviolet light for two cycles in the laminar flow tissue culture hood (which amounted to 1 hour).

### 3.6.3. The non-representative coal dose *in vitro* tests

Given that the sample used in the *in vitro* tests is of such a minute mass (stock sample 1mg coal/mL cell media) technical replicates were conducted within each experiment to test for the variability within the sample. Following the work from Gormley et al (1979) which highlighted the extreme difficulty of obtaining a truly representative coal dust sample, consistency among replicates from a given stock solution were favoured.

### 3.6.4. Controls for immunological tests

The intra-assay variation for each assay tested was accounted for by the use of controls. This section will describe the specific controls used and their role in assessing the performance of the assay. For the LDH assay, a commercial reference material (Min-U-Sil 5, obtained from U.S.Silica) was tested with each plate to provide a standard for which the performance of the assay can be compared. The Min-U-Sil was chosen for its well-established dose-dependent and highly cytotoxic nature. In addition, a positive and negative control was included in the plate to assess the health of the cells in relation to the exposure treatments (cells treated with Triton X and cells in media as the negative and positive control respectively). All the experiments for this assay were carried out in triplicate to assess the intra-assay variability and potential variation within the heterogeneous sample.

For the lipid peroxidation, this measurement was quantified using a standard curve. As a result, a series of controls were measured within each plate. In addition to this, a separate control sample of known concentration was used to assess the performance of the assay. All experiments for the lipid peroxidation and cytotoxicity assays were run in duplicate, due to the number of samples and limitations on the amount of reagents material within the kits. However, a t-test statistic was employed to assess the significance of the measured value relative to the low control (unexposed cells).

## 3.7. Statistical analysis

In assessing the relevance of coal dust particle characteristics to toxicological/immunological responses, Chapter 2 cited several studies which have attempted to relate the physicochemical and mineralogical components of coal dust to adverse cellular responses. However, the relationships defining the pneumoconiotic potency of coal dust have been limited to either linear or multiple linear regressions. With these regression types, the relationship analysis is restricted to few variables per model, even so the performance of the models is greatly hampered by collinear variables. To overcome these limitations, two kinds of latent variable models can be applied, namely, the principal component regression and the partial least squares regression. These models focus on dimensionality reduction before applying a linear model to the data which allows for the computation of large sets of explanatory variables whilst removing collinearity. The key differences between the two models are that the principal component regression

focuses on variance while performing dimensionality reduction, whereas the partial least squares regression prioritises covariance while reducing dimensionality. Additionally, the partial least squares regression defines components for the explanatory variables that are related to the components of the responses, whereas the principal component regression creates components for the explanatory variables without consideration of the response.

Considering this, the partial least squares regression was chosen as the main method for the statistical analysis of the data generated from the various experimental and analytical means. It should be highlighted that the application of such a model has not yet been presented in this field of study but presents a promising method of analysis for understanding the pneumoconiotic potency of coal dust demonstrated by this study. The subsequent sections will (1) outline the modelling approach used in the study, (2) specify and define the algorithm used, (3) describe the tools used to assess variation and uncertainty in the model, (4) provide a brief introduction to the Biplot (a graphical representation of the relationships), and (5) briefly outline the variable ranking and scoring methodologies applied on the regression products.

## 3.7.1. Modelling approach: Partial Least Squares Regression (SIMPLS)

The partial least squares (PLS) model is a broad class of methods for modelling relations between sets of observed quantities through the projection of latent structures. Generally, it can be stated that PLS models can also define new components by maximising the covariance between two blocks of data (explanatory-X and response-Y variables). Based on this, the PLS builds a latent space where measured data is reprojected as linear combinations of weighted latent variables.

PLS models are regarded as multivariate models which can capture the maximum variance and correlation between explanatory and response variables while removing collinearity. This differentiates them from multiple linear, multivariant, and principal components regressions. PLS models also can perform in cases where the number of individuals is much lower than the set of variables observed. Furthermore, the model has few requirements as the data do not need to come from normal or known distributions (residuals are assumed to be independent and identically distributed random normal variables). From this point on the content will revolve around describing the most common PLS model, known as the Partial least squares regression (PLSR). More specifically, focus will be given to the SIMPLS algorithm outlined in Mevik and Wehrens, (2007) derived from De Jong, (1993).

Before the initialisation of the SIMPLS algorithm, the equation for the multiple linear regression (MLR) or multivariant regression is outlined (Eq. 3-1.) as this represents the objective format for the PLSR model. Having said this, the key differentiating feature for PLSR is based on the least squares solution for the regression coefficient (B). For the MLR regression coefficient (Eq. 3-2.), the X term is required to have more samples than variables and be independent. The PLSR model circumvents this by decomposing X

into matrices of orthogonal scores/latent variables T and loadings P (components) and regressing Y on the components of the T scores.

$$Y = XB + \varepsilon \qquad \text{Eq. 3-1.}$$

Where X and Y are sets defined as $X = \{x_i\}_{i=1}^{n} \in R^p$ and $Y = \{y_i\}_{i=1}^{n} \in R^q$. B is a p-dimensional column vector $(B_1, \dots B_p)^T$, and $\varepsilon$ is a $(nxm)$ matrix of random errors.

$$B = (X^TX)^{-1}X^TY \qquad \text{Eq. 3-2.}$$

To compute all PLS models the standardised matrices of X and Y are decomposed by the following formulas (mean = 1, standard deviation = 0):

$$X = TP^T + E \qquad \text{Eq. 3-3.}$$

$$Y = UQ^T + F \qquad \text{Eq. 3-4.}$$

Where T and U are the latent components (scores) that explain the variance in X and Y reactively, P and Q are the orthogonal loading matrices for X and Y respectively, and E and F are error terms for X and Y respectively (assumed to be random, independent, and identically distributed).

Specifically, concerning the SIMPLS algorithm, initialisation begins with the singular value decomposition (SVD) of the crossproduct matrix $S = X^TY$, thereby including information from both X and Y and the correlation between them. To obtain the variable needed to solve this the following steps are applied:

**Step 1**: The left and right singular vectors $w$ and $q$ (product of SVD decomposition of $S = X^TY$ Eq. 3-7.) are used as the weight vectors for X and Y respectively to calculate the $t$ and $u$ scores (Eq. 3-5. & 6.):

$$t = Xw \qquad \text{Eq. 3-5.}$$

$$u = Yc \qquad \text{Eq. 3-6.}$$

From this, the X scores $t$ are often normalised. The Y scores $u$ are not necessary for the regression but are kept for interpretation purposes.

Once all the terms have been defined the goal of the algorithm is to maximise the covariance between the $t$ and $u$ scores (relationships based on the projection of latent structures):

$$cov(t,u) = cov(Xw, Yc) = t^Tu = (Xw)^TYc = w^TX^TYc \rightarrow \max cov \qquad \text{Eq. 3-7.}$$

**Step 2**: Next the X and Y loadings are obtained by regressing the $t$ scores against the orthogonal vectors of X and Y (Eq. 3-8. & 9.):

$$p = X^Tt \qquad \text{Eq. 3-8.}$$

$$q = Y^Tt \qquad \text{Eq. 3-9.}$$

**Step 3**: Finally, the data matrices are 'deflated' – the information related to the latent variables in the form of products $tp^T$ and $tq^T$ are subtracted from the current data matrices for X and Y respectively (Eq. 3-10 & 11.):

$$X_{n+1} = X_n - tp^T \qquad \text{Eq. 3-10.}$$

$$Y_{n+1} = Y_n - tq^T \qquad \text{Eq. 3-11.}$$

The estimation of the next component can start from the SVD crossproduct matrix $S = X^T_{n+1}Y_{n+1}$. After each iteration, the terms $w$, $t$ , $p$ and $q$ are saved in the columns W, T, P and Q respectively. To compare the columns of the matrix W – the successive deflation of the X and Y matrices do not have comparable weights – the weights have been recalculated in such a way that they relate to the original X matrix (Eq. 3-12.):

$$R = W(P^T W)^{-1} \qquad \text{Eq. 3-12.}$$

Revisiting the objective format of the PLSR equation (Eq. 3-1. & 2.), instead of regressing Y on X, the T scores are used to calculate the regression coefficients (Eq. 3-13.). At a later stage these are converted back to the realm of the original variable by multiplying with the matrix R (through the relationship $T = XR$):

$$B = R(T^T T)^{-1} T^T Y = RT^T Y = RQ^T \qquad \text{Eq. 3-13.}$$

It should be noted that only the first $a$ components are used, otherwise, the number of components that are optimal for the model must be determined through cross-validation.

In the final computation of the regression, the PLSR defines the relationship between X and Y as $Y = BX$, where the linear combinations of the latent variables and associated loadings are used as the modelled data.

### 3.7.2. Assessment of variation in model

Within this section the variation in the model will be discussed around the (1) preparation of data before computation, (2) optimisation of the number of components, and (3) the assessment of the model fit the measured data. Prior to initialising the model, both X and Y data are standardised/centred to ensure that the mean and standard deviation are 0 and 1 respectively. This step removes numeric bias from the different units of the variables, allowing them to be compared. In defining the model elements used to fit the data, the number of components and validation type needs to be chosen. Upon initialisation, the model is allowed to define as many components needed to maximally explain the variance in both X and Y and compute the validation as cross-validated predictions per component. Following this, the number of components chosen for the model is optimised using the following selection criteria:

1. The percentage variance explained X and Y per component
2. An assessment of the model error with increasing components, the components with the least error are "optimal" (derived from the cross-validated predictions-RMSEP)
3. An assessment of Pearson correlation coefficient ($R^2$) of the measured versus predicted values with increasing components, the components with an $R^2$ value closest to 1 are "optimal"

The fit of the model was assessed in three parts by determining the parity of the measured and fitted values. This was further coupled with the evaluation of the residuals (error components) by plotting the distribution of the errors (errors are assumed to be normally distributed) and the fitted versus measured values (assumed to be randomly distributed). A summary of the model uncertainty is also given reporting the root mean square error (RMSE), mean absolute error (MAE) and the $R^2$ of the final model.

### 3.7.3. Relationship analysis of multivariant data

Through modelling the latent variables of the X and Y data, one can build an understanding of the hypothetical actors involved in complex systems. Furthermore, information from these variables allows the investigator the ability to gain insights into the magnitude and effects such actors have on the system. This section will briefly outline and describe the data visualisation tools used to interpret the latent variables derived from the PLSR. This step is taken to provide clarity on the meaning of each plot and their contribution to describing the relationship between the samples and the variables as well as between the variables themselves.

### 3.7.3.1. Cluster analysis and outlier determination: Scores plot

Referring to the scores calculated in Eq. 3-5. and 6, the score value geometrically represents the distance from the origin along the direction of the first component ($a$) up to where the observation projects, up to the direction vector (the loadings defined by Eq. 3-8 and 9). For a single observation of the $a^{th}$ component the X scores can be represented as:

$$t_{i,a} = x_{i,1}P_{1,a} + x_{i,2}P_{2,a} + \ldots\ldots + (x_{i,k}P_{k,a}) = K \ terms \qquad \text{Eq. 3-14.}$$

While this represents the weighting of the X variables relative to the loadings, the magnitude of $t_{i,a}$ will not equal that of the $t$scores calculated in Eq. 3-5, as they are calculated differently. Thus, the K terms computed for $t_{i,a}$ represent the deviation of each X variable (per sample) from the mean. The $u$ scores are not often included as they are not always available, but since this study does not extend to prediction the $u$ scores have been computed. The scores of the first and second components are computed and plotted against one another (for X and Y respectively) in what is called a score plot. Here, clusters of variables can be observed, highlighting groups hypothesised to have similar behaviour. Additionally, outliers can be detected using the K terms defined in Eq. 3-14. As both X and Y data have been standardised and scaled, the variables which report at mean levels will have a value roughly equal to zero (outliers will have values higher than zero). The representation of the K terms for each component (relative to the mean) is referred to as the contribution plot.

3.7.3.2. Relative contribution of variables to XY components: Loadings plot

As referred to in the subsection above, the direction vector is defined by the loadings of the model and thus the loadings plot displays the direction vectors of both X and Y. In doing so the contribution of each variable can be assessed per component in the model (variables which have little contribution to a direction will have a weight close to zero). Variables that are correlated can also be identified from this plot, as strongly correlated variables will have approximately the same weight (when positively correlated) and will appear close together, whereas negatively correlated variables will plot diagonally opposite one another. It should, however, be noted that while the sign of the vector may be useful when comparing vectors, the vector can be rotated 180° and still have the same interpretation. A separate issue that can occur in the context of this plot is that highly correlated variables can have equivalent weights (signifying that the variables are individually important but contribute uniformly to the model). Finally, one can distinguish "unimportant variables" to the model by determining which variables have the smallest weights (the least contribution) across all the components.

3.7.3.3. Exploratory analysis of variable relationships: Biplot

The ability of the PLSR model to compute the scores and loadings for both the X and Y variables allows for the superimposition of this data for exploratory analysis of the relationships between groups of variables and the responses of interest. Before this can be done the scores and loadings need to be scaled to be on the same plane. The Biplot allows for this to happen by simultaneously plotting information on the observations and variables from a multidimensional dataset onto a 2-dimensional space.

3.7.3.4. Variable correlation: Coefficient plot

In terms of correlation, the coefficient plot is used to learn how the X-variables are related to the Y across all components. The regression format $Y = XB$ is used in this case, where $B$ is a standardised $K \times M$ matrix containing columns of the regression coefficient for all $K$ terms of the X variable and their relation to each $M$ terms of the Y variables. From this plot, the relative significance of the X variables to Y variables is derived and compared for all components (since they have been standardised). With regards to interpretation, the absolute value of the coefficient indicates its significance, where a higher $B$ value represents a greater strength in relative significance to the model.

## 3.8. References

Adamis, Z. and Timar, M. (1978) 'Studies on the effect of quartz, bentonite and coal dust mixtures on macrophages in vitro', *British Journal of Experimental Pathology*, 59, pp. 411–415.

De Boer, A. H., Gjaltema, D., Hagedoorn, P. and Frijlink, H. W. (2002) 'Characterization of inhalation aerosols: A critical evaluation of cascade impactor analysis and laser diffraction technique', *International Journal of*

*Pharmaceutics*, 249(1–2), pp. 219–231. doi: 10.1016/S0378-5173(02)00526-4.

Cannon, G. J. and Swanson, J. A. (1992) 'The macrophage capacity of phagocytosis', *Journal of Cell Science*, 101, pp. 907–913. doi: 10.4135/9781452218991.n13.

Dalal, N., Suryan, M., Vallyathan, V., Green, F., Jafari, B. and Wheeler, R. (1989) 'Detection of Reactive Free Radicals In Fresh Coal Mine Dust and Their Implication for Pulmonary Injury', *The Annals of Occupational Hygiene*, 33(1), pp. 79–84. doi: 10.1093/annhyg/33.1.79.

Gormley, I. P., Collings, P., Davis, J. M. G. and Ottery, J. (1979) 'An Investigation into the Cytotoxicity of Respirable Dusts from British Collieries', *British Journal of Experimental Pathology*, 60, pp. 526–536.

De Jong, S. (1993) 'SIMPLS: an alternative approach squares regression to partial least', *Chemometrics and Intelligent Labratory Systems*, 18, pp. 251–263.

Kaya, E., Hogg, R. and Mutmansky, J. M. (1996) 'Evaluation of procedures for production of dust samples for biomedical research', *Applied Occupational and Environmental Hygiene*, 11(7), pp. 745–750. doi: 10.1080/1047322X.1996.10389964.

Lee, C. Y., Lee, S. L., Sheehan, C. E. and Wang, Y. (1996) *Composition of coal dusts and their cytotoxicity on alveolar macrophages*. Technical report ARCCB-TR-96026. Available at: https://pdfs.semanticscholar.org/8185/85459224e1ac9db8dce8b006c415033ec7d9.pdf.

León-Mejía, G., Silva, L. F. O., Civeira, M. S., Oliveira, M. L. S., Machado, M., Villela, I. V., Hartmann, A., Premoli, S., Corrêa, D. S., et al (2016) 'Cytotoxicity and genotoxicity induced by coal and coal fly ash particles samples in V79 cells', *Environmental Science and Pollution Research*, 23(23), pp. 24019–24031. doi: 10.1007/s11356-016-7623-z.

Liu, T. and Liu, S. (2020) 'The impacts of coal dust on miners' health: A review', *Environmental Research*. Elsevier Inc., 190(June), p. 109849. doi: 10.1016/j.envres.2020.109849.

Marsalek, R. and Sassikova, M. (2016) 'Characterization of the size distribution of subbituminous coal by laser diffraction', *Instrumentation Science and Technology*, 44(3), pp. 233–240. doi: 10.1080/10739149.2015.1113429.

Mevik, B.-H. and Wehrens, R. (2007) 'The pls Package: Principal Component and Partial Least Squares Regression in R', *Journal of Statistical Software*, 18(2), pp. 1–24.

Pilcer, G., Vanderbist, F. and Amighi, K. (2008) 'Correlations between cascade impactor analysis and laser diffraction techniques for the determination of the particle size of aerosolised powder formulations', *International Journal of Pharmaceutics*, 358, pp. 75–81. doi: 10.1016/j.ijpharm.2008.02.014.

Vallyathan, V. (1994) 'Generation of Oxygen Radicals by Minerals and Its Correlation to Cytotoxicity', *Environmental Health Perspectives*, 102, pp. 111–115.

Vallyathan, V., Schwegler, D., Reasor, M., Stettler, L., Clere, J. and Green, F. H. Y. (1988) 'Comparative in vitro cytotoxicity and relative pathogenicity of mineral dusts', *Annals of Occupational Hygiene*, 32(inhaled_particles_VI), pp. 279–289. doi: 10.1093/annhyg/32.inhaled_particles_VI.279.

Ward, C. R. (2016) 'Analysis, origin and significance of mineral matter in coal: An updated review', *International Journal of Coal Geology*. Elsevier, 165, pp. 1–27. doi: 10.1016/j.coal.2016.07.014.

# Chapter 4

## CHARACTERISATION OF COAL DUST
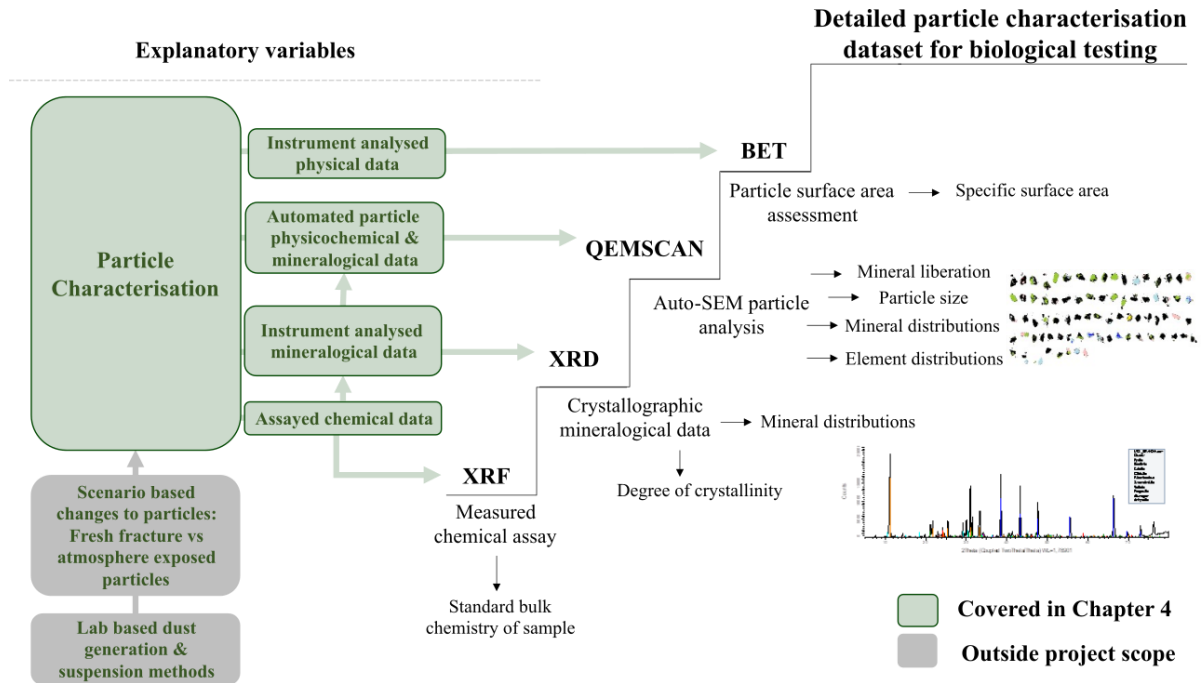


This graphic describes the breakdown of the different analytical tools used to develop the detailed particle characterisation precursor dataset for biological testing.

## 4.1. Overview

The work represented in this chapter is a product of the following overarching objective and associated key questions:

**Overarching objective 1:**
To develop a detailed and quantitative particle characterisation dataset for coal dust in preparation for biological testing, using a combination of QEMSCAN (quantitative evaluation of minerals by scanning electron microscopy), XRD (X-ray Powder Diffraction) and XRF (X-ray fluorescence) and complementary physical analysis methods for the analysis of physical, compositional, mineral specific characteristics.

Key question 1: Considering that the QEMSCAN is conceived to be the main tool, how should the coal sample be prepared before analysis and what operational requirements need to be made to successfully analyse the coal particles?

Key question 2: How will the characteristics of the coal particles be quantified and furthermore, how can supporting techniques be used to build confidence in the accuracy of the dataset?

Key question 3: Do the characteristics defined by the various techniques allow for trends to be identified in the nature of the particles generated, considering that they have been mechanically broken down and can different source characteristics be identified between samples?

For this study the QEMSCAN is used as the main particle analysis tool which provides detailed mineralogical, textural, and physical data on the coal particles. As a result, a significant proportion of the chapter discusses the development of an auto-SEM protocol specifically for the analysis of the coal particle samples utilised in this study. Technical paper 1 details the developmental decisions taken to measure and analyse coal particles on auto-SEM-EDS systems using the QEMSCAN as the application. The paper further highlights (1) the sample preparation requirements particular to coal analysis with such a method, (2) the operational optimisation required by the system to successfully run the measurement, and (3) the use of complementary mineralogical and chemical datasets to validate the mineral mapping of the particles, which all directly relate to the first two study objectives.

To address the third question which is outside the scope of paper 1, a separate chapter section has been included. In this section the variation in physiochemical and mineralogical characteristics obtained from the complete dataset are analysed. Insights obtained from this analysis highlight the different levels of information obtainable from a detailed particle characterisation dataset and further demonstrate the main features of the coal particles which could explain the variation in the sample set.

Post preparation of paper 1 for submission to *Frontiers in Earth Science* an article titled "QEMSCAN automated mineralogical analysis of PM2.5 and PM4: A preliminary study of underground coal mine dust from Poland and Slovenia" by Johnson et al 2022 was published. For this reason, the article is not referenced in paper 1, however, it is acknowledged that this paper displays elements of an analysis routine for coal dust particles using QEMSCAN. While there may be similarities, both studies provide complementary information on how to successfully analyse coal dust particles using auto-SEM techniques. Paper 1 is set apart from this paper in the sense that it discusses and reports a wider array of parameters which can be quantified. Additionally, the protocol in paper 1 demonstrates the integration of complementary datasets (XRD and XRF data) to validate the results. Lastly the protocol serves as a blueprint for the broader application of the analysis strategy to be used by other auto-SEM systems.

Technical paper 1: Development of a SEM-EDS-XRD Protocol for the Physicochemical and Automated Mineralogical Characterisation of Coal Dust Particles

## Abstract

Exposure to coal dust from mining-related activities has historically been linked to several preventable but incurable respiratory diseases. Although the findings of numerous biological studies have determined that the physicochemical and mineralogical aspects of dust particles greatly influence both cytotoxic and proinflammatory pathways, robust datasets which quantitatively define these characteristics of coal dust remain limited. This study aims to develop a robust characterisation routine applicable for real-world coal dust, using an auto-SEM-EDS system. In doing so, the study addresses both the validation of the particle mineralogical scans and the quantification of a range of coal particle characteristics relevant to respiratory harm. The findings presented demonstrate the application of auto-SEM-EDS-XRD systems to analyse and report on the physicochemical and mineralogical characteristics of thousands of dust-sized particles. Furthermore, by mineralogically mapping the particles, parameters such as liberation, mineral association and elemental distribution can be computed to understand the relationships between elements and minerals in the particles, which have yet to be quantified by other studies.

## 4.2. Introduction

The exposure to coal dust has been well recognised as a critical health issue for both mine workers and communities proximal to collieries. Through epidemiological research, links have been established between coal dust exposure and various preventable but incurable diseases. These include coal workers' pneumoconiosis, chronic obstructive pulmonary disease, and emphysema (Hurley et al, 1982; Heppleston, 1992; Petsonk et al, 2013; Cohen, 2016; Leonard et al, 2020).

Previous studies have shown that particle-cell reactions and their products play a vital role in the pathway of disease development (Vallyathan et al, 1988b, 1998; Castranova and Vallyathan, 2000; Harrington et al, 2013, 2015). In particular, the biologically reactive mineralogy present in coal particle composites has been established as a trigger for inflammatory reactions (Zhang et al, 2002; Cohn et al, 2006a; Schoonen et al, 2010; Harrington et al, 2012). Thus, it is generally understood that a detailed physicochemical and mineralogical characterisation of the dust is needed to effectively understand the inter-

relationships between the inherent properties of the particles and their impact on lung physiology. However, datasets quantitatively describing coal dust characteristics remain limited in the range of characteristics considered. This has contributed to the lack of consensus regarding the toxic agents leading to coal dust related diseases (Gormley et al, 1979; Reisner et al, 1982; Le Bouffant et al, 1988; Zosky et al, 2021; Sun et al, 2022).

The ability to assess the individual particle characteristics of coal dust has been explored by studies using SEM-EDS (scanning electron microscopy coupled with energy dispersive X-ray spectroscopy) analysis to manually assess the particle size, shape, and composition of particle populations (Huertas et al, 2012b; Ram et al, 2012; Liu and Liu, 2020; Trechera et al, 2020). However, obtaining high particle counts for statistical analysis using such methods can be time consuming. Other studies have used a semi-automated Computer Controlled-SEM-EDS routine (Sellaro et al, 2015; Bharti et al, 2017; Johann-Essex et al, 2017b) for the selection of particles and extraction of raw data on physicochemical particle characteristics. This routine reports on the physical characteristics of the particles, but the mineralogy only considers phase abundances without describing their texture. There are also studies which use automated mineralogical analysis systems that identify and classify particles scanned across a predefined area using commercial software packages (Petruk and Skinner, 1997; Petruk, 2000; French et al, 2008; French and Ward, 2009; Elmes et al, 2020; LaBranche et al, 2021, 2022). The software developed for auto-SEM-EDS systems provides additional functionality to mineralogically map particles and quantitatively assess textural aspects of particles (French et al, 2008; Pirrie and Rollinson, 2011; Schulz et al, 2020). The FEI QEMSCAN (Quantitative Evaluation of Minerals by Scanning Electron Microscopy) has been used to mineralogically map particles (Williamson et al, 2013; Little et al, 2015; Elmes et al, 2020; Schulz et al, 2020; Vickery and Eckardt, 2021). However, the application has mainly been in the context of natural dust, mineral processing, and the geo- and material sciences. Recent studies have utilised the FEI Mineral Liberation Analyser to assess physical and mineralogical characteristics of coal dust (LaBranche et al, 2021, 2022). However, to date the application of such systems has focused on extracting particle size and composition-related information.

These studies highlight the potential for automated mineralogical systems to serve as a robust tool for providing quantitative reporting of mineral specific characteristics of coal dust. As particle reactivity has been linked to pulmonary responses, this should provide additional dimensions for assessing the bio-reactivity of problematic minerals. Currently, no study has presented a description of a rigorous and generalisable characterisation routine using an auto-SEM-EDS system to analyse coal dust or dust-sized particles. This is despite its potential to provide both rapid analyses of thousands of particles and detailed particle characterisation datasets. In this study, an auto-SEM-EDS workflow was conceptualised for coal

dust particles utilising an FEI QEMSCAN instrument. In this context, this study aims to develop and demonstrate: (1) quantitative definitions for a range of coal particle characteristics relevant to respiratory harm for application to real-world coal dust; (2) an auto-SEM-EDS protocol to analyse dust-sized coal particles as a case study; and (3) a demonstration of the application and rigorous validation of the characterisation data reported.

## 4.3. Protocol Description and Setup

### 4.3.1. Approach

As all auto-SEM-EDS systems operate through a combination of a hardware and software platforms, to perform image analysis and data processing the development of a workflow for a given material should consider: (1) what information is to be extracted from the measurement? (2) which settings/choices need to be defined to reliably obtain this information? and (3) how confidence in the reported data can be increased? In this context, a generalised workflow is presented to highlight the key steps taken to perform a successful particle analysis measurement across auto-SEM-EDS systems (see Figure 4-1).

Based on this workflow, the two primary considerations to inform aspects of the measurement setup are the bulk material and objective particle properties. This is particularly relevant for the sample mounting, measurements settings and mineral identification. To perform mineral identification of the sample, auto-SEM-EDS systems employ a user-defined reference list of mineral compositions. This needs to be developed based on the material, and further requires the use of complementary analyses to provide a positive identification for the major phases present.

In addition to the primary analysis of the sample, the complementary analyses provide an objective set of information with which to optimise the mineral identification list and assess the performance of the measurement.

Ultimately the study provides a demonstration of the discussed workflow utilising the FEI QEMSCAN as the auto-SEM-EDS system. However, such a workflow can also be applied to similar tools such as the FEI Mineral Liberation Analyser, TESCAN TIMA-X mineral analyser or the ZEISS Mineralogic, thus highlighting its broader applicability across different instruments.
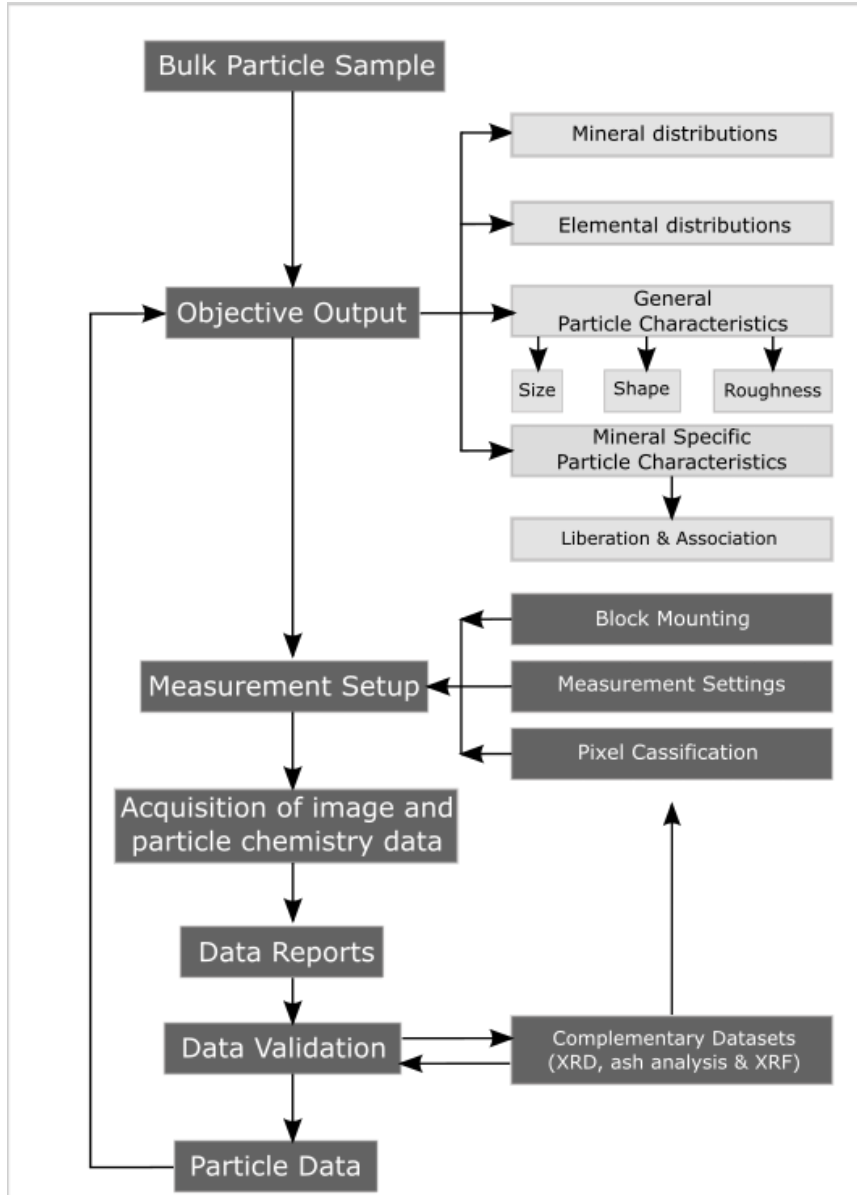
Figure 4-1 Generalised workflow describing the key elements required for the analysis of the physicochemical and mineralogical characterisation of dust-sized particles using auto-SEM-EDS systems.

## 4.3.2. Outline of Particle Characteristics Investigated

To address the objective output of the workflow, a description of the key particle characteristics relevant to particle toxicity and inflammation in the lung was first outlined (see Table 1). Based on this, sets of rules were then defined to extract mineral grades, element distributions and both general and mineral specific data from the particle scans. To provide a quantitative definition for each characteristic, the equations are further described for the various characteristics as listed in Table 4-1.

Table 4-1 List of the particle characteristics considered in the study and their relevance to various biological factors related to toxicity and inflammation in the lung.

| Characteristics Investigated | Relevance To Respiratory Toxicity and Inflammation | References |
|---|---|---|
| Mineral and element distributions | Minerals serve as hosts for reactive elements as well as providing surface reactive sites potentially producing harmful bio-reactive compounds. Elements can also be leached into the lung fluids where they can biogeochemically react depending on their form | (Zhang et al, 2002; Schoonen et al, 2006; Harrington et al, 2012) |
| General particle characteristics | | |
| Particle size | Determines the probability of where the particle may be deposited and potentially phagocytosed (digestion of foreign material by defence cells called macrophages) | (Bair, 2000; Maynard and Kuempel, 2005) |
| Particle roughness and shape | Surface texture and particle shape have been found to impact phagocytosis irrespective of the size and volume of the particles | (Fubini and Otero Areán, 1999; Plumlee et al, 2006) |
| Mineral specific characteristics | | |
| Liberation and association | Phases which are encapsulated and/or associated with non-reactive phases will be rendered inert, thus the degree to which a phase is liberated will impact its potential bio-reactivity | (Ruby et al, 1999; Plumlee and Ziegler, 2003) |

4.3.2.1. Mineral and Element Distributions

To quantify the mineral compositions and element distributions of scanned particles, the QEMSCAN and similar software-based auto-SEM-EDS initially isolate particles from the background by utilising differences in the BSE (backscattered electron) brightness. Following this, each particle is overlayed on a predetermined grid defining the pixel size and the point spacing where X-ray analysis is conducted. Utilising the collected spectra, each pixel is assigned a mineral/phase identity based on predetermined criteria, for the QEMSCAN this is defined as a Species Identification Profile (SIP) list.

To determine both the abundance of the minerals/phases present and elemental distribution, the user must provide specific detail on the basic characteristics of each mineral/phase such as the density and chemical composition (see Appendix A).

These characteristics are computed in a "primary list" which consolidates multiple SIP entries into mineral or chemical groupings to which the composition and specific gravity of each mineral/phase can be

assigned. Once assigned, both the mineral mass and the elemental distributions can be calculated by the software. As the primary list tends to be extensive, a user-defined "secondary list" is created to further consolidate the minerals into the most abundant phases and high-level groups constituting the bulk mineralogy.

In the case of the elemental distribution, each element listed is computed by back-calculating the element chemistry from the mineral formula defined in the primary list, relative to their respective abundances (see Appendix 4.3.2.1 for detail on the mineral compositions used). Based on this, the weight percentage of each element is computed as the sum of the percentage element of interest in each of its host minerals, multiplied by the respective mass abundance of each host mineral.

4.3.2.2. Particle Size

The reporting of particle size is highly dependent on the technique employed, however, for two-dimensional image analysis of particles the Equivalent Circular Diameter (ECD)—represented in equation 4-1—is the most widely used parameter (Li et al, 2005). To account for the resolution at which the scan is set, the area of a given particle is multiplied by the area of a single pixel. This was done to obtain a more accurate representation of the particle area, scaled by resolution.

Particle size = 2 × √((n pixels × Area of 1 pixel)/π)                    Eq. 4-1

4.3.2.3. Particle Shape

Currently, studies utilising Computer-Controlled SEM-EDS routines to define the shape of coal dust particles primarily assess this by quantifying the aspect ratio of the particle (Sellaro et al, 2015; Johann-Essex et al, 2017a, 2017b). While this may give the user an idea of how needle-like or circular a particle is, a metallurgical-based study using the QEMSCAN proposed a categorisation of particle shape using the parameters roundness and aspect ratio (Little et al, 2015) (further defined in Table 4-2). Their analysis showed that by a combination of these two parameters, the resulting data matrix could be used to define zones of particles with similar shape properties that describe more than just particle elongation (represented in Table 4-3). This study demonstrates the broader applicability of this alternative particle shape description on dust-sized particles.

Table 4-2 Description of the formula and visual depiction for both aspect ratio and roundness.

| Descriptor | Description | Formula | Visual Description |
|---|---|---|---|
| Roundness | The ratio of the surface area of an object over the area of a circle with a diameter equal to the maximum diameter of the object. Scaled to values between 0 and 1 | $\dfrac{4 \times n\ pixels}{\pi \times Long\ axis^2}$ |  High roundness / Low roundness |
| Aspect ratio (inverse) | The ratio of an object's length over width. The inverse of such can be taken to scale the values between 0 and 1 | $\dfrac{Short\ axis}{Long\ axis}$ |  High Aspect ratio / Low Aspect ratio |

Table 4-3 Shape categories as defined in Little et al (2015). Each category represents a zone in the matrix of aspect ratio and roundness values. Selected false colour images illustrate the different categories.

| Shape category | Round | Elongate and smooth | Equant | Angular | Elongate and Angular |
|---|---|---|---|---|---|
| |  | | | | |
| Aspect ratio | 0.5–1 | 0–0.5 | 0.5–1 | 0.5–1 | 0–0.5 |
| Roundness | 0.75–1 | 0.4–0.75 | 0.4–0.75 | 0–0.4 | 0–0.4 |

4.3.2.4. Particle Roughness

In addition to the matrix defining shape (based on ranges of aspect ratio and roundness), a "diagonal division" of the matrix was suggested to distinguish roughness as a textural characteristic over a range of aspect ratios (Little, 2016). This division takes the form of a straight line, representing the shape matrix as a Cartesian plane, where roundness and aspect ratio are a function of one another.

For the gradient and constants, values were chosen based on a qualitative assessment of the particle divisions. This resulted in three roughness categories namely, Jagged, Intermediate and Smooth (Equations 4-2 – 4-4, respectively).

Jagged = Roundness > 0.75 × Aspect ratio + 0                                    Eq. 4-2

Intermediate = Roundness ≤ 0.75 × Aspect ratio − 0.05                              Eq. 4-3

Smooth = Roundness > 0.75 × Aspect ratio + 0.05                                    Eq. 4-4

4.3.2.5. Mineral Liberation and Association

The liberation of potentially harmful phases from geological materials and their associations with otherwise inert or soluble phases have been discussed as influential factors relating to the bioaccessibility of potentially toxic elements from mineral assemblages (Ruby et al, 1999; Plumlee and Ziegler, 2003). While no study has defined liberation in this biological context, the concept of mineral liberation is well-established in the field of process mineralogy.

In its classical definition, liberation is defined by the percentage volume occupied by a mineral of interest (MOI) in the total volume of a particle (Barbery, 1992). For auto-SEM-EDS systems, liberation is classed by bound ranges in the percentage area of a target phase (Fandrich et al, 2007). By adapting this concept to understand the potential bioreactivity of minerals, based on their accessibility, this study developed a measure for the degree to which a target phase is either liberated or encapsulated (further defined in Table 4-4).

Table 4-4 Description of the liberation classes defined for this study.

| Liberation Classes | Percentage Area Range Of Target Phase | Example of False Colour Particles (MOI-Quartz) |
| --- | --- | --- |
| Liberated | % Area MOI ≤ 100 and% Area MOI ≥ 70 |  |
| Moderately liberated | % Area MOI < 70 and% Area MOI ≥ 40 |  |
| Mostly encapsulated | % Area MOI < 40 and% Area MOI ≥ 10 |  |
| Fully encapsulated | % Area MOI < 10 and% Area MOI ≥ 0 |  |

MOI-mineral of interest, Quartz-pink, Clays-green, Carbonaceous matter-black.

4.3.3. Instrumentation

For this study, the basic elements of the auto-SEM-EDS system used included: a QEMSCAN 650F field emission gun-scanning electron microscope (FEG-SEM); two Bruker ASX XFlash 6 series Energy Dispersive Spectrometers (EDS); and commercial image analysis and processing software packages.

As auto-SEM-EDS systems may be fitted with different SEMs, it should be noted that the use of a FEG-SEM over a tungsten filament-SEM greatly improves both the stability and reproducibility of the

delivered electron beam over several hours (Humphreys and Brough, 1999). As a result, FEG-SEMs can acquire high-resolution and better-quality BSE scans than their counterparts.

Furthermore, by coupling the SEM hardware with EDS detectors, the software developed for auto-SEM-EDS systems facilitates the communication between the SEM and EDS detector, allowing for the high-speed acquisition of X-ray spectra for element identification from silicon drift detectors (Gatti et al, 1984) (such as the Bruker ASX XFlash 6 series detector).

In combining the two sets of scan information (BSE and X-ray) as a raster matrix, auto-SEM-EDS systems are able to develop mineral maps of the scan based on the classification of the measured spectra to a reference library of synthesised X-ray spectra of minerals and their expected BSE grey level ranges.

## 4.3.4. Measurement Setup

### 4.3.4.1. Sample Mounting Methodology

To prepare the material for auto-SEM-EDS analysis, the sample must be mounted in a material that provides adequate contrast from the sample when imaged on a BSE (Backscattered electron) greyscale. Unlike more conventional ore/rock preparation methods using epoxy resin, the BSE contrast between the epoxy and the carbonaceous matter is nearly identical (Straszheim et al, 1988). Without a significant level of discrimination between the background and the carbonaceous matter, both the volume of carbonaceous matter and the definition of particle boundaries may be misidentified or inaccurate. As a result, carnauba wax has been favoured in the preparation of coal for SEM analysis, due to its low BSE contrast relative to carbonaceous matter (Straszheim et al, 1988; French et al, 2008) (see Figure 4-2 for an example image of blocks).
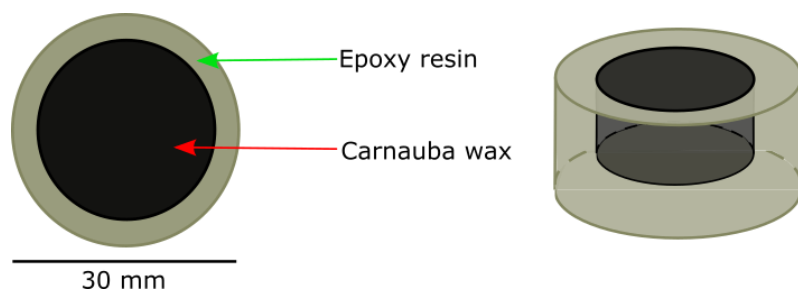


Figure 4-2 Annotated example of prepared sample blocks containing 25 mm diameter carnauba wax remounted in 30 mm diameter resin.

In addition to the specific use of wax over epoxy for the mounting coal samples, the incorporation of graphite particles as a 'filler' to separate touching particles cannot be used for coal as this would affect the estimation of carbonaceous matter. Thus, the sample preparation is aimed at producing a monolayer of the material.

For this study, 0.2 g of the coal particle samples were cast in 25 mm diameter carnauba wax moulds that were subsequently recast in epoxy resin to generate 30 mm diameter blocks (recasting in epoxy was used to provide stability to the sample block). The blocks were subsequently polished to reveal the surface of the block and smoothen the surface to a flat and level finish (see Appendix A1 for a full description of the wax block preparation procedure).

4.3.4.2. SEM Measurement Conditions

In execution of the measurement, the QEMSCAN was set to run at a beam energy of 15 keV, accelerating current of 9 nA, working distance of 13 mm and 1000 times magnification across all the samples. Prior to analysis, the BSE detector was calibrated on the quartz, copper, and gold standards. Additionally, the brightness and contrast of the scan was calibrated against the gold standard and faraday cup. Both calibration steps were conducted to ensure confidence in the BSE measurement. A further X-ray calibration was conducted on the copper standard to ensure confidence in the X-ray spectra captured by the EDS detector.

Apart from the operational setup for the SEM, the software requires the user to define the scanning and field parameters. For this study, the field of view was divided into areas sized at 500 µm with a 200 µm overlap (see Figure 4-3a, b for visual context). With respect to the scan, a resolution of $0.98 \times 0.98$ µm pixels with a point spacing of 1 µm was chosen to aid in the identification of features in the particles, given that they ranged between 25 and ~2 µm (see Figure 4-3c for visual context of the point spacing).



|       (a)       |       (b)       |       (c)       |
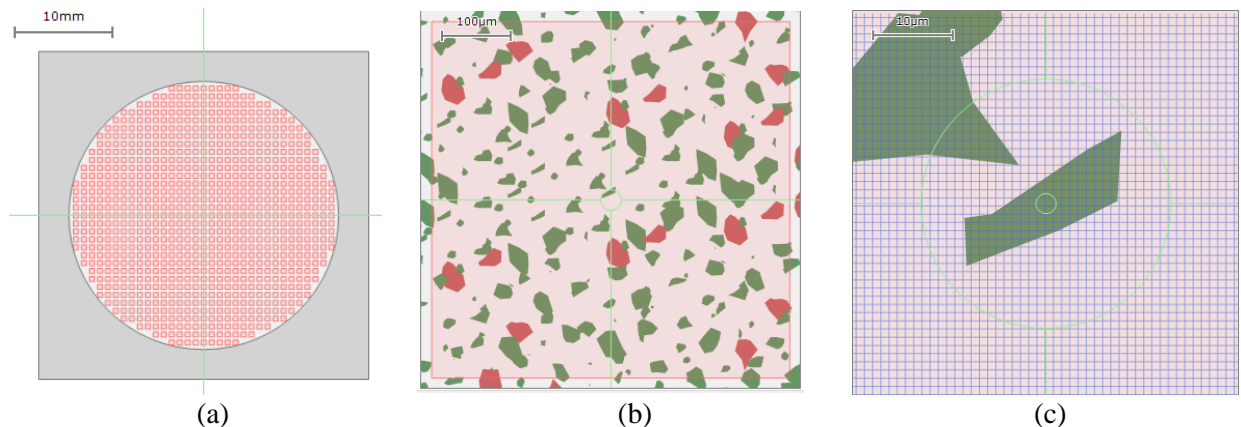
Figure 4-3 Visualisation of the simulated field and scan settings. (a) represents a view of the simulated block and the fields defined across the block, (b) displays a scaled image of the field sizes relative to a simulation of the expected particle sizes within a field, and (c) shows a representation of the point spacing across a given particle where each grid block shows a point where the X-ray spectra will be analysed.

To ensure that the scan could effectively select particles, both size exclusion criteria and a "separate touching particles" processor were included to refine the selection of particles during the measurement. Based on repeat measurement runs (data not shown) it was determined that defining a minimum limit for

the exclusion criteria is important for dust-sized material. This was observed from measurements which ran with no lower limit and were subsequently shown to contain a high proportion of single pixel artefacts.

To improve on this, the size exclusion criteria were set in the particle range between 30 and 2.5 µm. Furthermore, as the QEMSCAN cannot confidently determine detailed information on particles with less than 5 pixels, due to its maximum theoretical pixel spacing and interaction volume of the electron beam, a post-processing filter removing all particles less than 5 pixels was used to remove particles which would otherwise produce pixel-based artefacts. Additionally, a separate post-processing rule was applied to remove the wax pixels from the scan and further disaggregate touching particles from the process.

4.3.4.3. Optimising Mineral Identification: Development of Pixel Classifiers

The cornerstone of developing mineral maps for auto-SEM-EDS relies on a combination of the BSE and X-ray information acquired. For the QEMSCAN this is a result of a two-stage process. The first stage involves spectral analysis and element identification from the X-ray data using what is known as the spectral analysis engine. During the measurement, the EDS detector collects fast and reliable low-count energy spectra for each pixel, to be used in the classification of minerals. Using this as the raw spectrum, the spectral analysis engine fits a synthesised X-ray spectrum to the raw spectrum which allows the software to report the element concentrations of the synthesised spectrum.

In the second stage, a Species Identification Protocol (SIP) list is used to translate the element concentrations reported by the spectral analysis engine to minerals and compare the element ranges in mineral compositions to those defined for each pixel. As the EDS information captured reflects multiple iterations of low count spectra (<1000 photons) of a single high-count spectrum, statistical variation may occur in the reported element concentrations (Haberlah et al, 2012). Additionally, element ranges may differ from ideal compositions due to natural chemical variation in the minerals. Thus, the SIP list displays the composition as element ranges to account for such variation. To develop a robust and reliable SIP, various optimisation stages were employed to refine the mineral definitions used in the final maps.

Primarily, the basis of the minerals reported in the SIP originated from the minerals commonly reported in coal (Ward, 2016). Compositions for each mineral were extracted from the built-in reference library and were duplicated for each mineral to create a "simulated" and "measured" entry (where the measured entry was manually altered based on the element ranges observed in the sample). Initially, a drill core sample from a local mine was used to develop compositional entries for the carbonaceous matter (this was not present in the reference library) and to adjust the measured entries for quartz and clays, such as kaolinite and illite (as these comprised ~ 90% of the mineral matter in the drill core analysed).

Figure 3-6a highlights the classification performance of the generated SIP in distinguishing the carbonaceous matter versus mineral matter in the drill core standard. A coarse sample of wash product ultrafines (<180 µm in size) was subsequently set in the carnauba wax to generate compositional ranges to differentiate the wax background from the carbonaceous matter (Figure 4-4c further highlights the classification performance of the SIP and contrast between background and sample).



(a)

| | |
|---|---|
| ☐ | Background |
| ◼ | Coal |
| ◼ | Clays |
| ◼ | Quartz |
| ◼ | Other silicates |
| ◼ | Pyrite |
| ◼ | Other sulfides |
| ◼ | Dolomite |
| ◼ | Siderite |
| ◼ | Calcite |
| ◼ | Sulfates |
| ◼ | Rutile |
| ◼ | Iron oxidies |
| ◼ | Gibbsite |
| ☐ | Carnuba wax |
| ◼ | Others |

(c)

5.0 µm
180.0 µm

5.0 µm
180.0 µm

(b)

(d)
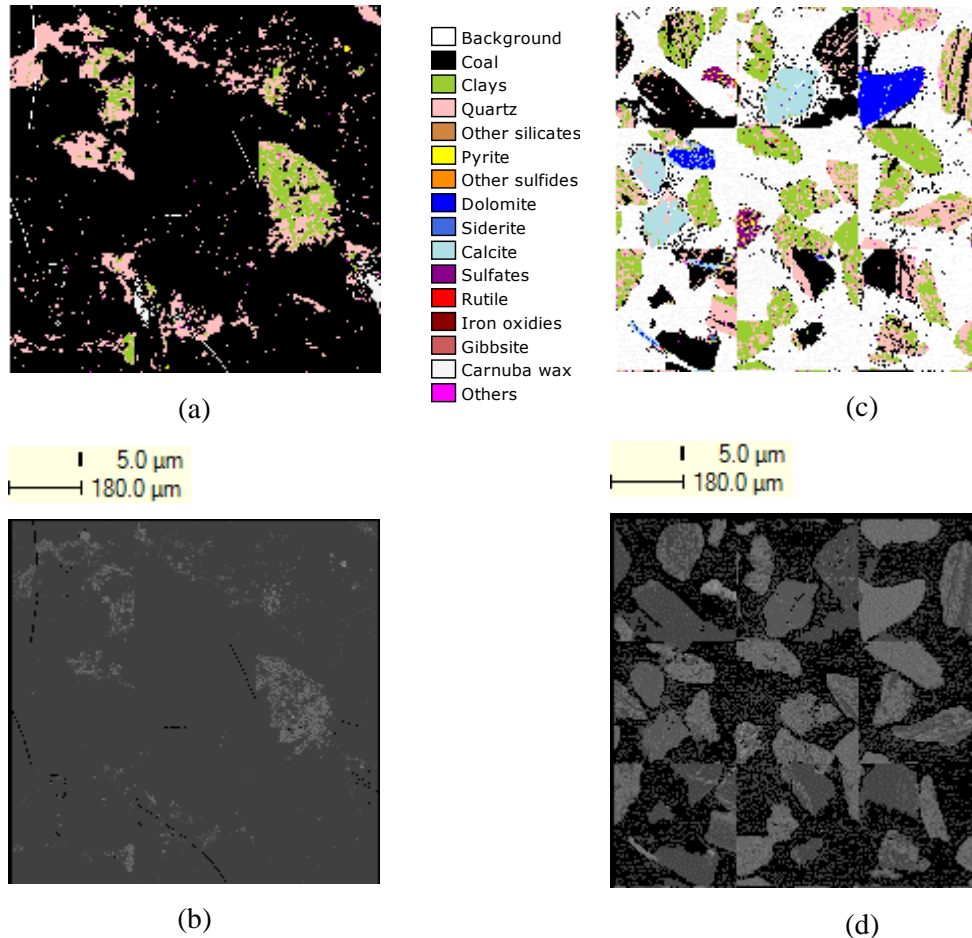
Figure 4-4 Images of the coal standards prepared to calibrate the initial SIP list. (a) represents the false colour mineral map of the drill core, below is the corresponding Back Scattered Electron (BSE) image to assess how the features were captured (b). (c) represents the false colour mineral map of the coarse particle standard, which was used to distinguish and assess the carbonaceous matter from the wax and the clays from the quartz, accompanied by the BSE image below (d). Note the greyscale contrast for both BSE images was changed to aid visual interpretability.

In combination with the mineral composition refinement, the BSE ranges were compared for the main phases (carbonaceous matter, quartz, and clays) and the background to define another degree of discrimination in cases where element ranges may be similar. This was particularly evident when analysing the dust-sized samples, as the balance between composition-based discriminators and the BSE difference between background and sample played a critical role in the mapping of the sample.

The drill core and coarse particle standards were again used to extract individual pixel information of the BSE ranges of the phases mentioned above. In Figure 4-5a, the BSE information from 33,307 pixels—extracted from a field image of the drill core (Figure 4-4a)—showed a narrow and unimodal BSE distribution range for carbonaceous matter.



(a)                                                    (b)
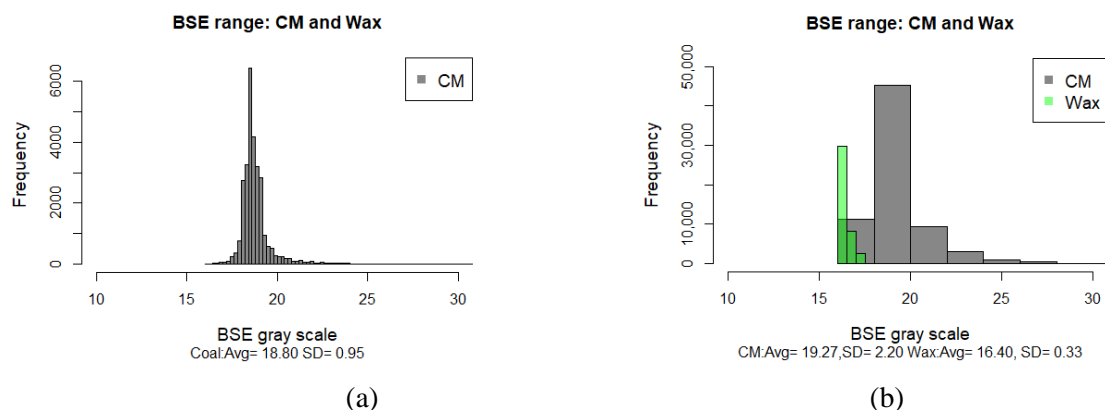
Figure 4-5 Frequency distribution of the BSE ranges for carbonaceous matter (CM) and wax. (a) shows the BSE ranges for pixels defined as carbonaceous matter in the drill core standard. (b) shows the BSE ranges for pixels defined as carbonaceous matter in the coarse particle standard.

To contrast this with the ranges of the wax background, BSE information extracted from the coarse particle standard (194,615 pixels, based on Figure 3-7c) revealed a slight overlap in ranges between the carbonaceous matter and wax (Figure 3-7b). However, the overlap was considered marginal and by determining the cut-off ranges between the elements present in carbonaceous matter versus wax, proper discriminations could be made between the background and the carbonaceous matter.

## 4.3.5. Complementary XRF and XRD Data

To assess the accuracy of the measurement two levels of data validation were employed. In the first level, the major element chemistry measured by the QEMSCAN was compared against an externally measured major element chemical assay using X-ray fluorescence spectrometry (XRF). The measurement was conducted by the Central Analytical Facilities, Stellenbosch University, Stellenbosch, South Africa, using a PANalytical Axios Wavelength Dispersive spectrometer on homogenised fusion disks. Major elements were analysed on a fused glass disk using a 2.4 kW Rhodium tube. Matrix effects in the samples were corrected by applying theoretical alpha factors and measured line overlap factors to the raw intensities measured with the SuperQ PANalytical software.

Secondly, the mineral abundances quantified by the QEMSCAN measurement were compared against mineral abundances determined through X-ray diffraction (XRD). The measurement was conducted by XRD Analytical and Consulting using a Malvern Panalytical Aeris diffractometer with a PiXcel detector and fixed slits with Fe-filtered Co-K$\alpha$ radiation. A randomly ordered powder mount of the sample was

prepared for analysis using the back-loading method. From this, the diffraction patterns were measured in the scan range 5.0000–80.0002° of 20 with a step size 0.0217° and a count time of 48.195 s per step. To identify and quantify the crystalline phases from the diffractogram, the Bruker DIFFRAC.EVA software was used by applying the Rietveld refinement method (Scrivener et al, 2004). The amount of carbonaceous matter could not be quantified by the diffractogram due to its amorphous structure. Hence, to determine an estimate of the carbonaceous matter, the XRD results were normalised to the percentage of mineral matter using (Equation (5)) established in Ward et al, (1999).

% mineral matter = % ash (SO$_3$ free) × 100/(100 − (%CO$_2$ + %H$_2$O + %S))                    (5)

In applying this method, the ash content of the coals was determined using the ASTM D3174-12 methodology for obtaining the ash in coal. Furthermore, the percentages of CO$_2$, H$_2$O and S in the relevant minerals identified were obtained from the Webmineral mineralogy database (Barthelmy, 1997).

## 4.4. Application and Evaluation of the Auto-SEM-EDS-XRD Protocol: A Case Study

### 4.4.1. Sample Description and Preparation

For this study, a sample set of bituminous coals from South Africa, Brazil and Mozambique were used as a case study to obtain a variety of particle populations and particle characteristics. For context, the description of each sample is represented in Table 4-5.

Table 4-5 Description of samples presented in the study, their replicate type and the D50 representing the median particle size determined from the Malvern Mastersizer 2000.

| Sample Name | Replicate Type | Description | D50 (µm) |
|---|---|---|---|
| Br-Dis | Single block with duplicate scans | Brazilian coal discard | 7.70 |
| SA-UF2 | Repeat block was made, blocks represent two separate sampling batches of the parental coal | South African ultrafine thickener underflow | 9.53 |
| Br-PyC | Single block with duplicate scans | Brazilian coal pyrite concentrate (waste product) | 10.42 |
| Mz-ROM1 *,† | Repeat block was made, blocks represent a single batch of the | Mozambican coal run of mine | - |
| Mz-ROM2 *,† | parental coal sub-samples into two splits | Mozambican coal run of mine | - |

* Coals Mz-ROM1 and Mz-ROM2 are from the same sampling batch but are different split samples; † Coals that displayed hydrophobic properties, no reading size could be collected.

Upon receipt, the samples were coarse (ranging from 5 cm to 180 µm) and thus required milling to reduce the particle size to the size range of dust. To achieve this, a process was developed to reduce the

final particle size of the population to approximately 25 µm or less applying methods defined by previous authors (Dalal et al, 1989; Kaya et al, 1996; Harrington et al, 2012; León-Mejía et al, 2016) (further described in Chapter 3, section 3.2.3.).

Although this study acknowledges that applying laboratory-based methods to generate dust-sized particles may not be representative of real-world coal dust, the practicality of using dust-sized coal particles was viewed as sufficient to develop critical aspects of the workflow, namely, the composition classification and size requirements needed to successfully run the measurement.

To cross-check the relevance of the samples as representative of an inhalable fraction, the relative proportion of sub-10 µm particles was quantified using the Malvern Mastersizer 2000. In all cases, the particle size reduction methods used produced particle populations with approximately 50 percent of the final sample containing particles <10 µm in size (tested on 17 independent coals, data not shown). Reliable Malvern measurements were not possible to obtain for some of the coal samples due to their natural hydrophobicity, which impaired the Malvern measurement. Instead, these samples were assumed to follow the trend of the non-hydrophobic coals as they were prepared using the same methods. All samples could be classified as dust-sized. Sub-samples of each coal were prepared for the QEMSCAN analysis using a benchtop rotary sample divider and micro rotary riffle splitter.

To evaluate the performance of the characterisation data reported, a subset of wax blocks was chosen to assess the representativity between replicate scans and blocks (refer to Table 5). Based on an analysis of these samples, the relevance of measurement representativity is discussed with respect to a validation of the mineralogical and chemical analyses using the complementary XRD and XRF data.

## 4.4.2. Measurement Validation

In assessing the consistency and accuracy of auto-SEM based reports, an understanding of the representativity of the measurement is important in the context of potential sources of uncertainty. The bulk mineralogy or mineral grades, as reported by QEMSCAN, (see Figure 4-6) represents a baseline for understanding the representativity of the measurement.
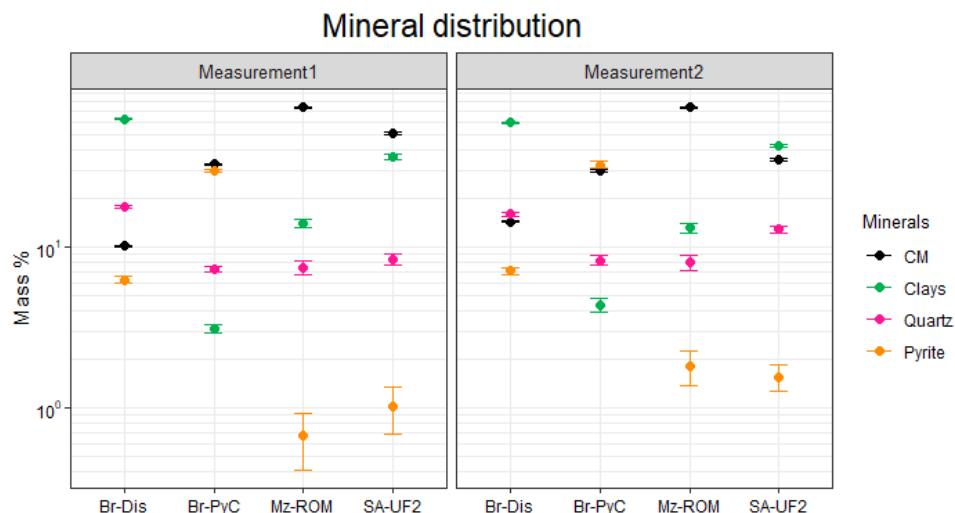
Figure 4-6 Mineral distribution across all the samples investigated. Reported errors show the 95% confidence in the reported abundance using methods in Van der Plas and Tobi, (1965).[1]

For the samples analysed, the combination of carbonaceous matter, quartz, clays, and pyrite accounted for approximately 80–95 percent of the sample by mass%. To assess the reliability of these reported abundances, the 95% confidence limits were calculated for each mineral based on the number of points analysed (Van der Plas and Tobi, 1965) – (see Figure 4-6). Through the uncertainty assessment, an error of less than 1% mass abundance was reported for all the phases identified. By assessing the uncertainty related to the mineral grades it was generally found that when the grades were lower the magnitude of the uncertainty was higher relative to the value, as displayed in Figure 4-6.

To provide a means of validating the representativity of measurements, two assessments relating to the mineral abundances and major element chemistry were made. The first assessment involved comparing the abundance of the major phases between the QEMSCAN and XRD analyses (see Figure 4-7).

Based on the comparison reported in Figure 3-9, a reasonable level of similarity for both sets of replicate measurements was established ($R^2 > 0.8$ for M1 and 2). Furthermore, by assessing the mean differences between the two analysis methods per phase, it was found that measurement 1 (M1) presented a lower percentage difference with respect to the XRD abundances than measurement 2 (M2). Sample SA-UF2 displayed the greatest disparity between measurements, with M2 reporting 16, 6, and 4 mass% more carbonaceous matter, clays, and quartz, respectively, than M1. As the measurements were conducted on two separate blocks, processed from different preparation batches, it can be assumed that the variation observed could be attributed to sub-sampling of batches from the starting bulk.

---

[1] CM refers to carbonaceous matter
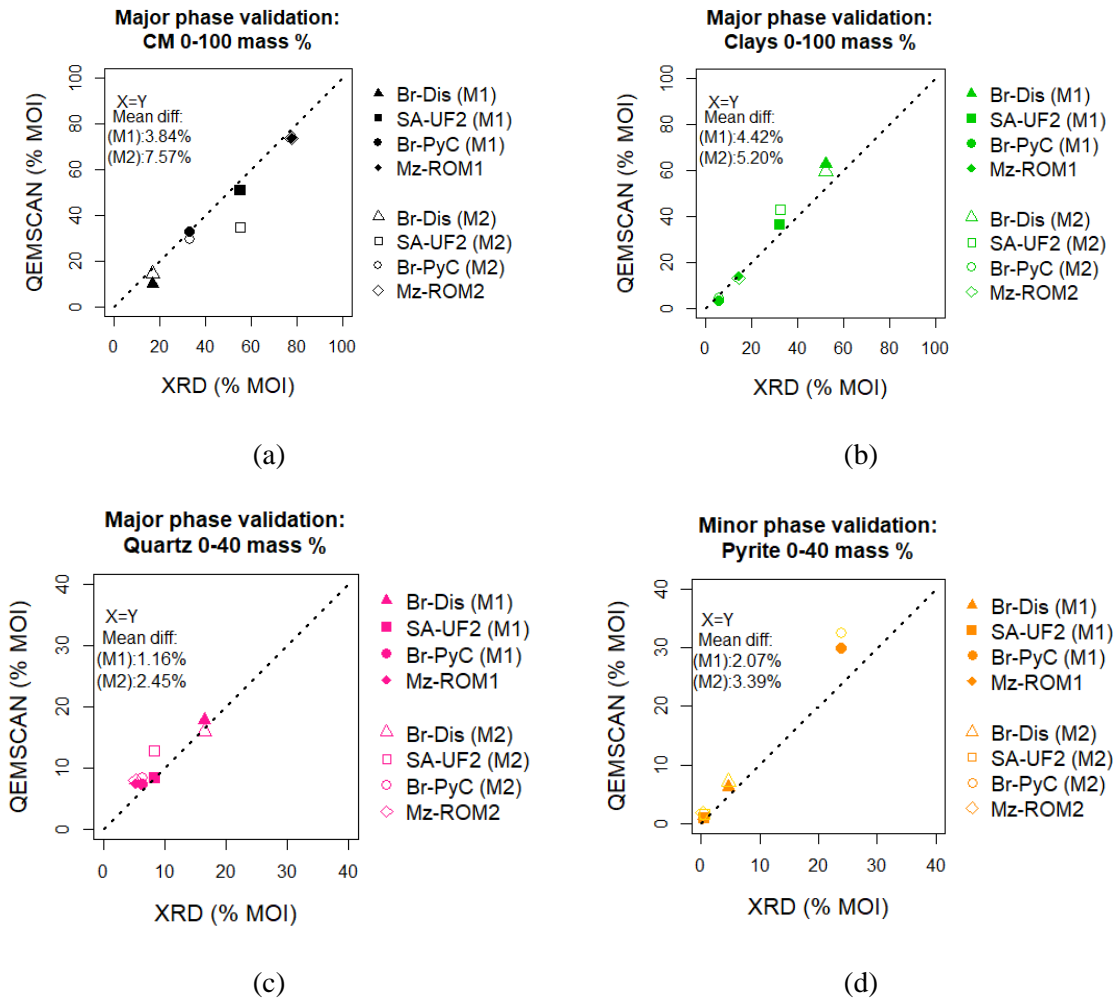
Figure 4-7 Parity charts for the main minerals and carbonaceous matter between the QEMSCAN and XRD analyses. Figures a – d show the parity for carbonaceous matter, clays, quartz, and pyrite, respectively, where the parity for both measurement 1 (M1) and measurement 2 (M2) have been contrasted.

For the performance of measurements 1 and 2 in identifying pyrite, it was observed that sample Br-PyC showed the greatest disparity between measurements compared to the other samples (3 mass% difference between measurements 1 and 2). As the measurements were acquired from the same block, the discrepancies relating to the composition between scans could be a result of the number of points analysed. Further analysis on the level of confidence expressed by the number of points counted revealed that for M1 with 35,056 pyrite points an error of ~1 mass% was determined. By contrast, M2 with 9045 points displayed an error of ~3 mass%. This confirms that the deviation in pyrite content in M2 could be because of sampling-related errors based on the number of points analysed.

Ultimately, based on the comparative deviation between the QEMSCAN and XRD analyses coupled with an understanding of the source of uncertainty, the measurements analysed can be considered representative of the bulk sample within 3.6% error by mass on average.

For the second validation assessment, the major element chemistry back-calculated by the QEMSCAN using supplied mineral compositions (see Appendix B), and a measured chemical assay conducted by XRF analysis were compared. For Al, Si and Fe (Figure 4-8a), it was generally found that there was a reasonable level of similarity for both sets of replicate measurements ($R^2 > 0.9$).



(a)

(b)
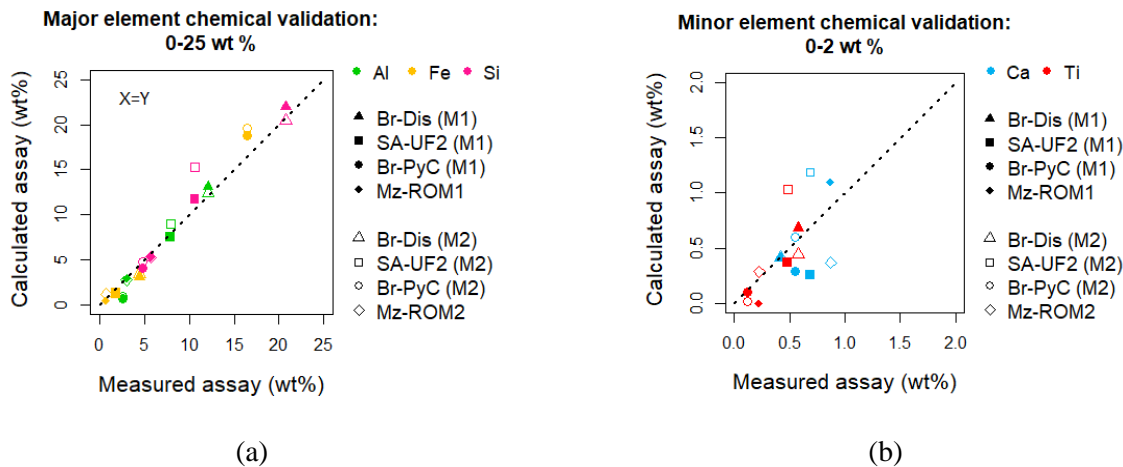
Figure 4-8 Parity charts for the calculated assay of the major and minor elements derived from the QEMSCAN and an independently measured chemical assay performed by XRF. (a) shows elements within the range 0–25 wt.% and (b) shows elements in the range 0–2 wt.%.

The mean difference reported for Al, Si, and Fe between the two analysis methods was 0.84, 0.85, and 1.1 wt.%, respectively, for measurement 1 and 0.83, 1.35, 1.29 wt.%, respectively, for measurement 2. As the differences were found to be less than 2 wt.%, the compositions were determined to be representative relative to the standard chemistry.

Parity charts for the minor elements Ti and Ca (<1.5 wt%) are shown in Figure 4-8b. The Pearson coefficient between the calculated and measured assay for Ti was 0.77 for M1 and 0.54 for M2, suggesting that Ti may not be fully accounted for in the defined mineral compositions.

The Pearson coefficient for Ca showed a poor indication of agreement with the measured and calculated assay data. The random nature of the errors further suggests that the error is neither related to measurement nor identification related errors. As Ca can be found in multiple minerals, as opposed to Ti (which was accounted for in rutile), the uncertainty derived from the calculation of Ca may be compounded by the uncertainty of its host minerals.

Ultimately, the mean deviation in Ca reported between the calculated and measured assay were found to be 0.56 (±0.28) and 0.65 (±0.29) wt.% on average for M1 and M2, respectively. In the context of

these results, it should be acknowledged that the parities reported are mostly indicative of the accuracy between major and minor phases, as derived from the four samples. Ultimately, the mineral and element distributions are optimised to obtain a general best fit for the major element chemistry. As such, this entails a compromise between the overall fit and the fit of major and minor phases.

## 4.4.3. Elemental Distributions

By extracting the contribution of selected elements (Si, Fe and Ca) within each mineral identified, the elemental deportment amongst host minerals was extracted as a percentage of the total element content (see Table 4-6). To obtain a more accurate indication of the element distributions, the percentages were normalised to the element concentration measured by XRF. By normalising the data, confidence in the accuracy of the element distributions was strengthened by utilising the XRF chemistry.

Table 4-6 Representation of the percentage distribution of Si, Fe and Ca between the various minerals calculated from the QEMSCAN dataset; errors reported are based on the deviation between measurement 1 and 2). The presence of the unmarked minerals was positively confirmed with XRD, while the remaining minerals classified by the QEMSCAN would have been present below the detection limit of XRD based on the abundance of each element.

| Minerals | Br-Dis | SA-UF2 | BR-PyC | Mz-ROM1&2 |
|---|---|---|---|---|
| Mean Element Distribution: Si (% in total) | | | | |
| Clays | 61.91 (±0.32) | 62.43 (±0.51) | 18.11 (±0.11) | 4.13 (±0.00) |
| Quartz | 38.09 (±0.32) | 37.57 (±0.51) | 81.87 (±0.11) | 1.53 (±0.00) |
| Mean Element Distribution: Fe (% in total) | | | | |
| Ankerite | 0.02 | - | - | - |
| Chalcopyrite *,[†] | 0.03 | 1.27 (±0.03) | <0.01 | - |
| Goethite *,[†] | 0.27 (±0.01) | 0.36 (±0.01) | <0.01 * | - |
| Hematite [†] | 0.49 (±0.01) | 8.89 (±0.22) | 0.06 (±0.01) | - |
| Jarosite | 0.19 | - | 0.03 | - |
| Pyrite | 89.18 (±0.22) | 40.15 (±0.17) | 79.24 (±0.37) | 74.93 (±0.00) |
| Rhomboclase | 5.52 (±0.13) | 2.00 (±0.04) | 15.75 (±0.19) | 3.87 (±0.00) |
| Siderite [†] | 3.19 (±0.00) | 46.14 (±0.02) | 0.09 (±0.00) | 18.85 (±0.00) |
| Sphalerite *,[†] | 0.03 (±0.00) | 0.30 | <0.01 | - |
| Szomolnokite | 2.30 | 1.05 (±0.02) | 4.83 (±0.18) | 2.31 (±0.00) |
| Mean Element Distribution: Ca (% in total) | | | | |
| Ankerite [†] | 0.26 | - | - | - |
| Apatite [†] | 6.33 (±0.02) | 0.36 | - | 0.48 |
| Calcite | 85.57 (±0.00) | 50.44 (±0.03) | 35.85 (±0.17) | 87.91 (±0.00) |
| Dolomite | - | 0.36 (±0.00) | 0.17 | 4.50 (±0.00) |
| Gypsum | 7.97 (±0.01) | 49.02 (±0.03) | 64.06 (±0.17) | 7.12 (±0.00) |

* Trace abundance < 0.01%; [†] Not confirmed by XRD but below detection limit.

Regarding the distributions of Si, which mainly was reported in quartz and clays, the Ca and Fe were found to be distributed amongst several host mineral groups (see in Appendix A for reference on mineral groups and chemical formula). As the presence of some minerals may be difficult to distinguish based on the nature of how the mineral identification is performed, XRD analysis was used to positively confirm the presence of the minerals described. In the case of minerals identified by the QEMSCAN but present at levels too low to be detected by XRD (chalcopyrite, goethite, hematite, siderite, sphalerite, ankerite and apatite), the composition was tightly constrained to the reference mineral chemistry to ensure confidence in their presence.

## 4.4.4. General Particle Characteristics

### 4.4.4.1. Size Distributions

To assess the reliability of the QEMSCAN in providing a consistent analysis of the particle sizes and their distributions for dust-sized particles, the distribution of particle sizes was assessed for each sample by determining the cumulative frequency of particles reporting to size categories (<5, <10, <15, …, <25).

The results in Figure 9 indicate that for Br-Dis, and Mz-ROM1&2, the particle size distributions were nearly the same for both sets of replicate measurements (Figure 4-9a, d, respectively). Similarly, the size distributions between blocks 1 and 2 of SA-UF2 were found to be highly similar, even though the resulting measurements were found to be compositionally dissimilar (see Figure 4-9b). Such findings support the notion that for sample SA-UF, the differences between measurements can be related to the variability in the sample batches and not measurement-related errors. For sample with Br-PyC, the particle size distributions were found to differ on average by 5 mass%, resulting in a 1.28 µm difference in the mean size. This may again be a result of the difference in the number of particles between measurements.
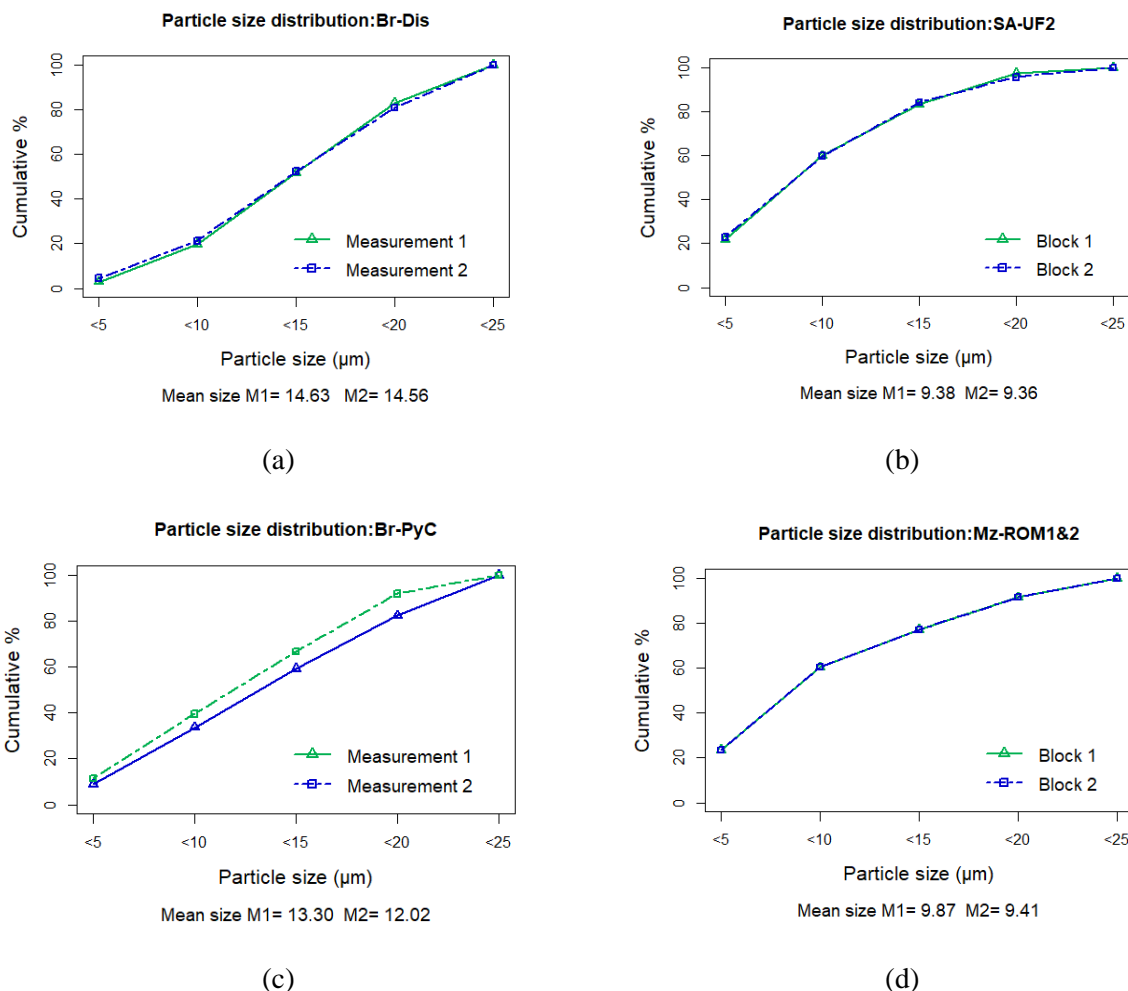
Figure 4-9 Particle size distribution for the samples analysed. Figures a – d show the variability in the distribution of particle size between replicate scans/blocks. For each sample, the mean size was described based on the midpoint of the size classes <5 to <25.

It was also observed that the particles in Br-Dis and Br-PyC were coarser on average than the particles in SA-UF2 and Mz-ROM1&2 (see Figure 3-11). In accordance with this observation, it was determined that samples SA-UF2 and Mz-ROM1&2 produced a greater proportion of particles less than 5 µm than samples Br-Dis and Br-PyC. Considering that the parental coals were crushed, and both SA-UF2 and Mz-ROM1&2 contain appreciable amounts of carbonaceous matter, it was suggested that a higher abundance of more easily friable carbonaceous matter may result in a greater proportion of fines. This was tested by assessing the mass% of carbonaceous matter in the fine particles (<5 µm class) compared to the coarser particles (>5 µm) (see Figure 4-10).
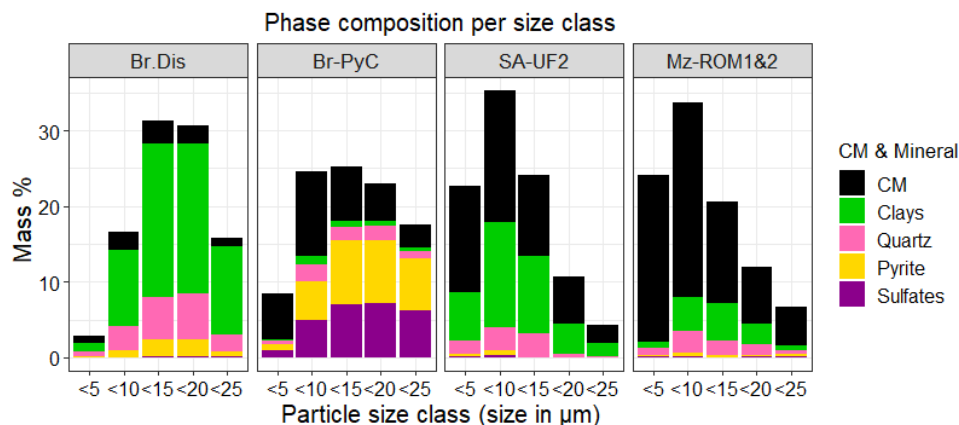
Figure 4-10 Representation of the composition of particles reporting to the different size classes.

A high abundance of fines was reported for coals which composed >50 mass% carbonaceous matter (51 mass% for SA-UF2 and 74 mass% for Mz-ROM1&2, respectively), relative to the other samples (mass% fines was 22 and 24%, respectively). Furthermore, a significant proportion of these particles were found to compose of carbonaceous matter (61 and 90% for samples SA-UF2 and Mz-ROM1&2, respectively). While it was clear that the fines mostly comprise carbonaceous matter in Mz-ROM1&2, SA-UF2 displayed appreciable amounts of clays in the fines (see Figure 4-10). Considering that the bulk composition of SA-UF2 comprised of ~36% clays, such observations may suggest that either a portion of the fines may be composed of clay grains or that there is a strong association of the carbonaceous matter with the clays.

Between the coals which contained the lowest mass of carbonaceous matter (33 and 10 mass% for Br-PyC and Br-Dis, respectively) a low abundance of fines was reported (10 mass% for Br-PyC and 3 mass% Br-Dis, respectively). By assessing the composition of fines, approximately 70% and 33% of the fines were composed of carbonaceous matter for Br-PyC and Br-Dis, respectively. Considering that Br-Dis contained extremely low abundances of carbonaceous matter in the bulk (~12 mass%), this may account for the low proportion of carbonaceous matter in the fines relative to other minerals such as clays and quartz.

Based on the observations described, the abundance of carbonaceous matter in a coal may impact its propensity to generate fines. However, samples SA-UF2 and Br-Dis highlight that when coals are crushed, inherently fine-grained minerals such as clays can additionally contribute to the proportion of fines. The presence of associations or texture needs to be considered when assessing the composition as a function of particle size, since the particle population includes both grains (particles containing a single phase) and composites (particles containing a mixture of phases).

4.4.4.2. Shape and Roughness

In this study, the total population of particles per sample was classified using the shape and roughness categories defined in sections 4.3.2.3 and 4.3.2.4, respectively. The percentage of particles reporting to each class was subsequently determined for both shape and roughness (see Table 4-7 and Table 4-8, respectively).

Table 4-7 Percentage of particles reporting to each shape class defined as a proportion of the total population (errors reported are based on the deviation between replicates).

| Particle Population: Distributed by Mean% Abundance Reporting to Shape Classes | | | | |
|---|---|---|---|---|
| Particle Classes | Br-Dis | SA-UF2 | Br-PyC | Mz-ROM1&2 |
| % Round | 0.03 (±0.01) | 0.72 (±0.30) | 0.18 (±0.05) | 0.42 (±0.01) |
| % Equant | 47.26 (±5.08) | 70.50 (±4.57) | 65.84 (±5.44) | 71.74 (±0.77) |
| % Elongate and smooth | 0.02 (±0.00) | 0.11 (±0.04) | 0.04 (±0.00) | 0.13 (±0.00) |
| % Elongate and angular | 8.27 (±1.37) | 8.92 (±1.55) | 5.06 (±1.83) | 7.72 (±1.34) |
| % Angular | 44.43 (±3.70) | 19.78 (±2.76) | 28.91 (±3.73) | 19.97 (±0.58) |
| Total% abundance | 100 (±0.00) | 100 (±0.00) | 100 (±0.00) | 100 (±0.00) |

Table 4-8 Percentage of particles reporting in each roughness class defined as a proportion of the total population (errors reported are based on the deviation between replicates).

| Particle Population: Distributed by Mean% Abundance of Reporting to Particle Roughness Classes | | | | |
|---|---|---|---|---|
| Roughness Classes | Br-Dis | SA-UF2 | Br-PyC | Mz-ROM1&2 |
| % Jagged | 83.03 (±5.06) | 51.96 (±10.87) | 78.46 (±2.43) | 54.92 (±1.40) |
| % Intermediate | 12.94 (±3.09) | 29.59 (±2.70) | 15.97 (±2.61) | 29.75 (±0.61) |
| % Smooth | 4.04 (±1.97) | 18.45 (±8.16) | 5.58 (±0.18) | 15.33 (±2.01) |
| Total% abundance | 100 (±0.00) | 100 (±0.00) | 100 (±0.00) | 100 (±0.00) |

For particle shape, the results from Table 4-7 show that most of the particles were reported as equant (roughly box-like or ball-like) or angular across all the samples (mean across samples: 64 (±11.34), 28 (±11.58) mass% for equant and angular particles, respectively). This may be a result of the milling processes, which in turn fracture the material to produce such shapes.

Based on the results on particle roughness in Table 4-8, the majority of the population analysed reported to the jagged and intermediate classes, while only a minor percentage of particles reported smooth (mean abundance across samples 67 (±4.24), 22 (±1.12) and 10 (±3.49) mass%, respectively). Such

observations are consistent with the particle shapes reported as a function of the breakage mechanism involved in the milling process (Little et al, 2016b; Semsari et al, 2020).

## 4.4.5. Mineral Specific Particle Characteristics: Liberation and Association

In addition to determining the bulk mineralogy in the particle population, the QEMSCAN software allows users to quantitatively determine the composition of the individual particles within the population. For this study, the degree to which the main minerals (clays, quartz, and pyrite) were liberated was assessed by determining the cumulative liberation yield (CLY) based on the liberation classes defined in Section 4.3.2.5. Additionally, 95% confidence limits were computed for each class using methods outlined in Leigh et al, (1993).

Across the samples analysed, the liberation of particles containing clays was found to vary based on the CLY profiles for each sample (see Figure 4-11). For Br-Dis, SA-UF2, Br-PyC and Mz-ROM1, the percent of liberated particles was 64 (±0.33), 46 (±2.42), 3 (±7.65), and 22 (±4.92) %, respectively. This suggests that when some coals are crushed a substantial portion of the clays may occur as liberated grains, while for others the clays more readily occur as composites.
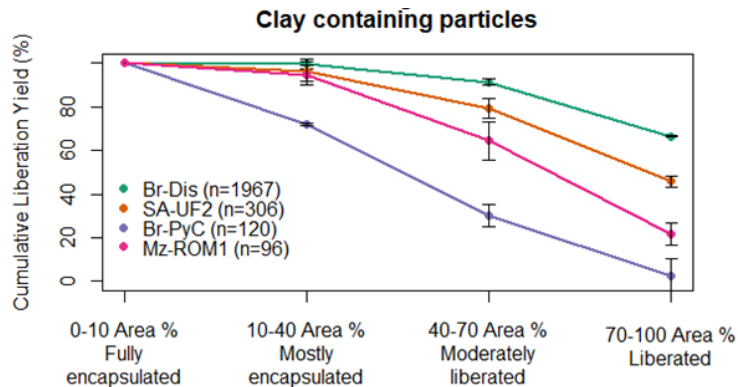


Figure 4-11 Assessment of the liberation for clay containing particles across the sample analysed using the cumulative liberation yield, where the uncertainty is expressed as the 95% confidence limits. For reference, the number of particles containing clays is represented per sample as "n".

Regarding the liberation of quartz, represented in Figure 4-12, little variation was reported across the samples (the percent of liberated quartz was found to be 22 (±2.85), 46 (±8.69), 31 (±4.46), and 43 (±7.61) mass% for samples Br-Dis, SA-UF2, Br-PyC and Mz-ROM1, respectively). These results indicate that quartz derived from pulverised coal tends to mostly occur in composite particles.

(a)  (b)
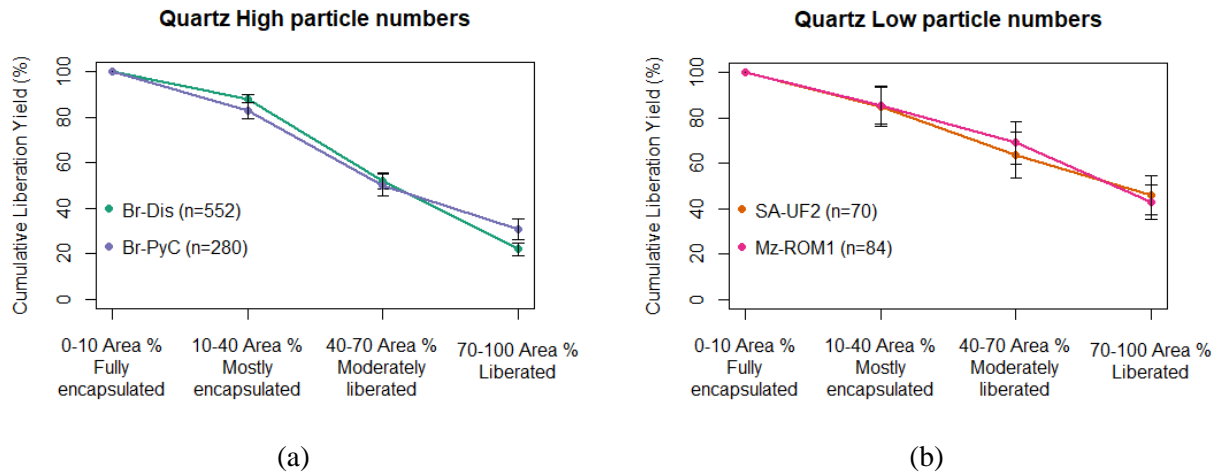
Figure 4-12 Assessment of the liberation for quartz-containing particles across the sample analysed using the cumulative liberation yield, where the uncertainty is expressed as the 95% confidence limits. For reference, the number of particles containing quartz is represented per sample as "n". Figures a and b contrast the impact of high and low particle numbers on uncertainty, respectively.

Furthermore, it was observed that the magnitude of the confidence limits displayed a dependence based on the number of particles containing quartz. For samples Br-Dis and Br-PyC, which obtained relatively high particle numbers, the confidence limits displayed no overlap between liberation classes (see Figure 4-12a). However, for samples SA-UF2 and Mz-ROM1, with considerably lower particle numbers, a higher magnitude of error resulted in an overlap between liberation classes (see Figure 4-12b).

For samples SA-UF2 and Mz-ROM1 the liberation of particles containing pyrite could not be reliably determined as the particle numbers were too low (2 and 7 particles, respectively). The results for samples Br-Dis and Br-PyC in Figure 4-13 show that Br-Dis displayed a higher proportion of liberated pyrite grains than Br-PyC (13 (±7.32) and 0.44 (±2.03) mass%, respectively). Even though Br-Dis displays a slightly higher liberation than Br-PyC, the majority of the particles containing pyrite were still composites.
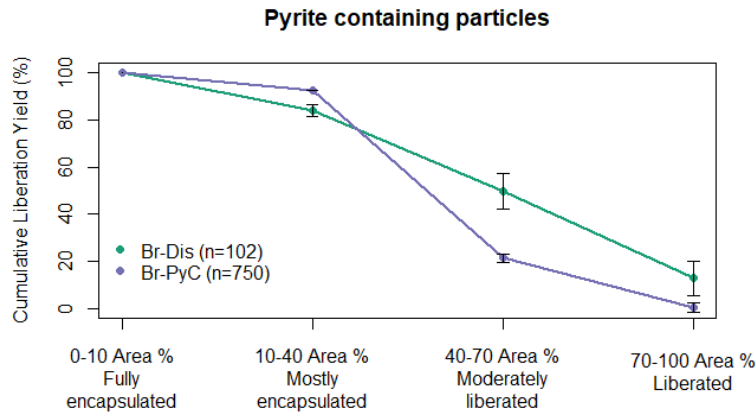
Figure 4-13 Assessment of the liberation for pyrite-containing particles across the sample analysed using the cumulative liberation yield, where the uncertainty is expressed as the 95% confidence limits. For reference, the number of particles containing pyrite is represented per sample as "n".

Mineral associations for the non-liberated fraction as well as the percentage of liberated particles were computed and are presented in Figure 4-14. The results indicate that the composite particles containing clays are mostly associated with carbonaceous matter. However, in some coals, notable associations between the clays and quartz were also observed (36, 28, and 19% association for Br-Dis, Br-PyC, and Mz-ROM1, respectively). Additionally, for Br-PyC, minor associations of the clays with pyrite and sulfates were reported (~7% association for both minerals).
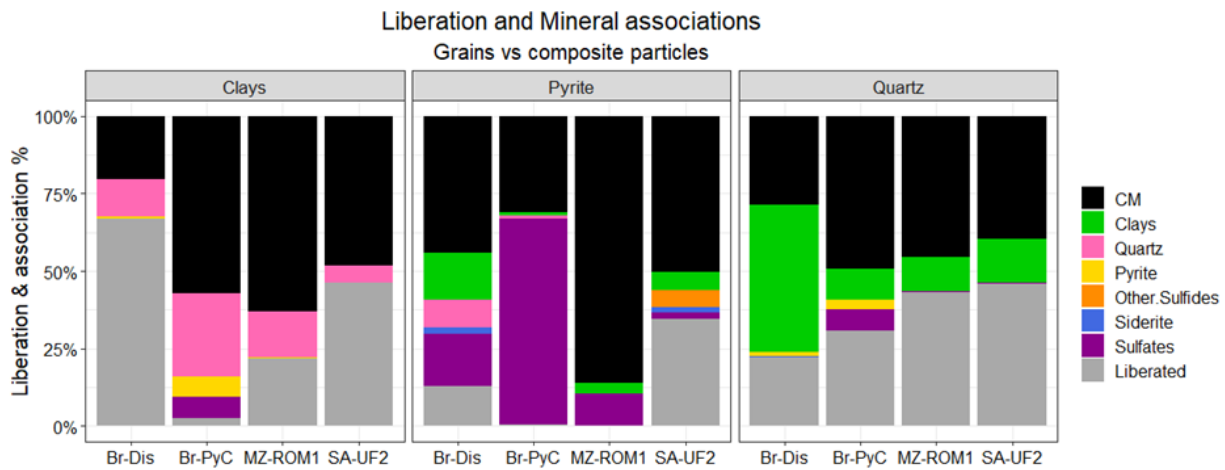


Figure 4-14 Representation of the particle liberation and association grouped by clays, pyrite, and quartz-containing particles. The liberated fraction described grains of either clays, quartz, or pyrite, whereas the associations depict the proportion of boundary minerals/carbonaceous matter associated with unliberated grains in each mineral group.

Particles containing pyrite were mostly associated with carbonaceous matter, as well as sulfates. The latter association was particularly significant in the case of Br-PyC (67% association) but was found to vary across the samples (19, 10, 3% association for Br-Dis, Mz-ROM1 and SA-UF2, respectively). As

pyrite can readily oxidise to sulfates in the presence of oxygen and water, such an association may allude to the state of weathering the mineral has undergone. Apart from sulfates, the pyrite-containing composites showed minor associations with additional minerals such as quartz, clays, and siderite in Br-Dis (10, 17 and 2% association, respectively) and clays, other sulfides, and siderite in SA-UF2 (9, 9 and 3% association, respectively).

Concerning the associations with quartz composites, carbonaceous matter was determined to be the predominantly associated phase with quartz across the samples. This was with the exception of sample Br-Dis, which showed only 36% association of carbonaceous matter with quartz. For this sample, the quartz was strongly associated with clays (60% association) in comparison to the other samples where this association was only weak (14, 19 and 25% association for Br-PyC, Mz-ROM1 and SA-UF2, respectively). Additionally, it was found that the quartz displayed minor associations with pyrite and sulfates for Br-PyC (5 and 10% association, respectively).

## 4.4.6. Limitations and Broader Implications of the Dataset

Through this study, an auto-SEM-EDS-XRD protocol was developed for the particle analysis of coal dust using the dust-sized coal particles. By applying laboratory-based methods to generate dust-sized particles, this study recognises that the particles analysed may not be representative of real-world coal dust. However, the analysis of dust-sized coal particles in the absence of real-world dust provided a practical means with which to develop the protocol to suit both the composition classification and size requirements needed to successfully run the measurement. Thus, despite such a limitation, the applicability of the protocol renders itself useful to real-world samples and the analysis of several coals which can be used to develop large datasets of particle information as a prerequisite for future biological testing of the material.

Through recent research, it has been demonstrated that geoanthropogenic activities at collieries can produce variation in the characteristics of coal dust (Johann-Essex et al, 2017a; LaBranche et al, 2022). The results of this study have indicated that the amount of carbonaceous matter—and in some cases clays—may influence the proportion of fines produced when coal is crushed. Furthermore, it was proposed that the breakage induced by crushing and milling coal produces particles that are mainly equant and angular. Ultimately, these properties could have significant implications in terms of potential health risks post-exposure.

In the context of developing a nuanced understanding of bio-accessibility, auto-SEM-EDS systems such as the QEMSCAN provide a quantitative measurement for mineral liberation and associations. As mineral associations have been found to impact the way certain reactive minerals behave in biological systems, the quantification of such information may prove useful in the interpretation of dose–response testing. Similarly, information of the element distributions within host minerals provides a more nuanced understanding of the bio-accessibility of potentially harmful elements than a standard chemical assay.

Despite these advantages and opportunities, the QEMSCAN system (or any equivalent platform) requires a substantial initial time investment to set up a robust SIP list, as well as repeated scans to optimise field and scan parameters to the size range of dust particles. Additionally, the data need to be validated to understand whether the measurement is representative of the bulk sample, and if sufficient particles were analysed to obtain the level of accuracy needed for the application.

As a result, it is recommended that an auto-SEM-EDS-based protocol should include the collection of independently analysed mineralogical (e.g., QXRD) and elemental data (supporting chemistry datasets). Recent work aimed at understanding the uncertainties in quantitative mineralogy from auto-SEM-EDS analyses demonstrated the effectiveness of bootstrap resampling methods to determine uncertainties in the reported data (Blannin et al, 2021).

Ultimately, such exercises should be considered essential components of a dust characterisation routine, as such datasets can form critical primary information for decision-making. While the accuracy of the measurement can be verified based on its mineral grades and element composition, it should be recognised that the auto-SEM-EDS scans generated from polished blocks generate cross-sectional images of the particles. This entails that the results obtained for general physical characteristics such as particle size will not be comparable with other methods which have a fundamental difference in the way the particle image is acquired (Little et al, 2016a). As such, the particle information extracted from auto-SEM-EDS should be carefully considered for its intended application and should be compared against complementary datasets, where possible, to ensure a robust analysis.

## 4.5. Conclusions

Previous studies, utilising auto-SEM-EDS systems to characterise coal dust particulates, have mainly focused on determining mineral compositions and establishing size distributions for a population of particles. While such information can be considered as baseline characteristics to establish an understanding of the potential risk associated with the dust, the auto-SEM-EDS protocol developed in this study targets a much wider range and provides a quantitative definition of particle properties—such as host mineral chemistry represented as element deportment, particle shape, and mineral liberation and association data.

Considering that toxicological studies have found direct and indirect relationships between these characteristics and respiratory damage, the ability to characterise a wide array of particle-related properties has significance for both assessment and management of coal dust related health risks and as prerequisite information for further biological testing.

Through an applied demonstration of the protocol, data reports from repeat measurements were rigorously validated. Based on an assessment of the sources of uncertainty, it was determined that errors in the protocol may arise from sampling-related uncertainty determined by the number of particles analysed.

Ultimately, the results presented show the use of the developed protocol to effectively determine both general and mineral specific particle characteristics from auto-SEM-EDS systems similar to the QEMSCAN, highlighting how such tool can be utilised for the reliable analysis of dust-sized coal.

## 4.6. References

Bair, W. (2000) 'The ICRP Human Respiratory Tract Model for Radiological Protection', *Radiation Protection Dosimetry*, 60(4), pp. 307–310.

Barbery, G. (1992) 'Liberation 1, 2, 3: Theoretical analysis of the effect of space dimension on mineral liberation by size reduction', *Minerals Engineering*, 5(2), pp. 123–141. doi: 10.1016/0892-6875(92)90038-B.

Barthelmy, D. (1997) *Webmineral-Mineralogy database*. Available at: https://www.webmineral.com.

Bharti, S. K., Kumar, D., Anand, S., Poonam, Barman, S. C. and Kumar, N. (2017) 'Characterization and morphological analysis of individual aerosol of PM10 in urban area of Lucknow, India', *Micron*. Elsevier, 103(September), pp. 90–98. doi: 10.1016/j.micron.2017.09.004.

Blannin, R., Frenzel, M., Tuşa, L., Birtel, S., Ivăşcanu, P., Baker, T. and Gutzmer, J. (2021) 'Uncertainties in quantitative mineralogical studies using scanning electron microscope-based image analysis', *Minerals Engineering*, 167, p. 106836. doi: 10.1016/j.mineng.2021.106836.

Bouffant, L. Le, Bruyet, B., Daniel, H., Demarez, J., Kovacs, P., Martin, J. C., Addison, J., Bolton, R. E., et al (1988) 'Compared in vitro and in vivo toxicity of coalmine dusts. relationship with mineralogical composition', *Annals of Occupational Hygiene*, 32(Inhaled Particles VI), pp. 611–620. doi: 10.1093/annhyg/32.inhaled_particles_VI.611.

Castranova, V. and Vallyathan, V. (2000) 'Silicosis and Coal Workers' Pneumoconiosis', *Environmental Health Perspectives*, 108, pp. 675–684. Available at: https://ehp.niehs.nih.gov/doi/pdf/10.1289/ehp.00108s4675.

Cohen, R. A. (2016) 'Resurgent coal mine dust lung disease: Wave of the future or a relic of the past?', *Occupational and Environmental Medicine*, 73(11), pp. 715–717. doi: 10.1136/oemed-2016-103737.

Cohn, C. A., Laffers, R., Simon, S. R., O'Riordan, T. and Schoonen, M. A. (2006) 'Role of pyrite in formation of hydroxyl radicals in coal: Possible implications for human health', *Particle and Fibre Toxicology*, 3, pp. 1–10. doi: 10.1186/1743-8977-3-16.

Colinet, J. F., Rider, J. P., Listak, J. M., Organiscak, J. A. and Wolfe, A. L. (2021) *Best Practices for Dust Control in Coal Mining*, *NIOSH*. Available at: http://www.cdc.gov/niosh/mining/UserFiles/works/pdfs/2010-110.pdf.

Dalal, N., Suryan, M., Vallyathan, V., Green, F., Jafari, B. and Wheeler, R. (1989) 'Detection of Reactive Free Radicals In Fresh Coal Mine Dust and Their Implication for Pulmonary Injury', *The Annals of Occupational Hygiene*, 33(1), pp. 79–84. doi: 10.1093/annhyg/33.1.79.

David, W. I. F., Leoni, M. and Scardi, P. (2010) 'Domain size analysis in the Rietveld method', *Materials Science Forum*, 651(June 2014), pp. 187–200. doi: 10.4028/www.scientific.net/MSF.651.187.

Elmes, M., Delbem, I., Gasparon, M. and Ciminelli, V. (2020) 'Single-particle analysis of atmospheric particulate matter using automated mineralogy: the potential for monitoring mine-derived emissions', *International Journal of Environmental Science and Technology*. Springer, 17(5), pp. 2743–2754. doi: 10.1007/S13762-020-02660-W/FIGURES/5.

Fandrich, R., Gu, Y., Burrows, D. and Moeller, K. (2007) 'Modern SEM-based mineral liberation analysis', *International Journal of Mineral Processing*, pp. 310–320. doi: 10.1016/j.minpro.2006.07.018.

French, D., Ward, C. and Butcher, A. R. (2008) *QEMSCAN for Characterisation of Coal and Coal Utilisation By-products*.

French, D. and Ward, C. R. (2009) 'The Application of Advanced Mineralogical Techniques to Coal Combustion Product Characterisation', in *2009 World of Coal Ash Conference*. Lexington. Available at: http://www.flyash.info/.

Fubini, B. and Otero Areán, C. (1999) 'Chemical aspects of the toxicity of inhaled mineral dusts', *Chemical Society Reviews*, 28, pp. 373–381. doi: 10.1039/a805639k.

Gatti, E., Rehak, P. and Walton, J. T. (1984) 'Silicon drift chambers - first results and optimum processing of signals', *Nuclear Inst. and Methods in Physics Research, A*, 226(1), pp. 129–141. doi: 10.1016/0168-9002(84)90181-5.

Gormley, I. P., Collings, P., Davis, J. M. G. and Ottery, J. (1979) 'An Investigation into the Cytotoxicity of Respirable Dusts from British Collieries', *British Journal of Experimental Pathology*, 60, pp. 526–536.

Haberlah, D., Owen, M., Botha, P. W. S. K. and Gottlieb, P. (2012) 'SEM-EDS-based protocol of subsurface drilling mineral identification and petrological classification', in *Proceedings of the 10th International Congress for Applied Mineralogy (ICAM)*, pp. 265–266. doi: 10.1007/978-3-642-27682-8.

Harrington, A. D., Hylton, S. and Schoonen, M. A. (2012) 'Pyrite-driven reactive oxygen species formation in simulated lung fluid: implications for coal workers' pneumoconiosis', *Environmental Geochemistry and Health*. Springer Netherlands, 34(4), pp. 527–538. doi: 10.1007/s10653-011-9438-7.

Harrington, A. D., Smirnov, A., Tsirka, S. E. and Schoonen, M. A. (2015) 'Metal-sulfide mineral ores, Fenton chemistry and disease – Particle induced inflammatory stress response in lung cells', *International Journal of Hygiene and Environmental Health*. Urban & Fischer, 218(1), pp. 19–27. doi: 10.1016/J.IJHEH.2014.07.002.

Harrington, A. D., Tsirka, S. E. and Schoonen, M. A. A. (2013) 'Inflammatory stress response in A549 cells as a result of exposure to coal: Evidence for the role of pyrite in coal workers' pneumoconiosis pathogenesis', *Chemosphere*, 93(6), pp. 1216–1221. doi: 10.1016/j.chemosphere.2013.06.082.

Heppleston, A. G. (1992) 'Coal workers' pneumoconiosis: a historical perspective on its pathogenesis.', *American Journal Of Industrial Medicine*, 22(6), pp. 905–923.

Huang, X., Zalma, R., Pezerat, H. and Huang, X. (1994) 'Factors That Influence the Formation and Stability of Hydrated Ferrous Sulfate in Coal Dusts. Possible Relation to the Emphysema of Coal Miners', *Chemical Research*

*in Toxicology*, 7(3), pp. 451–457. doi: 10.1021/tx00039a025.

Huertas, J. I., Huertas, M. E. and Solis-Casados, D. A. (2012) 'Characterization of airborne particles in an open pit mining region', *Science of the Total Environment*. Elsevier B.V., 423, pp. 39–46. doi: 10.1016/j.scitotenv.2012.01.065.

Humphreys, F. J. and Brough, I. (1999) 'High resolution electron backscatter diffraction with a field emission gun scanning electron microscope.', *Journal of microscopy*, 195(Pt 1), pp. 6–9. Available at: http://www.ncbi.nlm.nih.gov/pubmed/10444296.

Hurley, J. F., Burns, J., Copland, L., Dodgson, J. and Jacobsen, M. (1982) 'Coalworkers' simple pneumoconiosis and exposure to dust at 10 British coalmines', *British Journal of Industrial Medicine*, 39, pp. 120–127. doi: 10.1136/oem.39.2.120.

Johann-Essex, V., Keles, C., Rezaee, M., Scaggs-Witte, M. and Sarver, E. (2017a) 'Respirable coal mine dust characteristics in samples collected in central and northern Appalachia', *International Journal of Coal Geology*. Elsevier, 182(September), pp. 85–93. doi: 10.1016/j.coal.2017.09.010.

Johann-Essex, V., Keles, C. and Sarver, E. (2017b) 'A Computer-Controlled SEM-EDX Routine for Characterizing Respirable Coal Mine Dust', *Minerals*, 7(15), pp. 1–15. doi: 10.3390/min7010015.

Johnson, D., Rollinson, G. K., Arif, A. T., Moreno, T., Ruiz, P. T., Lah, R., Lubosik, Z., Pindel, T., et al (2022) 'QEMSCAN® automated mineralogical analysis of PM2.5 and PM4: A preliminary study of underground coal mine dust from Poland and Slovenia', *Frontiers in Earth Science*, 10(September), pp. 1–12. doi: 10.3389/feart.2022.788928.

Kaya, E., Hogg, R. and Mutmansky, J. M. (1996) 'Evaluation of procedures for production of dust samples for biomedical research', *Applied Occupational and Environmental Hygiene*, 11(7), pp. 745–750. doi: 10.1080/1047322X.1996.10389964.

Kongsuebchart, W., Praserthdam, P., Panpranot, J., Sirisuk, A., Supphasrirongjaroen, P. and Satayaprasert, C. (2006) 'Effect of crystallite size on the surface defect of nano-TiO2 prepared via solvothermal synthesis', *Journal of Crystal Growth*, 297(1), pp. 234–238. doi: 10.1016/J.JCRYSGRO.2006.09.018.

LaBranche, N., Keles, C., Sarver, E., Johnstone, K. and Cliff, D. (2021) 'Characterization of particulates from Australian underground coal mines', *Minerals*, 11(5), pp. 1–10. doi: 10.3390/min11050447.

LaBranche, N., Teale, K., Wightman, E., Johnstone, K. and Cliff, D. (2022) 'Characterization Analysis of Airborne Particulates from Australian Underground Coal Mines Using the Mineral Liberation Analyser', *Minerals*, 12(796), pp. 1–13.

Leigh, G. M., Sutherland, D. N. and Gottlieb, P. (1993) 'Confidence limits for liberation measurements', *Minerals Engineering*, 6(2), pp. 155–161. doi: 10.1016/0892-6875(93)90129-B.

León-Mejía, G., Silva, L. F. O., Civeira, M. S., Oliveira, M. L. S., Machado, M., Villela, I. V., Hartmann, A., Premoli, S., et al (2016) 'Cytotoxicity and genotoxicity induced by coal and coal fly ash particles samples in V79

cells', *Environmental Science and Pollution Research*. Environmental Science and Pollution Research, 23(23), pp. 24019–24031. doi: 10.1007/s11356-016-7623-z.

Leonard, R., Zulfikar, R. and Stansbury, R. (2020) 'Coal mining and lung disease in the 21st century', *Current Opinion in Pulmonary Medicine*, 26(2), pp. 135–141. doi: 10.1097/MCP.0000000000000653.

Li, M., Wilkinson, D. and Patchigolla, K. (2005) 'Comparison of particle size distributions measured using different techniques', *Particulate Science and Technology*, 23(3), pp. 265–284. doi: 10.1080/02726350590955912.

Little, L. (2016) *The Development and Demonstration of a Practical Methodology for Fine Particle Shape Characterisation in Minerals Processing*. University of Cape Town.

Little, L., Becker, M., Wiese, J. and Mainza, A. N. (2015) 'Auto-SEM particle shape characterisation: Investigating fine grinding of UG2 ore', *Minerals Engineering*. Elsevier Ltd, 82, pp. 92–100. doi: 10.1016/j.mineng.2015.03.021.

Little, L., Becker, M., Wiese, J., Yorath, G., Mainza, A. and Tonzetic, I. (2016a) 'Shape characterisation: Can different devices produce comparable data for particulate samples?', in *Proceedings of the XXVIII th International Mineral Processing Congress*.

Little, L., Mainza, A. N., Becker, M. and Wiese, J. G. (2016b) 'Using mineralogical and particle shape analysis to investigate enhanced mineral liberation through phase boundary fracture', *Powder Technology*. Elsevier, 301, pp. 794–804. doi: 10.1016/J.POWTEC.2016.06.052.

Liu, T. and Liu, S. (2020) 'The impacts of coal dust on miners' health: A review', *Environmental Research*. Elsevier Inc., 190(June), p. 109849. doi: 10.1016/j.envres.2020.109849.

Maynard, A. D. and Kuempel, E. D. (2005) 'Airborne nanostructured particles and occupational health', *Journal of Nanoparticle Research*, 7(6), pp. 587–614. doi: 10.1007/s11051-005-6770-9.

Pan, L., Golden, S., Assemi, S., Sime, M. F., Wang, X., Gao, Y. and Miller, J. (2021) 'Characterization of particle size and composition of respirable coal mine dust', *Minerals*, 11(3), pp. 1–12. doi: 10.3390/min11030276.

Petruk, W. (2000) 'Applied Mineralogy in the Mining Industry', in *Applied Mineralogy in the Mining Industry*. Elsevier, pp. 198–199. doi: 10.1016/b978-0-444-50077-9.x5000-7.

Petruk, W. and Skinner, H. C. W. (1997) 'Characterizing Particles in Airborne Dust by Image Analysis', *Review of Extraction & Processing*, pp. 58–61.

Petsonk, E. L., Rose, C. and Cohen, R. (2013) 'Coal mine dust lung disease: New lessons from an old exposure', *American Journal of Respiratory and Critical Care Medicine*, 187(11), pp. 1178–1185. doi: 10.1164/rccm.201301-0042CI.

Pirrie, D. and Rollinson, G. K. (2011) 'Unlocking the applications of automated mineral analysis', *Geology Today*, 27(6), pp. 226–235. doi: 10.1111/j.1365-2451.2011.00818.x.

Van der Plas, L. and Tobi, A. C. (1965) 'A chat for judging the reliability of point counting results', *American*

*Journal of Science*, 263(1), pp. 87–90.

Plumlee, G. S., Morman, S. and Ziegler, T. (2006) 'The Toxicological Geochemistry of Earth Materials: An Overview of Processes and the Interdisciplinary Methods Used to Understand Them', *Reviews in Mineralogy and Geochemistry*, 64(1), pp. 5–57. doi: 10.2138/rmg.2006.64.2.

Plumlee, G. S. and Ziegler, T. L. (2003) *The Medical Geochemistry of Dusts, Soils, and Other Earth Materials*. 9th edn, *Environmental geochemistry*. 9th edn. Elsevier. doi: 10.1016/B0-08-043751-6/09050-2.

Ram, S. S., Majumdar, S., Chaudhuri, P., Chanda, S., Santra, S. C., Maiti, P. K., Sudarshan, M. and Chakraborty, A. (2012) 'SEMEDS: An important tool for air pollution bio-monitoring', *Micron*. Elsevier Ltd, 43(2–3), pp. 490–493. doi: 10.1016/j.micron.2011.07.007.

Reisner, M. T. R., Bruch, J., Hilscher, W., Kriegseis, W., Prajsnar, D., Robock, K., Rosmanith, J., Scharmann, A., et al (1982) 'Specific harmfulness of respirable dusts from west German coal mines VI: Comparison of experimental and epidemiological results', *Annals of Occupational Hygiene*, 26(4), pp. 527–539. doi: 10.1093/annhyg/26.4.527.

Ruby, M. V., Schoof, R., Brattin, W., Goldade, M., Post, G., Harnois, M., Mosby, E., Casteel, S. W., et al (1999) 'Advances in evaluating the oral bioavailability of inorganics in soil for use in human health risk assessment', *Environmental Science and Technology*, 33(21), pp. 3697–3705. doi: 10.1021/es990479z.

Schoonen, M. A., Harrington, A. D., Laffers, R. and Strongin, D. R. (2010) 'Role of hydrogen peroxide and hydroxyl radical in pyrite oxidation by molecular oxygen', *Geochimica et Cosmochimica Acta*, 74, pp. 4971–4987. doi: 10.1016/j.gca.2010.05.028.

Schoonen, M. A., Roemer, E. J. and Simon, S. (2006) 'Mineral-Induced Formation of Reactive Oxygen Species Chemistry of surfaces and nanoparticles View project', *Reviews in Mineralogy and Geochemistry*, 64, pp. 179–222. doi: 10.2138/rmg.2006.64.7.

Schulz, B., Sandmann, D. and Gilbricht, S. (2020) 'Sem-based automated mineralogy and its application in geo-and material sciences', *Minerals*, 10(11), pp. 1–26. doi: 10.3390/min10111004.

Scrivener, K. L., Füllmann, T., Gallucci, E., Walenta, G. and Bermejo, E. (2004) 'Quantitative study of Portland cement hydration by X-ray diffraction/Rietveld analysis and independent methods', *Cement and Concrete Research*. Pergamon, 34(9), pp. 1541–1547. doi: 10.1016/J.CEMCONRES.2004.04.014.

Sellaro, R., Sarver, E. and Baxter, D. (2015) 'A standard characterization methodology for respirable coal mine dust using SEM-EDX', *Resources*, 4(4), pp. 939–957. doi: 10.3390/resources4040939.

Semsari, P. P., Parian, M. and Rosenkranz, J. (2020) 'Breakage process of mineral processing comminution machines – An approach to liberation', *Advanced Powder Technology*. Society of Powder Technology Japan, 31(9), pp. 3669–3685. doi: 10.1016/j.apt.2020.08.005.

Straszheim, W. E., Younkin, K. A., Greer, R. T., Markuszewski, R. and Younkinl, K. A. (1988) 'Mounting Materials for Automated Image Analysis of Coals Using Backscattered Electron Imaging', *Scanning Microscopy*

*International*. AMF O'Hare, 2(3), pp. 1257–1264.

Sun, Y., Kinsela, A. S. and Waite, T. D. (2022) 'Elucidation of alveolar macrophage cell response to coal dusts: Role of ferroptosis in pathogenesis of coal workers' pneumoconiosis', *Science of the Total Environment*. Elsevier B.V., 823, p. 153727. doi: 10.1016/j.scitotenv.2022.153727.

Trechera, P., Moreno, T., Córdoba, P., Moreno, N., Zhuang, X., Li, B., Li, J., Shangguan, Y., et al (2020) 'Mineralogy, geochemistry and toxicity of size-segregated respirable deposited dust in underground coal mines', *Journal of Hazardous Materials*. Elsevier, 399, p. 122935. doi: 10.1016/j.jhazmat.2020.122935.

Vallyathan, V., Shi, X. and Castranova, V. (1998) 'Reactive Oxygen Species: Their Relation to Pneumoconiosis and Carcinogenesis', *Environmental Health Perspectives*, 106, pp. 1151–1155.

Vallyathan, V., Shi, X., Dalal, N. S., Irr, W. and Castranova, V. (1988) 'Generation of free radicals from freshly fractured silica dust. Potential role in acute silica-induced lung injury', *American Review of Respiratory Disease*, 138(5), pp. 1213–1219. doi: 10.1164/ajrccm/138.5.1213.

Vickery, K. and Eckardt, F. (2021) 'A closer look at mineral aerosol emissions from the Makgadikgadi Pans, Botswana, using automated SEM-EDS (QEMSCAN®)', *South African Geographical Journal*. Routledge, 103(1), pp. 7–21. doi: 10.1080/03736245.2020.1824805.

Ward, C. R. (2016) 'Analysis, origin and significance of mineral matter in coal: An updated review', *International Journal of Coal Geology*. Elsevier B.V., 165, pp. 1–27. doi: 10.1016/j.coal.2016.07.014.

Ward, C. R., Spears, D. A., Booth, C. A., Staton, I. and Gurba, L. W. (1999) 'Mineral matter and trace elements in coals of the Gunnedah Basin, New South Wales, Australia', *International Journal of Coal Geology*, 40(4), pp. 281–308. doi: 10.1016/S0166-5162(99)00006-3.

Warr, L. N. and Nieto, F. (1998) 'Crystallite thickness and defect density of phyllosilicates in low-temperature metamorphic pelites: A TEM and XRD study of clay-mineral crystallinity-index standards', *Canadian Mineralogist*, 36(6), pp. 1453–1474.

Weaver, C. E. (1976) 'The Nature of TiO2 in Kaolinite', *Clays and Clay Minerals*. Springer, 24(5), pp. 215–218. doi: 10.1346/CCMN.1976.0240501.

Williamson, B. J., Rollinson, G. and Pirrie, D. (2013) 'Automated mineralogical analysis of PM10: New parameters for assessing PM toxicity', *Environmental Science and Technology*, 47(11), pp. 5570–5577. doi: 10.1021/es305025e.

Zhang, Q., Dai, J., Ali, A., Chen, L. and Huang, X. (2002) 'Roles of bioavailable iron and calcium in coal dust-induced oxidative stress: Possible implications in coal workers lung disease', *Free Radical Research*, 36(3), pp. 285–294. doi: 10.1080/10715760290019309.

Zosky, G. R., Bennett, E. J., Pavez, M. and Beamish, B. B. (2021) 'No association between pyrite content and lung cell responses to coal particles', *Scientific Reports*, 11(1), p. 8193. doi: 10.1038/s41598-021-87517-z.

Complete analysis of the coal particle samples: defining and assessing distributions in the characteristics

In paper 1, four of the seventeen samples were characterised for their physicochemical and mineralogical characteristics using the QEMSCAN as the main tool to generate the data reports and XRD and XRF data as complementary data to assess its accuracy. This section provides a complete analysis of the coal particle samples for all seventeen coals, describing the characteristics derived from QEMSCAN, XRD, XRF and BET (Brunauer–Emmett–Teller) analysis.

## 4.7. Mineral and major element distributions

To obtain an understanding of the mineralogical and chemical compositions across the full set of coals analysed in this study, the sections below discuss the mineral grades obtained via QEMSCAN and XRD and the element distributions defined by XRF and QEMSCAN.

### 4.7.1. Description of mineral grades

For this study, two methods of analyses were performed to identify and understand the distribution of minerals in the bulk sample and on a particle level. As discussed in the previous section, XRD analysis was utilised to positively identify the minerals present within each coal particle samples (shown in Figure 4-15). Secondly, mineral maps of individual particles were generated by QEMSCAN to broadly understand the distribution of specific minerals and groups of minerals within a population of particles (shown in Figure 4-16).

XRD analysis confirmed that the main mineral assemblages across the wider set of coal particulates were predominantly composed of quartz, aluminosilicate clays (specifically kaolinite and illite), pyrite, and gypsum (see appendix Table C-5 for mineral formulae). Apart from these minerals, appreciable amounts of rutile, carbonates (calcite and dolomite) and additional sulfate (szomolnokite and rhomboclase) species were observed. Regarding the mineral grades defined by QEMSCAN, the analysis of the coal particles reflected that the mineral content across samples mainly consisted of clays, quartz, pyrite, calcite, and sulfates. As clay minerals such as kaolinite and illite are difficult to differentiate based on their collected X-ray composition with QEMSCAN, these minerals were grouped as clays. In addition to this grouping, gypsum, szomolnokite, jarosite, and rhomboclase were aggregated to sulfates due to their relatively low abundances. Additionally, traces of minerals such as rutile, dolomite, siderite, and hematite/goethite (grouped as iron oxides) were identified through QEMSCAN analysis (see Figure 4-17).

## XRD Major mineral distribution
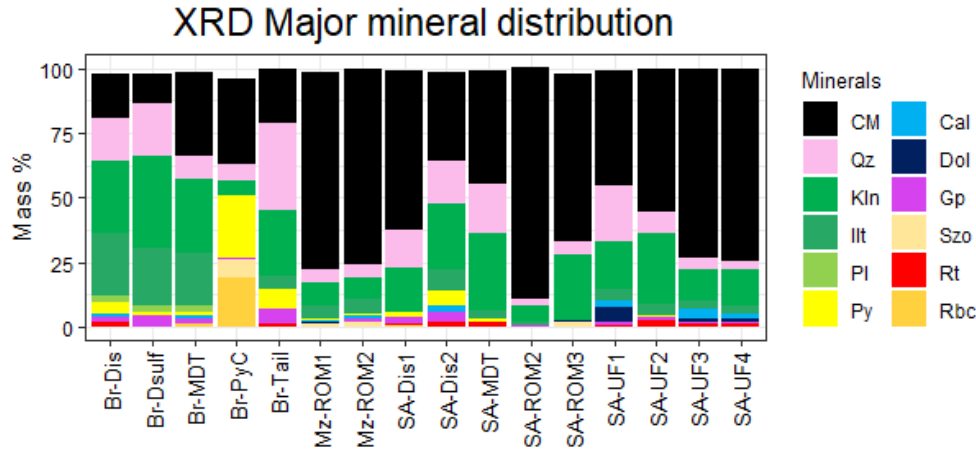


For sample US-ROM the amorphous content was too high to perform the XRD refinement.
Sample Br-PyC is the only sample to contain < 1 wt.% amphibole and voltatite in addition to ~ 1.5 wt. % alunogen.

CM-carbonaceous matter, Qz-quartz ($SiO_2$), Kln-kaolinite ($Al_2Si_2O_5(OH)_4$),
Ilt-illite ($K_{0.6}(H_3O)_{0.4}Al_{1.3}Mg_{0.3}Fe^{2+}_{0.1}Si_{3.5}O_{10}(OH)_2 \cdot (H2O)$), Pl-plagioclase ($Na_{0.5}Ca_{0.5}Si_3AlO_8$), Py-pyrite ($FeS_2$), Cal-Calcite ($CaCO_3$), Dol-dolomite ($CaMg(CO_3)_2$), Gp-gypsum ($Ca(SO_4)\cdot2(H_2O)$), Szo-szomolnokite ($Fe^{2+}(SO_4)\cdot(H_2O)$), Rt-rutile ($TiO_2$), and Rbc-rhomboclase ($HFe^{3+}(SO_4)_2\cdot4(H_2O)$)

Figure 4-15 Major mineral distribution defined for each sample determined by XRD analysis.

## QEMSCAN Major mineral distribution
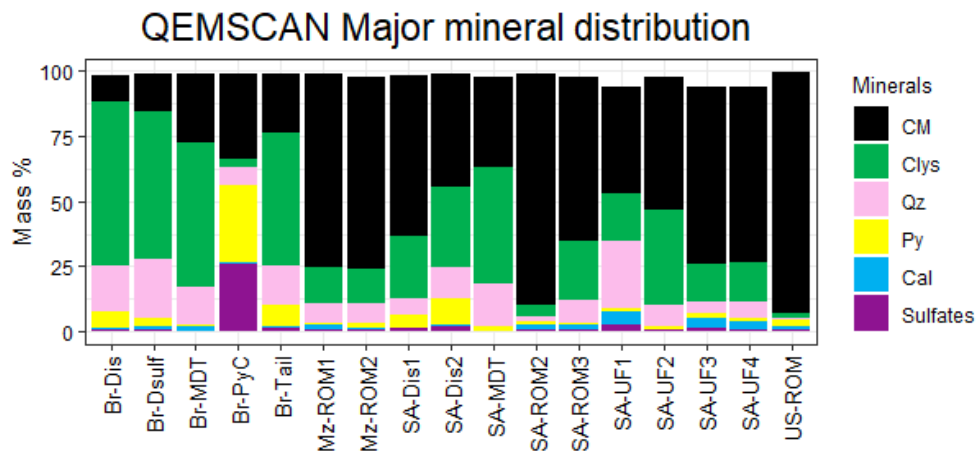


CM-carbonaceous matter, Clys-clays, Qz-quartz, Py-pyrite, Cal-calcite
Clays = Kaolinite + Illite content

Figure 4-16 Major mineral distribution defined for each sample determined by QEMSCAN analysis for major and minor phases.
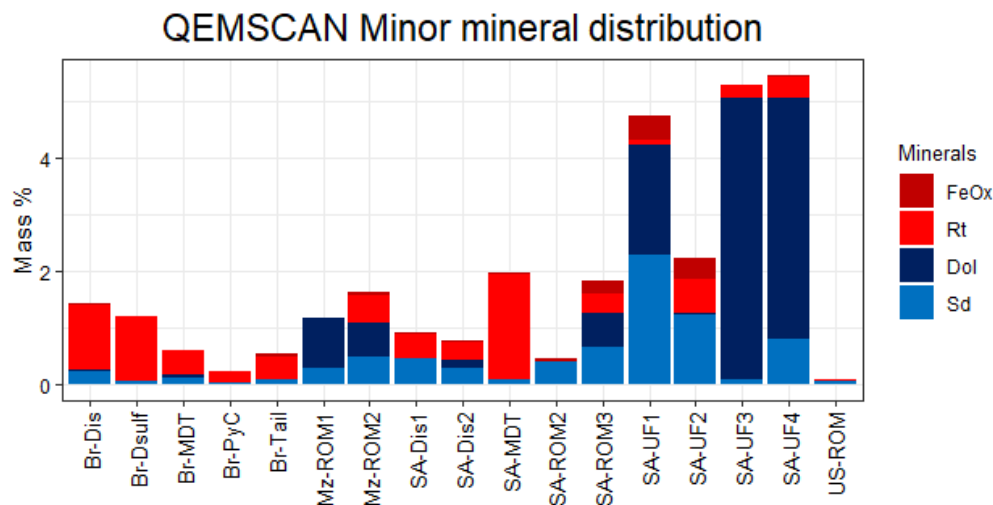
FeOx-iron oxides, Rt-rutile, Dol-dolomite, Sd-siderite (Fe$^{2+}$(CO3))

Figure 4-17 Minor mineral distribution defined for each sample determined by QEMSCAN analysis for trace phases.

Regarding the abundance of carbonaceous matter, the results from both XRD and QEMSCAN analyses show a similar distribution in the proportion of carbonaceous matter to mineral content (ranging from 11 to >90 % carbonaceous matter across the sample set). To assess how well these two methods compared against one another once the mineral matter identified by XRD was normalised to an estimate of carbonaceous content, parity plots were constructed (see Appendix C, Figure C-3). The results confirmed that these analysis methods produce reasonably consistent quantifications of both carbonaceous and mineral matter across the samples analysed (R$^2$ > 0.6 for minor phases and R$^2$ > 0.7 for major phases).

To show the chemical representativity of the mineral distributions between QEMSCAN and XRD analyses, the back-calculated chemistry from the minerals was compared to the measured chemistry obtained by XRF (see Appendix C, Figures 1 and 2). The correlations between the major elements Si, Al, Fe, Ca, and Ti showed that both analyses were chemically in good agreement with the XRF assay, yielding R$^2$ > 0.5 (see Appendix C, Table C-4). The results demonstrated that Si, Al, and Fe were accounted for – to a reasonable degree – by both mineral lists defined. This was exhibited by the Pearson correlation across both methods reporting as > 0.93. Regarding Ca and Ti, these elements were reasonably accounted for by both mineral lists across the full dataset (R$^2$ 0.62 and 0.50 and 0.74 and 0.60 for the XRD and QEMSCAN-based lists respectively).

While the previous section (paper 1) noted poor agreement between the calculated and measured abundances of Ca and Ti, the results from a larger set of coals show that the abundance of Ca is well represented by XRD and QEMSCAN analysis. However, the degree of variability in calculated Ca and Ti is still relatively higher compared to the other major elements. In the case of Ca, this is to be expected as it is derived from multiple minerals (calcite, dolomite, gypsum, and siderite) whose abundances are minor in

terms of wt. % (see Figures 4-15, 16, and 17). Regarding the variability in the calculated Ti abundance, rutile was assumed to be the only mineral host, however, the moderate correlation of the measured and calculated values suggests that Ti may be present in additional phases. Of the minerals present in coal, kaolinite has previously been observed to occur as $TiO_2$-kaolinite aggregates cemented to kaolinite particles in clay-bearing ores (Weaver, 1976). Upon assessing the particle maps, the results showed that the available rutile not only co-occurs with kaolinite but further demonstrate that Ti signatures can be detected in kaolinite-based EDS spectra (see Figure 4-18). This further supports the possible occurrence of $TiO_2$-kaolinite aggregates within the coal particulates. By assessing the correlation between the measured Ti content and the abundance of kaolinite and rutile respectively, the results suggest that a fraction of the Ti assayed may be contained in kaolinite (see Figure 4-19). The strong statistical relationship between Ti and clay content (specifically kaolinite), represented in Figure 4-19a and b, serve as evidence for an intrinsic relationship between kaolinite and Ti across a range of coal samples. In accordance with this, the relatively high variability and moderate predictability of Ti by rutile (defined by the QEMSCAN) supports the hypothesis that rutile is not the sole host of Ti in coal particles. While the same relationship expressed using rutile content demined via XRD suggests that rutile has a very poor relationship to Ti, the high level of variability observed was accounted for as measurement related uncertainty linked to the detection limit of this technique (detection limit ~ 2-3 wt. %).
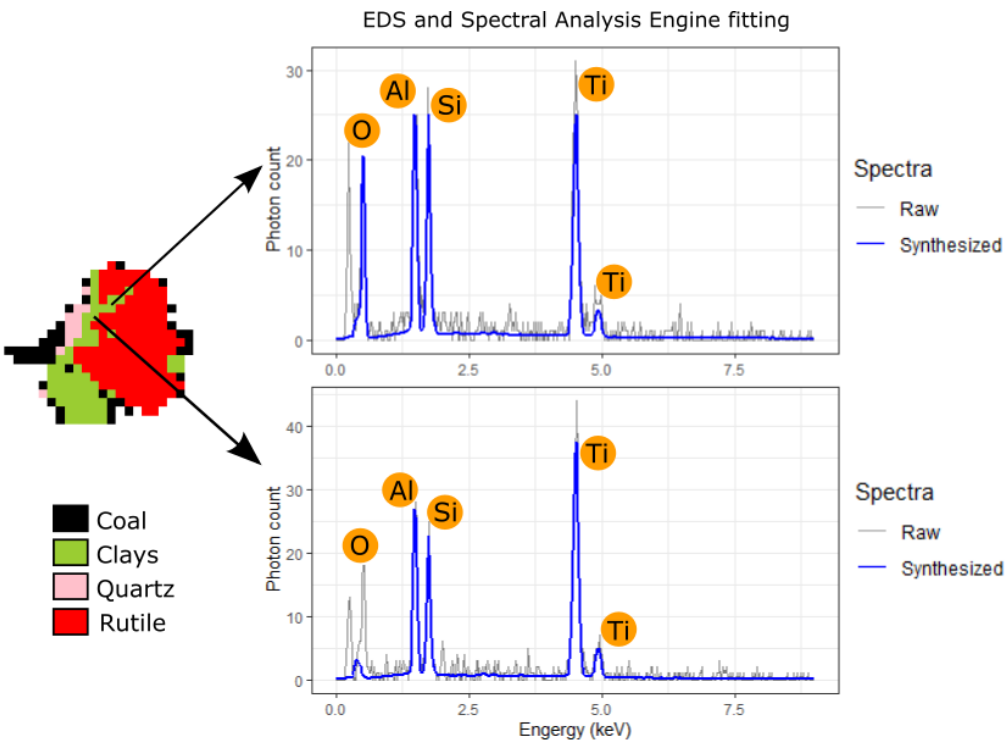


Figure 4-18 Kaolinite and rutile pixel analysis, depiction of collected EDS spectra representing the inclusion of Ti in kaolinite-based chemistry.
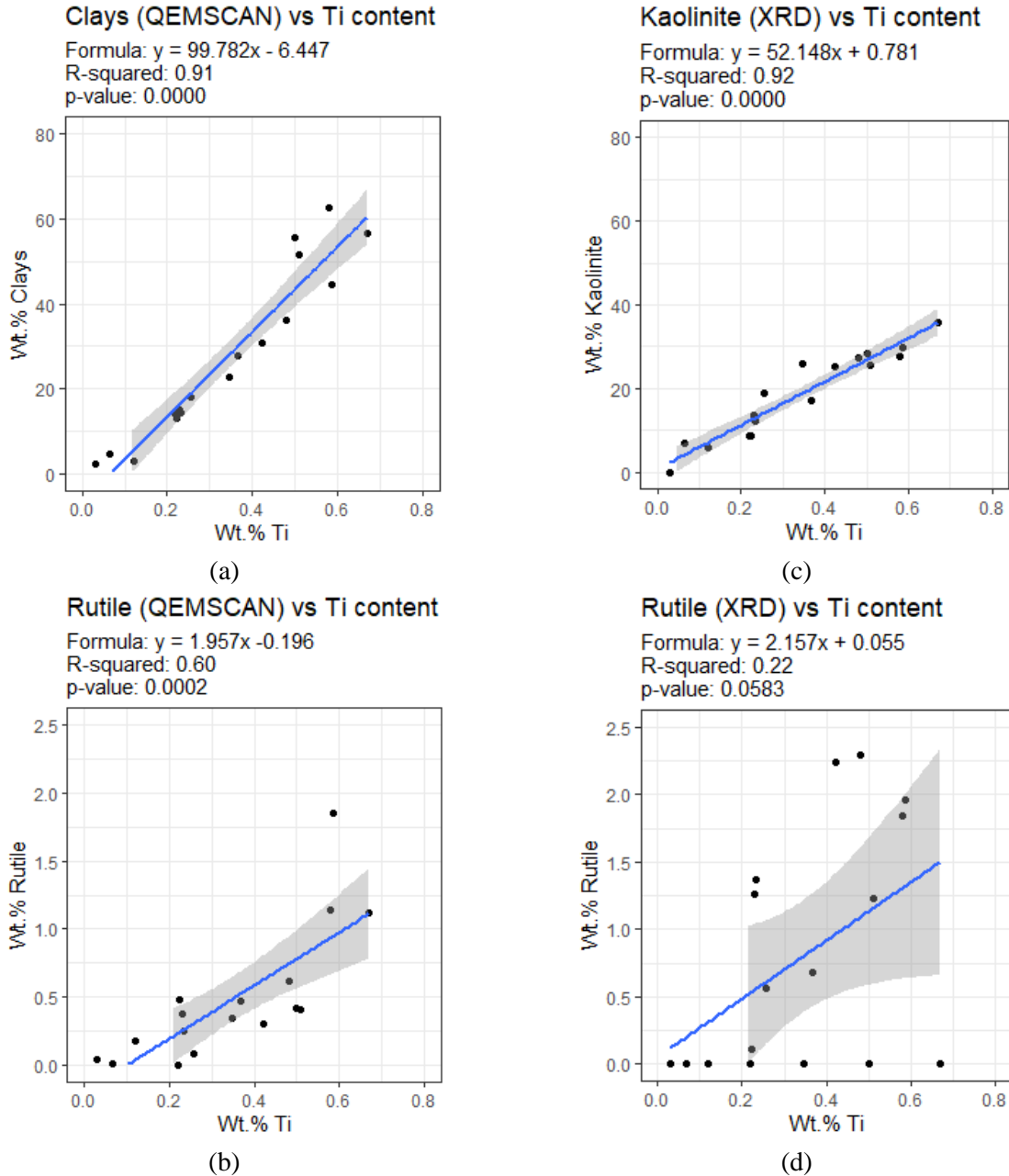
Figure 4-19: Description of titanium accountability by minerals hosts. (a) and (b) represent the relationship between the abundance of clays and rutile (defined by QEMSCAN) to the total assayable titanium content respectively. (c) and (d) represent the relationship between the abundance of kaolinite and rutile (defined by XRD) to the total assayable titanium content respectively. The blue line represents the regression line, and the grey shaded area shows the range of uncertainty.

4.7.2. Description of major element distributions

In paper 1 the distribution of Si, Fe, and Ca was investigated amongst the minerals mapped from the QEMSCAN analysis. As a baseline the major element chemistry (defined by XRF analysis) was assayed to show the distribution profile of elements within each coal. The results showed that the total element content can vary greatly across a range of different coal particle samples. This was based on their relative amounts of carbonaceous and mineral matter (see Figure 4-20a). The assay results also showed that Si, Al, and Fe make up the dominant element species across the samples analysed. While Ca was found to be present in most samples, its abundance was generally much lower than the other elements and variable across the coals. In addition to the elements described, trace abundances of Ti were found across almost all the samples.

To breakdown the distribution of these elements amongst host minerals in the coal particles, the percentage contribution of Si, Fe, and Ca-bearing minerals to the total content of each respective element was analysed (see Figure 4-20b-d). From this analysis it was determined that Si is mainly distributed between quartz and clays. Within the sample set it was generally observed that slightly more silica is distributed in the clays than in quartz (on average 54 and 45 % of the total Si respectively). However, samples Br-PyC and SA-UF1 demonstrate that some coals may contain significantly more Si distributed in quartz than in clays.

Regarding Fe content, Figure 4-20c shows that Fe is distributed amongst a range of minerals (Fe-sulfate, sulfides, carbonates, and iron oxides). Amongst the coals analysed, pyrite was the dominant iron-bearing species for most of the samples. Appreciable amounts of siderite (> 20 % of the total Fe) were observed in several samples, with sample SA-UF1 showing that in some coal particle samples siderite can be the dominant iron hosting phase. Some of the minor Fe-bearing species included minerals such as szomolnokite and rhomboclase, accounting for < 5 % of the total Fe across the samples. The sample Br-PyC displayed a relatively high abundance of rhomboclase (16 % of the total Fe) compared to the other samples. Given that this sample is pyrite rich, this suggests that the sample is likely to have undergone aggressive weathering. In the context of potential health effects, the abundance of secondary alteration products is particularly important to track, as these minerals have been found to more readily release metal cations in solution compared to their primary counterparts (Huang et al, 1994; Plumlee and Ziegler, 2003). Apart from the major and minor phases mentioned, trace proportions of Fe were observed in hematite, goethite, and chalcopyrite. Samples SA-UF1 and SA-UF2, however, reported relatively higher proportions of hematite compared to the other samples (13 and 18 % of the total Fe respectively). The elevated abundance of iron in hematite between these samples suggests the secondary alteration of pyrite to hematite under alkaline conditions, further supported by the elevated abundance of siderite in both samples.

Looking at the distribution of Ca amongst the host minerals defined, the results showed that calcite was the dominant Ca-bearing phase across the sample set (see Figure 4-20d). Generally, the presence of gypsum was also observed at relatively moderate abundances (accounting 25 % of the total Ca on average). However, samples Br-Tail, SA-Dis2, SA-Dis1, SA-MDT, SA-UF2 and Br-PyC show that gypsum can account for substantial proportions of the total Ca in some coals (accounting for 59 % of the total Ca averaged between these 6 samples). The results also highlighted that minor proportions of Ca report to dolomite amongst some of the coal samples, however, this was not consistent across the whole dataset. Similarly, trace proportions of Ca were hosted by apatite in some of the samples, but this was determined to be mostly a rare occurrence based on the relative magnitude.
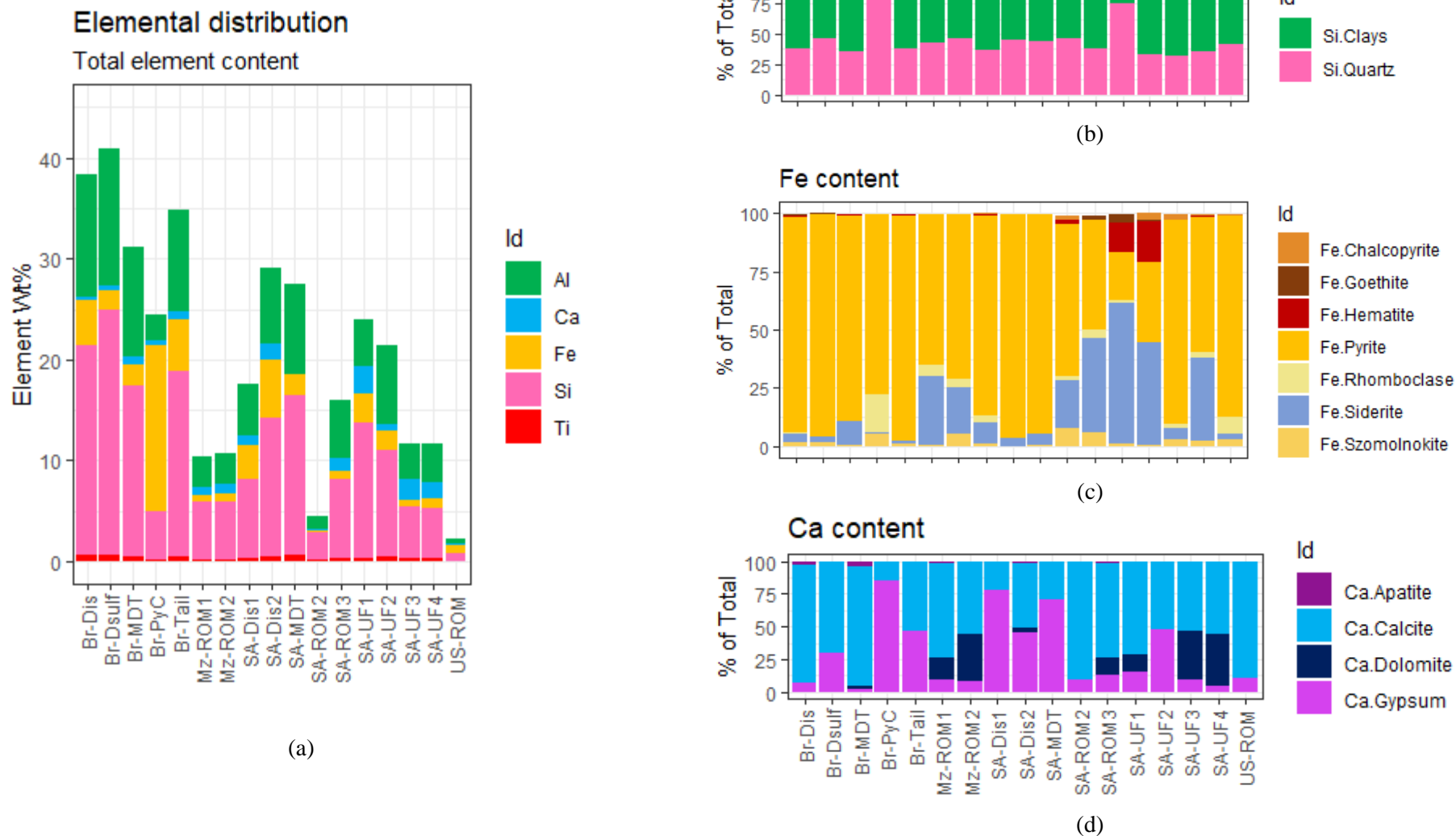
Figure 4-20 Total element content determined by XRF analysis. Figure 4-20a displays the major element content across the samples. Figure 4-20b, c and d show the distribution of Si, Fe, and Ca within host minerals, across the samples analysed respectively computed by the QEMSCAN.

## 4.8. General particle characteristics

In paper 1 a distinction between general and mineral specific particle characteristics was made. This distinction was made to highlight the different classes of information that can be acquired from the particle analysis using QEMSCAN. Apart from composition-based data, additional characteristics such as specific surface area and crystallite size (determined from the XRD diffractograms) were added to the description of general and mineral specific particle characteristics respectively.

### 4.8.1. Particle size

Regarding particle size, the results from paper 1 suggested that samples which displayed a coarser mean size contained a smaller proportion of fines, while samples which reported a finer mean size contained a larger proportion of fines. To determine whether the average particle size could mostly be explained by the fine fraction (particles $< 5$ μm in size), regression analysis was conducted on the larger set of coals. The results of this analysis showed that the percentage of fines in each sample displayed a statistically strong inverse relationship with the mean particle size (see Figure 4-21), thus confirming that the mean particle size is expected to be finer in samples which can produce high proportions of fine particles.
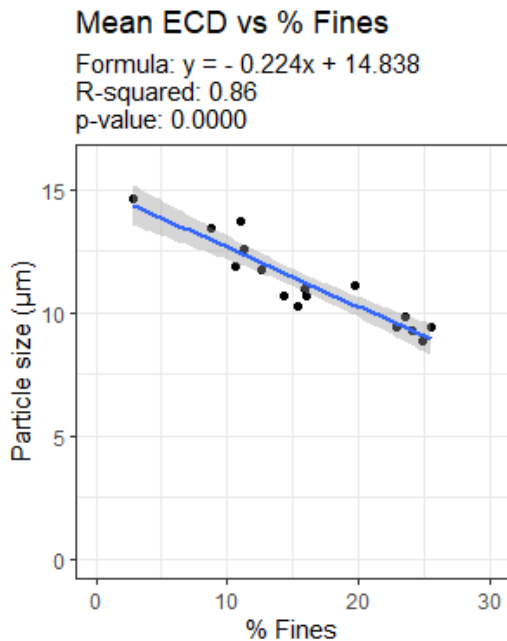


Figure 4-21: Relationship analysis between the mean particle size and the percentage of fines (particles $< 5$ μm in size) reported for each coal particulate sample.

In this context, understanding the potential factors which may result in a greater generation of fines from a parental coal may be important in detecting shifts in the particle size distribution of sampled dust. Studies have shown that ore composition, rock strength, and rock cutting-related factors have been linked

to the generation of fines in the mining context (Colinet et al, 2021; LaBranche et al, 2021; Pan et al, 2021). Paper 1 discussed a potential relationship between the proportion of fines reported and the abundance of clay and carbonaceous matter for each sample. As this relationship was based on the results from four samples, a multilinear regression analysis was conducted on the full set of samples to assess the combined influence of carbonaceous and clay content on the proportion of fines produced. Overall, the analytical results (presented in Table 4-9) show that the abundance of carbonaceous matter and clays in the samples poorly explain the proportion of fines reported by each coal ($R^2 = 0.32$, p-value = 0.0687). Despite this, the model did identify that the abundance of carbonaceous matter (and not clay content) was statistically significant to this weak relationship. Considering the particles were mechanically broken, the result from the analysis suggests that the amount of carbonaceous matter in coal, and by extension a coal's composition-based friability, plays a very limited role in the final proportion of fines. Rather, parameters which relate to the elastic strength of the different minerals, intrinsic grain size, and degree of interconnectivity between grains could play more of an influence on the resulting particle size distributions. In summary, parameters related to the rheology, deformation, and mechanical breakage of the parental material may be more relevant in accounting for the proportion of fines produced from a parental coal than compositional make-up of the particles.

Table 4-9 Multilinear analysis of the relationship between the proportion of fines generated from a sample and the total abundance of carbonaceous matter and clays in each sample.

| Parameter | Value | Estimate p-value relative to model |
|---|---|---|
| Coefficient (Carbonaceous matter) | 0.270 | 0.0339 |
| Coefficient (Clays) | 0.203 | 0.1821 |
| R-squared | 0.32 | |
| Overall model p-value | 0.0687 | |

### 4.8.2. Particle roughness and shape

Regarding particle roughness and shape, the results from paper 1 suggested that fractures generated by the milling processes tended to produce mostly jagged particles with either equant (roughly box-like or ball-like) or angular shapes. To assess whether this observation remained consistent over a wider variety of coal particle samples, boxplots were constructed to understand the distribution of roughness and particle shape categories across the sample population (represented in Figure 4-22). The resulting distributions confirmed that in terms of particle roughness, the majority (35 to 84 %) of the particles analysed reported as jagged (see Figure 4-22a). Additionally, the results showed that of the non-jagged particles, it is more likely that the particles will be intermediate rather than smooth. Amongst the particle shape classes the results demonstrated that particles within this dataset are most likely to report as equant or angular (see Figure 4-22b). Between these two shapes, the results further highlighted that by total proportion particles are mostly likely equant-shaped over angular (between 51 to 84 % abundance equant-shaped particles

across the samples). Considering that these particle shapes and roughness features were suggested to result from fracturing during the milling process, the coupling of these results with those of particle size further suggest that parameters related to particle breakage may be integral in understanding the general particle characteristics of coal particulates.



(a)                                                                                         (b)
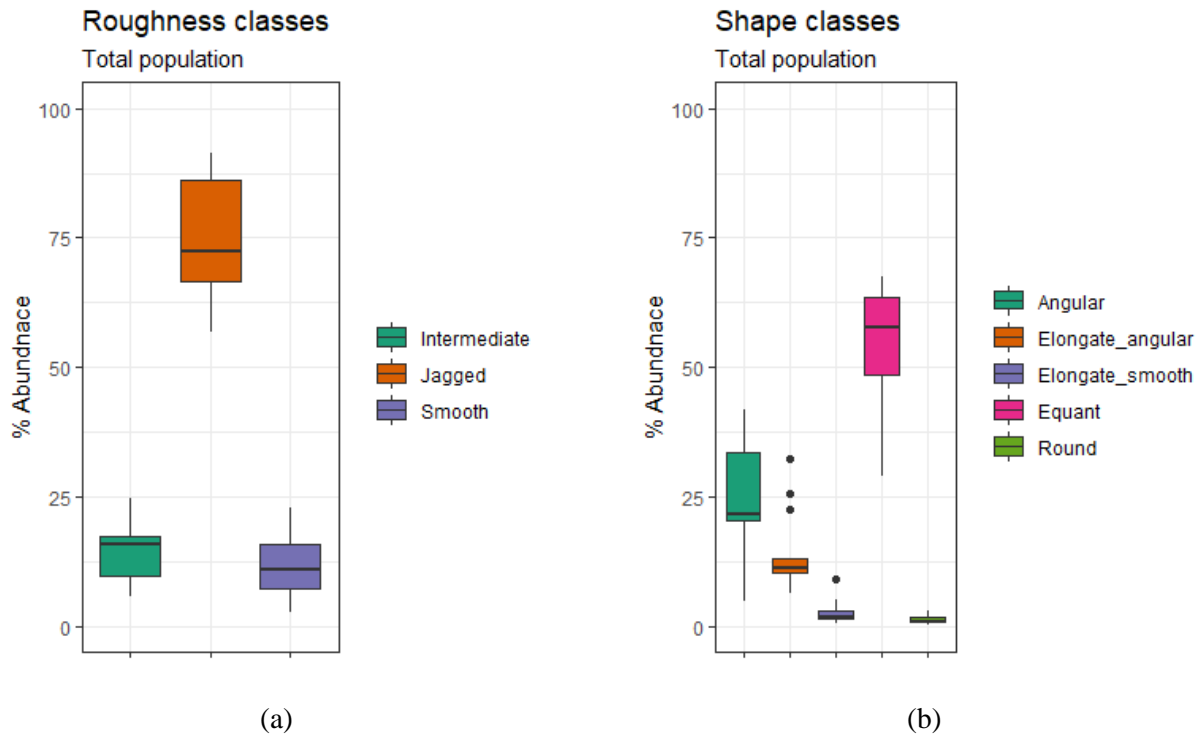
Figure 4-22 Distribution of the particle roughness and shape classes across the sample population. (a) and (b) represent the percentage abundance of the roughness and shape classes amongst the samples analysed respectively.

To assess the relationships between particle roughness and shape, a correlation matrix was constructed comparing the classes from each parameter (see Figure 4-23). The shape classes "elongate and angular" and "elongate and smooth" were omitted from Figure 4-23 as they displayed no relationship between either of these classes. Amongst the remaining classes, strong positive relationships ($R^2 > 0.7$) were observed between round-shaped particles and the roughness classes "smooth" and "intermediate". This suggests that the round particles in the population analysed, are likely to be smoother. The equant particles were observed to have a weak positive relationship with round-shaped particles and a strong positive association with "intermediate" particle roughness ($R^2 = 0.7$). This observation was coupled with the weak relationship equant particles share with angular shapes and jagged particle roughness, which is consistent with the expected box-like/ball-like habit. Angular-shaped particles were found to be negatively associated with other particle shapes and moderately associated with jagged particle roughness ($R^2 = 0.61$). This observation is consistent with the suspected fracturing of particles and the formation of jagged surfaces (suggested in paper 1).
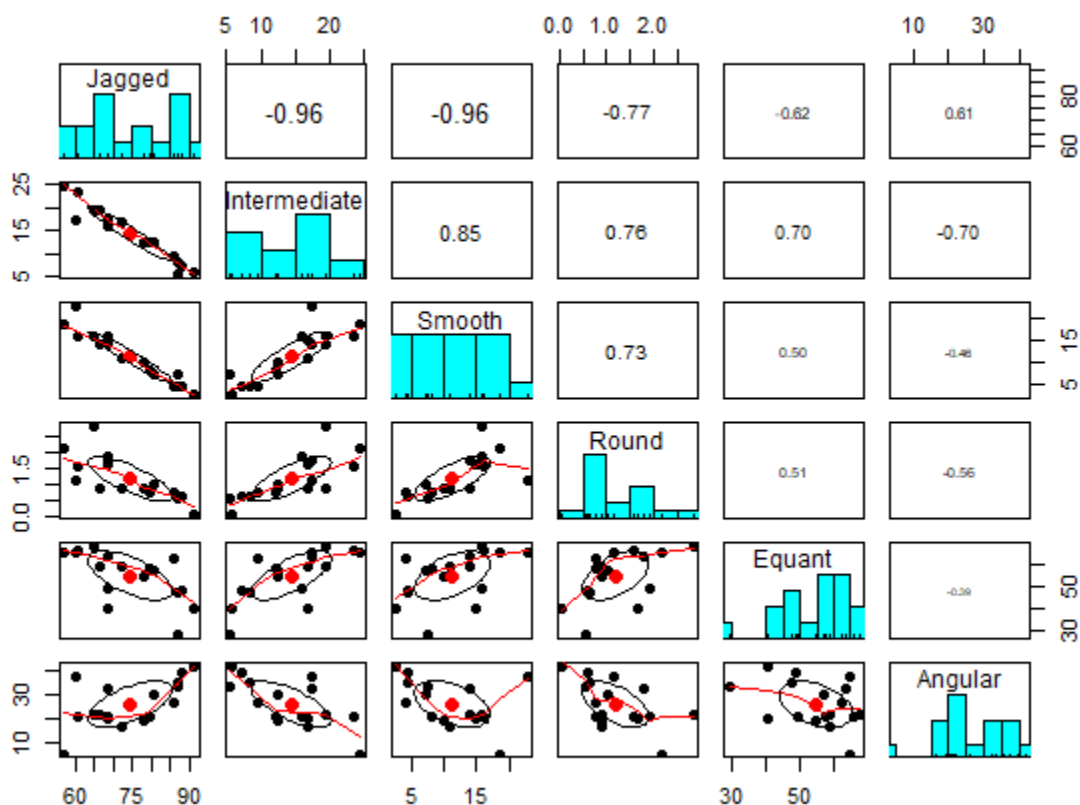
Figure 4-23 Correlation matrix of standardised values of the shape classes: Angular, Equant and Round compared to the roughness classes: Jagged, Intermediate and Smooth. The lower half of the plot shows the spread around the correlation related to the width of the ellipse, the diagonal section of the figure shows the density distribution of each parameter, and the top half of the plot shows the Pearson correlation associated which each association.

### 4.8.3. Specific surface area (SSA)

In the context of biogeochemical reactions, particle specific surface area (SSA) is an important physical parameter which can describe the total surface area available for reaction. As it is not possible to measure specific surface area using either QEMSCAN or XRD analysis, the Brunauer–Emmett–Teller analysis technique was used to quantify the SSA for each sample (see operational information in section 3.4.5). Initially it was assumed that the particulate samples with a higher proportion of fines would yield a larger SSA, however, no relationship was found between SSA and the percentage of fines. As the samples came from different continental locations and geological settings, the SSA for each sample was grouped by the country of origin and represented as boxplots (see Figure 4-24a). The results showed that the mean SSA of coal particulates derived from Brazilian coals was higher than the SSA of particulates generated from South African, Mozambiquan, and USA-based coals. Generally, the Brazilian coals contained more mineral matter than the other localities, and it was thus postulated that the higher relative SSA in these samples

could be related to the formation of milling-related microcracks in the minerals. To test this hypothesis, a regression between SSA and the mineral matter content per samples was constructed (see Figure 4-24b). The results showed that SSA and the total mineral content possess a moderate but statistically significant linear relationship, suggesting that some artefacts of the minerals have an impact on the effective SSA of the sample. Given that mineral reactivity is a key factor in the toxicity of coal dust, understanding the total surface area for reaction may be important parameter in differentiating the effects of composition-based toxicity between coal dust samples. To understand the contribution of the main minerals to this relationship a multivariant model was constructed. Table 4-10 shows that kaolinite and pyrite are the main minerals related to the positive linear relationship between mineral matter and SSA, and quartz does not significantly contribute to this relationship. Furthermore, the results show that pyrite particles have a greater influence on the relationship than kaolinite.

Table 4-10 Multivariant comparison of the main minerals and SSA (model p-value = 0.001).

| Mineral | Coefficient | P-value |
|---|---|---|
| Kaolinite | 0.17 | 0.002 |
| Quartz | -0.08 | 0.115 |
| Pyrite | 0.27 | 0.001 |



(a)                        (b)
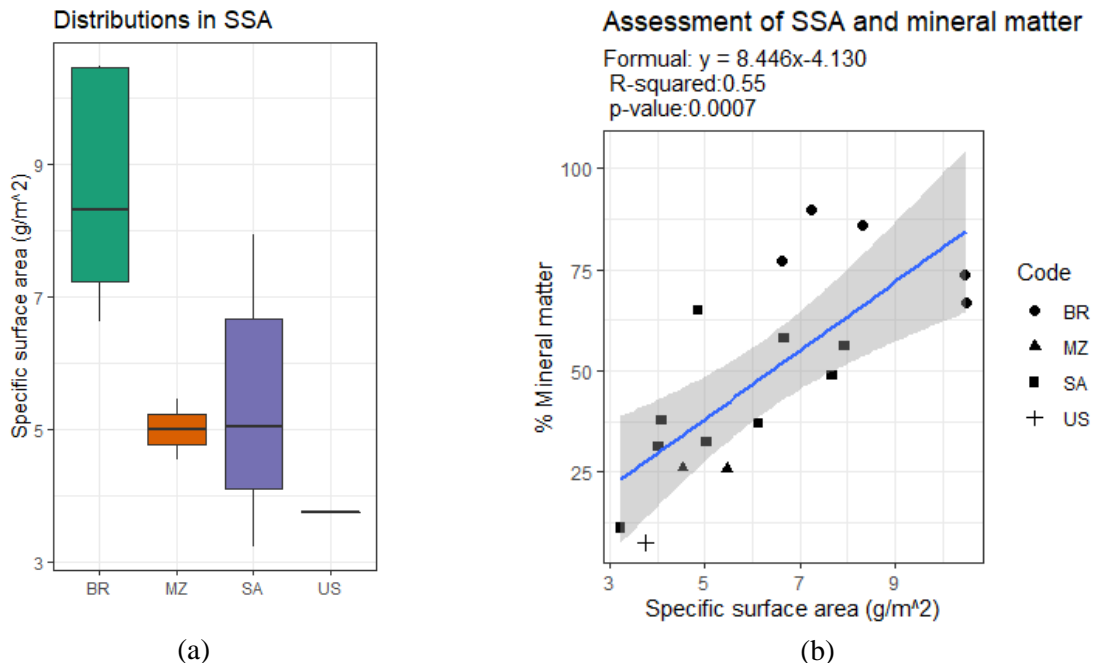
Figure 4-24 Distribution in SSA across the different sample locations. (a) represents these distributions as a boxplot describing the range and median across the sample set. (b) shows the relationship between mineral matter and SSA across the locations.

## 4.9. Mineral specific particle characteristics

Although most coal dust characterisation efforts focus heavily on determining composition and general physical characteristics, it is well understood that mineral specific characteristics such as mineral association and surface structure play an important role in the reactivity of particles on a molecular level. The subsequent sections demonstrate and discuss (1) the distributions of liberated and composite particles, (2) mineral/carbonaceous associations between the main minerals (clays, quartz, and pyrite), and (3) the differences in crystallite size and its relationship with surface reactivity.

### 4.9.1. Liberation and association

In paper 1, the proportion of liberated clay grains greatly varied between the small set of samples analysed. The results from the analysis of a larger set of 17 coals similarly found that the proportion of liberated clays varied widely across samples (see Figure 4-25). This further confirms that when crushed, some coals may contain high proportions of liberated clay grains while others may contain clays in composite particles. For pyrite containing particles, the results demonstrated in paper 1 showed that a low proportion of pyrite occurred as liberated grains while the majority of the pyrite was reported in composites. Whereas the results presented in Figure 4-25 do generally show that a higher proportion of pyrite occurs within composites, the results also display that the proportion of liberated pyrite grains can vary from ~ 2 to 41 % of the pyrite detected. Regarding quartz, the proportion of liberated quartz grains showed little variation (between 22 and 46 % of the quartz detected). Similar results were found across the larger set of coals, however some samples showed as little as ~ 3 % liberated quartz gains. Conversely, some coal contained as high as 58 % liberated quartz gains. Based on the distribution of quartz across the larger set of coals, the results confirm that, whilst the proportion of liberated grains may be higher in some samples, in general, quartz in crushed coal particles mainly occurs within composites.
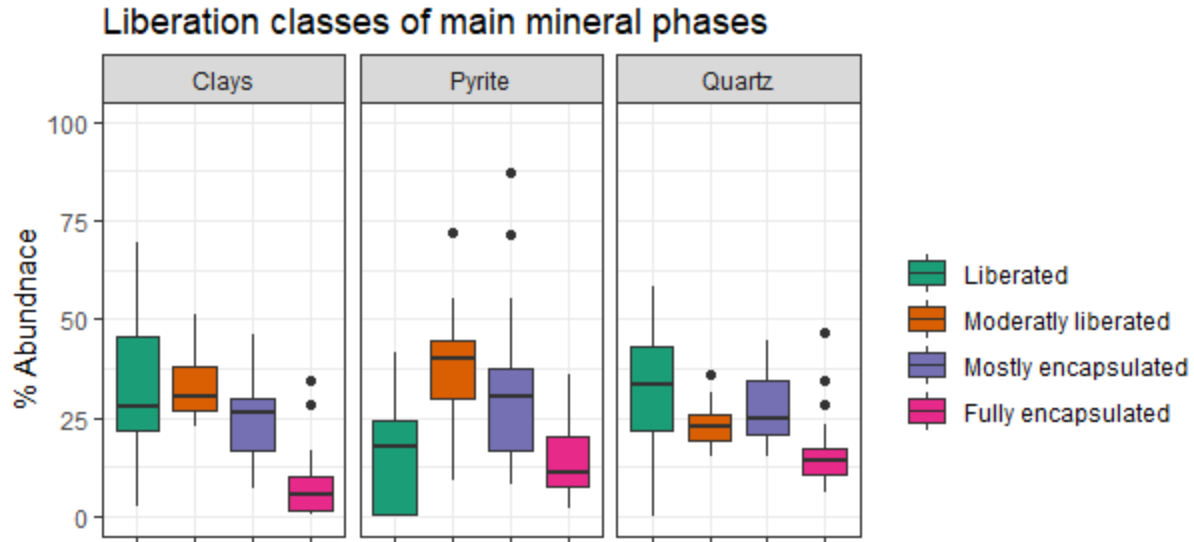
Figure 4-25 Degree of liberation amongst particles containing quartz, pyrite, or clays across the 17 samples investigated.

Considering that the liberation results showed that a substantial proportion of the main mineral phases were contained within composite particles, an understanding of the associated phases in the non-liberated fraction gives a quantitative indication of textural relationships between minerals. In paper 1, the results showed that, apart from carbonaceous matter, clay composites were commonly associated with quartz. Conversely, quartz composites were commonly associated with clays. By assessing the associations of quartz and clay composites across a larger set of coals the results showed similar trends, however, it was found that quartz composites had a higher association to clays than clay composites had to quartz (see Figure 4-26). As the association parameter is a function of pixel adjacency, this result may suggest that the fraction of unliberated quartz is likely to be coated to some degree by clays. Regarding the pyrite composites, the results from paper 1 showed that pyrite was mainly associated with carbonaceous matter and sulfates. Minor associations between additional minerals such as quartz, clays and siderite were also observed within these composites. Similar results were reported in Figure 4-26, which showed that, apart from carbonaceous matter, some of the pyrite composites were highly associated with sulfates and to a minor extent additional phases such as quartz, clays, carbonates, and other sulfides. Ultimately, the results across the larger set of coals reflect that pyrite composites are often oxidised to some extent and are thus commonly associated with sulfates.
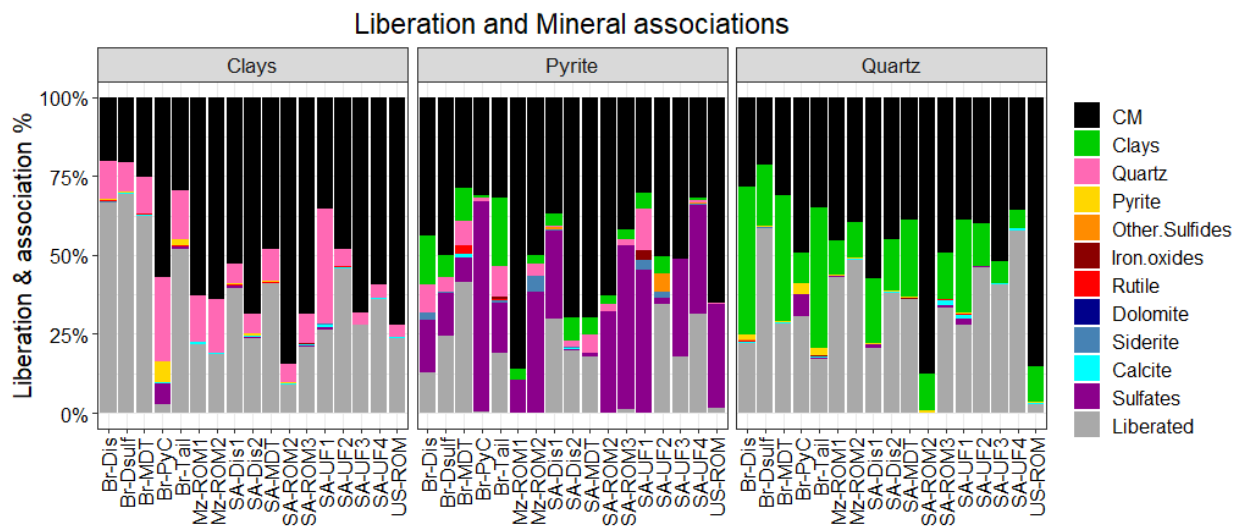
Figure 4-26 proportions of liberated and composite particles. The sets of bar graphs show the percentage association of unliberated clays, pyrite, and quartz particles with other minerals identified.

## 4.9.2. Crystallite size

On a microscale level, crystallite size represents the smallest single crystal in a powdered form. XRD is commonly used to obtain an estimate of crystallite size for each mineral represented in a diffractogram (David et al, 2010). In the context of powders, the size of mineral crystallites has been linked to the prevalence of surface defects in minerals (Warr and Nieto, 1998; Kongsuebchart et al, 2006). As surface defects are known to serve as sites for ROS generation in biological contexts, an investigation into the possible distribution of crystallite sizes between critical minerals may be a useful in understanding the potential surface-related reactivity of these minerals in coal dust.

As the samples came from different continental locations and geological settings, the crystallite size estimates for each target mineral were grouped by the country of origin (represented as boxplots in Figure 4-27). The results show that kaolinite, in comparison to pyrite and quartz, consists of smaller crystallites. This is in line with the fine grain nature of clays and further suggests that kaolinite particles may have fewer surface defects compared to the other target minerals. For pyrite, the crystallite size was found to be roughly consistent across the countries of origin, this was except for the Mozambique samples. The crystallite size of quartz was found to vary widely across the different countries of origin. The quartz analysed from the Brazilian samples was found to show the largest crystallite sizes, with some degree of variation. Additionally, the quartz analysed from the South African samples showed a wide distribution of crystallite sizes, suggesting that different coalfields may possess quartz grains with different crystallite sizes. Based on these results, it can be suggested that quartz grains in coal particles may have the widest variability in crystallite size and by extension surface defects. Given the complex surface reactivity of quartz

in biological systems crystallite size potentially provide an indication of surface reactivity, however, this needs to be explored further and will be addressed in Chapter 5.
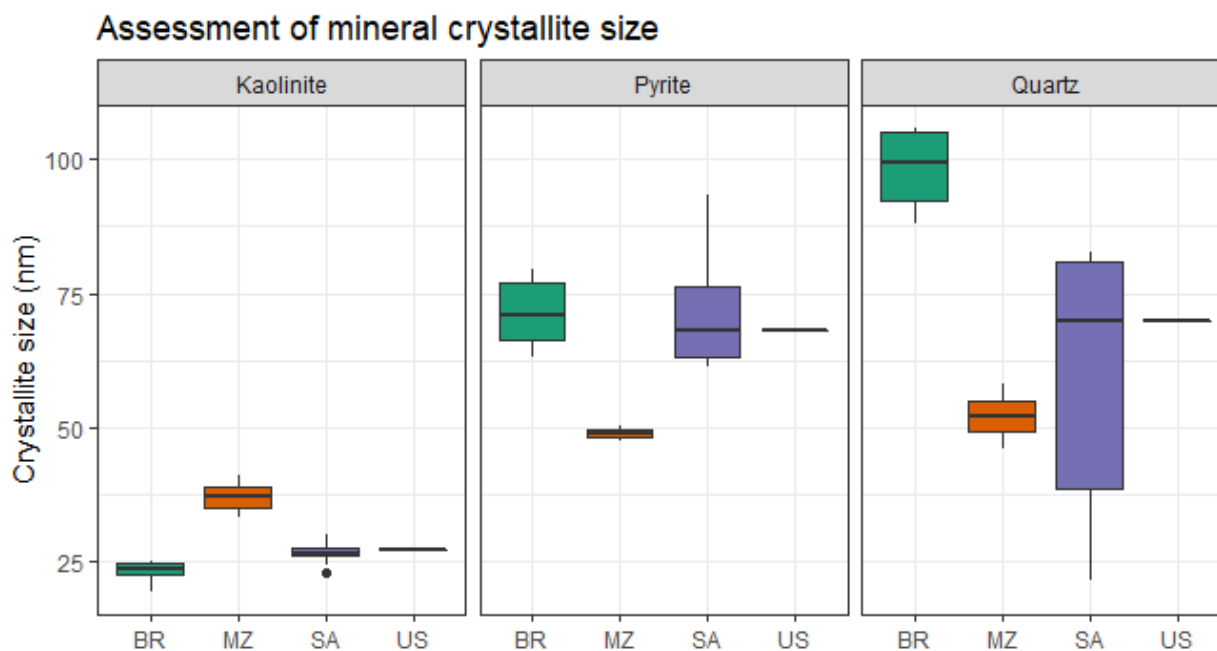


Figure 4-27 Distributions of crystallite size in kaolinite, pyrite and quartz across the samples analysed.

## 4.10. Additional references

Barthelmy, D. (1997) *Webmineral-Mineralogy database*. Available at: https://www.webmineral.com.

Colinet, J. F., Rider, J. P., Listak, J. M., Organiscak, J. A. and Wolfe, A. L. (2021) *Best Practices for Dust Control in Coal Mining, NIOSH*. Available at: http://www.cdc.gov/niosh/mining/UserFiles/works/pdfs/2010-110.pdf.

David, W. I. F., Leoni, M. and Scardi, P. (2010) 'Domain size analysis in the Rietveld method', *Materials Science Forum*, 651(June 2014), pp. 187–200. doi: 10.4028/www.scientific.net/MSF.651.187.

Deer, W. A., Howie, R. A. and Zussman, J. (1992) *An introduction to the rock forming minerals*. 2nd edn. Pearson Parentice Hall.

Huang, X., Zalma, R., Pezerat, H. and Huang, X. (1994) 'Factors That Influence the Formation and Stability of Hydrated Ferrous Sulfate in Coal Dusts. Possible Relation to the Emphysema of Coal Miners', *Chemical Research in Toxicology*, 7(3), pp. 451–457. doi: 10.1021/tx00039a025.

Kongsuebchart, W., Praserthdam, P., Panpranot, J., Sirisuk, A., Supphasrirongjaroen, P. and Satayaprasert, C. (2006) 'Effect of crystallite size on the surface defect of nano-$TiO_2$ prepared via solvothermal synthesis', *Journal of Crystal Growth*, 297(1), pp. 234–238. doi: 10.1016/J.JCRYSGRO.2006.09.018.

LaBranche, N., Keles, C., Sarver, E., Johnstone, K. and Cliff, D. (2021) 'Characterization of particulates from Australian underground coal mines', *Minerals*, 11(5), pp. 1–10. doi: 10.3390/min11050447.

Pan, L., Golden, S., Assemi, S., Sime, M. F., Wang, X., Gao, Y. and Miller, J. (2021) 'Characterization of particle size and composition of respirable coal mine dust', *Minerals*, 11(3), pp. 1–12. doi: 10.3390/min11030276.

Plumlee, G. S. and Ziegler, T. L. (2003) *The Medical Geochemistry of Dusts, Soils, and Other Earth Materials*. 9th edn, *Environmental geochemistry*. 9th edn. Elsevier. doi: 10.1016/B0-08-043751-6/09050-2.

Rasheed, M. A., Rao, P. L. S., Boruah, A., Hasan, S. Z., Patel, A., Velani, V. and Patel, K. (2015) 'Geochemical Characterization of Coals Using Proximate and Ultimate Analysis of Tadkeshwar Coals, Gujarat', *Geosciences*, 5(4), pp. 113–119. doi: 10.5923/j.geo.20150504.01.

Warr, L. N. and Nieto, F. (1998) 'Crystallite thickness and defect density of phyllosilicates in low-temperature metamorphic pelites: A TEM and XRD study of clay-mineral crystallinity-index standards', Canadian Mineralogist, 36(6), pp. 1453–1474.

Weaver, C. E. (1976) 'The Nature of TiO2 in Kaolinite', *Clays and Clay Minerals*. Springer, 24(5), pp. 215–218. doi: 10.1346/CCMN.1976.0240501.

# Chapter 5

# MULTIVARIANT ANALYSIS OF *IN VITRO* RESPONSES TO COAL

# DUST EXPOSURE
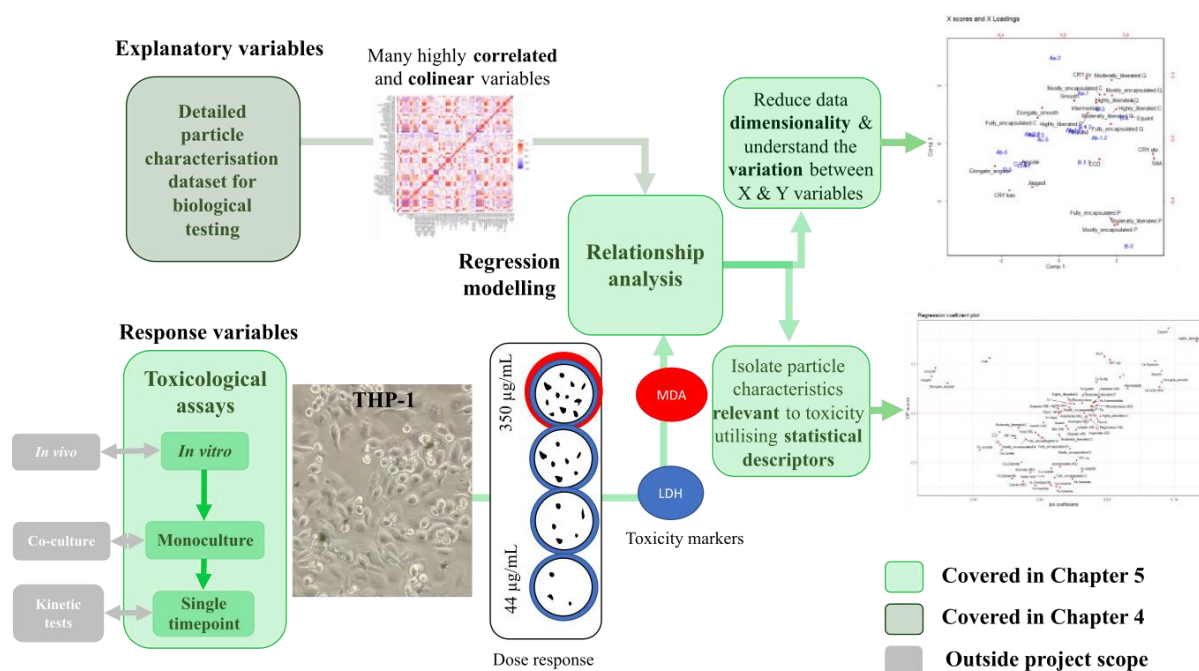


This graphic abstract shows the integration of the particle and toxicological data through relationship analysis and further demonstrates examples of graphical formats for dimensionality reduction (biplot) and the isolation of variables relevant to the response (coefficients plot)

## 5.1. Overview

The work represented in this chapter is a product of the following objective and associated key questions:

> **Overarching objective 2:**
> To investigate the multivariant relationships between the coal particle characteristics and immunological responses (cytotoxicity and oxidative stress) generated from exposed macrophage cells.

> Key question 1: What is the relative significance of the various physicochemical characteristics in relation to their effect on the cells and on what basis can this be determined?

> Key question 2: Is there a difference between the characteristics linked to cytotoxicity compared to those related to oxidative stress?

> Key question 3: Does the addition of detailed particle characteristics (the quantification of mineralogical, chemical and physical characteristics) provide a more holistic picture of the factors influencing toxicity and the underpinning mechanisms compared to more generalised particle characteristics (quantitative phase identification and physical characteristics)?

Within this study, the relationships between an array of particle characteristics and toxic cellular responses were investigated using multivariant regression analysis. As a result, this chapter focuses on developing an approach for assessing the relative significance of particle characteristics in relation to their effects on cells. This was conceived and further demonstrated in technical paper 2 where a Partial Least Squares Regression (PLSR) was used to identify the key influencing characteristics for a number of coal samples. This allowed for the direct discussion of key question 1 and 2 as the two responses were analysed in parallel. Ultimately, this paper illustrates the need to consider a wide range of chemical, mineralogical and physical characteristics in terms of assessing potential toxicity of coal dust. This in turn links back to the third key question for this objective.

---

## Technical paper 2: Multivariant investigation into the relationship between cytotoxicity, oxidative stress, and the physicochemical characteristics of coal dust

---

## Abstract

Mine dust has historically been linked to the development of pneumoconiotic diseases such as silicosis and coal workers' pneumoconiosis. Although studies have established the potential role of physicochemical and mineralogical characteristics in the cytotoxic and proinflammatory nature of dust particles, it remains unclear which parameter(s) could account for the differential toxicity of coal dust. Studies have applied multilinear regressions to elucidate relationships between the characteristics of coal dust and markers of cellular toxicity. While this method allows for the comparison of multiple variables to a response, collinearity between different classes of particle characteristics can affect the model fit and its interpretation. This study aims to address this issue by demonstrating the use of Partial Least Squares Regression (PLSR) to relate and compare the influence of a large array of coal particle characteristics to the markers of cellular damage. The results reflect that the PLSR can define a consistent linear relationship between 72 particle characteristics and markers of cytotoxicity and oxidative stress. Furthermore, by comparing the relative influence of each characteristic to the modelled response, the results reflect that physical characteristics such as shape and particle roughness may have a greater impact on cytotoxicity than composition-based parameters. Based on these results, the significance of a PLSR as a screening tool is discussed in the context of defining variables which represent the "toxic potency" for a set of coal dust samples.

**Status:** This manuscript is planned to be submitted for peer review after the submission of this thesis

## 5.2. Introduction

Mine dust remains a critical issue for the respiratory health of both workers in the occupational settings and proximal communities to mines (Ghose and Majee, 2000b, 2007; Huertas et al, 2012a; Yadav and Jamal, 2018). Historically, dust generated from the mining environment has been linked to the development of pneumoconiotic diseases such as silicosis, asbestosis, and coal workers' pneumoconiosis (CWP). Epidemiological trends in the prevalence of these diseases have shown that CWP is still a pertinent occupational dust disease, accounting for 25 % of the total pneumoconiosis cases reported in a 2017 global disease burden study (Shi et al, 2020). Apart from CWP, it has also been established that other chronic respiratory diseases may also result from coal dust exposure (Leonard et al, 2020).

By investigating the pathways leading to coal dust-induced disease development, several mechanistic studies have attributed cell/tissue damage to perpetual cycles of stress and inflammation (Dalal et al, 1995; Vallyathan et al, 1998; Zhang et al, 2002; Cohn et al, 2006a; Huang et al, 2006). To sustain these cycles, it was established that biogeochemical interactions between the deposited particles and the lung physiology could create a feedback loop producing both cell and particle-mediated generation of reactive oxygen species (ROS). Under these circumstances perpetuated oxidative damage is expected to lead to cytokine and chemokine synthesis, and the production of growth factors and lysosomal enzymes (Vallyathan et al, 1998; Schins and Borm, 1999).

In assessing the potential role that particle characteristics play in the molecular and cellular mechanisms leading to coal dust toxicity, physical, chemical, and mineralogical particle characteristics have been found to contribute to ROS production, lipid peroxidation, cytotoxicity, and collagen production (Gormley et al, 1979; Reisner et al, 1982; Vallyathan et al, 1998; Trechera et al, 2020; Song et al, 2022; Sun et al, 2022). Based on the relationships described in these studies and other mechanistic research by Lison et al (1997); Champion and Mitragotri (2006); Fubini and Fenoglio (2007); Turci et al (2016); and Sun et al (2021, 2022), characteristics such as particle surface area and reactivity, shape, bioavailable iron content and free quartz content have been identified as agents responsible for cellular damage. While these studies have demonstrated the importance of particle-based parameters in the generation of ROS and proinflammatory responses, no consensus could be reached on a single causal agent across the analyses. Ultimately, the complex relationships between the characteristics of coal dust and their combined relation to the toxic responses on a cellular level remains unclear.

To address the lack of clarity in the combined relationships between the physicochemical and mineralogical characteristics of coal dust and cellular responses, multiple linear regression analysis has been applied to a large array of parameters (Trechera et al, 2021b, 2021a; Shangguan et al, 2022). By regressing pairwise combinations of geochemical and mineralogical parameters on the measures of oxidative potential for each coal sample, several statistically significant relationships explaining the

variability in the response could be interpreted. However, the application calls for the construction of a multitude of parameter combinations which would then need to be filtered based on statistical significance. Apart from this, the analysis of any coefficients from these models could potentially be impacted by collinearity, which is a particular issue for large datasets of complementary information (such as geochemical and mineralogical data). Moreover, such an approach does not provide a holistic understanding of how the variation in the sample characteristics impacts the response or how the magnitude of their influence can be compared between different classes of particle characteristics.

Currently, there is no concise and reproducible application of multivariant analysis to define dependency relationships between a large array of variables in the context of coal dust characteristics and cellular responses. This study aims to demonstrate the use of a Partial Least Squares Regression (PLSR) and discriminant analysis to determine associations between a large array of physicochemical and mineralogical characteristics of coal particles to the markers of cytotoxicity and oxidative stress in a single linear function. In doing so the study shows the relative significance of an array of physicochemical and mineralogical characteristics to different levels of cytotoxicity and lipid peroxidation amongst different coals. As part of this application, the study further demonstrates the significance of discriminant analysis as a screening tool for the selection for variables which can represent the "toxic potency" of a set of coal dust samples. In this way, the study presents a reproducible application of multivariant analysis that can be used to assess the characteristics of dust-sized coal particles which strongly influence cellular damage and stress, whilst discussing the relevance of different data classes in describing variability in the toxic responses observed.

## 5.3. Materials and methods

Apart from a description of the materials used in this study, two datasets representing the set of explanatory and response variables are reported. Dataset 1 describes the characteristics represented in the detailed particle characterisation dataset (Section 2 of Chapter 4) and the methods used to acquire the data. Dataset 2 reports the *in vitro* assays used and the experimental setup used to obtain the response data. Finally, the statistical analysis methods are described.

### 5.3.1. Coal particle samples

A set of bituminous coals from collieries-based in South Africa, Brazil, the USA and Mozambique were used to obtain a spectrum of different coal particle populations (see Table 5-1). As this study utilised run of mine, tailings and discard coal samples sourced from various stages of the coal processing plants, the size of the parental coal samples ranged considerably between 5 cm and 180 μm. As a result, the samples were milled to a passing size of 25 μm, where the material was sieved to reach an appropriate mass for all the analyses and experiments. To further understand the distribution of particle sizes in each sample the

size distributions were quantified using laser diffraction. For this, a Mastersizer 2000 (based at the Department of Environmental and Geographical Sciences, University of Cape Town) was used. From this the D50 (median particle size) was determined to be approximately 10 μm. On the basis of this, the particulate samples were defined to represent dust-size coal particulates.

Table 5-1 Description of samples presented in the study and the D50 representing the median particle size determined with the Malvern Mastersizer 2000 (Pananalytical)

| Sample name | Waste stream | Country | Coal field | D50 (μm) |
|---|---|---|---|---|
| SA-Dis1* | Discard | South African | Mine G Waterberg coal field | - |
| SA -UF1 | Ultrafine thickener underflow | South African | Mine G Waterberg coal field | 11.02 |
| SA -MDT | Medium dense wash waste | South African | Mine L Witbank coal field | 8.49 |
| SA -Dis2 | Discard | South African | Mine G Witbank coal field | 9.73 |
| SA -UF2 | Ultrafine thickener underflow | South African | Mine L Witbank coal field | 9.53 |
| SA -UF3* | Ultrafine coal | South African | Mine G Witbank coal field | - |
| SA -UF4 | Ultrafine coal | South African | Mine P Witbank coal field | 9.78 |
| SA -ROM3 | Run of mine | South African | Sasolburg coal field | 9.66 |
| SA -ROM2* | Run of mine | South African | Witbank coal field | - |
| Br-MDT | Medium dense wash waste | Brazilian | Santa Catarina coal field | 7.18 |
| Br-DSulf | Desulfurised coal | Brazilian | Santa Catarina coal field | 8.85 |
| Br-PyC | High pyrite concentrate waste | Brazilian | Santa Catarina coal field | 10.42 |
| Br-Tail | Coal from Dump | Brazilian | Santa Catarina coal field | 8.36 |
| Br-Dis | Discard | Brazilian | Santa Catarina coal field | 7.70 |
| Mz-ROM1* | Run of mine | Mozambican | | - |
| Mz-ROM2* | Run of mine | Mozambican | | - |
| US-ROM* | Run of mine | USA | Pittsburgh coal field, Pennsylvania | - |

\* For coals that displayed hydrophobic properties, no reading size could be collected

## 5.3.2. Dataset 1: Sample Characterisation information

To develop a robust understanding of the sample characterisation, various methods were employed to quantitatively measure the physicochemical and mineralogical parameters of the particles. Dataset 1 therefore represents a description of the mineral and element distributions, as well as the general and mineral specific characteristics of the particles. In Appendix D, Figure D-1 demonstrates the associations between parameters within each class of data and the groups of samples with similar particle characteristics.

### 5.3.2.1. Mineralogical data

To understand the mineral assemblages present within each of the samples, XRD analysis was employed to positively identify minerals based on their crystal structure. The measurements were conducted by XRD Analytical and Consulting using a Malvern Panalytical Aeris diffractometer with a PiXcel detector and fixed slits with Fe-filtered Co-Kα radiation. A randomly ordered powder mount of the sample was prepared for analysis using the back-loading method. From this, the diffraction patterns were measured in the scan range 5.0000–80.0002° at 2Θ, with a step size 0.0217° at a count time of 48.195 s per step. To identify and quantify the crystalline phases from the diffractogram, the Bruker DIFFRAC.EVA software

was used by applying the Rietveld refinement method (Scrivener et al, 2004). Refer to Section 4.7.1. for a full description of the minerals identified.

In addition to the XRD analysis, the particles were mineralogically mapped using a FEI QEMSCAN 650F auto-SEM-EDS instrument. For this analysis the SEM was operationally set to at run at a beam energy of 15 keV, accelerating current of 9 nA, working distance of 13 mm and 1000 times magnification across all the samples. The resulting mineral maps represent simplified groups of minerals which have been outlined in section 4.7.1. and Appendix C.

5.3.2.2. Chemical data

An understanding of the major element distributions was established by assaying each coal via XRF analysis. Each coal sample was milled split and then homogenised into a fusion disk where it was subsequently analysed using a Panalytical Axios Wavelength Dispersive spectrometer. These measurements were conducted at the Central Analytical Facilities, Stellenbosch University, Stellenbosch, South Africa. Major elements were analysed on a fused glass disk using a 2.4 kW Rhodium tube. Matrix effects in the samples were corrected by applying theoretical alpha factors and measured line overlap factors to the raw intensities measured with the SuperQ PANalytical software. Refer to section 4.7.2 for a full description of the major element chemistry.

To further understand how these elements are distributed amongst host minerals, the mineral maps defined by the QEMSCAN were used to quantitatively assess the distribution of the major elements amongst the mineral groups identified. Refer to section 4.7.2 for a full description of element distributions.

5.3.2.3. General and mineral specific particle characteristics

In earlier work by Kamanzi et al (2022), coal particle characteristics were grouped as general characteristics (shape and size) and mineral specific characteristics (mineral liberation), based on the types of data generated from the auto-SEM-EDS characterisation of these particles using QEMSCAN. Refer to sections 4.8 and 4.9.1. for a full description of these parameters across the sample set.

As these parameters cannot capture surface related features additional parameters such as specific surface area and crystallite size were added to the general and mineral specific characteristics respectively. To measure specific surface area, a Micromeritics Tristar II 3020 instrument was used to measure the amount of adsorbed nitrogen corresponding to a monomolecular layer on the surface of the sample. This was conducted at the Analytical Laboratory based at the Department of Chemical Engineering within the University of Cape Town. To ensure that no absorbed gasses or vapours are present on the sample through handling, preparations were made by "outgassing" before the measurement at 120°C for 12 hours.

To determine estimates of the crystallite size of target minerals, the XRD diffractograms were processed in the Bruker software TOPAS using the Scherrer equation in the Rietveld method (David et al, 2010).

### *5.3.3.* Dataset 2: Exposure responses *in vitro*

To demonstrate the relative potential of a variety of the coal particulate samples to induce cellular damage, an *in vitro* THP-1 macrophage cell culture model was established to measure cell viability and oxidative stress induced by the respective characterised particle samples. Dataset 2 therefore represents the quantitative measures of cytotoxicity and lipid peroxidation which provide an indication of cell death and oxidative stress respectively across the sample set.

#### 5.3.3.1. Cell culture and treatment

For this study, THP-1 cells (a human leukemia monocytic cell line) purchased from ATCC (American Type Culture Collection) were cultured in T75 tissue culture treated flasks (Greiner CELLSTAR) with RPMI 1640 culture medium supplemented with 10% Fetal Calf Serum (FCS) (Gibco) and 1% Penicillin-Streptomycin (Gibco) at 37°C in a humidified 5% $CO_2$ atmosphere. To assay for the compounds relevant to cytotoxicity and lipid peroxidation, a generalisable experimental setup was developed to assess the toxicity of the 17 coal particulate samples based on prior *in vitro* experimental procedures described in Lee et al, (1996); Maanen et al, (1999); Schins and Borm, (1999); Basil and Zosky, (2019). Figure 5-1 depicts the plate configuration used for the two response markers, as the nature of these assays differed in terms of the mass of sample utilised (number of cells), separate plate configurations were used.

## Cytotoxicity plate design

N= 4 samples/plate, 2-3 replicates
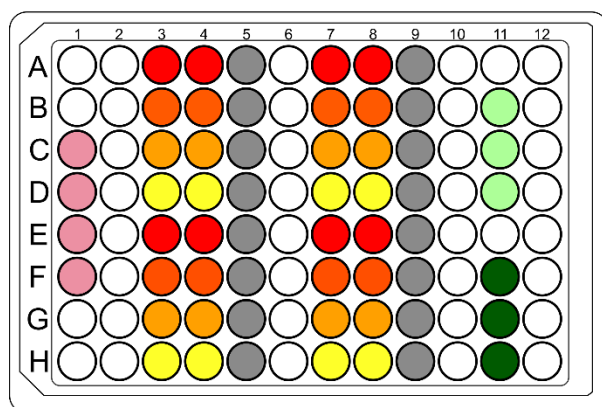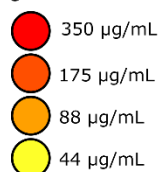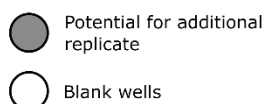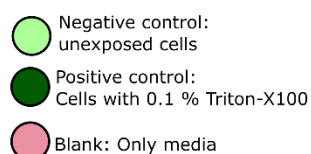
## Lipid peroxidation plate design

N= 5 samples/plate with negative control or 6 samples/plate, 2 replicates
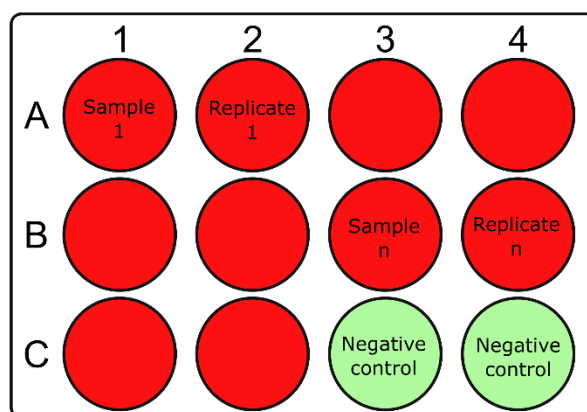


Figure 5-1 Experimental plate design of the two plate configurations for the cytotoxicity and lipid peroxidation assays

For the LDH assay, flatbottom 96-well plates were seeded at $23x10^4$ cells/well (143 750 cell/cm$^{2)}$) (~ 40% confluency) with 50 ng/mL phorbol 12-myristate-13-acetate (PMA) to allow the cells to differentiate to macrophages (final volume of 200μL/well). In contrast the experimental setup for the lipid peroxidation assay utilised a 12-well plate that was seeded at a density of $1x10^6$cells/well (263 157,9 cells/cm$^{2)}$) in medium containing 50 ng/mL of PMA (final volume 1 mL/well). For both assays the media was removed twenty-four hours after seeding and replaced with UV-sterilised stock coal particle suspensions.

A concentration gradient of 350, 175, 88, 44 μg/mL ( 218,8; 109,4; 55; 27,5 μg/cm$^2$ respectively) was used for the cytotoxicity assay (illustrated in Figure 5-1). Each experimental well was only replicated once, this was due to the high volume of samples and limited availability of reagents. In addition to the experimental wells, blank wells (only media) as well as negative and positive controls (media only and 0.1% Triton X-100 respectively) were added to each plate.

Preliminary data from the cytotoxicity assay showed that a more pronounced signal could be measured at the 72-hour timepoint compared to the 24-hour point. For this reason, the subsequent tests were thus conducted at the 72-hour timepoint. Additionally, the preliminary analysis showed that a particle concentration of 350 μg/mL produced responses that were statistically significant from the negative control. Based on this, the exposure conditions for the lipid peroxidation assay were set at a particle concentration

of 350 µg/mL incubated for 72-hours, to obtain a strong measurement signal. Notably, the lipid peroxidation assay was only conducted on coals which displayed cytotoxicity greater than 10 % at this concentration.

5.3.3.2. LDH assay

The amount of LDH produced in the sample was assayed using a colourimetric assay kit (Roche) developed for the quantification of cell death and cell lysis. At the end of the 72-hour exposure period, 100 µL of the culture supernatant from each well was carefully removed and transferred to a clear flat bottom microplate (Nunc, Thermo Scientific). To determine the activity of LDH from the supernatant, 100 µL of the kit reaction mixture (containing the reaction catalyst and dye solution) was added to each well of the microplate and set to incubate protected from light for 30 minutes and the absorbance read at 490 nm using an ELISA reader (VersaMax, Molecular Devices). In determining the percentage cytotoxicity, the average absorbance values of the sample replicates were subtracted from the background control and substituted in equation 5-1.

$$\% \; Cytotoxicity = \frac{sample\;value - low\;control}{high\;control - low\;control} \times 100 \qquad \text{Eq. 5-1}$$

As a baseline, the dependency relationship between the coal particle dose and the elicited response was assessed for the cytotoxicity results by initially plotting the data to assess the fit of the relationship. Thereafter, the data was fitted to a linear function where the strength and significance of the relationship was examined by the Pearson correlation and the p-value ($< 0.05$ was deemed as significant). Based on these defined relationships, the gradient of each model was extracted as a single value to represent the dose-relationship of each coal.

5.3.3.3. Lipid Peroxidation assay

Lipid peroxidation is considered as a useful marker of oxidative stress as the degradation of lipids (polyunsaturated lipids), resulting from oxidative damage, produces a well-defined chain of reaction end-products such as malondialdehyde (MDA). The extent of oxidative damage produced from the particle-cell interaction was measured using a lipid peroxidation assay kit (Sigma-Aldrich) which quantified the MDA concentration through its reaction with thiobarbituric acid (TBA) forming a colourimetric product proportional to the MDA present in the sample. After the 72-hour exposure period, the sample was prepared by removing the supernatant and washing the cells with ice cold PBS (Phosphate-Buffered Saline, Gibco) after which, 300 µL of lysis buffer and 3 µL BHT (butylated hydroxytoluene) were added to the samples and placed on ice for 45 minutes. The wells were subsequently scrapped, and the cell samples were placed in microcentrifuge tubes and spun at 7 600 rpm for 10 minutes. From this, 200 µL of the supernatant was

placed in new microcentrifuge tubes with 600 μL of the TBA solution and incubated at 95°C for 60 minutes. Afterwards, the tubes were allowed to cool for 2 minutes in an ice bath. Finally, 200 μL of the reaction solution from each vial was pipetted into a 96 well plate and at the absorbance was read at 532 nm using an ELISA reader (VersaMax, Molecular Devices). The final MDA concentration was quantified by comparing the samples to a standard curve determined synchronously with the samples. The results were then normalised to the percentage viable cells as the dead cells would not contribute to the MDA concentrations.

### 5.3.4. Statistical analysis

To assess the relative significance of the coal particle characteristics (X variables) to the resulting exposure-based responses expressed *in vitro* (Y variables), a Partial Least Squares regression (PLSR) was applied as a tool to model the multivariant relationships between these variables. Generally, the PLSR operates by regressing the X and Y variables as a function of the product of two smaller matrices called scores (latent components) and loadings (Abdi, 2010). In its final form Y is regressed by the X scores instead of X (in the form of a linear regression Y=BX), this allows the model to perform in cases where variables are colinear and where there are more variables than samples (further expanded in Mevik and Wehrens (2007)). The PLSR model was conducted in R 4.0.3 (RStudio Team, 2020) using the *pls* package (Mevik, 2022) with the SIMPLS algorithm (De Jong, 1993) on standardised data with a cross-validation (CV) step to assess the model performance per component generated.

## 5.4. Results

### 5.4.1. Effect of dust-sized coal on macrophage viability and ROS-related damage

As a baseline for understanding the direct particle-induced cytotoxicity, an LDH assay was conducted to measure cell death related to cytosolic damage. Figure 5-2 demonstrates the dose response nature of the various coal samples across a concentration gradient of 350, 175, 88, and 44 μg/mL. Through inspection of the results, three degrees of cytotoxicity could be identified for the coals (high, moderate, and low), based on distinct clusters of samples at the 350 μg/mL dose.

In addition to defining the toxicity classes, the dose-response relationships were modelled based on a linear regression to determine whether the gradient of each modelled sample could be used as a summary descriptor for the intensity of cytotoxic responses. From these results, it was established that all responses relationships could be explained by separate linear regressions. This further suggests that different coal particles display a similar mechanism of cytotoxicity which can be modelled linearly, but the intensity of the response may differ due to the inherent properties of the particles. In determining the validity of the defined relationships, the goodness of fit and strength of the relationship was defined using the adjusted correlation coefficient and p-value (represented in Appendix D, Table D-1).
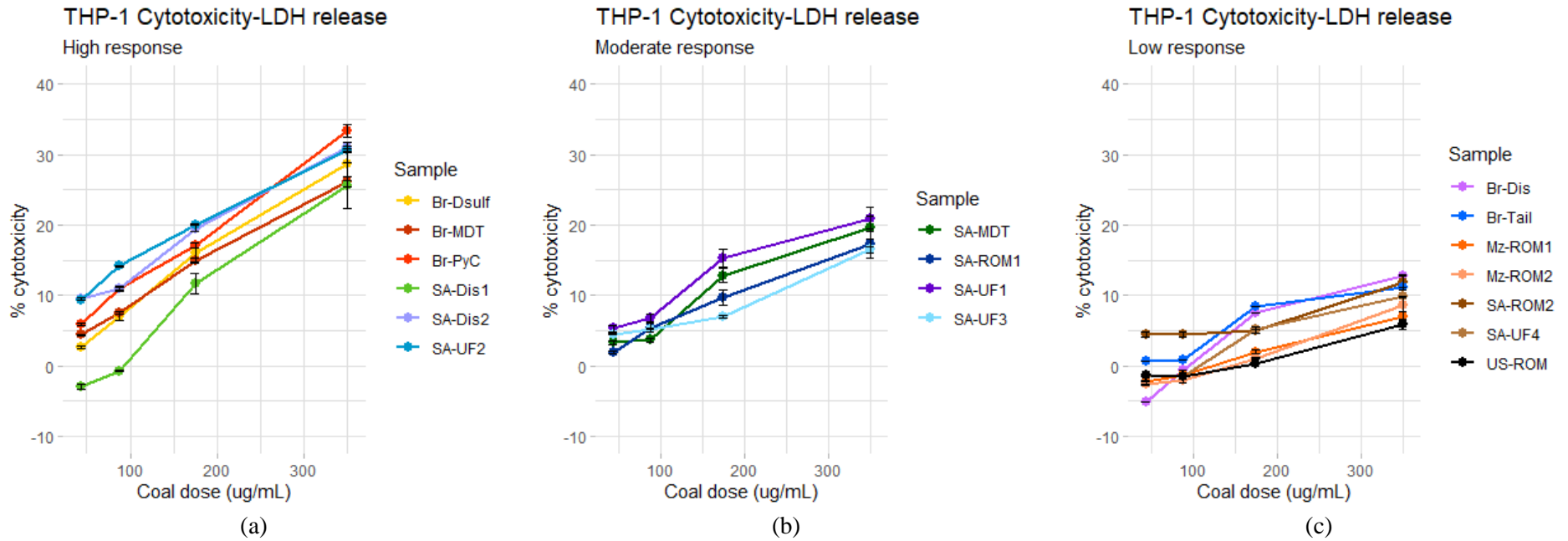
Figure 5-2 depicts the dose-response relationship between the different coal particle samples at the 72-hour timepoint (exposure concentrations 350, 175, 88, 44 µg/mL (218,8; 109,4; 55; 27,5 µg/cm² respectively)). Figures a, b and c represent the samples that have been subdivided into high, medium, and low cytotoxic responses based on clusters observed at the 350 µg/mL concentration. For reference the relative error reported at each concentration was less than 3.5 % across the samples analysed

To determine the extent to which macrophages can be affected by ROS-related damage an MDA assay was conducted which measured the extent of lipid peroxidation induced from the exposure. The results from this assay are represented in Figure 5-3 which reflect the amount of MDA produced from viable cells relative to a baseline of unexposed cells. Only samples which displayed greater than 10 % cytotoxicity were assayed due to limitations in reagent availability. The results reflected that samples which displayed the highest levels of cytotoxicity generally elicited a higher release of MDA than samples which showed low toxicity. Such findings are in line with a similar study by Vallyathan, (1994) which observed a positive correlation between the extent of lipid peroxidation and cytotoxicity and additional studies such as Zhang et al (2002); Harrington et al (2013); Orona et al (2014); and Sun et al (2021), which have demonstrated links between oxidative stress and cytotoxicity. This may further imply that the mechanisms related to oxidative stress may also influence the level of cytotoxicity as suggested by Yang et al (2009) and Sun et al (2022).
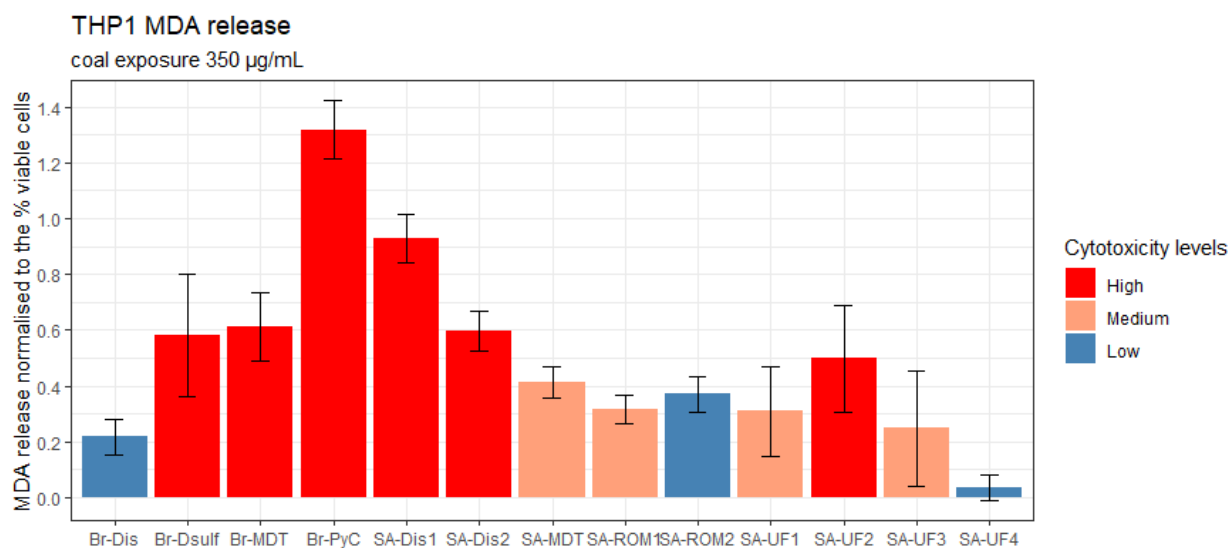


Figure 5-3 Displays the degree of lipid peroxidation produced from the THP-1 cells from a 72-hour exposure with 350 µg/mL ( 92,1 µg/cm$^{2)}$ of the particle samples (classed by colour based on their cytotoxicity response). The amount of MDA released relative to the negative control was normalised by the percentage of viable cells based on the results of the LDH assay. For reference, the relative error across all measurements was observed to be less than 0.2 units.

## 5.4.2. Analysis of particle-cell relationships

Separate models were constructed for each response to compare whether the parameters relevant to lipid peroxidation can also be identified as influential to cytotoxicity.

5.4.2.1. Demonstration of particle-cell relationships using latent structures

Upon initialisation, the model was allowed to define as many components needed to maximally explain the variance in both X and Y whilst computing the cross-validated predictions per component (see Table D-2 in Appendix D). From this process, the PLSR determined 3 and 4 components which accounted for 91 and 98 % of the variance in the LDH and MDA responses respectively. As overfitting is a common issue for PLSR, due to the number of correlated variables, the cross-validated predictions per component were chosen to assess whether the model was subject to overfitting. In doing so, the difference between the RMSEP (root mean squared error of prediction) generated from the model with n components (CV) and the cross-validated model with the sample number of components (adjCV) was computed and considered based on their similarity – (see Table D-2 in Appendix D).

Figures 5-4 to 5-6 provide a visual description of the defined relationships in the form of a loadings plot. To aid in the interpretability of the plots the characteristics were broken into groups representing: mineral and element-related data (Figure 5-4); mineral specific data (Figure 5-5); and general particle characteristics (Figure 5-6). The characteristics represented in each figure were further classified by relative importance using VIP (Variable of Importance) scores. By definition model parameters which report a VIP score greater than 1 signifies a relevant contribution to the model and those with a score less than 1 may be excluded (Galindo-Prieto et al, 2014; Gómez-Gener et al, 2018). For the Biplots shown in Figures 5-4 to 5-6 the categories less, moderately, and highly influential relate to parameters with VIP scores less than 1, between 1 and 1.25, and greater than 1.25 respectively.

(a)                                                                                           (b)
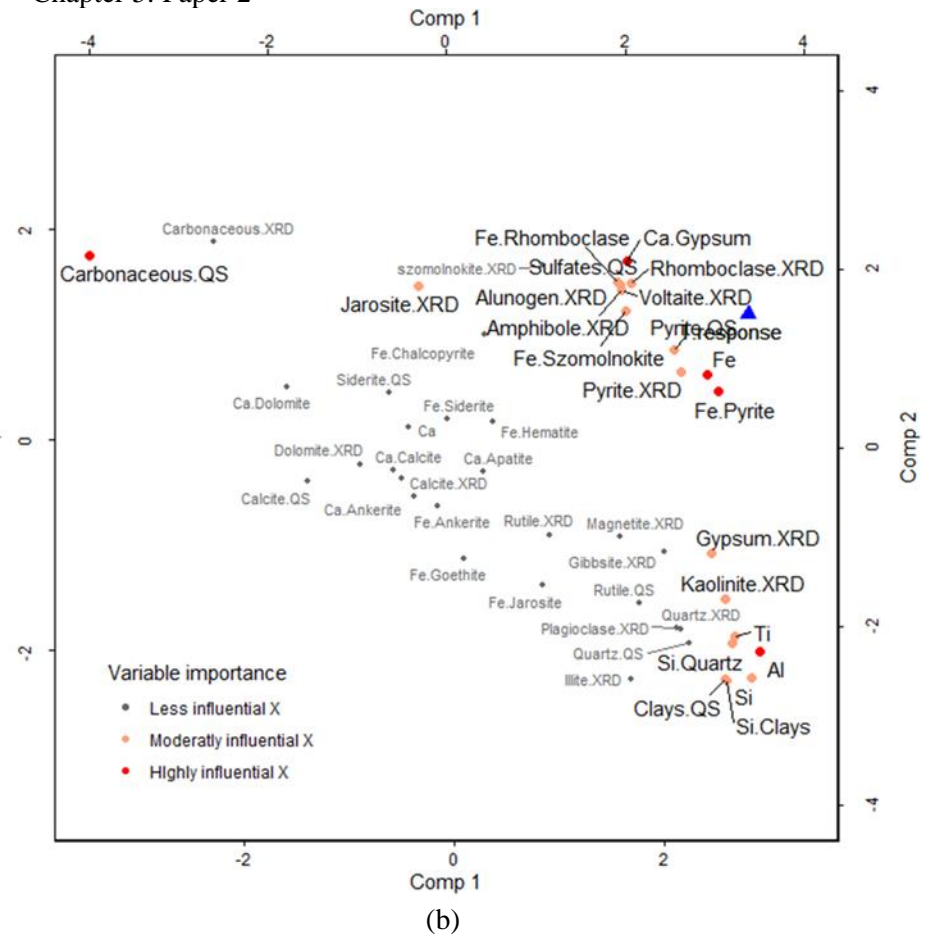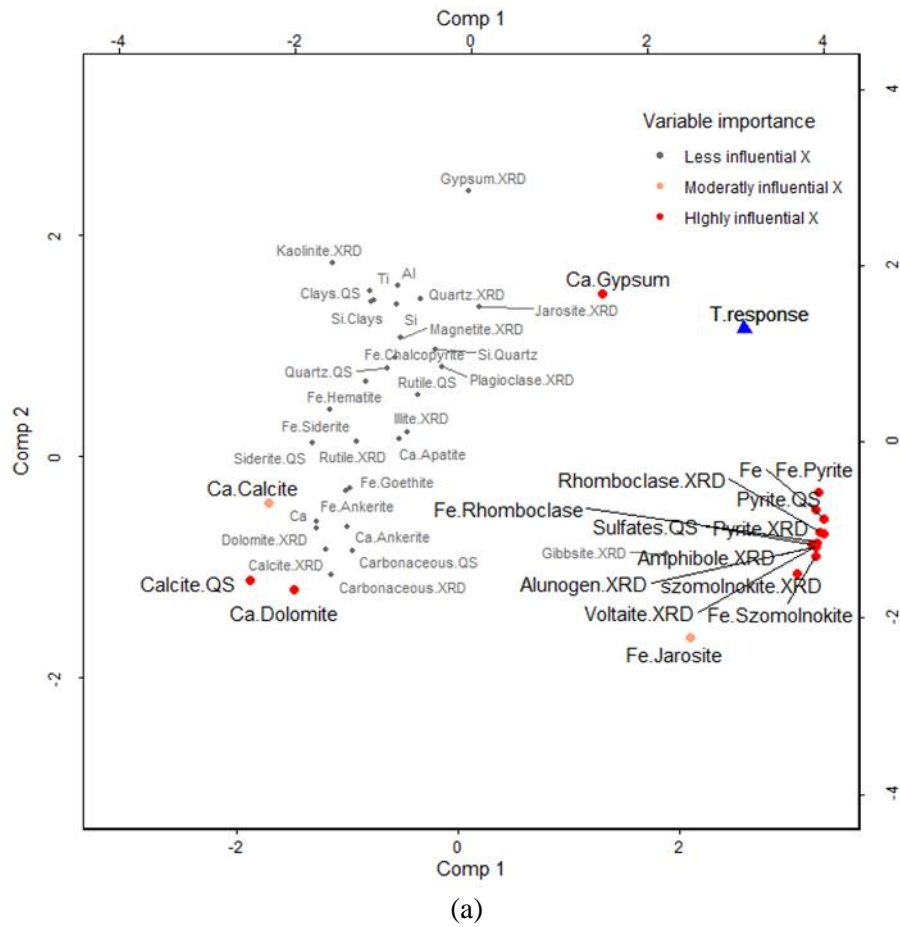
Figure 5-4 Loadings plots representing the relationships between the mineral and elemental-based data (red, orange, and grey dots) and the two measured responses (blue triangles). Figures a and b show the loadings plot for MDA and LDH respectively. VIP scores were used to class the characteristics by importance to the model. The total variance explained by components 1 and 2 across all variables in the MDA model were comp1=21.86 %, comp2=15.09 %). The total variance explained by components 1 and 2 across all variables in the LDH model comp1=19.94 %, comp2=12.39 %)

Regarding the MDA-based model, Fe-bearing sulfate and sulfide minerals were found to be significant to the model and positively associated with the release of MDA (see Figure 5-4a). Additionally, the Ca distributed in gypsum was found to be significant and positively associated to the response, whereas the Ca distributed in calcite and dolomite were significant but negatively associated to the response. Generally, mineral specific characteristics represented in Figure 5-5a were not found to be influential to the model, however, the crystallite size of quartz (CRY.qtz) was found to be positively associated and highly influential to MDA release. Additionally, quartz encapsulation displayed a moderate level of influence to the model, however, due to its isolated position in the loadings plot relative to the other classes of liberation this may be a result of outlier expression (see Figure D-1 for comparison of variability between samples). General particle characteristics such as particle shape and specific surface area (SSA), were found to be moderately influential to MDA release (see Figure 5-6). Based on the loadings plot, angular-shaped particles and smooth and equant-shapes were observed to oppose one another in the loadings plot relative to smooth and equant-shapes, thus suggesting that these parameters have opposite effects to the response (see Figure 5-6a).

Similarly to the MDA based model, Fe-bearing sulfate and sulfide minerals were found to be positively associated with the release of LDH (see Figure 5-4b). However, the LDH-based model determined that total Fe content and the Fe distributed in pyrite displayed a higher level of significance to the model compared to other Fe-bearing minerals. Apart from elemental Fe, Ca distributed in gypsum and the total Ti content were found to be highly influential and positively associated with the release of LDH. The minerals quartz and kaolinite as well as the associated Si and Al distributed in these minerals were observed to be both moderately influential and positively associated with the response (see Figure 5-4b). Considering that the silicate and Fe-bearing minerals were observed as opposing clusters, it can be suggested that these two mineral groups affect the cells though different and potentially independent mechanisms.

(a)                                                                                              (b)
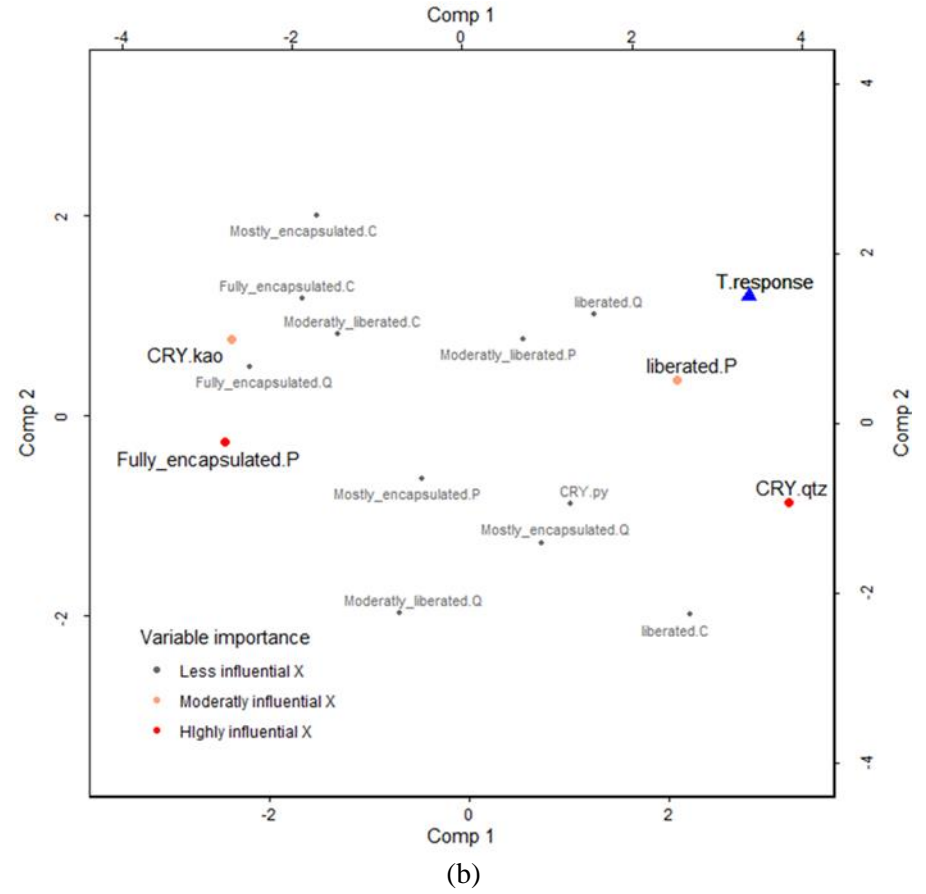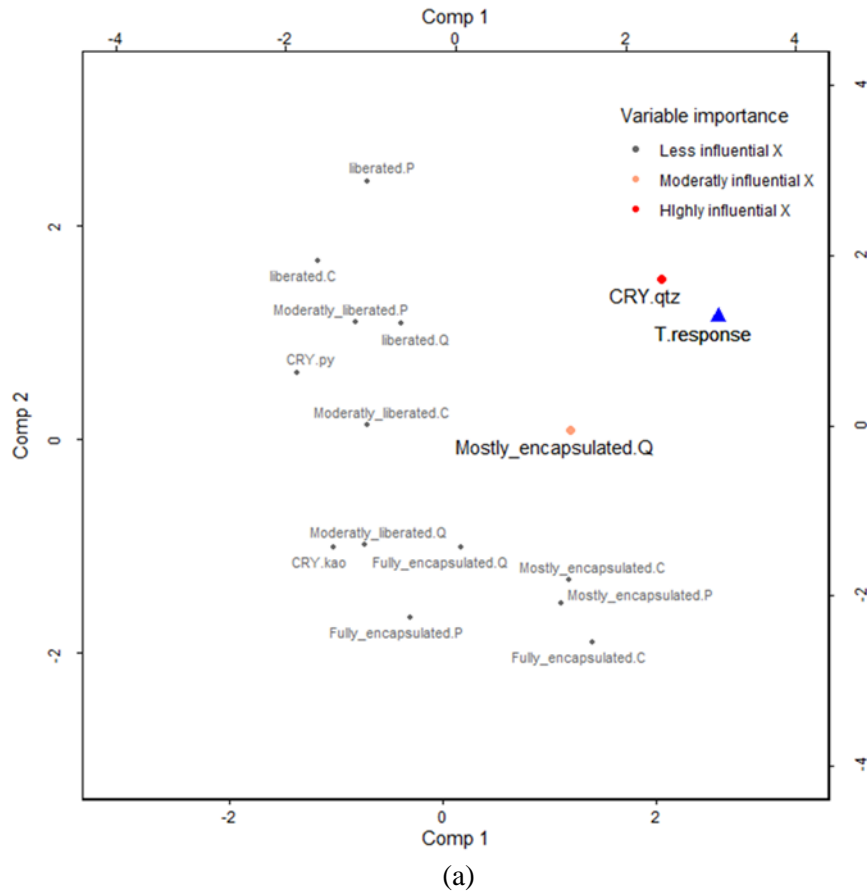
Figure 5-5 Loadings plots representing the relationships between the mineral specific particle data (red, orange, and grey dots) and the two measured responses (blue triangles). Figures a and b show the loadings plot for MDA and LDH respectively. VIP scores were used to class the characteristics by importance to the model. The total variance explained by components 1 and 2 across all variables in the MDA model were comp1=21.86 %, comp2=15.09 %). The total variance explained by components 1 and 2 across all variables in the LDH model comp1=19.94 %, comp2=12.39 %)

The abundance of gypsum was observed to occur between these clusters, suggesting that cytotoxicity related to gypsum may occur via a pathway independent to Fe-bearing sulfates/sulfides and silicates. In contrast to these positive associations, carbonaceous content was found to be highly influential and negatively associated with LDH release. This suggests that the composition-based effects related to cytotoxicity are a function of the mineral matter and not the carbonaceous content. Regarding the influence of mineral specific characteristics on LDH release, the crystallite size of quartz was found to be highly influential and positively associated with the response. In contrast the crystallite size of kaolinite (CRY.kao) was found to be moderately influential and negatively associated with LDH release (see Figure 5-5b).

Apart from crystallite size, the liberation of pyrite containing particles was found to be influential to the model. Specifically, liberated pyrite grains showed a moderate positive association to LDH release, whereas pyrite which is fully encapsulated displayed a highly influential negative association to the response. In Figure 5-6b the loadings plot showed that particle shape and SSA significantly impact the release of LDH. The distribution of the parameters in the plot suggests that particle shape and SSA impact the release of LDH release via different mechanisms. Furthermore, the same opposing distribution of equant and angular-shaped particles reported in the MDA-based model was observed in the results of the LDH-based model. This suggests that particle shape may play a significant role in both lipid peroxidation and cytotoxicity.

(a)



(b)
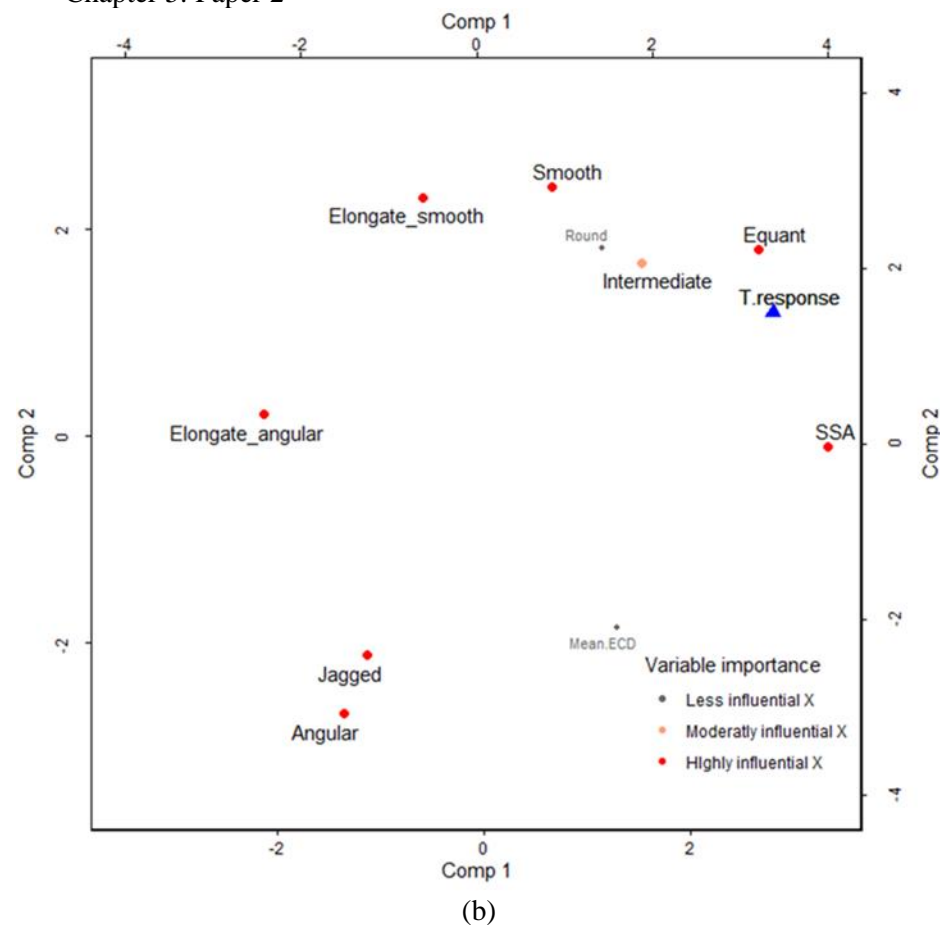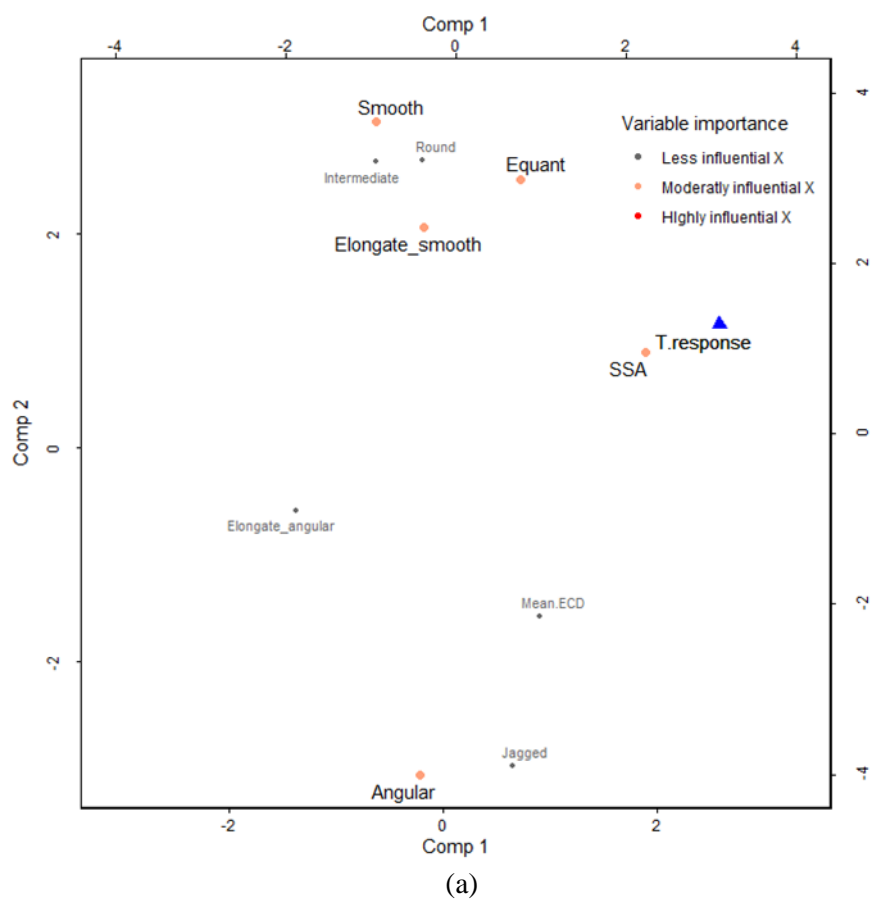
Figure 5-6 Plate Loadings plots representing the relationships between the general particle data (red, orange, and grey dots) and the two measured responses (blue triangles). Figures a and b show the loadings plot for MDA and LDH respectively. VIP scores were used to class the characteristics by importance to the model. The total variance explained by components 1 and 2 across all variables in the MDA model were comp1=21.86 %, comp2=15.09 %). The total variance explained by components 1 and 2 across all variables in the LDH model comp1=19.94 %, comp2=12.39 %)

5.4.2.2. Relative influence of particle characteristics on cytotoxicity and oxidative stress

To assess the contribution of each variable to the MDA and LDH-based models, coefficient plots were constructed using the VIP scores of each variable to screen for the characteristics which significantly influenced the respective responses in the model (see Figure 5-7 and 5-8 respectively). By comparing the relative contribution of the characteristics deemed influential in the MDA-based model, the results show that the crystallite size of quartz, presence of elongate and smooth particles, and the amount of Ca hosted in gypsum have the highest positive coefficient values compared to the other parameters (see Figure 5-7). Quartz that was mostly encapsulated reported a coefficient value similar to these parameters, however, the relative importance of this parameter was considered to be biased based on outlier samples. The second highest positive coefficient values were reported for characteristics which reflect the abundance and distribution of Fe in Fe-bearing sulfate and sulfide minerals as well as particles which are smooth and equant. Specific surface area (SSA) was found to impact MDA release to a lesser extent compared to the crystallite size of quartz, SSA and composition-based parameters. Apart from the characteristics which yielded positive coefficient values, the abundance and distribution of Ca in carbonate minerals as well as angular-shaped particles displayed high negative coefficient values. Additionally, the Fe distributed in jarosite displayed a moderate negative coefficient value.

Regarding the relative contribution of characteristics deemed relevant to the LDH-based model, particle shape was observed to strongly influence the release of LDH more so compared to composition-based parameters (see Figure 5-8). Specifically, equant particles with smooth roughness as well as elongate and smooth-shaped particles displayed a high positive coefficient value while more jagged and angular particles displayed a high negative coefficient value. Regarding particles with intermediate roughness, the moderate but positive coefficient observed shows that particles with this characteristic have less of a positive impact on LDH release than equant and smooth particles. This suggests that smoother and equant particles may exacerbate LDH release.

Apart from particle shape, Ca hosted in gypsum displayed a high positive coefficient with a magnitude similar to the equant and smooth shaped particles. In the LDH-based model, mineral specific characteristics such as pyrite liberation and the crystallite size of quartz and kaolinite had a moderate impact of the modelled response. The coefficient values for pyrite liberation show that fully encapsulated pyrite particles have a relatively high but negative coefficient value, whereas liberated pyrite had a moderate positive value. This suggests that the negative effect of fully encapsulated pyrite has a stronger influence on LDH release compared to the positive effect of liberated pyrite grains. Regarding the crystallite size, the crystallite size of quartz displayed a moderate positive coefficient compared to that of kaolinite which showed a moderate negative value. The coefficient value of carbonaceous content was observed to be

similar to that of kaolinite crystallite size, which could suggest that more amorphous structures may have a negative effect on LDH release based on the relatively small crystallite size of kaolinite.

In terms of the relative significance of mineral and elemental characteristics, the abundance of jarosite was observed to have the highest positive coefficient value amongst the minerals. Across the other composition-based characteristics the distribution of Fe in pyrite as well as the abundance of kaolinite and other Fe-bearing sulfates were observed to cluster with moderate coefficient values. This shows that the relative impact of various minerals were considered similar in the LDH-based model. Although quartz content was reported with a VIP score less than 1 the Si distributed in quartz displayed a moderate but positive contribution to LDH release. Similarly, Ti content was observed to have a moderate but positive contribution to the model even though the main Ti-bearing phase rutile reported a VIP score less than 1. Lastly, SSA displayed a moderate but positive contribution to LDH release which yielded a coefficient value in a range similar to the mineral and element data. This shows that particle SSA has a similar impact to LDH release as composition-based characteristics.
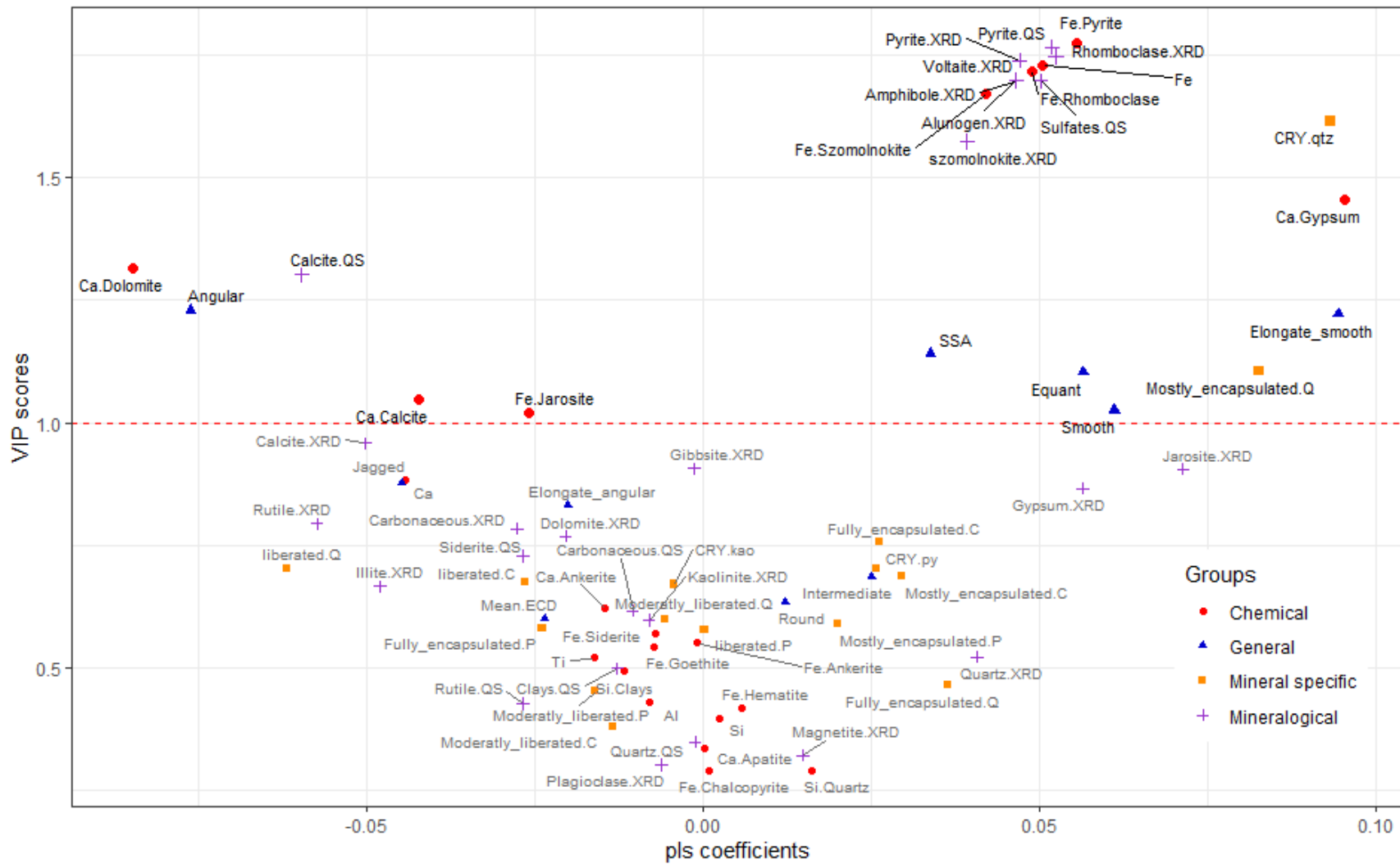
Figure 5-7 Coefficient plot for the MDA model comparing the impact of the coefficients for each parameter to their relevance to the model (based on the VIP scores).

Figure 5-8 Coefficient plot for the LDH model comparing the impact of the coefficients for each parameter to their relevance to the model (based on the VIP scores).

## 5.5. Discussion

By conducting a multivariant analysis on the relationships between the physicochemical and mineralogical characteristics of dust-sized coal with markers of cytotoxicity and oxidative stress, this study has shown that various particle characteristics affect cellular responses to different degrees when compared directly. Among the different classes of characteristics defined in this study, particle shape and roughness were observed to be highly influential to both cytotoxicity and lipid peroxidation. In the case of lipid peroxidation, the effects that particle shape and roughness had on the response were of a similar level to composition-based characteristics (see Figure 5-7). This suggests that both parameters may be equally important when trying to understand the effect that coal particles have on oxidative stress. However, when considering macrophage cytotoxicity, the influence of particle shape was found to be greater than composition-based characteristics (see Figure 5-8). A previous study by Champion and Mitragotri (2006) it was found that particle geometry could affect the successful internalisation of particles which may potentially lead to cell stress and eventual apoptosis. Based on their results it was demonstrated that the unsuccessful internalisation of a particle could occur where the contact angle between the particle surface and the macrophage was high. In such cases, particles with concave or flatter surfaces were found to promote spreading over clearance in macrophages, as depicted in Champion and Mitragotri (2006) and Champion et al (2007). From the results in Figure 5-8 it was shown that equant and smoother shaped particles displayed a positive impact on cytotoxicity whereas more angular and jagged particles displayed a negative impact. Such results are congruent with the findings of Champion and Mitragotri (2006) as equant particles display a block-like/ball-like habit which would lead to higher contact angles compared to angular and jagged particles.

Apart from particle shape, the Ca distributed in gypsum ($Ca(SO_4)\cdot2(H_2O)$) was shown to be highly influential to both lipid peroxidation and cytotoxicity. As gypsum is a readily soluble mineral, Ca can be easily released and thus become available to macrophages. The observed relationship between Ca in gypsum and these responses is congruent with studies by Kass and Orrenius (1999) and Donaldson et al (2003) which have shown that elevated levels of extracellular and intracellular Ca can disrupt cellular functions which utilise Ca via signalling mechanisms, as well as induce apoptosis. Moreover, studies by Dolmetsch et al (1997, 1998) showed that elevated levels of calcium could lead to the activation and transcription of nuclear factor of activated T cells and NF-κB, which are both involved in inflammatory pathways which could further promote cellular stress.

Regarding the mineral chemistry, both models showed that the Fe related chemistry and mineralogy played an influential role in both lipid peroxidation and cytotoxicity. The loadings plots related to the mineralogical and chemical characteristics (Figure 5-4) show that pyrite and sulfate minerals such as rhomboclase, jarosite and szomolnokite clustered together, suggesting that these minerals are associated.

In the natural environment the presence of sulfates in coal are commonly derived from the oxidation of pyrite either in buffered or highly acidic systems (Ward, 2016). For coals which contain carbonates ($CaCO_3$/$CaMg(CO_3)_2$) the reaction between pyrite ($FeS_2$) and the carbonate phases can produce gypsum. However, under highly acidic conditions any carbonates present are likely to be consumed and through separate reactions, secondary iron sulfate minerals such as jarosite, rhomboclase ($HFe^{3+}(SO_4)_2 \cdot 4(H_2O)$) and szomolnokite ($Fe^{2+}(SO_4) \cdot (H_2O)$) can form as acidic alteration products of pyrite. As these alteration products are more readily soluble than pyrite, studies by Huang et al (1994, 2005) have proposed that the presence of sulfate minerals can actively release bioavailable iron in addition to pyritic iron. As a result, the iron derived from sulfates in combination with pyritic iron is proposed to aggravate the levels of Fenton-based reactive oxygen species (ROS), thus leading to lipid peroxidation and eventual cytotoxicity. While the loadings plot reflected the association between pyrite and the various sulfates (Figure 5-4), the coefficients plot related to lipid peroxidation showed that Fe distributed in jarosite displayed a negative impact on lipid peroxidation as opposed to Fe distributed in rhomboclase and szomolnokite which showed a strong positive impact (Figure 5-7). In a study by Sun et al, (2021) it was demonstrated that sulfate minerals displayed marginal associations with oxidative stress and cytotoxicity. Based on the disparity observed between the different effects of sulfate species (jarosite versus rhomboclase and szomolnokite), some Fe-bearing sulfates may be more reactive than others and thus may have different impacts on the Fe-mediated radical production. This was further affirmed by the inclusion of Fe distributed in rhomboclase and szomolnokite and exclusion of Fe distributed in jarosite by the LDH-based model.

While the above context discussed the effects of coals with mineral assemblages that reflect an acidic environment, coals which contain a high abundance of carbonate minerals are expected to contribute less to oxidative stress and cytotoxicity. This is due to the buffering capacity of carbonate minerals which alter pyrite to its chemically non-reactive iron hydroxide products (Zhang et al, 2002). This was reflected in the MDA-based model which showed that Ca derived from calcite and dolomite have a strong negative impact on the lipid peroxidation.

In the LDH-based model, the silicate chemistry reflective of quartz and kaolinite were found to be moderately influential to cytotoxicity (see Figure 5-8). Despite the moderate but positive coefficient reported for Si distributed in quartz, the abundance of quartz was found to show no contribution to the model (Figure 5-8). Such an observation is not inconsistent with literature despite the known toxicity of quartz, with studies by Tourmann and Kaufmann (1994) and Wallace et al (1994) having shown that aluminosilicate clays (such as kaolinite) play a depressive role in the bio-reactivity of other silicates such as quartz. In contrast to this observation, the crystallite size of quartz was determined to be highly influential to lipid peroxidation and less so to cytotoxicity. This suggests that the cytotoxicity of quartz is potentially better reflected by its crystallite size than by abundance. Mechanistically this can be explained by the

positive link between mineral crystallite size and surface defects reported by Warr and Nieto (1998) and Kongsuebchart et al (2006). As surface defects are known to serve as sites for ROS generation in biological contexts, the relatively large crystallite size of quartz (refer to section 4.9.2. Chapter 4 for reference) compared to other minerals such as kaolinite supports this observation.

Conventionally kaolinite content is generally considered to only play a mitigative role in supressing the toxicity of quartz. However, the LDH-based model defined kaolinite a similar weighted effect to pyrite. Such findings are consistent with studies by Davies (1983); Davies et al (1984); and Wastiaux and Daniel (1990) which demonstrated a link between kaolinite and cytotoxicity in macrophages. Despite this apparent link, little research has been conducted to further understand the mechanism of kaolinite toxicity.

While studies by Trechera et al (2020, 2021b) have shown a positive association between Ti content and oxidative potential based on non-cellular chemical assays, the results presented show that neither Ti content nor its mineral host rutile ($TiO_2$) report a significant effect on lipid peroxidation in macrophages. However, the results of the LDH-based model show that Ti content is moderately influential on cytotoxicity despite rutile displaying no significant contribution to the model. Separate analysis presented in section 4.7.1. has shown that Ti is highly associated with kaolinite, which also is moderately associated cytotoxicity. This finding is supported by Weaver (1976), who described the occurrence of $TiO_2$-kaolinite aggregates cemented to kaolinite particles in clay deposits. It is thus possible that the relative significance of Ti content to cytotoxicity could be a result of its association with kaolinite. As the effects of these aggregates on cellular function has not been discussed in literature this could be a potential avenue for studies seeking to further understand the mechanics associated with kaolinite-induced cytotoxicity.

## 5.6. Conclusions

Through the results presented, the application of a PLSR was demonstrated to provide a robust understanding of how the characteristics of dust-sized coal particulates influence cellular damage in macrophages. It should, however, be acknowledged that the dust particles generated within this study might not be representative of real world mine dust samples or samples within what is considered the respirable fraction. Despite this limitation, the results showed that a stable and robust model could be developed using a PLSR to determine the multivariant relationships between 72 characterisation parameters and 2 responses, whilst accounting for the effects of collinearity. By using an analytical approach such as discriminant analysis (visualised by the loadings plots) and the VIP scores, this study was able to demonstrate a systematic screening approach to determine the most significant variables to each response measured. Additionally, the study presented the first comparative analysis of the effect of numerous physicochemical and mineralogical characteristics on oxidative stress and cytotoxicity expressed from exposed macrophages.

The results showed that between the two responses, similar groups of characteristics could be identified. This included parameters such as particle shape and roughness, iron-based chemistry and mineralogy, quartz crystallite size, and Ca hosted in gypsum. Ultimately, such results are consistent with the links known between oxidative stress and eventual cell death. By contrast, parameters related to silicate chemistry and kaolinite abundance were not determined to have an impact on lipid peroxidation but were rather found to impact cytotoxicity. Although the mechanisms related to kaolinite-related toxicity are not known, the results suggest that kaolinite exposure to macrophages may be direct and not related to ROS generating pathways.

Ultimately, the study demonstrated the usefulness of including different data types (encompassing general, chemical, mineralogical, and mineral specific data) to provide a holistic understanding of the potential mechanisms occurring between macrophages and coal particulates. With the understanding developed from both the discriminant analysis and model coefficients, this study proposes the importance of the following relationships with respect to particle toxicity derived from parental coals: (1) particle shape for its role in phagocytosis and potential to lead to inflammation, (2) chemical availability of Ca from soluble minerals such as gypsum, for its role in oxidative stress and cytotoxicity, (3) the crystallite size of quartz as a more reliable measure of quartz-mediated radical induced damage than quartz abundance, (4) the chemical availability of Fe derived from pyrite and Fe-bearing sulfates for its role in Fenton-related ROS production and subsequent cytotoxicity, and (5) the potential contribution of kaolinite to cytotoxicity which requires further research to understand the mechanism of toxicity. In stating these relationships it should be acknowledged that the dominance of these relationships may change if the same strategy were applied to real-world samples.

## 5.7. References

Abdi, H. (2010) 'Partial least squares regression and projection on latent structure regression (PLS Regression)', *Wiley Interdisciplinary Reviews: Computational Statistics*, 2(1), pp. 97–106. doi: 10.1002/wics.51.

Basil, B. and Zosky, G. (2019) *Assessment of pyritic coal dust induced pneumoconiosis*.

Champion, J. A., Katare, Y. K. and Mitragotri, S. (2007) 'Particle shape: A new design parameter for micro- and nanoscale drug delivery carriers', *Journal of Controlled Release*, 121(1–2), pp. 3–9. doi: 10.1016/j.jconrel.2007.03.022.

Champion, J. A. and Mitragotri, S. (2006) 'Role of target geometry in phagocytosis', *Proceedings of the National Academy of Sciences of the United States of America*, 103(13), pp. 4930–4934. doi: doi.org/10.1073/pnas.0600997103.

Cohn, C. A., Laffers, R., Simon, S. R., O'Riordan, T. and Schoonen, M. A. (2006) 'Role of pyrite in formation of hydroxyl radicals in coal: Possible implications for human health', *Particle and Fibre Toxicology*, 3, pp. 1–10. doi: 10.1186/1743-8977-3-16.

Dalal, N., Newman, J., Pack, D., Leonard, S. and Vallyathan, V. (1995) 'Hydroxyl Radical Generation by Coal Mine Dust: Possible Implication to Coal Workers' Pneumoconiosis (CWP)', *Free Radical Biology and Medicine*, 18(I), pp. 11–20.

David, W. I. F., Leoni, M. and Scardi, P. (2010) 'Domain size analysis in the Rietveld method', *Materials Science Forum*, 651, pp. 187–200. doi: 10.4028/www.scientific.net/MSF.651.187.

Davies, R. (1983) 'Factors Involved in the Cytotoxicity of Kaolinite towards Macrophages in Vitro', *Environmental Health Perspectives*, 51, pp. 249–274.

Davies, R., Griffiths, D. M., Johnson, N. F., Preece, A. W. and Livingston, D. C. (1984) 'The cytotoxicity of kaolin towards macrophages in vitro', *British Journal of Experimental Pathology*, 65, pp. 453–466.

Dolmetsch, R. E., Lewis, R. S., Goodnow, C. C. and Healy, J. I. (1997) 'Differential activation of transcription factors induced by Ca2+ response amplitude and duration', *Nature*, 386(6627), pp. 855–858. doi: 10.1038/386855a0.

Dolmetsch, R., Xu, K. and Lewis, R. S. (1998) 'Calcium oscillations increase the efficiency and specificity of gene expression', *Nature*, 392, pp. 933–936. Available at: https://www.metabolic-economics.de/pages/seminar_regulationsnetze_2005/literatur/Dolmetsch_Calcium_1998_Nature.pdf.

Donaldson, K., Stone, V., Borm, P. J. A., Jimenez, L. A., Gilmour, P. S., Schins, R. P. F., Knaapen, A. M., Rahman, I., et al (2003) 'Oxidative stress and calcium signaling in the adverse effects of environmental particles (PM10)', *Free Radical Biology and Medicine*. Elsevier, 34(11), pp. 1369–1382. doi: 10.1016/S0891-5849(03)00150-3.

Fubini, B. and Ivana, F. (2007) 'Toxic Potential of Mineral Dusts', *Elements*, 3(6), pp. 407–414. doi: 10.2113/GSELEMENTS.3.6.407.

Galindo-Prieto, B., Eriksson, L. and Trygg, J. (2014) 'Variable influence on projection (VIP) for orthogonal projections to latent structures (OPLS)', *Journal of Chemometrics*, 28(8), pp. 623–632. doi: 10.1002/cem.2627.

Ghose, M. K. and Majee, S. R. (2000) 'Assessment of the impact on the air environment due to opencast coal mining - An Indian case study', *Atmospheric Environment*, 34(17), pp. 2791–2796. doi: 10.1016/S1352-2310(99)00302-7.

Ghose, M. K. and Majee, S. R. (2007) 'Characteristics of hazardous airborne dust around an Indian surface coal mining area', *Environmental Monitoring and Assessment*, 130(1–3), pp. 17–25. doi: 10.1007/s10661-006-9448-6.

Gómez-Gener, L., Gubau, M., von Schiller, D., Marcé, R. and Obrador, B. (2018) 'Effect of small water retention structures on diffusive CO2 and CH4 emissions along a highly impounded river', *Inland Waters*. Taylor & Francis, 8(4), pp. 449–460. doi: 10.1080/20442041.2018.1457846.

Gormley, I. P., Collings, P., Davis, J. M. G. and Ottery, J. (1979) 'An Investigation into the Cytotoxicity of Respirable Dusts from British Collieries', *British Journal of Experimental Pathology*, 60, pp. 526–536.

Harrington, A. D., Tsirka, S. E. and Schoonen, M. A. A. (2013) 'Inflammatory stress response in A549 cells as a result of exposure to coal: Evidence for the role of pyrite in coal workers' pneumoconiosis pathogenesis', *Chemosphere*, 93(6), pp. 1216–1221. doi: 10.1016/j.chemosphere.2013.06.082.

Huang, X., Gordon, T., Rom, W. N. and Finkelman, R. B. (2006) 'Interaction of Iron and Calcium Minerals in Coals and their Roles in Coal Dust-Induced Health and Environmental Problems', *Reviews in Mineralogy and Geochemistry*, 64(1), pp. 153–178. doi: 10.2138/rmg.2006.64.6.

Huang, X., Li, W., Attfield, M. D., Nádas, A., Frenkel, K. and Finkelman, R. B. (2005) 'Mapping and prediction of coal workers' pneumoconiosis with bioavailable iron content in the bituminous coals.', *Environmental health perspectives*, 113(8), pp. 964–8. doi: 10.1289/ehp.7679.

Huang, X., Zalma, R., Pezerat, H. and Huang, X. (1994) 'Factors That Influence the Formation and Stability of Hydrated Ferrous Sulfate in Coal Dusts. Possible Relation to the Emphysema of Coal Miners', *Chemical Research in Toxicology*, 7(3), pp. 451–457. doi: 10.1021/tx00039a025.

Huertas, J. I., Huertas, M. E., Izquierdo, S. and Gonzalez, E. D. (2012) 'Air quality impact assessment of multiple open pit coal mines in northern Colombia', *Journal of Environmental Management*. Elsevier, 93(1), pp. 121–129. doi: 10.1016/j.jenvman.2011.08.007.

De Jong, S. (1993) 'SIMPLS: an alternative approach squares regression to partial least', *Chemometrics and Intelligent Labratory Systems*, 18, pp. 251–263.

Kamanzi, C., Becker, M., Von Holdt, J. and Broadhurst, J. (2022) 'Development of a SEM-EDS-XRD Protocol for the Physicochemical and Automated Mineralogical Characterisation of Coal Dust Particles', *Resources*. Multidisciplinary Digital Publishing Institute, 11, p. 114. doi: 10.3390/RESOURCES11120114.

Kass, G. and Orrenius, S. (1999) 'Calcium Signaling and Cytotoxicity', *Environmental Health Perspectives*, 107, pp. 25–35. Available at: http://ehpnet1.niehs.nih.gov/docs/1999/Suppl-1/25-35kass/abstracthtml.

Kongsuebchart, W., Praserthdam, P., Panpranot, J., Sirisuk, A., Supphasrirongjaroen, P. and Satayaprasert, C. (2006) 'Effect of crystallite size on the surface defect of nano-TiO2 prepared via solvothermal synthesis', *Journal of Crystal Growth*, 297(1), pp. 234–238. doi: 10.1016/J.JCRYSGRO.2006.09.018.

Lee, C. Y., Lee, S. L., Sheehan, C. E. and Wang, Y. (1996) *Composition of coal dusts and their cytotoxicity on alveolar macrophages*. Technical report ARCCB-TR-96026. Available at: https://pdfs.semanticscholar.org/8185/85459224e1ac9db8dce8b006c415033ec7d9.pdf.

Leonard, R., Zulfikar, R. and Stansbury, R. (2020) 'Coal mining and lung disease in the 21st century', *Current Opinion in Pulmonary Medicine*, 26(2), pp. 135–141. doi: 10.1097/MCP.0000000000000653.

Lison, D., Cile Lardot, C., Ois Huaux, F., Zanetti, G. and Fubini, B. (1997) 'Inuence of particle surface area on the toxicity of insoluble manganese dioxide dusts', *Archives of toxicology*, 71, pp. 725–729. Available at: https://link.springer.com/content/pdf/10.1007/s002040050453.pdf.

Maanen, J. M. S. Van, Borm, P. J. A., Knaapen, A., Herwijnen, M. Van, Schilderman, P. A., Smith, K. R., Aust, A. E. and Tomatis, M. (1999) 'In vitro effects of coal fly ashes: Hydroxyl Radical Generation , Iron Release , and DNA Damage and Toxicity in Rat Lung Epithelial Cells', *Inhalation Toxicology*, 11, pp. 1123–1141.

Mevik, B.-H. W. (2022) 'Introduction to the pls Package', *CRAN*. Netherlands, pp. 1–24. Available at: https://cran.r-project.org/web/packages/pls/vignettes/pls-manual.pdf.

Mevik, B.-H. and Wehrens, R. (2007) 'The pls Package: Principal Component and Partial Least Squares Regression in R', *Journal of Statistical Software*, 18(2), pp. 1–24.

Orona, N. S., Astort, F., Maglione, G. A., Saldiva, P. H. N., Yakisich, J. S. and Tasat, D. R. (2014) 'Direct and indirect air particle cytotoxicity in human alveolar epithelial cells', *Toxicology in Vitro*, 28, pp. 796–802. doi: 10.1016/j.tiv.2014.02.011.

Reisner, M. T. R., Bruch, J., Hilscher, W., Kriegseis, W., Prajsnar, D., Robock, K., Rosmanith, J., Scharmann, A., et al (1982) 'Specific harmfulness of respirable dusts from west German coal mines VI: Comparison of experimental and epidemiological results', *Annals of Occupational Hygiene*, 26(4), pp. 527–539. doi: 10.1093/annhyg/26.4.527.

RStudio Team (2020) 'RStudio: Integrated Development Environment for R'. Boston: RStudio, PBC. Available at: http://www.rstudio.com/.

Schins, R. P. F. and Borm, P. J. A. (1999) *Mechanisms and Mediators in Coal Dust Induced Toxicity: A Review*, *Annals of Occupational Hygiene*. Available at: https://academic.oup.com/annweh/article-abstract/43/1/7/162163.

Scrivener, K. L., Füllmann, T., Gallucci, E., Walenta, G. and Bermejo, E. (2004) 'Quantitative study of Portland cement hydration by X-ray diffraction/Rietveld analysis and independent methods', *Cement and Concrete Research*. Pergamon, 34(9), pp. 1541–1547. doi: 10.1016/J.CEMCONRES.2004.04.014.

Shangguan, Y., Zhuang, X., Querol, X., Li, B., Moreno, N., Trechera, P., Sola, P. C., Uzu, G., et al (2022) 'Characterization of deposited dust and its respirable fractions in underground coal mines: Implications for oxidative potential-driving species and source apportionment', *International Journal of Coal Geology*, 258(December 2021). doi: 10.1016/j.coal.2022.104017.

Shi, P., Xing, X., Xi, S., Jing, H., Yuan, J., Fu, Z. and Zhao, H. (2020) 'Trends in global, regional and national incidence of pneumoconiosis caused by different aetiologies: An analysis from the Global Burden of Disease Study 2017', *Occupational and Environmental Medicine*, 77(6), pp. 407–414. doi: 10.1136/oemed-2019-106321.

Song, Y., Southam, K., Basil, B., Zosky, G. R., Graeme Zosky, C. R., Bardin, P. and Reynolds, P. (2022) 'Effects of chemical composition on the lung cell response to coal particles: Implications for coal workers' pneumoconiosis', *Rispirology*, 12, pp. 447–454. doi: 10.1111/resp.14246.

Sun, Y., Kinsela, A. S., Cen, X., Sun, S., Collins, R. N., Cliff, D. I., Wu, Y. and Waite, T. D. (2021) 'Impact of reactive iron in coal mine dust on oxidant generation and epithelial lung cell viability', *Science of the Total Environment*. Elsevier B.V., 810, p. 152277. doi: 10.1016/j.scitotenv.2021.152277.

Sun, Y., Kinsela, A. S. and Waite, T. D. (2022) 'Elucidation of alveolar macrophage cell response to coal dusts: Role of ferroptosis in pathogenesis of coal workers' pneumoconiosis', *Science of the Total Environment*. Elsevier B.V., 823, p. 153727. doi: 10.1016/j.scitotenv.2022.153727.

Tourmann, J.-L. and Kaufmann, R. (1994) 'Laser Microprobe Mass Spectrometric (LAMMS) Study of Quartz-Related and Non-Quartzrelated Factors of the Specific Harmfulness of Coal Mine Dusts', *The Annals of Occupational Hygiene*, 38, pp. 455–467. doi: 10.1093/ANNHYG/38.INHALED_PARTICLES_VII.455.

Trechera, P., Moreno, T., Córdoba, P., Moreno, N., Amato, F., Cortés, J., Zhuang, X., Li, B., et al (2021a) 'Geochemistry and oxidative potential of the respirable fraction of powdered mined Chinese coals', *Science of The Total Environment*. Elsevier, 800, p. 149486. doi: 10.1016/J.SCITOTENV.2021.149486.

Trechera, P., Moreno, T., Córdoba, P., Moreno, N., Zhuang, X., Li, B., Li, J., Shangguan, Y., et al (2021b) 'Comprehensive evaluation of potential coal mine dust emissions in an open-pit coal mine in Northwest China', *International Journal of Coal Geology*. Elsevier, 235, p. 103677. doi: 10.1016/J.COAL.2021.103677.

Trechera, P., Moreno, T., Córdoba, P., Moreno, N., Zhuang, X., Li, B., Li, J., Shangguan, Y., et al (2020) 'Mineralogy, geochemistry and toxicity of size-segregated respirable deposited dust in underground coal mines', *Journal of Hazardous Materials*. Elsevier, 399, p. 122935. doi: 10.1016/j.jhazmat.2020.122935.

Turci, F., Pavan, C., Leinardi, R., Tomatis, M., Pastero, L., Garry, D., Anguissola, S., Lison, D., et al (2016) 'Revisiting the paradigm of silica pathogenicity with synthetic quartz crystals: the role of crystallinity and surface disorder', *Particle and Fibre Toxicology*. doi: 10.1186/s12989-016-0136-6.

Vallyathan, V. (1994) 'Generation of Oxygen Radicals by Minerals and Its Correlation to Cytotoxicity', *Environmental Health Perspectives*, 102, pp. 111–115.

Vallyathan, V., Shi, X. and Castranova, V. (1998) 'Reactive Oxygen Species: Their Relation to Pneumoconiosis and Carcinogenesis', *Environmental Health Perspectives*, 106, pp. 1151–1155.

Wallace, W. E., Harrison, J. C., Grayson, R. L., Keane, M. J., Bolsaitis, P., Kennedy, R. D., Wearden, A. Q. and Attfield, M. D. (1994) 'Aluminosilicate surface contamination of respirable quartz particles from coal mines dust and from clay works dusts', *Annals of Occupational Hygiene*, 38, pp. 439–445.

Ward, C. R. (2016) 'Analysis, origin and significance of mineral matter in coal: An updated review', *International Journal of Coal Geology*. Elsevier, 165, pp. 1–27. doi: 10.1016/j.coal.2016.07.014.

Warr, L. N. and Nieto, F. (1998) 'Crystallite thickness and defect density of phyllosilicates in low-temperature metamorphic pelites: A TEM and XRD study of clay-mineral crystallinity-index standards', *Canadian Mineralogist*, 36(6), pp. 1453–1474.

Wastiaux, A. and Daniel, H. (1990) 'Pulmonary Toxicity of Kaolin in Rats Exposed by Inhalation', *Health Related Effects of Phyllosilicates*. Springer, pp. 405–414. doi: 10.1007/978-3-642-75124-0_36.

Weaver, C. E. (1976) 'The Nature of TiO2 in Kaolinite', *Clays and Clay Minerals*. Springer, 24(5), pp. 215–218. doi: 10.1346/CCMN.1976.0240501.

Yadav, A. K. and Jamal, A. (2018) 'Impact of mining on human health in and around mines', *Environmental Quality Management*, 28(1), pp. 83–87. doi: 10.1002/tqem.21568.

Yang, H., Liu, C., Yang, D., Zhang, H. and Xi, Z. (2009) 'Comparative study of cytotoxicity, oxidative stress and genotoxicity induced by four typical nanomaterials: the role of particle size, shape and composition Comparative study of cytotoxicity, oxidative stress and genotoxicity', *Journal of Applied Toxicology*, 29, pp. 69–78. doi: 10.1002/jat.1385.

Zhang, Q., Dai, J., Ali, A., Chen, L. and Huang, X. (2002) 'Roles of bioavailable iron and calcium in coal dust-induced oxidative stress: Possible implications in coal workers lung disease', *Free Radical Research*, 36(3), pp. 285–294. doi: 10.1080/10715760290019309.

# Chapter 6

# FRAMEWORK FOR CLASSIFYING RELATIVE RISK OF COAL

# DUST
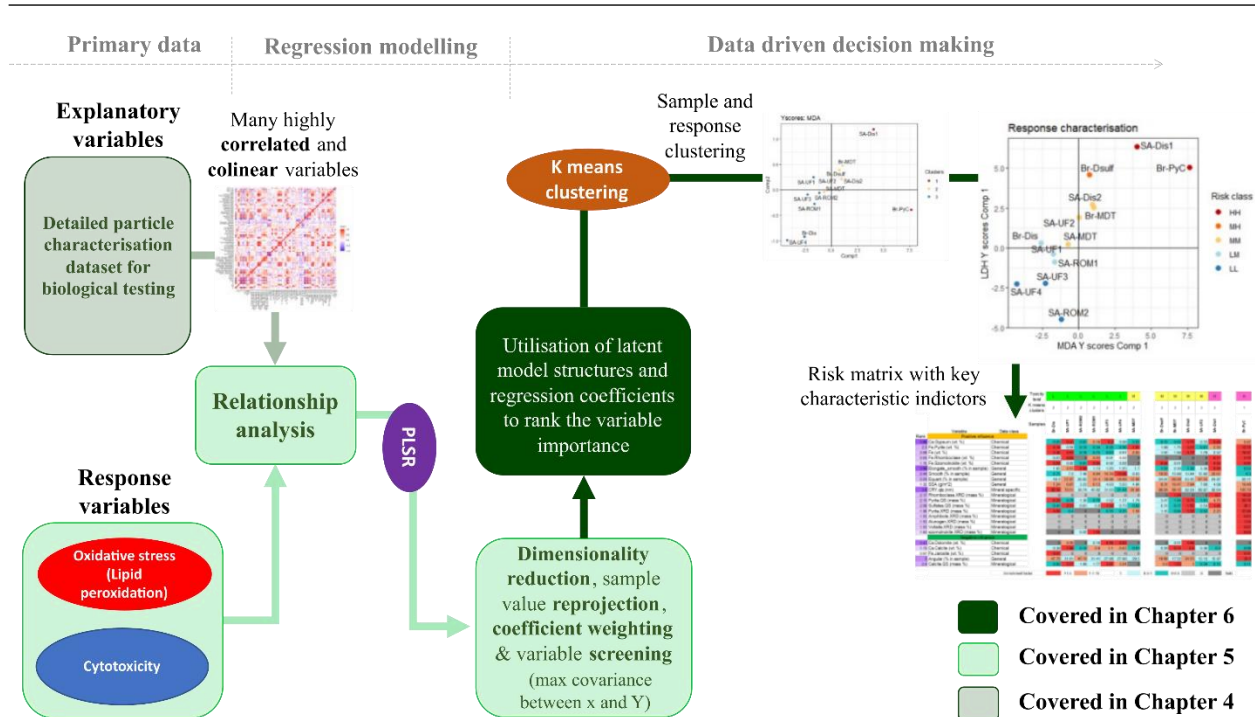


This graphic abstract depicts the integration and analysis of information from primary data to the outputs used for data driven decision- making.

## 6.1. Overview

In the context of this study, relative risk is used to describe the observed cellular harm induced by the exposure of cells to coal dust particulates. In Chapter 5 it was established that different samples exhibited differing degrees of oxidative stress (determined by the intensity of lipid peroxidation) and cytotoxicity. Apart from this, the regression analysis between the detailed particle characterisation dataset (presented in Chapter 4) and the two cellular responses further demonstrated that, while many variables can be attributed to these responses, some characteristics displayed a greater magnitude of influence over others. By expanding on the relationship analysis conducted in Chapter 5, the subsequent work presented in this Chapter further shows how the latent variable structures of the Partial Least Squares Regression (PLSR) model can be used to (1) construct a ranking system to identify the most influential particle characteristics

to cytotoxicity and oxidative stress, and (2) develop hazard matrices to understand the potential health risks associated with coal dust on a cellular scale.

The work presented in this chapter is a product of the following overarching objective and associated key questions:

> Overarching objective 3:
> To empirically characterise the relative risk of coal dust related damage on a cellular level based on the ranking of the most influential particle characteristics contributing to the harm of pulmonary cells and determining if there are distinct classes of harm.

> Key question 1: From the understanding developed in objective 2, on what basis will the empirical ranking of respiratory harm criteria be determined?

> Key question 2: Through the understanding developed under objective 1 and 2, how can the various data classes be combined to provide relevant and interpretable information to decision makers and other stakeholders?

Objective 1: To develop a detailed and quantitative particle characterisation dataset for coal dust in preparation for biological testing, using a combination of QEMSCAN (quantitative evaluation of minerals by scanning electron microscopy), XRD (X-ray Powder Diffraction) and XRF (X-ray fluorescence) and complementary physical analysis methods for the analysis of physical, compositional, mineral specific characteristics.

Objective 2: To investigate the multivariant relationships between the coal particle characteristics and immunological responses (cytotoxicity and oxidative stress) generated from exposed macrophage cells.

## 6.2. Introduction

The potential public health concerns associated with coal dust exposure have been documented by many studies including Ávila Júnior et al (2009); Yadav and Jamal (2018); and Batool et al (2020). Through such work both Ávila Júnior et al (2009) and Batool et al (2020) independently found that individuals chronically exposed to coal dust showed depleted antioxidant levels and markers of oxidative stress in their blood relative to unexposed control groups. While both studies found a gradation of antioxidant levels between underground and surface miners (with underground miners exhibiting lower levels of antioxidants compared to surface miners), the study by Ávila Júnior et al (2009) found that residents living in proximity to the mine and surface miners showed higher levels of oxidant related damage relative to underground miners. In the context of coal dust related health risks, the intensity of oxidant-related damage (and depleted antioxidant levels) is consistent with the prolonged exposure to coal dust (as discussed in Chapter 2). However, the expression of these markers in blood could also indicate a potential risk for cardiovascular damage. In a review describing the mechanisms by which particulate matter may induce cardiovascular damage, Fiordelisi et al (2017) described two hypothesised mechanisms. These involve damage induced

through ROS-related processes that either occur through the translocation of particles to the cardiovascular region, or from an indirect systemic inflammatory state resulting from pulmonary oxidative stress (Costa and Dreher, 1997; Kennedy et al, 1998; Donaldson et al, 2003). In this context, it becomes critical to understand the characteristics of coal particulates which can activate pathways to oxidative damage and direct cytotoxicity to understand what interventions can be made to mitigate their effects.

Currently, the concept of relative risk has not been extended beyond attempting to identifying the particle characteristics which can account for measured differences in oxidative potential. Studies by Trechera et al (2021b, 2021a); and Shangguan et al (2022) have constructed relationship pairs between oxidative potential and the physicochemical and mineralogical characteristics of coal particulates. However, these studies have not further investigated whether these relationships could be used to holistically define the relative risk of coal dust induced oxidative damage by a set of indicators. In a study by Zazouli et al (2021), the physicochemical data from coal dust samples as well as their oxidative potential were compared to a USEPA (United States Environmental Protection Agency) risk assessment of the dust samples in an attempt to understand how particle characterisation data could be complementary in a health risk assessment. In their analysis, the health risk assessment focused on the probability of carcinogenic and non-carcinogenic element risk while the measured oxidative potential was correlated with the mass concentration and element distribution of dust at each sampling point. Based on the comparison of these two indicators the results suggested that inhalation posed the most prominent non-carcinogenic risk over ingestion and dermal contact. Furthermore, transition metals were determined to have the strongest and most significant relationship to oxidative potential. In the study by Zazouli et al (2021), no attempt was made to integrate the two indicators of risk and oxidative potential, thus no understanding of the impact of the investigated particle characteristics with these measures could be reached. While these analyses provide some information for decision makers, the mere identification of chemical characteristics which relate to oxidative potential does not completely resolve whether a certain dust can be classified as "high risk" as many other physicochemical and mineralogical characteristics in coal dust have been observed to directly and indirectly affect oxidant levels (Maynard and Kuempel, 2005; Fubini and Fenoglio, 2007; Huang and Finkelman, 2008; Sun et al, 2022).

In the context of nanomaterials, it is understood that the toxicity of these particles is highly impacted by their physicochemical characteristics (Oberdörster, 2000; Maynard and Kuempel, 2005; Stoeger et al, 2006; Wittmaack, 2007). As a result, studies such as Linkov et al (2009); and Landsiedel et al (2017) utilised multicriteria decision making tools to understand the relative risk of various types of nanoparticles based on their particle characteristics and measure of cytotoxicity. By utilising the framework of scoring the characteristics relative to their cytotoxic response and ranking the risk categories describing

the impact, these strategies were able to quantify the relative risk of different nanoparticle types on a single scale. The previous chapters demonstrated that coal particulates are inherently complex and can vary in terms of their properties and measured responses based on the original source and mode of generation. Based on this it can be argued that utilising a ranking and/or scoring-type approach to define relative risk may be beneficial in determining a more holistic indication of the cytotoxic/ oxidative potential of a given dust. In this context the sections below describe the empirical risk characterisation protocol developed here to classify the relative risk of the sample set of coals analysed using the model coefficients and latent structures of the PLSR to weight and rank the characteristics to the responses. As the framework of the PLSR has been discussed in previous chapters the subsequent sections aim to provide a detailed description of the various protocol elements which feed into an ultimate "shortlist" of suggested particle-based risk factors for cellular stress and cytotoxicity.

## 6.3. Protocol description

In determining the relative risk of cellular damage from sampled coal dust, it is well understood that several particle characteristics may be involved in the expression of cytotoxicity, oxidative stress, and inflammation. Apart from the high number of potential factors to consider, many of the characteristics may have correlative associations which make the relation of numerous characteristics to a given response particularly challenging. In Chapter 5 it was shown that the PLSR could successfully perform both a regression of the numerous characteristics on cellular responses as well as a dimensionality reduction step to resolve a large set of particle characteristics to few components (whilst still capturing the variation between sample characteristics and responses). In doing so, the resulting relationships were discussed in the context of the latent structures of the model. While this approach is common practice when reporting the resulting relationships defined by a PLSR, the format of the information cannot be easily interpreted.

For this reason, there is a need to determine a systematic protocol for disseminating the information from the PLSR or similar multivariant linear regressions such that various stakeholders are able discern the key findings from the regression analysis. Based on this context, Figure 6-1 represents an overview of the workflow developed to translate the information from the PLSR to an interpretable format which describes the relative risk of sampled coal particulates. The main elements of the protocol can be described as (1) modelling the relationships between the particle characteristics and the measure of cellular harm, followed by (2) screening the variables for their significance to the relationship defined. Element (3) involves variable ranking and response classing, which then leads to (4) formatting the final data matrix for ease of interpretation. For reference, elements 1 and 2 were completed in Chapter 5, whilst elements 3 and 4 are the subject of this Chapter.
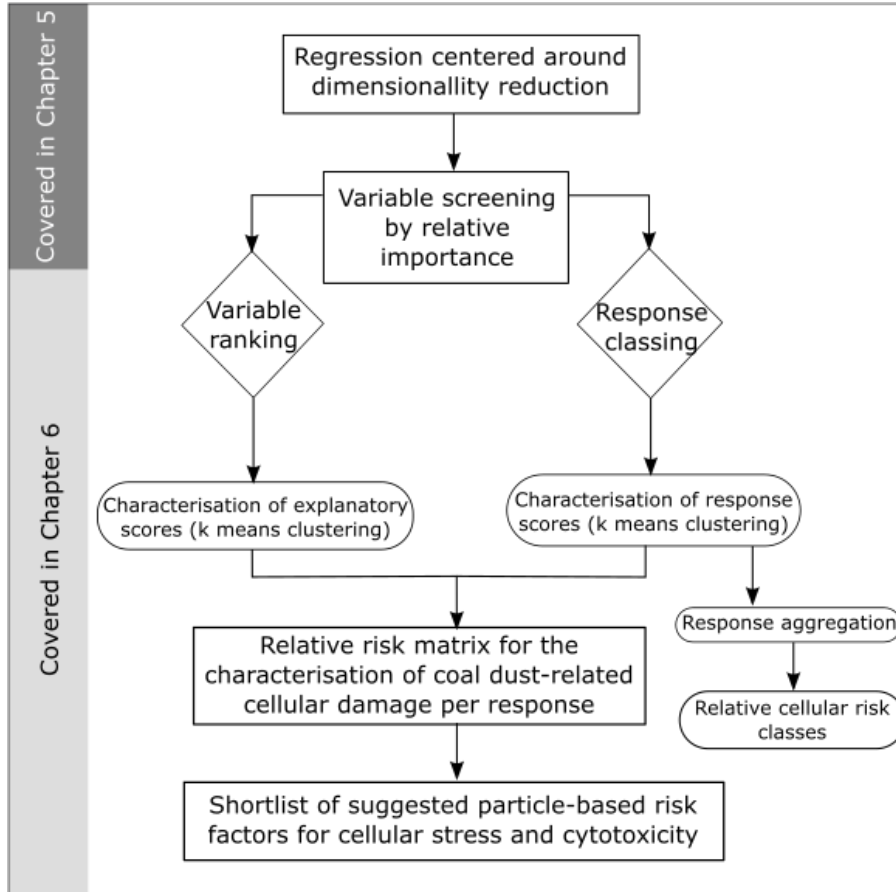
Figure 6-1 Overview of the protocol workflow demonstrating the key elements used to rank and class the particle characteristics and samples most relevant to defining coal dust-related cellular damage.

## 6.4. Case study description: Variable importance screening and ranking

In Chapter 5 a range of 72 particle characteristics were used to model the differences between cytotoxicity (determined by an LDH assay) and lipid peroxidation (determined by an MDA assay) from 17 coal particulate samples. To understand which parameters contributed significantly to the model, the VIP (variable of importance) scores were calculated for each parameter. Based on these scores, variables which computed a value ≥ 1 and reported a coefficient value > 0.01 were deemed influential to the model. Tables E-1 and E-2 in Appendix E represent the list of characteristics which were found to be influential to describing the differences in cytotoxicity and lipid peroxidation respectively based on the results from Chapter 5. As the final form of the PLSR is a linear model, represented as $Y = BX$, the coefficient $B$ is commonly used as a weight for relative importance. However, the coefficient values need to be normalised to represent the absolute rank of the characteristics to the response. In both tables the characteristics are ranked by their relative importance to the respective response based on a normalisation of the regression coefficients of the model (see Eq. 6-1). Additionally, the characteristics represented in both tables were split between variables which showed a positive importance verses a negative importance.

154

$$B_i \times 100 \ / \ \sum_{i=1}^{n} |B_i| \qquad \qquad \text{Eq. 6-1}$$

Where $B_i$ is the coefficient value modelled for each characteristic in the PLS regression.

While these tables allow for the understanding of the relative importance of different characteristics on one scale, this format may suggest to users that few characteristics can be picked out as being the most influential while other characteristics may be deprioritised based on their rank. This may allow for users to bias the reporting of particle-based factors related to the hazard on individual parameters based on their importance rank without considering that groups of variables with similar ranks may be pointing to the presence of underlying mechanisms. Based on this understanding, it becomes important to classify any distinct groups between the response and explanatory variables to relate the magnitude of the coefficient ranks (defined by the latent model) to the real-world values recorded.

## 6.5. Case study results

### 6.5.2. Distinctions between sample characterisation clusters

For the classification of distinct sample groups which show similar characteristics, a k means algorithm was applied to the X scores of the PLSR developed in Chapter 5. Figure 6-2a and b show the clusters identified in the scores plots of both the MDA and LDH responses respectively. Through multiple iterations of the k means algorithm, a reasonable distinction among samples was defined by 3 clusters for both responses.

To interpret the differences between each of the clusters, the standardised mean values for each "influential" characteristic were compared (see Figures 6-3 and 6-4 for the MDA and LDH responses respectively). As the list of influential characteristics listed for each response is extensive, the composition-related information was grouped to generally represent the chemistry and abundance of silicate, carbonate, Ca-bearing sulfates, Fe-bearing sulfates, Fe-bearing sulfides phases (see Table E-3 in Appendix E for a full description of the grouped characteristics).

(a)                                                    (b)
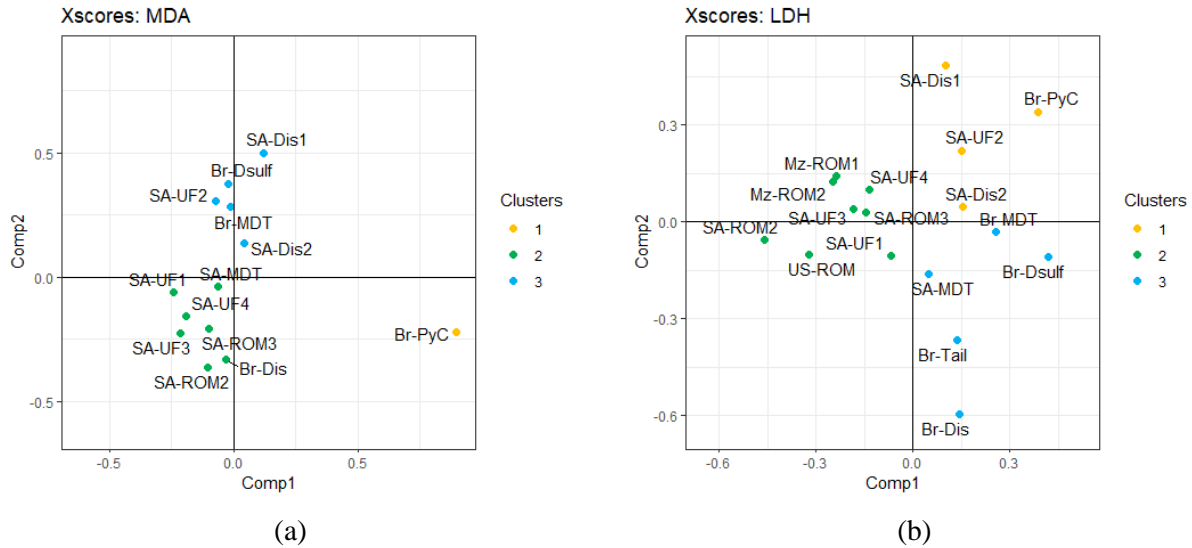
Figure 6-2 K means clustering of the MDA (a) and LDH (b) X scores represented as samples (% variability explained by comp1=21.86 %, comp2= 15.09 %) for MDA and by comp1= 19.94 %, comp2= 12.39 %) for LDH.

Regarding the cluster differentiation analysis for the MDA response, Figure 6-3 shows that the extreme sample in cluster 1 (Br-PyC) differs significantly from the other clusters in terms of its specific surface area (SSA), crystallite size of quartz and Fe-related chemistry and mineralogy. Notably, cluster 1 also displayed the lowest mean values of carbonate chemistry and mineralogy as well as particles with smooth roughness and elongate and smooth shapes compared to the other clusters. Between clusters 2 and 3, marginal differences were observed between the Fe-related chemistry and mineralogy. However, cluster 3 was observed to show lower mean value for carbonate-based chemistry and mineralogy on average compared to cluster 2. Additionally, cluster 3 displayed elevated levels of Ca derived from sulfates as well as higher values for SSA and quartz crystallite size relative to cluster 2. In terms of particle shape, it was observed that on average samples in cluster 3 have the lowest proportion of angular particles compared to the other clusters. In line with this, cluster 3 displayed the highest mean value of particles which were smooth with shapes that were either elongate and smooth or equant, thus further differentiating cluster 3 from the other clusters.
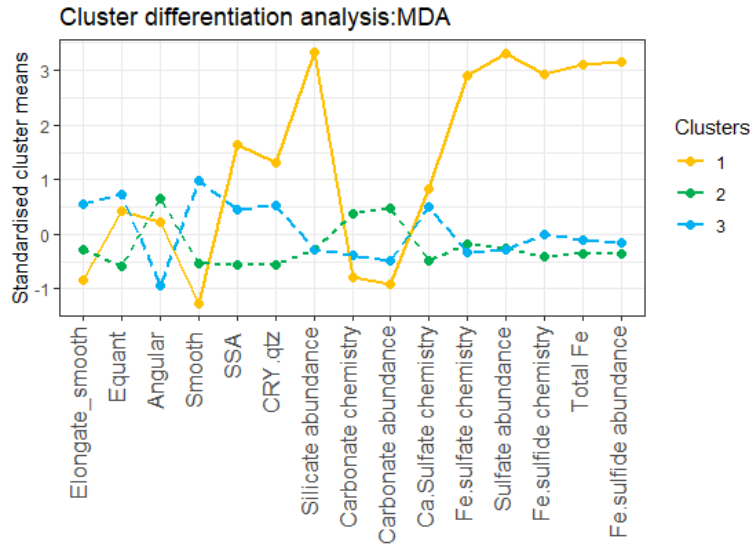
Figure 6-3 Analysis of the mean differences between the k means clusters defined from the X scores of the MDA-based model.

Regarding the clusters defined from the X scores of the LDH-based model, Figure 6-4a and b shows the distinction between these clusters based on their mean values for composition-related and non-composition-related variables respectively. Focusing on the non-composition-related variables, Figure 6-4a demonstrates that cluster 2 strongly deviates from clusters 1 and 3 with respect to the crystallite size of quartz and kaolinite as well as the proportion of liberated versus encapsulated particles. On average the samples in cluster 2 were found to exhibit much smaller mean value for the crystallite size of quartz whilst showing a much higher value of crystallite size for kaolinite compared to the other clusters. Additionally, cluster 2 was found to show much higher mean value of fully encapsulated pyrite compared to clusters 1 and 3. Apart from these mineral specific characteristics, cluster 2 also displayed a much lower mean value for SSA on average compared to the other clusters. Regarding particle roughness, clusters 2 and 3 displayed similar mean values for smooth and jagged particles, while cluster 1 showed a much higher value of smooth particles accompanied by a much lower mean value for jagged particles. In terms of particle shape, cluster 1 displayed the highest values of elongate and smooth and equant shaped particles further accompanied by the lowest mean value for elongate and angular and angular shaped particles. Between clusters 2 and 3, cluster 3 displayed a lower mean value for particles with the shapes elongate and smooth and elongate and angular compared to cluster 2. While both clusters reported the same mean value for angular particles, cluster 2 displayed a lower value of equant shaped particles than cluster 3.
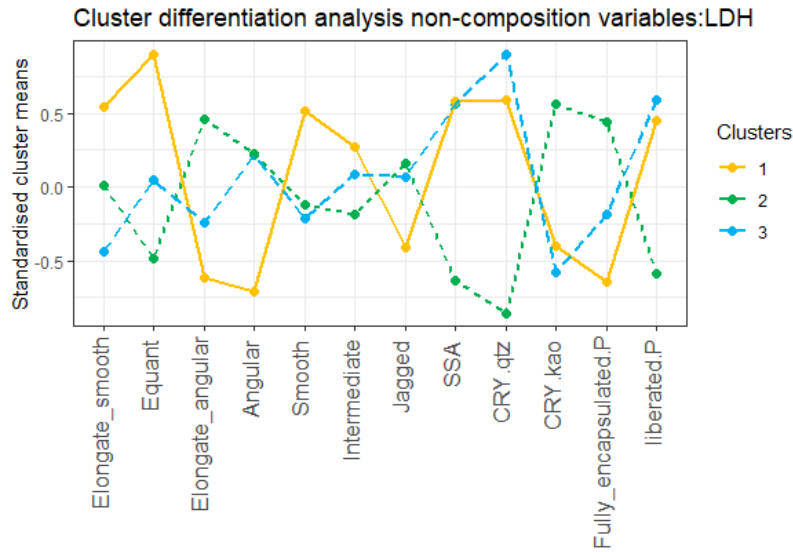
(a)
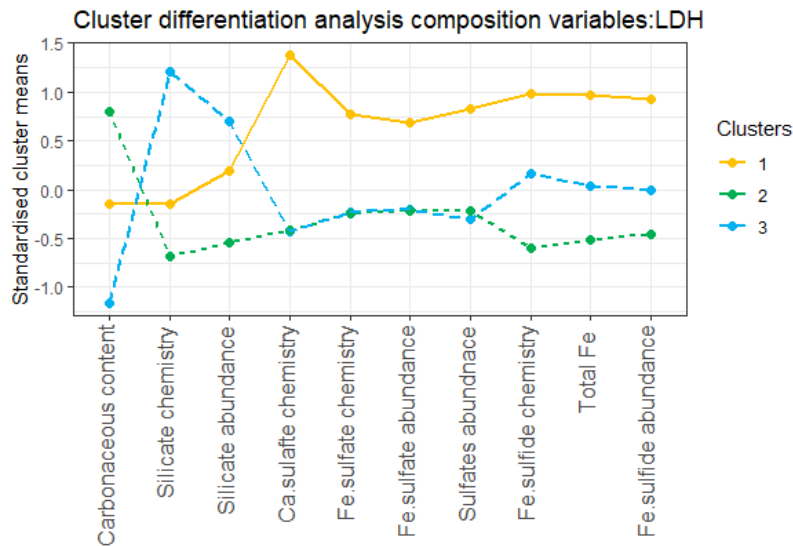


(b)

Figure 6-4 Analysis of the mean differences between the k means clusters defined from the X scores of the LDH-based model. (a) represents the mean differences between the non-composition related variables (general and mineral specific characteristics). (b) represents the mean differences of each cluster across composition-based variables (mineral abundances and chemistry).

With a focus on the composition-related variables and the influence on the clusters defined by the X scores of the LDH-based model, Figure 6-4b demonstrates that cluster 2 and 3 display the highest and lowest mean values for carbonaceous content respectively. In line with the high mean value of carbonaceous content characterised by cluster 2, this cluster generally reports lower values for most of the other mineral-related variables. This is with the exception of Ca-sulfate chemistry, Fe-sulfate chemistry, Fe-sulfate abundance, and general sulfate abundance, where cluster 2 and 3 shared similar mean values. Cluster 1

however 1 showed a distinct enrichment in Ca-sulfate chemistry and Fe-sulfate and sulfide related parameters which distinguishes this cluster relative to clusters 2 and 3. The cluster analysis further shows that cluster 3 is highly enriched in the abundance of silicate minerals and thus silicate chemistry relative to clusters 1 and 2. Additionally, cluster 3 shows an enrichment in the abundance of Fe-sulfide related parameters and total Fe compared to cluster 2.

## 6.5.3. Distinctions between response characterisation clusters

In the context of the two cellular responses measured, the PLSR models constructed in Chapter 5 reported that 98 and 91 % of the variation in the macrophage-based expression of LDH and MDA could be explained by the model. To understand how the sample Y scores relate to the response loading vector, a biplot was constructed of each model (see Figures E-1 and E-2 in Appendix E). Here it was shown that the majority of the sample variation was resolved in the first component, with samples mainly distributed either in the same direction as the response vector (more harmful) or on the opposite end of the vector (less harmful). To further understand whether classes in the response could be identified, a k means algorithm was applied to the Y scores of each response. Through multiple iterations it was determined that 3 clusters could be identified for both responses (see Figure 6-5).



(a)                                         (b)
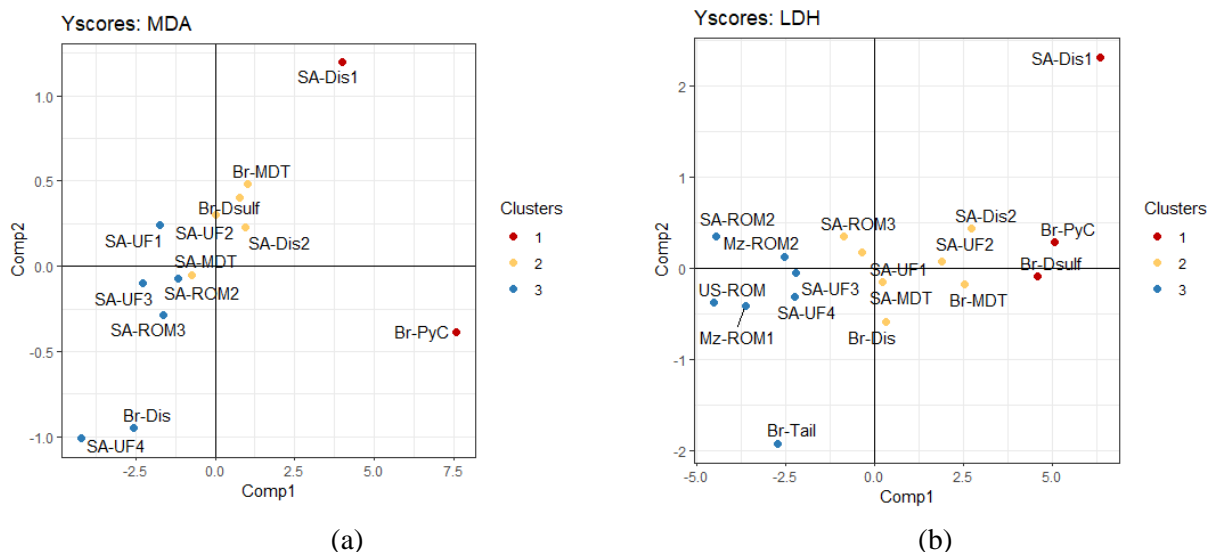
Figure 6-5 K means clustering of the MDA (a) and LDH (b) Y scores represented as samples (% variability explained by comp1=79.56 %, comp2= 13.72 % for MDA responses and by comp1= 71.49 %, comp2= 14.21 % for LDH responses).

To assist in distinguishing the differences between the different clusters, the mean differences between the rate of cytotoxicity and extent of lipid peroxidation were plotted in Figure 6-6. Based on the cluster differences it was found that for cytotoxicity the clusters could be categorised as high, medium, and low response coals. In terms of LDH intensity the distribution of the clusters could be summarised as cluster 1 > cluster 2 >> cluster 3 and cluster 1 >>> cluster 3. Similarly, the MDA intensity of the different clusters

displayed a stepped decrease in abundance of MDA produced, where cluster 1 > cluster 2 > cluster 3. This also suggests that different coals may have either a high, medium, and low propensity to induce lipid peroxidation. However, the MDA response showed that the difference between the low and medium clusters is not as drastic compared to the intensity of LDH expression. This observation may be due to the reduced sample set considered for the MDA response compared to LDH.
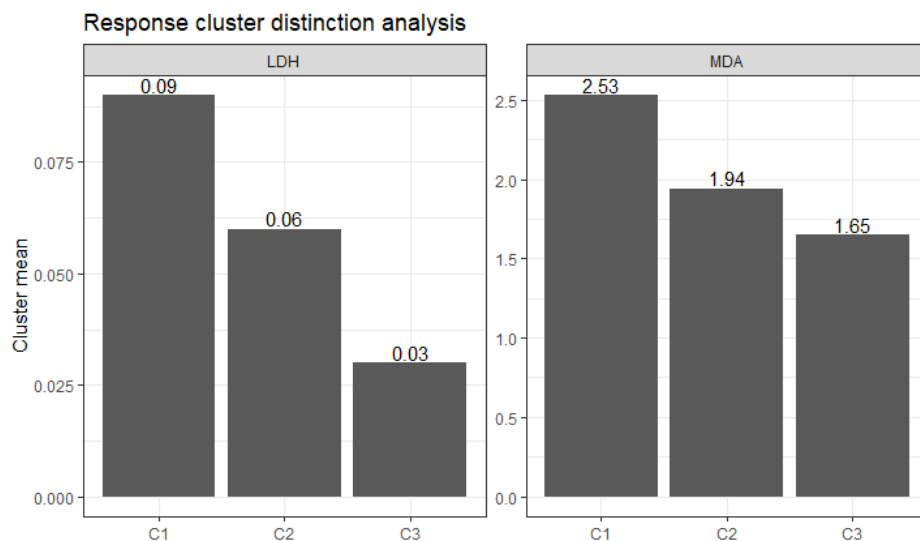


Figure 6-6 Assessment of the cluster mean differences between the rate of LDH intensity on the left-hand side and the average amount of MDA released within each cluster on the right-hand side.

To understand whether any relationships or generalisations could be drawn from the two cellular responses, the Y scores of component 1 (which explained the majority of the variation between samples) from the MDA and LDH-based models were plotted together in Figure 6-7. Here combinations of samples which represented either high, medium, or low category of each response were used to determine high-level hazard classes which accounted for cytotoxicity and oxidative damage in macrophages. Based on this analysis five hazard categories were determined and the trend between the two components showed that for macrophages exposed to dust-sized coal particles, the rate of cytotoxicity and lipid peroxidation are covariant (travel in the same direction). Additionally, a separate analysis found that both the rate of cytotoxicity and lipid peroxidation are significantly correlated ($R^2$ = 0.63, p-value = 0.001). This may suggest that a PLSR with both responses could be constructed, however, more samples would be needed across the hazard categories to allow for any meaningful results to be determined.

**Response characterisation**
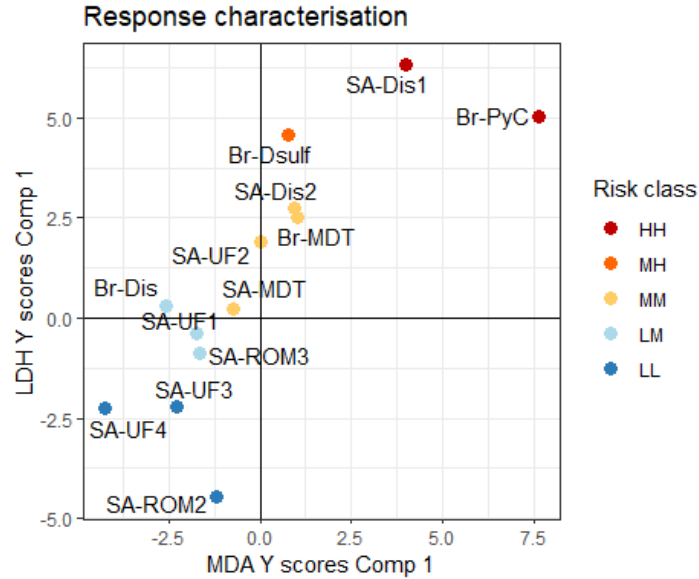
Figure 6-7 Response classification comparing the Y scores for the first component accounting for 78 and 71 % of the variation in the MDA and LDH responses respectively. The codes representing the classes show a combination of H = high; M = medium; or L = low, where the first letter corresponds to the class for the MDA response and the second for the LDH response.

### 6.5.4. Relative hazard characterisation of coal dust-related cellular damage

Thus far, the information relating to the variable importance and the analysis of variation with respect to the characteristics and responses were considered separately. While the interpretation of such information in isolation is straightforward, it can become challenging when attempting to integrate these different sets of information. To effectively understand how these parameters can be utilised to comprehensively describe the relative risk of coal particulates with respect to cellular damage, the format of a data matrix was used for both the ease of interpretation and the integration of different data. To further outline the elements of these matrices Figure 6-8 and 6-7 represent the: (1) variables of importance and their raw values, (2) their rank of importance relative to the responses, (3) the individual toxicity level of each sample, and (4) the cluster number defining samples with similar characteristics for the MDA and LDH-based models respectively.

In terms of the matrix structure, the columns represent the k means clusters of samples with similar characteristics and response classes (distinguishing samples that show a high, medium, or low response). The matrix rows correspond to the raw values for the variables of importance as well as their coefficient rank. To visually assess how each sample may differ from the cluster mean (average of the response clusters), the relative enrichment/depletion of each characteristic relative to the cluster mean was computed along with conditional formatting criteria. By investigating the pairwise comparisons within characteristic and response-based clusters, the toxicity level of a given sample and its characteristics could be compared

against the rank value of each characteristic to aid in the interpretation of which characteristics may be involved in dominant mechanisms in the system.

6.5.4.1 Lipid peroxidation related hazard characterisation

In terms of parameters related to levels of MDA release between samples, the matrix in Figure 6-8 shows that the majority of samples exhibiting low levels of MDA release (SA-UF1, SA-ROM 3&2, SA-UF3, and SA-UF4) are characterised by  relatively high abundance of angular-shaped particles (28-45% in sample) and angular/elongate and smooth particle ratios (14-22), and relatively low levels of smooth (7-14% in sample) and equant shaped samples (29-59%). Additionally, these samples were also characterised by relatively low levels of pyritic Fe (0.13-0.59 wt. %) and low ratios of Fe hosted in pyrite to Ca in carbonates – calcite and dolomite ($\leq$ 1.1). In terms of other relevant characteristics such as chemical, mineralogical, and mineral specific properties, the low MDA samples displayed lower levels of these parameters relative to the other clusters. Moreover, the values of these variables were found to vary quite significantly across the samples in this group. This was observed by ranges in the quartz crystallite size (21.44 – 70.51 nm), gypsum hosted Ca (0.01-0.41 wt. %), carbonate hosted Ca (0.12-0.21 wt. %). In comparison to the other samples in its cluster, SA-UF1 displayed a relatively large quartz crystallite size (70.51 nm), high abundance of gypsum hosted Ca (0.41 wt. %) and relatively high level of carbonate hosted Ca (2.21 wt. %).

Despite being in the low MDA release cluster, sample Br-Dis displayed relatively high levels of pyritic Fe (4 wt. %), low levels of carbonates (0.4 wt. % carbonate hosted Ca) and relatively large quartz crystallite sizes (92 nm). This sample, however, also displayed a significantly higher ratio of angular to elongate and smooth particles (50) compared to other samples in this toxicity group. Additionally, it contains lower levels of smooth (3 % in sample) and equant-shaped samples (40 % in sample).

| | | | Toxicity level | L | L | L | L | L | L | | M | M | M | M | M | | H | H | |
|---|---|---|---|---|---|---|---|---|---|---|---|---|---|---|---|---|---|---|---|
| | | | K means clusters | 2 | 2 | 2 | 2 | 2 | 2 | | 2 | 3 | 3 | 3 | 3 | | 3 | 1 | |
| Rank | Variable | Data class | Samples | Br-Dis | SA-UF1 | SA-ROM2 | SA-ROM3 | SA-UF3 | SA-UF4 | L Mean | SA-MDT | Br-Dsulf | Br-MDT | SA-Dis2 | SA-UF2 | M Mean | SA-Dis1 | Br-PyC | H Mean |
| | **Positive influence** | | | | | | | | | | | | | | | | | | |
| 3.88 | Elongate_smooth (% in sample) | General | | 1.05 | 2.21 | 2.96 | 1.73 | 1.25 | 1.25 | 1.74 | 1.7 | 1.52 | 2.39 | 1.32 | 3.38 | 2.06 | 8.94 | 0.53 | 4.74 |
| 2.44 | Smooth (% in sample) | General | | 2.73 | 7.2 | 7.46 | 9.84 | 10.76 | 14.09 | 8.68 | 8.03 | 18.65 | 15.98 | 13.94 | 15.92 | 14.5 | 22.67 | 4.3 | 13.49 |
| 2.24 | Equant (% in sample) | General | | 40.4 | 57.07 | 28.85 | 54.4 | 58.88 | 58.88 | 49.75 | 57.66 | 64.64 | 66.08 | 63.45 | 67.55 | 63.88 | 64.87 | 62.11 | 63.49 |
| 1.32 | SSA (g/m^2) | General | | 7.24 | 6.67 | 3.23 | 6.13 | 4.03 | 5.03 | 5.39 | 4.86 | 8.31 | 10.47 | 7.94 | 7.68 | 7.85 | 4.09 | 10.48 | 7.29 |
| 3.8 | CRY.qtz (nm) | Mineral specific | | 92.34 | 70.51 | 38.74 | 45.82 | 31.03 | 21.44 | 49.98 | 81.08 | 99.24 | 88.12 | 82.24 | 69.97 | 84.13 | 82.64 | 105.79 | 94.22 |
| 1.93 | Amphibole.XRD (mass %) | Silicate abundance | | 0 | 0 | 0 | 0 | 0 | 0 | 0 | 0 | 0 | 0 | 0 | 0 | 0 | 0 | 0.63 | 0.32 |
| 3.86 | Ca.Gypsum (wt. %) | Ca.Sulfate chemistry | | 0.03 | 0.41 | 0.01 | 0.16 | 0.2 | 0.08 | 0.15 | 0.03 | 0.12 | 0.02 | 0.75 | 0.33 | 0.25 | 0.69 | 0.47 | 0.58 |
| 2.03 | Fe.Rhomboclase (wt. %) | Fe.Sulfate chemistry | | 0.01 | 0.04 | 0 | 0.03 | 0.01 | 0.02 | 0.02 | 0 | 0 | 0 | 0 | 0 | 0 | 0.11 | 2.72 | 1.42 |
| 1.75 | Fe.Szomolnokite (wt. %) | Fe.Sulfate chemistry | | 0.08 | 0.02 | 0.01 | 0.05 | 0.02 | 0.02 | 0.03 | 0 | 0.04 | 0.01 | 0 | 0 | 0.01 | 0.04 | 0.91 | 0.48 |
| 2.3 | Fe.Pyrite (wt. %) | Fe.Sulfide chemistry | | 4.14 | 0.59 | 0.13 | 0.34 | 0.55 | 0.56 | 1.05 | 1.91 | 1.88 | 1.75 | 5.57 | 0.61 | 2.34 | 2.93 | 12.75 | 7.84 |
| 2.09 | Fe (wt. %) | Total Fe | | 4.46 | 2.91 | 0.19 | 0.73 | 0.63 | 0.97 | 1.65 | 2.03 | 1.97 | 1.98 | 5.77 | 1.78 | 2.71 | 2.57 | 16.41 | 9.49 |
| 2.15 | Pyrite.QS (mass %) | Fe.Sulfide abundance | | 6.24 | 0.78 | 1.36 | 0.79 | 1.52 | 1.37 | 2.01 | 1.78 | 3.47 | 1.04 | 9.75 | 1.01 | 3.41 | 4.75 | 29.78 | 17.27 |
| 1.96 | Pyrite.XRD (mass %) | Fe.Sulfide abundance | | 4.69 | 0.4 | 0 | 0 | 0.35 | 0.35 | 0.97 | 1.56 | 1.16 | 0.84 | 5.58 | 0.52 | 1.93 | 2.23 | 23.98 | 13.11 |
| 2.17 | Rhomboclase.XRD (mass %) | Fe.Sulfate abundance | | 0 | 0 | 0 | 0 | 0 | 0 | 0 | 0 | 0 | 1.29 | 0 | 0 | 0.26 | 0.7 | 19.32 | 10.01 |
| 2.08 | Sulfates.QS (mass %) | Fe.Sulfate abundance | | 0.41 | 2.31 | 0.61 | 0.9 | 1.39 | 0.73 | 1.06 | 0.02 | 0.74 | 0.17 | 1.62 | 0.54 | 0.62 | 1.42 | 26.1 | 13.76 |
| 1.93 | Alunogen.XRD (mass %) | Fe.Sulfate abundance | | 0 | 0 | 0 | 0 | 0 | 0 | 0 | 0 | 0 | 0 | 0 | 0 | 0 | 0 | 1.54 | 0.77 |
| 1.93 | Voltaite.XRD (mass %) | Fe.Sulfate abundance | | 0 | 0 | 0 | 0 | 0 | 0 | 0 | 0 | 0 | 0 | 0 | 0 | 0 | 0 | 0.67 | 0.34 |
| 1.63 | szomolnokite.XRD (mass %) | Fe.Sulfate abundance | | 0 | 0 | 0.22 | 1.93 | 0 | 0 | 0.36 | 0 | 0 | 0 | 0 | 0 | 0 | 0 | 6.63 | 3.32 |
| | **Negative influence** | | | | | | | | | | | | | | | | | | |
| 3 | Angular (% in sample) | General | | 47.72 | 31.61 | 45.13 | 31.41 | 27.88 | 27.88 | 35.27 | 29.5 | 18.66 | 17.52 | 24.53 | 13.12 | 20.67 | 15.97 | 30.2 | 23.09 |
| 3.41 | Ca.Dolomite (wt. %) | Carbonate chemistry | | 0 | 0.35 | 0 | 0.16 | 0.76 | 0.62 | 0.32 | 0 | 0 | 0.01 | 0.06 | 0 | 0.01 | 0 | 0 | 0 |
| 1.73 | Ca.Calcite (wt. %) | Carbonate chemistry | | 0.38 | 1.86 | 0.12 | 0.9 | 1.1 | 0.87 | 0.87 | 0.01 | 0.29 | 0.74 | 0.8 | 0.36 | 0.44 | 0.2 | 0.08 | 0.14 |
| 2.4 | Calcite.QS (mass %) | Carbonate abundance | | 0.92 | 5.57 | 1.66 | 1.77 | 3.91 | 3.24 | 2.85 | 0 | 0.9 | 1.65 | 1 | 0.34 | 0.78 | 0.15 | 0.11 | 0.13 |
| 0.97 | Fe.Jarosite (wt. %) | Fe.Sulfate chemistry | | 0.01 | 0 | 0 | 0 | 0 | 0 | 0 | 0 | 0 | 0 | 0 | 0 | 0 | 0 | 0.01 | 0.01 |

| Enrichment factor | >1.5 | 1-1.15 | 1 | 0.5-1 | 0-0.5 | 0 | NaN |
|---|---|---|---|---|---|---|---|

Figure 6-8 Relative lipid peroxidation hazard matrix for the full set of coals analysed showing the classes of characteristics which are most influential to the model and their relative magnitude of influence as well as the clusters of coal particulates with similar properties and their recorded toxicity level/class.

Samples exhibiting moderate MDA release (SA-MDT, Br-Dsulf, SA-Dis2, SA-UF2) have been observed to all contain: (1) lower levels of angular particles (13-30 % in sample), (2) higher levels of pyritic iron (0.6-6 wt. %), (3) higher ratios of Fe in pyrite to Ca in carbonates (1.7-191), and (4) larger quartz crystallite sizes (70-99 nm). Although samples in this toxicity level have lower ratios of angular to elongate-smooth particles (4-18) that overlap with those found in the low MDA release samples, the general trend of the moderate level samples showed higher levels of smooth particles (8-19% of sample). Ultimately, the overlaps in particle shape ranges were deemed a result of the relatively wide range of values for these characteristics. Similarly, samples in moderate level of MDA release displayed a wide range of gypsum and carbonate hosted Ca (0.03-0.75 wt. % and 0.01-0.86 wt. % respectively). For example, whilst sample SA-Dis2 has a relatively high pyritic Fe (5.57 wt. %) and gypsum hosted Ca content (0.75 wt. %), the carbonate content (0.86 wt. % carbonate hosted Ca) is also relatively high, as is the angular/elongate-smooth particle ratio (18). On the other hand, SA-UF2 has a relatively low pyritic Fe content (0.6 wt. %), low ratio of Fe in pyrite to Ca in carbonate ratio (1.7), smaller quartz crystalline quartz size (70nm). However, the abundance of elongate and smooth particles is high (3.38%) and angular/elongate and smooth ratio low (3.9).

The two samples with high toxicity based on MDA response (SA-Dis1 and Br-PyC) differ quite significantly in terms of their physicochemical properties. Both samples exhibit relatively high levels of gypsum hosted Ca (0.69 and 0.47 wt. %). Sample SA Dis1 has moderately large quartz crystallites (82.6 nm), as well as relatively high levels of Fe as pyrite (2.93 %) and gypsum hosted Ca (0.69 wt. %) in combination with a low carbonate content (0.2 wt. % carbonate hosted Ca). This results in a relatively high pyritic Fe: carbonate-associated Ca ratio (14.7) in comparison to most of the samples classified in the low-moderate toxicity level. Furthermore, the percentage of elongate and smooth particles (8.9 % of sample) is significantly higher than all the other samples across clusters, and the angular/elongate and smooth ratio (1.7) is significantly lower than other samples in cluster 3 with moderate toxicity.

In contrast, Br-PyC displays relatively low contents of elongate and smooth particles (0.53 % in sample) and a high angular/elongate and smooth particle ratio (56) in comparison to all samples tested. However, the pyritic Fe content is relatively high (12.8 wt. %) and the carbonate hosted Ca relatively low (0.08 wt. %), thus resulting in a significantly elevated pyritic Fe/ carbonate hosted Ca ratio (159). The sample is also characterised by relatively high gypsum hosted Ca (0.63) and a large quartz crystallite size (106 nm).

6.5.4.2 Cytotoxicity related hazard characterisation

In terms of LDH release, the agreement between sample clusters (classified on the basis of chemical characteristics) and toxicity levels (i.e. level of cytotoxicity) is not as well defined as it was for the MDA-based matrix (seen in Figure 6-9). For instance, whilst the majority of cluster 2 samples are associated with low toxicity levels, samples SA-UF1 and SA-ROM3 both exhibit moderate toxicity. Similarly, whilst 3 of 5 samples in cluster 3 exhibit moderate toxicity, Br-Tail shows low toxicity, whilst Br-Dsulf displays high levels of toxicity. Samples falling into cluster 1, exhibit both moderate toxicity (SA-Dis 2 and SA-UF2) and high toxicity (Br-PyC and SA-Dis1).

Of the parameters identified by the LDH-based model, particle shape and roughness were weighted strongly in terms of explaining the differences between the levels of cytotoxicity amongst the samples. Within and between the toxicity levels, samples display large variation between the proportions of particles reporting on the spectrum of more 'angular and jagged' or 'smooth and equant'. In the low and moderate toxicity clusters, most of the samples reported higher abundances of angular particles with jagged roughness compared to equant particles with smooth roughness. Samples Mz-ROM 1&2 and SA-UF 3 (in the low toxicity cluster); SA-MDT, SA-UF1, SA-ROM3, and SA-Dis2 (in the moderate toxicity cluster); and Br-PyC (high toxicity cluster) displayed a ratio of angular + jagged/ equant + smooth between 1.2 – 1.8, while Br-Dis (moderate toxicity) and US-ROM, SA-ROM2 and Br-Tail (low toxicity) had ratios between 2.4-3.6. By contrast, samples SA-UF4, Br-MDT and SA-UF2 (moderate toxicity) and Br-Dsulf and SA-Dis1 (high toxicity) displayed ratios between 1 and 0.9. Ultimately, while there is significant overlap between the clusters, the distribution on this limited dataset suggests that the low toxicity samples are more skewed to the spectrum of angular-shaped and jagged particles than the moderate and high toxicity samples. Based on the ratio between Angular + Jagged to Equant + Smooth particles sub-groups within each toxicity level were defined (see Table 6-1).

Table 6-1 Description of the shaped-based sample sub-groups defined by the ratio between angular + jagged and equant + smooth particles.

| Sub-group name | Definition: angular + jagged/ equant + smooth | Samples |
|---|---|---|
| Equivalent angular to equant | 0.9-1.0 | *Moderate toxicity:* SA-UF2, Br-MDT<br>*High toxicity:* Br-Dsulf, SA-Dis1 |
| Moderately angular | 1.1-1.8 | *Low toxicity:* SA-UF 3&4, Mz-ROM 1&2<br>*Moderate toxicity:* SA-Dis2, SA-MDT, SA-UF1, SA-ROM3<br>*High toxicity:* Br-PyC |
| Mostly angular | 2.4-3.6 | *Low toxicity:* Br-Tail, US-ROM, SA-ROM2<br>*Moderate toxicity:* Br-Dis |

| Toxicity level | | | L | L | L | L | L | L | L | | M | M | M | M | M | M | M | | H | H | H | |
|---|---|---|---|---|---|---|---|---|---|---|---|---|---|---|---|---|---|---|---|---|---|---|
| K means clusters | | | 2 | 2 | 2 | 2 | 2 | 2 | 3 | | 3 | 3 | 3 | 2 | 2 | 1 | 1 | | 3 | 1 | 1 | |
| Samples | | | Mz-ROM1 | Mz-ROM2 | US-ROM | SA-ROM2 | SA-UF3 | SA-UF4 | Br-Tail | | Br-MDT | Br-Dis | SA-MDT | SA-UF1 | SA-ROM3 | SA-Dis2 | SA-UF2 | | Br-Dsulf | Br-PyC | SA-Dis1 | |
| Rank | Variable | Data class | | | | | | | | L Mean | | | | | | | | M Mean | | | | H Mean |
| | **Positive influence** | | | | | | | | | | | | | | | | | | | | | |
| 5.31 | Elongate_smooth (% in sample) | General | 4.1 | 5.01 | 0.96 | 2.96 | 1.25 | 1.94 | 0.83 | 2.44 | 2.39 | 1.05 | 1.7 | 2.21 | 1.73 | 1.32 | 3.38 | 1.97 | 1.52 | 0.53 | 8.94 | 3.66 |
| 4.64 | Smooth (% in sample) | General | 15.69 | 14.85 | 4.55 | 7.46 | 10.76 | 14.09 | 4.55 | 10.28 | 15.98 | 2.73 | 8.03 | 7.2 | 9.84 | 13.94 | 15.92 | 10.52 | 18.65 | 4.3 | 22.67 | 15.21 |
| 4.12 | Equant (% in sample) | General | 49.1 | 40.35 | 48.54 | 28.85 | 58.88 | 65.19 | 47.67 | 48.37 | 66.08 | 40.4 | 57.66 | 57.07 | 54.4 | 63.45 | 67.55 | 58.09 | 64.64 | 62.11 | 64.87 | 63.87 |
| 2.69 | Intermediate (% in sample) | General | 15.85 | 16.69 | 7.12 | 5.56 | 16.9 | 19.36 | 8.27 | 12.82 | 23.4 | 5.8 | 12.3 | 12.33 | 12.34 | 17.35 | 19.36 | 14.70 | 24.5 | 9.65 | 17.44 | 17.20 |
| 1.39 | SSA (g/m^2) | General | 4.54 | 5.46 | 3.75 | 3.23 | 4.03 | 5.03 | 6.63 | 4.67 | 10.47 | 7.24 | 4.86 | 6.67 | 6.13 | 7.94 | 7.68 | 7.28 | 8.31 | 10.48 | 4.09 | 7.63 |
| 2.32 | liberated.Py (% in sample) | Mineral specific | 0 | 0 | 1.53 | 0 | 17.76 | 31.39 | 18.8 | 9.93 | 41.35 | 12.82 | 17.98 | 0 | 1.27 | 19.59 | 34.65 | 18.24 | 24.5 | 0.44 | 29.89 | 18.28 |
| 2.18 | CRY.qtz (nm) | Mineral specific | 46.27 | 58 | 69.88 | 38.74 | 31.03 | 21.44 | 104.93 | 52.9 | 88.12 | 92.34 | 81.08 | 70.51 | 45.82 | 82.24 | 69.97 | 75.73 | 99.24 | 105.79 | 82.64 | 95.89 |
| 1.36 | Si.Quartz (wt. %) | Silicate chemistry | 2.39 | 2.63 | 0.3 | 1.27 | 1.63 | 1.84 | 7.11 | 2.45 | 6 | 7.86 | 7.06 | 10.18 | 2.99 | 6.29 | 3.52 | 6.27 | 11.26 | 4.02 | 2.8 | 6.03 |
| 1.04 | Al (wt. %) | Silicate chemistry | 2.97 | 3.04 | 0.46 | 1.3 | 3.59 | 3.86 | 10.02 | 3.61 | 10.89 | 12.08 | 8.91 | 4.62 | 5.83 | 7.54 | 7.91 | 8.25 | 13.65 | 2.57 | 5.02 | 7.08 |
| 0.95 | Si (wt. %) | Silicate chemistry | 5.61 | 5.71 | 0.71 | 2.77 | 5.13 | 5.09 | 18.4 | 6.2 | 16.98 | 20.77 | 15.84 | 13.52 | 7.81 | 13.77 | 10.61 | 14.19 | 24.27 | 4.82 | 8.21 | 12.43 |
| 0.67 | Ti (wt. %) | Silicate chemistry | 0.22 | 0.22 | 0.03 | 0.07 | 0.23 | 0.23 | 0.51 | 0.22 | 0.5 | 0.58 | 0.59 | 0.26 | 0.35 | 0.42 | 0.48 | 0.45 | 0.67 | 0.12 | 0.26 | 0.35 |
| 0.32 | Si.Clays (wt. %) | Silicate chemistry | 3.22 | 3.08 | 0.41 | 1.5 | 3.5 | 3.25 | 11.29 | 3.75 | 10.96 | 12.91 | 8.78 | 3.34 | 4.82 | 7.47 | 7.09 | 7.91 | 13.01 | 0.79 | 4.92 | 6.24 |
| 1.91 | Kaolinite.XRD (mass %) | Silicate abundance | 8.83 | 8.66 | 0 | 6.88 | 12.26 | 13.68 | 25.73 | 10.86 | 28.44 | 27.81 | 29.88 | 18.78 | 25.82 | 25.15 | 27.43 | 26.19 | 35.94 | 5.84 | 16.95 | 19.58 |
| 1.26 | Amphibole.XRD (mass %) | Silicate abundance | 0 | 0 | 0 | 0 | 0 | 0 | 0 | 0 | 0 | 0 | 0 | 0 | 0 | 0 | 0 | 0.00 | 0 | 0.63 | 0 | 0.21 |
| 0.44 | Clays.QS (mass %) | Silicate abundance | 14.04 | 13.14 | 2.26 | 4.85 | 14.33 | 15.04 | 51.48 | 16.45 | 55.72 | 62.72 | 44.46 | 18.24 | 22.86 | 30.83 | 36.25 | 38.73 | 56.67 | 3.08 | 24.04 | 27.93 |
| 4.74 | Ca.Gypsum (wt. %) | Ca.Sulfate chemistry | 0.07 | 0.07 | 0.01 | 0.01 | 0.2 | 0.08 | 0.42 | 0.12 | 0.02 | 0.03 | 0.03 | 0.41 | 0.16 | 0.75 | 0.33 | 0.25 | 0.12 | 0.47 | 0.69 | 0.43 |
| 1.44 | Fe.Rhomboclase (wt. %) | Fe.Sulfate chemistry | 0.04 | 0.03 | 0.07 | 0 | 0.01 | 0.02 | 0 | 0.02 | 0 | 0.01 | 0 | 0.04 | 0.03 | 0 | 0 | 0.01 | 0 | 2.72 | 0.11 | 0.94 |
| 1.22 | Fe.Szomolnokite (wt. %) | Fe.Sulfate chemistry | 0 | 0.04 | 0.03 | 0.01 | 0.02 | 0.02 | 0.05 | 0.02 | 0.01 | 0.08 | 0 | 0.02 | 0.05 | 0 | 0 | 0.02 | 0.04 | 0.91 | 0.04 | 0.33 |
| 1.78 | Fe.Pyrite (wt. %) | Fe.Sulfide chemistry | 0.48 | 0.5 | 0.77 | 0.13 | 0.55 | 0.56 | 4.86 | 1.12 | 1.75 | 4.14 | 1.91 | 0.59 | 0.34 | 5.57 | 0.61 | 2.13 | 1.88 | 12.75 | 2.93 | 5.85 |
| 1.59 | Fe (wt. %) | Total Fe | 0.74 | 0.7 | 0.89 | 0.19 | 0.63 | 0.97 | 5.03 | 1.31 | 1.98 | 4.46 | 2.03 | 2.91 | 0.73 | 5.77 | 1.78 | 2.81 | 1.97 | 16.41 | 2.57 | 6.98 |
| 1.53 | Pyrite.QS (mass %) | Fe.Sulfide abundance | 0.67 | 1.82 | 2.62 | 1.36 | 1.52 | 1.37 | 7.98 | 2.48 | 1.04 | 6.24 | 1.78 | 0.78 | 0.79 | 9.75 | 1.01 | 3.06 | 3.47 | 29.78 | 4.75 | 12.67 |
| 0.83 | Pyrite.XRD (mass %) | Fe.Sulfide abundance | 0.23 | 0.33 | 0 | 0 | 0.35 | 0.35 | 7.63 | 1.27 | 0.84 | 4.69 | 1.56 | 0.4 | 0 | 5.58 | 0.52 | 1.94 | 1.16 | 23.98 | 2.23 | 9.12 |
| 3.71 | Jarosite.XRD (mass %) | Fe.Sulfate abundance | 0.49 | 0.5 | 0 | 0 | 0 | 0 | 0 | 0.14 | 0 | 0 | 0.76 | 0 | 0 | 0 | 0 | 0.11 | 0 | 0 | 0.91 | 0.30 |
| 1.54 | Rhomboclase.XRD (mass %) | Fe.Sulfate abundance | 0 | 0 | 0 | 0 | 0 | 0 | 0 | 0 | 1.29 | 0 | 0 | 0 | 0 | 0 | 0 | 0.18 | 0 | 19.32 | 0.7 | 6.67 |
| 1.41 | Sulfates.QS (mass %) | Fe.Sulfate abundance | 0.62 | 0.58 | 0.9 | 0.61 | 1.39 | 0.73 | 1.27 | 0.87 | 0.17 | 0.41 | 0.02 | 2.31 | 0.9 | 1.62 | 0.54 | 0.85 | 0.74 | 26.1 | 1.42 | 9.42 |
| 1.26 | Alunogen.XRD (mass %) | Fe.Sulfate abundance | 0 | 0 | 0 | 0 | 0 | 0 | 0 | 0 | 0 | 0 | 0 | 0 | 0 | 0 | 0 | 0.00 | 0 | 1.54 | 0 | 0.51 |
| 1.26 | Voltaite.XRD (mass %) | Fe.Sulfate abundance | 0 | 0 | 0 | 0 | 0 | 0 | 0 | 0 | 0 | 0 | 0 | 0 | 0 | 0 | 0 | 0.00 | 0 | 0.67 | 0 | 0.22 |
| | **Negative influence** | | | | | | | | | | | | | | | | | | | | | |
| 3.8 | Jagged (mass %) | General | 68.46 | 68.46 | 88.33 | 86.98 | 72.33 | 66.55 | 87.18 | 76.9 | 60.62 | 91.47 | 79.67 | 80.47 | 77.82 | 68.7 | 64.72 | 74.78 | 56.85 | 86.06 | 59.9 | 67.60 |
| 3.36 | Elongate_angular (% in sample) | General | 25.49 | 32.33 | 11.3 | 22.47 | 11.06 | 10.49 | 13.1 | 18.03 | 12.4 | 10.79 | 10.35 | 8.09 | 11.57 | 8.93 | 13.13 | 10.75 | 13 | 6.32 | 9.04 | 9.45 |
| 3.35 | Angular (% in sample) | General | 19.44 | 20.7 | 38.59 | 45.13 | 27.88 | 20.64 | 37.75 | 30.02 | 17.52 | 47.72 | 29.5 | 31.61 | 31.41 | 24.53 | 13.12 | 27.92 | 18.66 | 30.2 | 15.97 | 21.61 |
| 2.74 | Fully_encapsulated.Py (% in sample) | Mineral specific | 35.82 | 32.42 | 15.27 | 31.62 | 2.63 | 9.49 | 14.66 | 20.27 | 7.69 | 16.03 | 20.22 | 2.56 | 24.05 | 9.54 | 1.98 | 11.72 | 3.75 | 7.39 | 10.95 | 7.36 |
| 1.25 | CRY.kao (nm) | Mineral specific | 33.23 | 40.98 | 27.32 | 30.01 | 26.25 | 24.5 | 22.57 | 29.27 | 19.52 | 24.64 | 28.6 | 27.78 | 26.31 | 22.88 | 26.49 | 25.17 | 25.12 | 23.86 | 26.49 | 25.16 |
| 1.24 | Carbonaceous.QS (mass %) | Carbonaceous content | 73.83 | 73.76 | 92.28 | 88.4 | 68.3 | 67.33 | 22.41 | 69.47 | 25.95 | 10.1 | 34.72 | 41.14 | 62.6 | 43.55 | 50.88 | 38.42 | 14.05 | 32.76 | 61.42 | 69.47 |

| Enrichment factor | >1.5 | 1-1.15 | 1 | 0.5-1 | 0-0.5 | 0 | NaN |
|---|---|---|---|---|---|---|---|

Figure 6-9 Relative cytotoxicity hazard matrix for the full set of coals analysed showing the classes of characteristics which are most influential to the model and their relative magnitude of influence as well as the clusters of coal particulates with similar recorded toxicity level/class.

Regarding the distribution of elongate and smooth and elongate and angular particles, samples displayed more distinct ranges when classified by the shape-based subgroups defined in Table 6-1. Within the low toxicity cluster, the moderately angular subgroup of samples (Mz-ROM 1&2 and SA-UF 3&4) reported 1.3-5 % elongate and smooth particles and 10.5-32.3 % elongate and angular particles, while the mostly angular subgroup (Br-Tail, US-ROM and SA-ROM2) displayed a narrower distribution of the two shapes (0.8-3 % and 11.3-22.5 % respectively). In the moderate toxicity cluster, samples SA-UF2 and Br-MDT generally contained higher proportions of elongate and angular as well as elongate and smooth particles (2.4-3.4 % and 12.4-13.1 % respectively) compared to the moderately angular and mostly angular sub-groups (1.3-2.2, 1.1 % and 8.1-11.6, 10.8 % respectively). Regarding the high toxicity cluster, samples Br-Dsulf and SA-Dis1 in the equivalent angular to equant sub-group reported a wide range in the abundance of both shapes (1.5-8.9 and 9-13 % between the two respective shapes), while Br-PyC in the moderately angular subgroup displayed low values for these shapes in comparison to other samples in the same subgroup (0.5 % and 6.3 % between the two respective shapes).

In addition to particle shape, parameters related to silicate chemistry and clay content were deemed positively influential to cytotoxicity. Between the clusters, majority of samples which displayed a low level of LDH release (Mz-ROM1, Mz-ROM2, US-ROM, SA-ROM2, SA-UF3, and SA-UF4), also showed lower proportions of silicate related chemistry (1.20-9.18 combined wt. % of Al, Si, and Ti). This in turn translated to low abundances of clay content and kaolinite in particular (2.26-15 wt. % clays and 6.88-13.7 wt. % kaolinite). These observations were consistent with the fact that the low toxicity samples generally contained higher proportions of carbonaceous matter (67.3-92.3 wt. %) and thus low mineral content. In contrast the general trend in the low toxicity cluster, Br-Tail reported a relatively low amount of carbonaceous matter (22.41 wt. %) and higher abundances of silicate related chemistry (28.93 combined wt. % of silicate chemistry) and mineralogy (51.48 wt. % clays and 25.73 wt. % kaolinite).

For the samples in the moderate toxicity level (Br-MDT, Br-Dis, SA-MDT, SA-UF1, SA-ROM3, SA-Dis2, SA-UF2), the data trends generally showed higher abundances of silicate chemistry (18.4-33.43 combined wt. %), with lower but variable proportions of carbonaceous matter (10.1-62.6 wt. %) and higher amounts of clay content (18.2-62.7 wt. %) compared to samples in the low toxicity cluster. Regarding the samples in the high toxicity level (Br-Dsulf, Br-PyC, and SA-Dis1), a high level of variation was observed in the abundance of carbonaceous matter and thus silicate chemistry (38.59, 7.51, 13.49 combined wt. % respectively) and clay content (56.7, 3.08, 24 wt. % respectively).

Apart from the chemical parameters of silicate minerals, a closer examination of the relationships between quartz crystallite size and the distribution of Si in quartz showed that majority of low toxicity samples (Mz-ROM1, Mz-ROM2, US-ROM, SA-ROM2, SA-UF3, and SA-UF4) report small crystallite

sizes of quartz (21.4-69.9 nm) with very low abundances of Si hosted in quartz (0.3-2.63 wt. %), while the majority of the moderate toxicity samples (Br-MDT, Br-Dis, SA-MDT, SA-UF1, and SA-Dis2) reported higher abundances of Si in quartz (6-10.2 wt. %) and larger crystallite sizes of quartz than the low toxicity level (70.5-92.3 nm). SA-ROM3 and SA-UF2 however, displayed smaller crystallite sizes (45.8 and 70 nm respectively) and lower abundances of Si hosted in quartz (2.99-3.52 respectively) despite being in the moderate toxicity level. The high toxicity samples again showed a variation in parameter values between samples. However, between the samples (Br-Dsulf, Br-PyC, and SA-Dis1) the crystallite sizes of quartz were generally observed to be high (99.2, 105.8, 82.6 nm respectively) with variable amounts of Si hosted in quartz (11.3, 4.02, 2.8 wt. % respectively).

Apart from the influence of silicate mineralogy, the chemical and mineralogical parameters relating to pyrite and sulfate minerals have also been observed to contribute positively and significantly to cytotoxicity. Generally, most of the samples in the low and moderate toxicity level (Mz-ROM 1&2, US-ROM, SA-ROM 2&3, SA-UF 1,2,3&4, Br-MDT, SA-MDT) reported percentages of pyrite ranging from 0.67-2.62 wt. %. The samples Br-Tail (in the low toxicity level) as well as Br-Dis and SA-Dis1 (in the moderate toxicity level) reported 7.98, 6.24, and 9.75 wt. % pyrite respectively. The high toxicity level samples generally had higher levels of pyrite, with Br-PyC, Br-Dsulf and SA-Dis1 reporting 29.78, 3.47, and 4.75 wt. % respectively. Aside from the abundance of pyrite, the degree of pyrite liberation was also deemed influential. Many of the samples in the low toxicity level (Mz-ROM 1&2, US-ROM, and SA-ROM2) reported virtually no liberated pyrite grains, while the remaining samples SA-UF 3&4 and Br-Tail displayed appreciable levels of liberated pyrite grains (17.76, 31.39, and 18.8 %). Majority of the samples in the moderate toxicity level (Br-MDT, Br-Dis, SA-MDT, SA-Dis2, and SA-UF2) generally showed higher levels of pyrite liberation compared to the low toxicity samples (12.82-41.35 %). However, samples SA-UF1 and SA-ROM reported virtually no liberated pyrite grains (similarly to many of samples in cluster 2). In the case of samples in the high toxicity level, samples Br-Dsulf and SA-Dis1 displayed significant levels of liberated pyrite (24.5 and 29.89 % respectively), whereas Br-PyC reported < 1 % liberated pyrite.

Regarding the influence of sulfide-based parameters, the LDH-based model determined that the elemental contribution of sulfates (rhomboclase and szomolnokite and gypsum) play an important role in cytotoxicity. When considering the ratio between pyrite/total sulfate content, the comparison showed that there is a greater abundance of pyrite as opposed to sulfates across most of the samples in the population. However, samples SA-UF1 and SA-ROM3 (in the moderate toxicity level) reported 1.95 and 0.11 wt. % more sulfate content than pyrite. Between these samples, the elevated levels of sulfate content translated to a higher abundance in gypsum hosted Ca relative to the low toxicity coals (0.41 wt. % in SA-UF1 and 0.16 wt. % in SA-ROM3). Though a separate analysis of gypsum liberation, it was determined that while these

samples contained higher levels of Ca in gypsum, the gypsum in these samples were either mostly encapsulated or fully encapsulated (see Figure 6-10). In the case of samples Mz-ROM1, SA-UF3, and Br-PyC, similar values for pyrite and sulfate abundance were reported. For Mz-ROM1 and SA-UF3 the elemental contribution from gypsum hosted Ca were 1.8 and 6.7 times greater than the contribution from the Fe-bearing sulfates (rhomboclase and szomolnokite) respectively, while Br-PyC displayed 7.7 times more elemental contribution from Fe-bearing sulfates than gypsum hosted Ca. Similarly, samples US-ROM and Br-Dis reported a higher elemental contribution of Fe from Fe-sulfates than gypsum hosted Ca (10 and 3 times respectively). By contrast, samples Br-Tail, Br-MDT, Br-Dsulf and SA-Dis1, which reported higher ratios of pyrite to sulfate abundance (>3.4), displayed a higher elemental contribution of Ca hosted in gypsum compared to the Fe hosted in Fe-sulfates (8.4, 2, 3, 4.6 times respectively). In terms of the liberation of gypsum between these samples, Br-Dsulf and SA-Dis1 yielded 35 and 28 % liberated gypsum respectively, while Br-Tail and Br-MDT displayed 7.17 and 0 % respectively. Of the remaining samples in the low toxicity level, Mz-ROM2, SA-ROM2 displayed similar elemental contributions of gypsum hosted Ca and Fe hosted in Fe-bearing sulfates. Finally, samples SA-MDT, SA-Dis2 and SA-UF2 (in the moderate toxicity level) reported no elemental Fe derived from sulfates but did however display varying amounts of gypsum hosted Ca (0.03, 0.75, 0.33 wt. % respectively). By contrast, SA-MDT and SA-UF reported no liberated gypsum grains, while 15 % of the gypsum in SA-Dis2 was liberated.
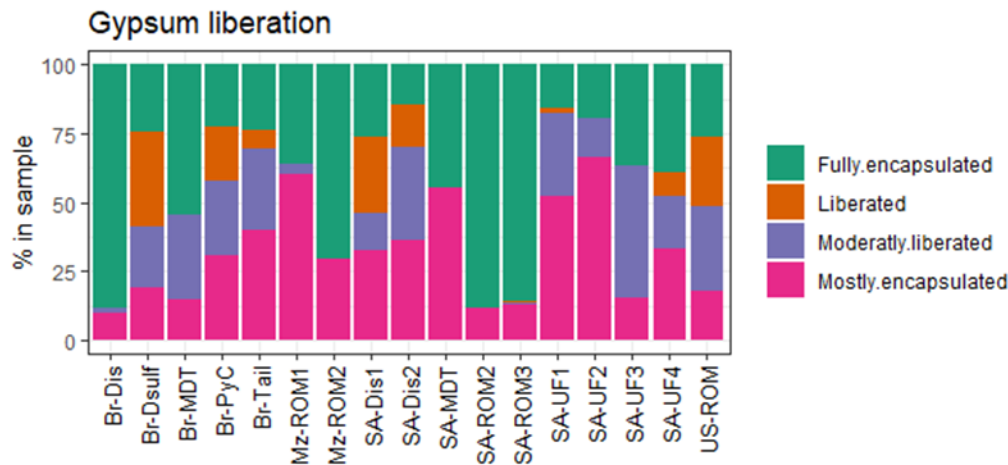


Figure 6-10 Gypsum liberation per sample analysed.

## 6.6. Discussion

In this Chapter, an analysis of a data matrix demonstrating the key elements of the relationship demonstrated in Chapter 5 was conducted as part of a protocol to shortlist key parameters that can be used by relevant stakeholders to assess the toxicity of different coal dust. In doing so, the latent structures of the PLSR applied in Chapter 5 were used to characterise samples with similar intrinsic properties and responses. The results showed that samples could be classified based on their characteristics by using a k means algorithm on the X scores of the PLSR. Additionally, these same samples could be characterised based on their level of toxicity (either high – H, Moderate – M, or low – L) using the same approach on the modelled Y scores. By combining the toxicity levels of the different responses (cytotoxicity and lipid peroxidation), five classes of cellular harm were determined. This same rationale was explored by Song et al, (2022) where they aggregated cytotoxic, proinflammatory and fibrogenic factors using Principal Components Analysis for the purposes of determining a single harm term. In this study the classes determined included: (1) $H_{MDA}H_{LDH}$, (2) $H_{MDA}M_{LDH}$, (3) $M_{MDA}M_{LDH}$, (4) $L_{MDA}M_{LDH}$, and (5) $L_{MDA}L_{LDH}$. These classes suggest that there is a wider spread of samples which report moderate reactive oxygen species (ROS)-related damage, but also show varying degrees of cytotoxicity. As ROS are an important feature of phagocytic cells' innate response to foreign matter, this observation is consistent with the fact that the inherent toxicity of some samples will be manageable by phagocytes, while others may require the activation of inflammatory pathways and, in the worst case, lead to a ROS imbalance and significant cell death and inflammation.

Between the two matrices, the MDA-matrix showed that the k means clusters which defined similar characteristic-based groups were mostly consistent with the samples in the toxicity levels. This suggests that the distinct parameter differences between the characteristic-based clusters can mostly translate to level of lipid peroxidation expected for a sample or set of samples. Some examples of this were expressed by considering (1) the ratio of Fe hosted in pyrite/ Ca hosted in carbonates, (2) ratio of angular/ elongate and smooth shaped particles, (3) the percentages of angular, equant and smooth particles, (4) quartz crystallite size, and (5) abundance of Ca hosted gypsum.

In the case of cytotoxicity, the characterisation-based clusters did not overlap well with the toxicity levels. This implies that the inter-relationships between the parameters are not as clear-cut as for lipid peroxidation. However, this is to be expected as cytotoxicity can result from a range of indirect/direct means which may or may not be from ROS-related pathways. The matrices did however show that many of the key parameters related to the MDA-based model were linked to cytotoxicity. These included the: (1) ratios of angular and jagged particles to equant and smooth particles, and (2) proportions of elongate and angular

to elongate and smooth shapes (3) the abundance of pyritic Fe and sulfate-hosted Fe, with the added consideration of pyrite liberation (4) quartz crystallite size, and (5) abundance of Ca hosted gypsum.

In terms of the non-ROS related parameters linked to cytotoxicity, the most distinctive characteristics identified were the proportion of carbonaceous matter, clay content and silicate-related chemistry. The results generally showed that carbonaceous content had a negative influence on cytotoxicity, further suggesting that the minerals in the coal particulates are operative to the direct or indirect effects between the particles and cells. In the case of the clay content, the low toxicity samples generally contained significantly lower abundance of clays (kaolinite in particular) compared to the moderate and high toxicity samples. While studies by Davies 1983; Gibbs 1990; and Carretero et al 2006 have discussed the toxicity of kaolinite, no mechanism relating to its toxicity has been established. In addition to the abundance of kaolinite the results further showed that the chemistry of kaolinite had a positive influence on cytotoxicity while the crystallite size of kaolinite displayed a negative but significant influence. This suggest that there may be an element of chemical reactivity which could be involved in the cytotoxic effects of kaolinite. By contrast, the fact that the crystallite size of kaolinite was found to have a negative influence of cytotoxicity may suggest a potential for kaolinite grains with small crystallite sizes to break apart into finer particles once mechanically milled. As clays are naturally fine grained ($< 2$ µm), the further breakdown of clay particles to submicron sizes (nanoparticles) may result in increased toxicity. The weak but significant relationship between SSA and kaolinite content (reported in Chapter 4) may imply that this process could occur on a small scale but could become impactful with greater abundances of kaolinite.

Between the two responses, the low MDA and LDH samples mostly showed lower crystallite sizes compared to the moderate and high MDA and LDH samples. Amongst the moderate and high toxicity samples there was some variation in the crystallite sizes of the quartz, however, on average the trend followed an increase in both cytotoxicity and lipid peroxidation with increasing crystallite size. These observations are consistent with the highly reactive nature of quartz surfaces. As crystallite size can be considered as a proxy for the abundance of surface defects, these results further confirm the potent reactivity of quartz and demonstrate the significance of using parameters related to quartz surface activity over reporting the abundance of quartz. This deduction is consistent with recent work by Pavan et al 2020, as they suggest that a characterisation of the surface functional groups would be the most effective way of understanding the toxic nature of quartz to macrophages. Considering that the modality of quartz-related cytotoxicity involves the damage of the cell membrane upon contact with the reactive surface species, it is unsurprising that the moderate and high toxicity samples display variation in terms of intra-cluster crystallite sizes. This is because quartz-related damage is one of many mechanisms that occur between coal-macrophage interactions.

Despite the results showing that the toxicity of quartz was mostly accounted for by the trends observed in the crystallite size of quartz, it should also be noted that aluminosilicate clays have been found to supress the toxicity of quartz in coal dust (Bégin et al, 1986; Wallace et al, 1994; Fubini, 1998). Looking at sample Br-Tail, this effect may be the main reason why this sample is classed in the low toxicity cluster despite having a large crystallite size for quartz (104.93 nm). Upon separate inspection of the quartz liberation data of this sample, it was established that 45% of the unliberated quartz composites (83 % of all the quartz in the sample) was associated with clay minerals. Based on this it can be suggested that the effects of the quartz in this sample have been supressed by clay associations.

While this may explain the inactivity of quartz in samples Br-Tail, this sample also displays significant amounts of pyritic Fe (4.86 wt. %). By comparing Br-Tail to its most similar counterpart sample Br-Dis, which reported moderate cytotoxicity, the key differences between these samples were in the percentage association that the unliberated pyrite composite had with the clays. Sample Br-Dis reported that 15 % of the unliberated pyrite (87 % of all the pyrite in this sample) was associated with clay minerals as opposed to Br-Tail which display a 22 % association of the unliberated pyrite (81 %) with clays. Additionally, Br-Dis showed a 2.15 % association of unliberated pyrite with siderite (an Fe carbonate), while Br-Tail reported only a 0.73 % association with unliberated pyrite. This suggests that the Fe from pyrite and other potential sources such as siderite may be more available in Br-Dis than Br-Tail, as the clay association may affect the total area for reaction between the pyrite and the biogeochemistry.

Apart from having elevated levels of pyrite, sample Br-Tail contained high amounts of Ca hosted in gypsum (0.42 wt. %) comparable to some of the samples in the high toxicity level. As Ca hosted in gypsum was deemed a highly influential characteristic to the model, this prompted further investigation into the liberation of gypsum particles across the samples. The results showed that Br-Tail only contained 7 % liberated gypsum while the samples in the high toxicity level reported 19-34 % liberated gypsum at near equivalent levels of Ca hosted gypsum (0.12, 0.47, and 0.69 between Br-Dsulf, Br-PyC, and SA-Dis1 respectively). Such observations highlight the importance of understanding the area available for reaction, as whole-rock geochemical analysis involves the breakdown of the sample material to liberate the elements and does not give an indication of the textural relationships between host minerals which may in fact render them inactive.

Thus far the observations between the chemical and mineralogical parameters were discussed in the context of both matrices. However, particle shape was observed to have a strong impact on both responses based on the modelled data. In the context of lipid peroxidation, a general trend in the abundance of angular particles was observed. The low MDA clusters samples generally displayed higher levels of angular particles along with lower levels of equant and smooth particles. By contrast, the majority of the samples in the moderate MDA cluster as well as sample SA-Dis1 in the high MDA cluster, reported lower

levels of angular particles and relatively higher abundances of equant and elongate and smooth shapes with smooth roughness. Based on the known effect that particle shape has on phagocytosis, these trends suggest that particle shape could be affecting the successful/unsuccessful internalisation of particles by the macrophages, and by extension, impacting the level of frustration experienced by the cell (as suggested by Champion and Mitragotri 2006 and Champion et al 2007). Under such circumstances, a low initial contact point between the cell and the particle is likely to result in the successful internalisation (experienced with more angular-shaped particles), while a high contact angle (experienced with more smooth or flat-sided particles) is likely to induce unsuccessful and frustrated phagocytosis. In the latter case this is expected to lead to the secretion of ROS by stressed cells.

Apart from this shape-effect on cell stress, the internalisation of particles by macrophages is proposed to occlude any further reactivity of the particles. This phenomenon has been observed in samples Br-Dis and SA-Dis2, which both reported higher than cluster average abundances of Fe hosted pyrite with high ratios of Fe-pyrite/ Ca-carbonate. These observations alone would suggest that both coals would be highly reactive based on the Fe available for Fenton-based ROS generation. However, both samples contain elevated levels of angular particles and lower than cluster average abundances of elongate and smooth, equant, and smooth particles, thus suggesting that the likely internalisation of these particles limited the ROS-based reactivity in the extracellular environment and rather concentrated the damage on their host phagocytes. This was supported by the fact that both samples reported moderated levels of cytotoxicity despite Br-Dis and SA-Dis2 displaying low and moderate MDA release respectively. By contrast, sample Br-PyC, which unlike the other samples displayed higher amounts of angular particles, additionally contained high levels of pyritic Fe (12.75 wt. % Fe compared to 0.13-0.59 wt. % Fe in samples with similar ranges of angular particles). Based on this observation it can be suggested that even though many of the particles are likely to be phagocytosed, the remaining particles in the extracellular environment are still able to react due to the high abundance of pyrite and Fe-bearing sulfates (52.14 wt. % in the sample). This hypothesis was supported by Br-PyC reporting high levels of both lipid peroxidation and cytotoxicity.

## 6.7. Conclusion

One of the greatest challenges faced by similar studies which attempt to model particle characteristics of coal dust particles to cellular damage is the phenomenon of samples with similar characteristics presenting different levels of toxicity or inflammation. For this reason, studies have found it difficult to identify the toxic agent(s) involved in the pathology of coal dust. Furthermore, the number of potential variables involved in coal dust-related cellular damage presents a challenge when attempting to model particle characteristics to responses due to collinearity. Ultimately, this study has demonstrated that the effect of particle shape in relation to whether a particle is likely to be successfully phagocytosed, can

confound the anticipated ROS-related damage from reactive mineralogy. This observation along with the impacts of pyrite and gypsum liberation, carbonate neutralisation capacity of pyritic Fe and the deactivation of quartz surfaces with kaolinite contamination have been identified by analysing the relative hazard matrix developed by the protocol in this Chapter.

As some of the key outcomes of the protocol, this study has ultimately shown that while the original format of the relationships from a PLSR may be interpretable by few, the data can be transformed to more accessible formats for different users of the data. Although the resulting relative hazard matrix may still be considered complex, it does highlight the important information needed to assess pairwise comparisons of samples and determine the key factors/ parameters relating to each cellular response. While the application of this model in this format is the first of its kind it has shown effectiveness in its performance to explain the variation in each response.  It should however be acknowledged that this model is limited in terms of the dataset on which it was trained. For this reason, the characteristics identified by this study are presented as a comprehensive and justifiable set of hazard factors to be taken into consideration when characterising the relative health risk of coal dust based on cellular damage.

## 6.8. References

Ávila Júnior, S., Possamai, F. P., Budni, P., Backes, P., Parisotto, E. B., Rizelio, V. M., Torres, M. A., Colepicolo, P., et al (2009) 'Occupational airborne contamination in south Brazil: 1. Oxidative stress detected in the blood of coal miners', *Ecotoxicology*, 18(8), pp. 1150–1157. doi: 10.1007/s10646-009-0364-8.

Batool, A. I., Naveed, N. H., Aslam, M., Da Silva, J. and Ur Rehman, M. F. (2020) 'Coal dust-induced systematic hypoxia and redox imbalance among coal mine workers', *ACS Omega*, 5(43), pp. 28204–28211. doi: 10.1021/acsomega.0c03977.

Bégin, R., Massé, S., Sébastien, P., Martel, M., Bossé, J., Dubois, F., Geoffroy, M. and Labbé, J. (1986) 'Sustained Efficacy of Aluminum to Reduce Quartz Toxicity in the Lung', *Experimental Lung Research*. Taylor & Francis, 13(2), pp. 205–222. doi: 10.3109/01902148709064319.

Carretero, M. I., Gomes, C. S. F. and Tateo, F. (2006) 'Clays and huamn health', in Bergaya, F., Theng, B., and Lagaly, G. (eds) *Developments in Clay Science*. Elsevier, pp. 717–740. doi: 10.1016/S1572-4352(05)01024-X.

Champion, J. A., Katare, Y. K. and Mitragotri, S. (2007) 'Particle shape: A new design parameter for micro- and nanoscale drug delivery carriers', *Journal of Controlled Release*, 121(1–2), pp. 3–9. doi: 10.1016/j.jconrel.2007.03.022.

Champion, J. A. and Mitragotri, S. (2006) 'Role of target geometry in phagocytosis', *Proceedings of the National Academy of Sciences of the United States of America*, 103(13), pp. 4930–4934. doi: doi.org/10.1073/pnas.0600997103.

Costa, D. L. and Dreher, K. L. (1997) 'Bioavailable Transition Metals in Particulate Matter Mediate Cardiopulmonary Injury in Healthy and Compromised Animal Models', *Environ Health Perspect*, 1(5), pp. 1053–1060.

Davies, R. (1983) 'Factors Involved in the Cytotoxicity of Kaolinite towards Macrophages in Vitro', *Environmental Health Perspectives*, 51, pp. 249–274.

Donaldson, K., Stone, V., Borm, P. J. A., Jimenez, L. A., Gilmour, P. S., Schins, R. P. F., Knaapen, A. M., Rahman, I., et al (2003) 'Oxidative stress and calcium signaling in the adverse effects of environmental particles (PM10)', *Free Radical Biology and Medicine*. Elsevier, 34(11), pp. 1369–1382. doi: 10.1016/S0891-5849(03)00150-3.

Fiordelisi, A., Piscitelli, P., Trimarco, B., Coscioni, E., Iaccarino, G. and Sorriento, D. (2017) 'The mechanisms of air pollution and particulate matter in cardiovascular diseases', *Heart Failure Reviews*. Heart Failure Reviews, 22(3), pp. 337–347. doi: 10.1007/s10741-017-9606-7.

Fubini, B. (1998) 'Surface Chemistry and Quartz Hazard', *Annals of occupational hygine*, 42(8), pp. 521–530. Available at: https://academic.oup.com/annweh/article/42/8/521/148104.

Fubini, B. and Ivana, F. (2007) 'Toxic Potential of Mineral Dusts', *Elements*, 3(6), pp. 407–414. doi: 10.2113/GSELEMENTS.3.6.407.

Gibbs, A. R. (1990) 'Human Pathology of Kaolin and Mica Pneumoconioses', in *Health Related Effects of Phyllosilicates*. Berlin Heidelberg: Springer, pp. 217–226. doi: https://doi.org/10.1007/978-3-642-75124-0_20.

Huang, X. and Finkelman, R. B. (2008) 'Understanding the Chemical Properties of Macerals and Minerals in Coal and its Potential Application for Occupational Lung Disease Prevention', *Journal of Toxicology and Environmental Health, Part B*, 11(1), pp. 45–67. doi: 10.1080/10937400701600552.

Kennedy, T., Ghio, A. J., Reed, W., Samet, J., Zagorski, J., Quay, J., Carter, J., Dailey, L., et al (1998) 'Copper-dependent inflammation and nuclear factor-κb activation by particulate air pollution', *American Journal of Respiratory Cell and Molecular Biology*. American Lung Association, 19(3), pp. 366–378. doi: 10.1165/AJRCMB.19.3.3042.

Landsiedel, R., Ma-Hock, L., Wiench, K., Wohlleben, W. and Sauer, U. G. (2017) 'Safety assessment of nanomaterials using an advanced decision-making framework, the DF4nanoGrouping', *Journal of Nanoparticle Research*, 19(5), p. 171. doi: 10.1007/s11051-017-3850-6.

Linkov, I., Steevens, J., Chappell, M., Merad, M., Tervonen, T. and Figueira, J. R. (2009) 'Classifying Nanomaterial Risk Using Multi-Criteria Decision Analysis', in *Nanomaterials: risks and benefits*. Springer, pp. 179–191. Available at: http://www.nanotechproject.org/inventories/.

Maynard, A. D. and Kuempel, E. D. (2005) 'Airborne nanostructured particles and occupational health', *Journal of Nanoparticle Research*, 7(6), pp. 587–614. doi: 10.1007/s11051-005-6770-9.

Oberdörster, G. (2000) 'Pulmonary effects of inhaled ultrafine particles', *International Archives of Occupational and Environmental Health*, 74(1), pp. 1–8. doi: 10.1007/s004200000185.

Pavan, C., Santalucia, R., Leinardi, R., Fabbiani, M., Yakoub, Y., Uwambayinema, F., Ugliengo, P., Tomatis, M., et al (2020) 'Nearly free surface silanols are the critical molecular moieties that initiate the toxicity of silica particles', *Proceedings of the National Academy of Sciences*. National Academy of Sciences, 117(45), pp. 27836–27846. doi: 10.1073/PNAS.2008006117/SUPPL_FILE/PNAS.2008006117.SAPP.PDF.

Shangguan, Y., Zhuang, X., Querol, X., Li, B., Moreno, N., Trechera, P., Sola, P. C., Uzu, G., et al (2022)

'Characterization of deposited dust and its respirable fractions in underground coal mines: Implications for oxidative potential-driving species and source apportionment', *International Journal of Coal Geology*, 258(December 2021). doi: 10.1016/j.coal.2022.104017.

Song, Y., Southam, K., Basil, B., Zosky, G. R., Graeme Zosky, C. R., Bardin, P. and Reynolds, P. (2022) 'Effects of chemical composition on the lung cell response to coal particles: Implications for coal workers' pneumoconiosis', *Rispirology*, 12, pp. 447–454. doi: 10.1111/resp.14246.

Stoeger, T., Reinhard, C., Takenaka, S., Schroeppel, A., Karg, E., Ritter, B., Heyder, J. and Schulz, H. (2006) 'Instillation of six different ultrafine carbon particles indicates a surface area threshold dose for acute lung inflammation in mice', *Environmental Health Perspectives*, 114(3), pp. 328–333. doi: 10.1289/ehp.8266.

Sun, Y., Kinsela, A. S. and Waite, T. D. (2022) 'Elucidation of alveolar macrophage cell response to coal dusts: Role of ferroptosis in pathogenesis of coal workers' pneumoconiosis', *Science of the Total Environment*. Elsevier B.V., 823, p. 153727. doi: 10.1016/j.scitotenv.2022.153727.

Trechera, P., Moreno, T., Córdoba, P., Moreno, N., Amato, F., Cortés, J., Zhuang, X., Li, B., et al (2021a) 'Geochemistry and oxidative potential of the respirable fraction of powdered mined Chinese coals', *Science of The Total Environment*. Elsevier, 800, p. 149486. doi: 10.1016/J.SCITOTENV.2021.149486.

Trechera, P., Moreno, T., Córdoba, P., Moreno, N., Zhuang, X., Li, B., Li, J., Shangguan, Y., et al (2021b) 'Comprehensive evaluation of potential coal mine dust emissions in an open-pit coal mine in Northwest China', *International Journal of Coal Geology*. Elsevier, 235, p. 103677. doi: 10.1016/J.COAL.2021.103677.

Wallace, W. E., Harrison, J. C., Grayson, R. L., Keane, M. J., Bolsaitis, P., Kennedy, R. D., Wearden, A. Q. and Attfield, M. D. (1994) 'Aluminosilicate surface contamination of respirable quartz particles from coal mines dust and from clay works dusts', *Annals of Occupational Hygiene*, 38, pp. 439–445.

Wittmaack, K. (2007) 'In search of the most relevant parameter for quantifying lung inflammatory response to nanoparticle exposure: Particle number, surface area, or what?', *Environmental Health Perspectives*, 115(2), pp. 187–194. doi: 10.1289/ehp.9254.

Yadav, A. K. and Jamal, A. (2018) 'Impact of mining on human health in and around mines', *Environmental Quality Management*, 28(1), pp. 83–87. doi: 10.1002/tqem.21568.

Zazouli, M. A., Dehbandi, R., Mohammadyan, M., Aarabi, M., Dominguez, A. O., Kelly, F. J., Khodabakhshloo, N., Rahman, M. M., et al (2021) 'Physico-chemical properties and reactive oxygen species generation by respirable coal dust : Implication for human health risk assessment', *Journal of Hazardous Materials*. Elsevier, 405, p. 124185. doi: 10.1016/j.jhazmat.2020.124185.

# Chapter 7

# CONCLUSIONS AND RECOMMENDATIONS

## 7.1. Overview

In this chapter the general outcomes of the thesis are discussed in the context of the overarching study aim, which is further resolved in the three main study objectives. This chapter also examines the hypothesis proposed in Chapter 3 with relation to the study findings. Finally, recommendations for the progression of the work demonstrated in the thesis are discussed in addition to the recommendation of potential separate studies stemming from the findings demonstrated.

## 7.2. Research context

The direct and indirect effects that coal dust has on pulmonary cells and tissue have been thoroughly investigated experimentally by numerous studies such as Rosmanith et al 1982; Le Bouffant et al 1988; Schins and Borm, 1999; Castranova and Vallyathan, 2000; Gulumian et al 2006; and Vanka et al 2022. Despite this body of work there is currently uncertainty on which characteristics act as catalysts for toxicological/immunological responses and which properties have depressive or even benign effects on cellular harm. As a result of this uncertainty there has been little development in determining the relative risk of coal dust generated from different sources. With regards to the resurgence patterns of coal dust-related diseases such as CWP, studies such as Hurley et al (1982), (1987); Attfield (1992); Attfield and Seixas (1995); and Soutar et al (2004) have progressively determined that mass concentration of dust plays a critical role in the prevalence of these diseases. However, despite managing the exposure levels of coal dust, cases of CWP continue to rise anomalously and disproportionally within geographic regions.

By attempting to understand the source characteristics of coal dust generated from various activities on the mine site, studies such as Johann-Essex et al (2017); LaBranche et al (2021); Sarver et al (2021); and Trechera et al (2021b, 2021a) established that coal dust characteristics may vary depending on the regional geology and the different mine operation and parental source of the dust. In further seeking to understand how these characteristics may impact biological conditions, Trechera et al (2021b, 2021a) investigated the oxidative potential of multiple particle characteristics in acellular conditions. While this investigation yielded multiple relationships between different classes of characterisation data (mineralogical and chemical), the information only served as indicators of various mechanisms which had been identified by previous studies. As a result, no synthesised picture of the relative risk of these parameters with respect to cellular damage could be derived. Furthermore, no understanding of the overall

importance or magnitude of the influence of the investigated characteristics relative to oxidative potential could be established.

In this context, the study aim focused on developing an advanced understanding of the relationships between the physicochemical and mineralogical characteristics of coal particles and pulmonary toxicity. Stemming from this understanding, the aim of the study further involved proposing an empirical protocol for characterising the potential health risks associated with inhalable coal particles, from the perspective of primary hazard identification. This aim was achieved progressively by the work demonstrated within Chapters 4-6. Within these chapters, three main objectives were established as the elements needed to achieve the overarching aim.

## 7.3. Objective 1: Particle characterisation

In Chapter 4 the first objective focused on the development and analysis of the detailed particle characterisation dataset using the QEMSCAN as the main analysis tool whilst combining additional information from complementary chemical, mineralogical, and physical analysis methods. This objective was met by:

i.   Determining a reliable and systematic protocol for analysing coal dust using the QEMSCAN.

ii.  Utilising complementary datasets to interrogate the accuracy of data from different analysis tools.

iii. Understanding how the various techniques explain the variation between the samples and the main feature differences between samples.

Ultimately, Chapter 4 provided a holistic description of the general, mineralogical, chemical, and mineral specific characteristics observed from the different source material. The results determined that both routine and advance particle analyses contribute to the definition of the different data classes as well as providing important information to assess the accuracy of the information reported. The results further demonstrate that features relating to general particle characteristics (size, shape, roughness, and surface area) are more strongly a function of mechanical breakage and deformation than compositional variation. This may suggest that for dust sources stemming from geo-anthropogenic activities such as cutting, blasting, or milling, characterisation datasets should incorporate more variables which reflect the mechanical breakage or rock-strength of the source material.

## 7.4. Objective 2: Relationship between particle characteristics and immunological responses

Following the description of the detailed characterisation dataset, objective 2 in Chapter 5 centred around the investigation of the multivariant relationships between the coal particle characteristics and the

two cellular responses (cytotoxicity and lipid peroxidation) assay on macrophage cells *in vitro*. In this context the achievement of objective 2 involved:

i. Determining the relative significance of the various physicochemical characteristics in relation to their effect on the cells

ii. Further investigating whether the addition of mineralogical, chemical, and physical characteristics provides a more holistic understanding of the factors influencing toxicity and their mechanisms compared to more generalised particle characteristics (mineral, chemical, and particle size distributions).

iii. Assessing any differences between the characteristics linked to cytotoxicity compared to those related to lipid peroxidation.

The application of the PLSR in Chapter 5 showed that by coupling a range of data classes (general, mineralogical, chemical, and mineral specific), the variability between sample characteristics and their impact on cytotoxicity and lipid peroxidation could successfully be explained with a reasonable level of confidence. The results from the regression analysis revealed that physical characteristics (particle shape in particular) displayed a greater influence on cytotoxicity and lipid peroxidation over mineral and chemical-based characteristics. This was explained by the established role of particle shape in successful/unsuccessful phagocytosis. In this context, the effects of the chemical and mineralogical reactivity of particles could either be expressed strongly in the extracellular environment, where indirect and direct damage may occur to many cells, or the detrimental effects of these chemical mechanisms may be incurred by the cells which successfully ingested the particles. Between the two responses it was established that mechanisms which promote lipid peroxidation (such as Fe-based Fenton reactions, Calcium signalling and the surface activity of quartz) can also be linked to cytotoxicity. However, cytotoxicity was also found to occur from non-ROS related pathways. This was observed by the toxic influence of kaolinite.

Ultimately, Chapter 5 presented a novel, reproducible and systematic analysis strategy for understanding the relationships between many highly correlated variables to single responses. Through this analysis, the study presented the first indication of the relative importance of an array of particle characteristic in relation to markers of cellular damage on a single scale. This allowed for the comparison of the influence of mineralogical, chemical, and physical-based parameters to cytotoxicity and lipid peroxidation.

## 7.5. Objective 3: Characterisation of the relative pulmonary risk of sampled coal particulates

Finally, objective 3 in Chapter 6 focused on determining a means to empirically characterise the relative risk of coal dust related damage on a cellular level based on the ranking of the most influential particle characteristics contributing to the harm of pulmonary cells and further determine if there are distinct classes of harm. In this context the achievement of objective 3 involved:

i. Defining a shortlist of the most relevant characteristics relative to each response and an importance rank for each variable.

ii. Determining how the various data classes can be combined to provide relevant information to decision makers and other stakeholders.

The elements described above were incorporated in a protocol to describe the empirical risk characterisation of the sample which was developed in Chapter 6. Here the structural information from the PLSR was translated into a more easily interpretable format to facilitate the use of this information in data-driven decision making. Tables 7-1 and 7-2 represent the future hazard factors for investigation concerning lipid peroxidation and cytotoxicity respectively. Through a combination of the findings in Chapters 5 and 6, some of the relationships that were identified by the PLSR suggested that multiple mechanisms could be involved in both lipid peroxidation and cytotoxicity. Generally, these revolved around: (1) iron related Fenton chemistry which can be mitigated by carbonate phases, (2) surface area-based reactivity indicated by the importance of SSA, (3) suggested positive increased quartz surface activity based on crystallite size, (4) and the potential for frustrated phagocytosis and cell stress to occur in particles which are more smooth than angular. Through the analysis of the relative hazard matrices, it was proposed that while mechanisms related to compositional reactivity could clearly be identified as a cause for cellular damage, the impact of complete/incomplete phagocytosis could determine whether particles were able to react in the extracellular environment and progress the damage. In this case, even if particles contain the typical chemical and mineralogical signatures for a "high risk" coal, if they can be phagocytosed then reactivity could be limited, and the damage would be mostly incurred by affected cells.

Table 7-1 Summary of key parameters characterising the hazards of lipid peroxidation-based cellular damage.

| | Characterisation class | Variable groups | | Association type | Potential ratios and data for analysis |
|---|---|---|---|---|---|
| **Decreasing importance** | General | Shape and roughness | Shapes equant & elongate and smooth with smooth roughness | Strong positive | Angular/Elongate and smooth |
| | | | Angular shapes | Strong Negative | |
| | Chemical | Ca distribution | Ca in Gypsum | Strong positive | Gypsum liberation |
| | Mineral specific | Crystallite size | Quartz | Strong positive | - |
| | Chemical | Ca distribution | Ca in dolomite | Negative | Fe in pyrite/ Ca in carbonates |
| | | | Ca in calcite | | |
| | Chemical | Fe distribution | Fe in Pyrite | Strong positive | Carbonates = calcite, dolomite |
| | | | Fe in Rhomboclase | Positive | |
| | | | Fe in Szomolnokite | | |
| | Mineralogical | Mineral abundances | Calcite | Negative | Pyrite/Calcite |
| | | | Pyrite | Positive | |
| | | | Fe-Sulfates | | |
| | General | SSA | | Positive | - |

Table 7-2 Summary of key parameters characterising the hazards of cytotoxicity.

| | Characterisation class | Variable groups | | Association type | Potential ratios and data for analysis |
|---|---|---|---|---|---|
| **Decreasing importance** | General | Shape and roughness | Shapes equant & elongate and smooth with smooth to intermediate roughness | Strong positive | Elongate and Angular/Elongate and smooth |
| | | | Shapes elongate and angular & angular with jagged roughness | Strong negative | Angular + Jagged/Equant + smooth |
| | Chemical | Ca distribution | Ca in Gypsum | Strong positive | Gypsum liberation |
| | Mineral specific | Pyrite liberation | Liberated pyrite | Positive | - |
| | | | Fully encapsulated pyrite | Negative | |
| | Mineral specific | Crystallite size | Quartz | Positive | - |
| | | | Kaolinite | Negative | |
| | Mineralogical | Mineral abundances | Fe-Sulfates | Strong positive | Pyrite/total sulfate |
| | | | Pyrite | | |
| | | | Kaolinite | | |
| | Chemical | Fe distribution | Fe in Pyrite | Positive | Element contribution from sulfates: Fe-bearing sulfates/Ca-bearing sulfates |
| | | | Fe in Rhomboclase | | |
| | | | Fe in Szomolnokite | | |
| | General | SSA | | Positive | - |
| | Mineralogical | Carbonaceous content | | Negative | - |
| | Chemical | Major silicate chemistry | $\sum [Al; Si; Ti]$ | Weak positive | - |
| | Chemical | Si distribution | Si in quartz | Weak positive | - |
| | | | Si in clays | | |

## 7.6. Discussion of research hypothesis

Since the establishment of Fenton-mediated oxidative damage, studies have debated the overall significance of pyrite in coal dust as a causal agent in pulmonary damage. As a result of several mechanistic studies demonstrating the immunological effects of pyritic iron in coal mine dust, a study by Huang et al 2005 utilised a simplistic measure of bioavailable Fe content to predict the prevalence of CWP across the USA. Several studies by Zhang et al 2002; Cohn et al 2006; Harrington et al 2012, 2013; and Sun et al 2022 have shown that pyritic Fe is a strong contributor to the production of ROS and more specifically hydroxyl radicals via the Fenton mechanism. Additionally, these studies have demonstrated that the elevated levels of Fe-related ROS have a strong relationship with markers of cellular damage such as: lipid peroxidation, cytotoxicity, and the release of inflammatory factors. It is in this context that this study hypothesised that:

Pyrite particles present in the coal with high surface area for reaction will have the highest potential to yield an inflammatory/toxic response in macrophages, due to the high surface exposure for oxidation and the release of soluble iron. As a result, these characteristics can provide an indication of pulmonary risk based on the interactions between the composite particles and primary phagocytes such as macrophages.

While the results presented in this study did not find the abundance of pyrite in coal to be the most influential parameter related to macrophage toxicity, it was demonstrated that ROS-related damage from pyrite had a significant impact on the overall toxicity level of a sample. In terms of the reactivity related to pyrite, various factors were found to confound the availability of Fe for reaction. In the case of lipid peroxidation, trends showed that low toxicity samples which reported high levels of carbonate minerals in relation to pyrite were likely able to mitigate the release of Fe and thus limited the Fenton-based reactivity. Regarding cytotoxicity, pyrite liberation was highlighted as an influential parameter related to understanding the reactivity of a sample. This demonstrated that, as hypothesised, the area for reaction is likely to have a direct effect on the chemical reactivity of pyrite.

Ultimately, when considering the validity of the hypothesis statement, the results from the relationship analysis in Chapters 5 and 6 confirm that pyritic Fe and the liberation of pyrite grains do serve as a relevant set of predictors which can account for some of the ROS-related damage. However, the combination of pyritic Fe and pyrite liberation cannot be considered the parameters with the highest potential to explain the toxicity among dust samples. This supports the notion that there is no single parameter or groups of parameters which can definitively explain the level of damage caused by coal particulates of differing sources.

Rather, the results of this study found that the overall toxicity of coal particulates is governed by multiple mechanisms relating to the reactivity of minerals and the response of cells to particle morphology.

In terms of ROS-mediated damage, pyritic Fe, the crystallite size of quartz, and Ca hosted in gypsum were all found to positively influence the level of lipid peroxidation. Amongst these parameters, Ca hosted in gypsum and quartz crystallite size were determined to be more potent to both lipid peroxidation and cytotoxicity than pyritic Fe. In relation to non-ROS-related damage, kaolinite content was identified to have a positive influence on only cytotoxicity. However, it should be acknowledged that while kaolinite has been observed to induce cytotoxicity in macrophages, the mechanisms for this are still unknown. In contrast to this relationship, the surface coating of quartz grains with kaolinite have been shown to suppress the toxicity of quartz. This effect was proposed for one of the low toxicity samples which displayed quartz with a large crystallite size and a high association of quartz with clays. These two observations suggest that the role of kaolinite in the overall reactivity of coal composites may be more complex and thus require further investigation.

Trends in the data additionally suggested a link between successful phagocytosis and the shape and roughness of particle. Based on mechanisms defined in literature and the observations in the data it was proposed that for samples with more angular and jagged particles, phagocytes are more able to successfully ingest particles and remove them from the extracellular environment thus reducing their reactive potential with other cells. As a result, samples which have a high abundance of reactive mineralogical/chemical actors may exhibit low levels of toxicity despite these active components.

## 7.7. Concluding remarks

As discussed in Chapters 2 and 6, one of the greatest challenges faced by similar studies which seek to relate the characteristics of coal dust particles to cellular damage is the phenomenon of samples with similar characteristics presenting different levels of toxicity or inflammation. This makes developing a generic understanding of coal dust toxicity from single or small groups of parameters (like pyrite or quartz content) infeasible. The statistical analysis strategy and results presented in Chapters 5 and 6 show that differences between samples can be resolved through the applications of models which are capable of removing collinearity and a collection of general, mineralogical, chemical, and mineral specific information. In conclusion, it is proposed that the toxic potential of coal dust is primarily a function of the reactive mineralogical and chemical components within the particles, however, the magnitude of this intrinsic reactivity is subject to the mitigative factors which can either neutralise of supress the anticipated reactivity. Having established the likelihood of multiple particle-related mechanisms and key particle-parameters involved in explaining coal dust-related cellular damage, such information may provide a means to understand how certain particle properties could mitigate the toxic effects caused by compositional reactivity and the disruption of phagocytosis.

## 7.8. Recommendations for future work

It is explicitly acknowledged in this study that the sampled materials are unlikely representative of any specific coal mine dust source or operation and have coarser particle size distributions than those conventionally considered to be "respirable" dust.. This could potentially result in different distributions being reported for the characteristics investigated, more specifically in relation to particle size, shape and even texture. As a result, it may be useful for future studies to apply the strategies employed in this research to real world mine dust samples to further understand whether the similar mechanisms identified in this study can be linked to particles in the respirable fraction. Such studies would be able to introduce additional complexities such as diesel exhaust contamination and the influence of dust suppression treatments on inhalable particles.

One of the most important elements of studies which aim to define relationships between coal dust characteristics and pulmonary toxicity is the data used in the relationship analysis. Chapter 4 demonstrated the use of complementary datasets to assess the accuracy of the composition data derived from an auto-SEM-EDS system. While this was successful for the compositional data, the same could not be done for the physical data (i.e. particle size and shape). This is because the particle analysis was conducted on 2D particle cross sections while other common tools of analysis for particle shape and size rely on images acquired from 3D projections of particles. Several studies have shown that Image J can be used to process particle dimensions from BSE images, and by using separate plug-ins prepare quantitative data for external analysis (Igathinathane et al, 2008; Mazzoli and Favoni, 2012; Rana, 2015). By performing a separate image analysis on high resolution BSE images taken within the frames analysed by the auto-SEM, a comparable set of particle size and shape information can be acquired to assess the accuracy of the physical data reported. Potentially by using this method the distinction between grain boundaries can be better resolved compared to those determined by the pixel dimensions from the auto-SEM scan. Additionally, to curb the effects of soteriological bias with respect to determining particle shape from 2D cross-sectional images, nano X-ray Computer Micro Tomography (nano-XCT) can be used to obtain a more realistic representation of the particle size distribution of coal mine dust. Considering that nano-XCT instruments can scan particles down to a resolution of 100 nm and produce 3D models of the particles, this approach may be useful for real-world dust samples in the respirable fraction (for reference see Becker et al (2016) and Zschech et al (2018)).

In relation to the different datasets used in this study, an array of particle information from various analytical tools were employed. However, more specialised analytical machinery such as the Synchroton using EXAFS (Extended X-ray absorption fine structure) have been used in a study by Sun et al (2021) to determine the oxidation states of Fe amongst the Fe-bearing mineral assemblages in coal dust. While these kinds of datasets are rare, such data could be incorporated in a similar PLSR routine as demonstrated in this

study to provide further information on the electrochemical mechanisms of different Fe-bearing minerals and their pathways to toxicity.

Apart from what can be done to add or improve on the detailed characterisation dataset used in this study, characteristics such as quartz crystallite size could potentially be used as an identifier of quartz populations from different sources. The ease of obtaining this parameter from XRD scans, via methods described in David et al (2010), should be stressed as these parameters showed significant potential to account for the differences in quartz-based toxicity amongst a wide variety of coals. In Chapter 4 it was shown that the crystallite size of quartz varied between the coal samples from different countries. Additionally, the inter-colliery variation between the South African samples showed that coals from different sources may display differences in the crystallite size of their associated quartz. Considering that studies have attributed wall-rock cutting as an additional source of quartz mixed in coal dust, future studies should look at the distribution of quartz crystallite sizes in the XRD diffractograms to understand if different modalities of quartz are present in coal dust.

Furthermore, as dust generation activities have been demonstrated to produce dust with differing characteristics, future studies should investigate how these different modes of dust generation impact the toxic effects observed. Such an example would be to investigate the difference between freshly fractured particles versus particles that have been exposed to ambient conditions over time in kinetic dose response tests. In doing so, such information may aid in understanding which parameters contribute to acute/chronic toxicity.

While this study only looked at two responses related to cell harm, future studies could use the PLSR routine on inflammatory indicators and cytokine expression. This would provide further insight as to whether the same parameters which result in elevated levels of lipid peroxidation and cytotoxicity also lead to the progression of inflammatory factors. Such information could further be aggregated with additional toxic responses (as demonstrated in Chapter 6) to understand the circumstances under which samples show signs of an inflammatory imbalance and whether the parameter ranges from those samples can be used to benchmark cut-off values of each active parameter. In such a case a greater number of samples would need to be considered in the analysis.

In the context of particle shape and roughness, the results of this study revealed that these parameters played a substantial role in the level of toxicity experienced by cells even in the case of highly reactive samples. Based on this, it is recommended that future studies should investigate the shape-effect phenomenon described to determine whether phagocytosis is indeed affected by particle shape in coal dust samples, and furthermore, if this has any impact on the reaction rates of biogeochemical reactions in the extracellular matrix. In doing so, confocal laser microscopy and SEM analysis can be used to observe the impact of particle shape on phagocytosis as explored by Tomašek et al (2016).

# BIBLIOGRAPHY

Abdi, H. (2010) 'Partial least squares regression and projection on latent structure regression (PLS Regression)', *Wiley Interdisciplinary Reviews: Computational Statistics*, 2(1), pp. 97–106. doi: 10.1002/wics.51.

Adamis, Z. and Timar, M. (1978) 'Studies on the effect of quartz, bentonite and coal dust mixtures on macrophages in vitro', *British Journal of Experimental Pathology*, 59, pp. 411–415.

Amato, F., Querol, X., Johansson, C., Nagl, C. and Alastuey, A. (2010) 'A review on the effectiveness of street sweeping, washing and dust suppressants as urban PM control methods', *Science of the Total Environment*. Elsevier, 408(16), pp. 3070–3084. doi: 10.1016/j.scitotenv.2010.04.025.

Attfield, M. D. (1992) 'British Data on Coal Miners' Pneumoconiosis and Relevance to US Conditions', *American Journal of Public Health*, 82(7), pp. 978–983.

Attfield, M. D. and Castellan, R. M. (1992) 'Epidemiological data on US coal miners' pneumoconiosis, 1960 to 1988', *American Journal of Public Health*, 82(7), pp. 964–970. doi: 10.2105/AJPH.82.7.964.

Attfield, M. D. and Morring, K. (1992a) 'An investigation into the relationship between coal workers' pneumoconiosis and dust exposure in U.S. coal miners', *American Industrial Hygiene Association Journal*, 53(8), pp. 486–492. doi: 10.1080/15298669291360012.

Attfield, M. D. and Morring, K. (1992b) 'The derivation of estimated dust exposures for U.S. coal miners working before 1970', *American Industrial Hygiene Association Journal*, 53(4), pp. 248–255. doi: 10.1080/15298669291359609.

Attfield, M. D. and Seixas, N. S. (1995) 'Prevalence of pneumoconiosis and its relationship to dust exposure in a cohort of U.S. Bituminous coal miners and ex-miners', *American Journal of Industrial Medicine*. John Wiley & Sons, 27(1), pp. 137–151. doi: 10.1002/ajim.4700270113.

Ávila Júnior, S., Possamai, F. P., Budni, P., Backes, P., Parisotto, E. B., Rizelio, V. M., Torres, M. A., Colepicolo, P. and Wilhelm Filho, D. (2009) 'Occupational airborne contamination in south Brazil: 1. Oxidative stress detected in the blood of coal miners', *Ecotoxicology*, 18(8), pp. 1150–1157. doi: 10.1007/s10646-009-0364-8.

Bair, W. (1991) 'Overview of ICRP Respiratory Tract Model', *Radiation Protection Dosimetry*, 38(1–3), pp. 147–152. doi: 10.1093/RPD/38.1-3.147.

Bair, W. (2000) 'The ICRP Human Respiratory Tract Model for Radiological Protection', *Radiation Protection Dosimetry*, 60(4), pp. 307–310.

Barbery, G. (1992) 'Liberation 1, 2, 3: Theoretical analysis of the effect of space dimension on mineral liberation by size reduction', *Minerals Engineering*, 5(2), pp. 123–141. doi: 10.1016/0892-6875(92)90038-B.

Barthelmy, D. (1997) *Webmineral-Mineralogy database*. Available at: https://www.webmineral.com.

Basil, B. and Zosky, G. (2019) *Assessment of pyritic coal dust induced pneumoconiosis*.

Batool, A. I., Naveed, N. H., Aslam, M., Da Silva, J. and Ur Rehman, M. F. (2020) 'Coal dust-induced systematic hypoxia and redox imbalance among coal mine workers', *ACS Omega*, 5(43), pp. 28204–28211. doi: 10.1021/acsomega.0c03977.

Becker, M., Wightman, E. and Evans, C. (2016) 'Process Mineralogy', in *Issue 6 of JKMRC monograph series in mining and mineral processing*. Julius Kruttschnitt Mineral Research Centre, pp. 133–148.

Bégin, R., Massé, S., Sébastien, P., Martel, M., Bossé, J., Dubois, F., Geoffroy, M. and Labbé, J. (1986) 'Sustained Efficacy of Aluminum to Reduce Quartz Toxicity in the Lung', *Experimental Lung Research*. Taylor & Francis, 13(2), pp. 205–222. doi: 10.3109/01902148709064319.

Bennett, J. G., Dick, J. A., Kaplan, Y. S., Shand, P. A., Shennan, D. H., Thomas, D. J. and Washington, J. S. (1979) 'The relationship between coal rank and the prevalence of pneumoconiosis', *British Journal of Industrial Medicine*, 36, pp. 206–210. doi: 10.1136/oem.36.3.206.

Bharti, S. K., Kumar, D., Anand, S., Poonam, Barman, S. C. and Kumar, N. (2017) 'Characterization and morphological analysis of individual aerosol of PM10 in urban area of Lucknow, India', *Micron*. Elsevier, 103(September), pp. 90–98. doi: 10.1016/j.micron.2017.09.004.

Blackley, D. J., Halldin, C. N. and Laney, A. S. (2018) 'Continued Increase in Prevalence of Coal Workers' Pneumoconiosis in the United States, 1970-2017', *American journal of public health*, 108, pp. 1220–1222. doi: 10.2105/AJPH.2018.304517.

Blannin, R., Frenzel, M., Tuşa, L., Birtel, S., Ivăşcanu, P., Baker, T. and Gutzmer, J. (2021) 'Uncertainties in quantitative mineralogical studies using scanning electron microscope-based image analysis', *Minerals Engineering*, 167, p. 106836. doi: 10.1016/j.mineng.2021.106836.

De Boer, A. H., Gjaltema, D., Hagedoorn, P. and Frijlink, H. W. (2002) 'Characterization of inhalation aerosols: A critical evaluation of cascade impactor analysis and laser diffraction technique', *International Journal of Pharmaceutics*, 249(1–2), pp. 219–231. doi: 10.1016/S0378-5173(02)00526-4.

Borda, M. J. and Schoonen, M. A. (2001) 'Pyrite-Induced Hydrogen Peroxide Formation as a Driving Force in the Evolution of Photosynthetic Organisms on an Early Earth Chemistry of surfaces and nanoparticles View project'. doi: 10.1089/15311070152757474.

Borish, L. C. and Steinke, J. W. (2003) 'Cytokines and chemokines', *Journal of Allergy and Clinical Immunology*, 111(2 SUPPL. 2), pp. 460–475. doi: 10.1067/mai.2003.108.

Borm, P. J. A. (2002) 'Particle Toxicology: From Coal Mining To Nanotechnology', *Inhalation Toxicology*, 14(3), pp. 311–324. doi: 10.1080/08958370252809086.

Bouffant, L. Le, Bruyet, B., Daniel, H., Demarez, J., Kovacs, P., Martin, J. C., Addison, J., Bolton, R. E., et al (1988) 'Compared in vitro and in vivo toxicity of coalmine dusts. relationship with mineralogical composition', *Annals of Occupational Hygiene*, 32(1), pp. 611–620. doi: 10.1093/annhyg/32.inhaled_particles_VI.611.

Broug-Holub, E., Toews, G. B., Van Iwaarden, J. F., Strieter, R. M., Kunkel, S. L., Paine, R. and Standiford, T. J. (1997) 'Alveolar macrophages are required for protective pulmonary defenses in murine Klebsiella pneumonia: elimination of alveolar macrophages increases neutrophil recruitment but decreases bacterial clearance and survival', *Infection and Immunity*. American Society for Microbiology, 65(4), pp. 1139–1146. doi: 10.1128/IAI.65.4.1139-1146.1997.

Brown, D. M., Wilson, M. R., MacNee, W., Stone, V. and Donaldson, K. (2001) 'Size-dependent proinflammatory effects of ultrafine polystyrene particles: A role for surface area and oxidative stress in the enhanced

activity of ultrafines', *Toxicology and Applied Pharmacology*, 175(3), pp. 191–199. doi: 10.1006/taap.2001.9240.

Bufton, M. W. and Melling, J. (2005) 'Coming up for air: Experts, employers, and workers in campaigns to compensate silicosis sufferers in Britain, 1918-1939', *Social History of Medicine*, 18(1), pp. 63–86. doi: 10.1093/sochis/hki007.

Cannon, G. J. and Swanson, J. A. (1992) 'The macrophage capacity of phagocytosis', *Journal of Cell Science*, 101, pp. 907–913. doi: 10.4135/9781452218991.n13.

Carley, S. and Konisky, D. M. (2020) 'The justice and equity implications of the clean energy transition', *Nature Energy*. Springer US, 5(8), pp. 569–577. doi: 10.1038/s41560-020-0641-6.

Carretero, M. I., Gomes, C. S. F. and Tateo, F. (2006) 'Clays and huamn health', in Bergaya, F., Theng, B., and Lagaly, G. (eds) *Developments in Clay Science*. Elsevier, pp. 717–740. doi: 10.1016/S1572-4352(05)01024-X.

Castranova, V. (2000) 'From Coal Mine Dust To Quartz: Mechanisms of Pulmonary Pathogenicity', *Inhalation Toxicology*, 12(3), pp. 7–14. doi: 10.1080/08958378.2000.11463226.

Castranova, V. and Vallyathan, V. (2000) 'Silicosis and Coal Workers' Pneumoconiosis', *Environmental Health Perspectives*, 108, pp. 675–684. Available at: https://ehp.niehs.nih.gov/doi/pdf/10.1289/ehp.00108s4675 (Accessed: 14 December 2018).

Champion, J. A., Katare, Y. K. and Mitragotri, S. (2007) 'Particle shape: A new design parameter for micro- and nanoscale drug delivery carriers', *Journal of Controlled Release*, 121(1–2), pp. 3–9. doi: 10.1016/j.jconrel.2007.03.022.

Champion, J. A. and Mitragotri, S. (2006) 'Role of target geometry in phagocytosis', *Proceedings of the National Academy of Sciences of the United States of America*, 103(13), pp. 4930–4934. doi: doi.org/10.1073/pnas.0600997103.

Chattopadhyay, D., Bazilian, M. D., Handler, B. and Govindarajalu, C. (2021) 'Accelerating the coal transition', *Electricity Journal*. Elsevier Inc., 34(2), p. 106906. doi: 10.1016/j.tej.2020.106906.

Cohen, R. A. (2016) 'Resurgent coal mine dust lung disease: Wave of the future or a relic of the past?', *Occupational and Environmental Medicine*, 73(11), pp. 715–717. doi: 10.1136/oemed-2016-103737.

Cohen, R. A., Almberg, S. and Sarver, E. A. (2022a) 'Pathology and Mineralogy Demonstrate Respirable Crystalline Silica is a Major Cause of Severe Pneumoconiosis in US Coal Miners'. ANNALSATS Articles in Press. Published. doi: 10.1513/AnnalsATS.202109-1064OC.

Cohen, R. A., Rose, C. S., Go, L. H. T., Zell-Baran, L. M., Almberg, K. S., Sarver, E. A., Lowers, H. A., Iwaniuk, C., et al (2022b) 'Pathology and Mineralogy Demonstrate Respirable Crystalline Silica Is a Major Cause of Severe Pneumoconiosis in U.S. Coal Miners', *Annals of the American Thoracic Society*, 19(9), pp. 1469–1478. doi: 10.1513/annalsats.202109-1064oc.

Cohn, C. A., Laffers, R., Simon, S. R., O'Riordan, T. and Schoonen, M. A. (2006a) 'Role of pyrite in formation of hydroxyl radicals in coal: Possible implications for human health', *Particle and Fibre Toxicology*, 3, pp. 1–10. doi: 10.1186/1743-8977-3-16.

Cohn, C. A., Mueller, S., Wimmer, E., Leifer, N., Greenbaum, S., Strongin, D. R. and Schoonen, M. A. (2006b) 'Pyrite-induced hydroxyl radical formation and its effect on nucleic acids', *Geochemical Transactions*.

Springer International Publishing, 7(1), p. 3. doi: 10.1186/1467-4866-7-3.

Cohn, C. A., Pak, A., Strongin, D. and Schoonen, M. A. (2005) 'Quantifying hydrogen peroxide in iron-containing solutions using leuco crystal violet', *Geochemical Transactions*, 6(3), pp. 47–51. doi: 10.1063/1.1935449.

Colinet, J. F., Rider, J. P., Listak, J. M., Organiscak, J. A. and Wolfe, A. L. (2021) *Best Practices for Dust Control in Coal Mining*, *NIOSH*. Available at: http://www.cdc.gov/niosh/mining/UserFiles/works/pdfs/2010-110.pdf.

Collis, E. L. and Gilchrist, J. C. (1928) 'Effects of Dust upon Coal Trimmers.', *Journal of Industrial Hygiene*, 10, pp. 101–10.

Costa, D. L. and Dreher, K. L. (1997) 'Bioavailable Transition Metals in Particulate Matter Mediate Cardiopulmonary Injury in Healthy and Compromised Animal Models', *Environ Health Perspect*, 1(5), pp. 1053–1060.

Cross, C. E., Van Der Vliet, A., O'neill, C. A., Louie, S. and Halliwell, B. (1994) 'Oxidants, Antioxidants, and Respiratory Tract Lining Fluids', *Environmental Health Perspectives*, 102, pp. 185–191.

D'arcy Hart, P. and Aslett, E. A. (1942) *Chronic Pulmonary Disease in South Wales Coalminers. I. Medical Studies. A.-Report by the Committee on Industrial Pulmonary Disease.*

D'Arcy Hart, P. and Tansey, E. M. (1998) 'Chronic Pulmonary Disease in South Wales Coal Mines: An Eye-Witness Account of the MRC Surveys (1937-1942)', *Social History of Medicine*, 11(3), pp. 459–468. doi: 10.1093/shm/11.3.459.

Dalal, N., Newman, J., Pack, D., Leonard, S. and Vallyathan, V. (1995) 'Hydroxyl Radical Generation by Coal Mine Dust: Possible Implication to Coal Workers' Pneumoconiosis (CWP)', *Free Radical Biology and Medicine*, 18(I), pp. 11–20.

Dalal, N., Shi, X. and Vallyathan, V. (1990) 'Role of free radicals in the mechanisms of hemolysis and lipid peroxidation by silica: Comparative esr and cytotoxicity studies', *Journal of Toxicology and Environmental Health*, 29(3), pp. 307–316. doi: 10.1080/15287399009531393.

Dalal, N., Suryan, M., Vallyathan, V., Green, F., Jafari, B. and Wheeler, R. (1989) 'Detection of Reactive Free Radicals In Fresh Coal Mine Dust and Their Implication for Pulmonary Injury', *The Annals of Occupational Hygiene*, 33(1), pp. 79–84. doi: 10.1093/annhyg/33.1.79.

David, W. I. F., Leoni, M. and Scardi, P. (2010) 'Domain size analysis in the Rietveld method', *Materials Science Forum*, 651, pp. 187–200. doi: 10.4028/www.scientific.net/MSF.651.187.

Davies, R. (1983) 'Factors Involved in the Cytotoxicity of Kaolinite towards Macrophages in Vitro', *Environmental Health Perspectives*, 51, pp. 249–274.

Davies, R., Griffiths, D. M., Johnson, N. F., Preece, A. W. and Livingston, D. C. (1984) 'The cytotoxicity of kaolin towards macrophages in vitro', *British Journal of Experimental Pathology*, 65, pp. 453–466.

Davis, J. M. G., Addison, J., Bruch, J., Bruyere, S., Daniel, H., Degueldre, G., Dodgson, J., Gade, M., et al (1982) 'Variations in cytotoxicity and mineral content between respirable mine dusts from the Belgian , British , French and German coalfields', *Annals of Occupational Hygiene*, 26(541), pp. 541–549.

Decuzzi, P., Godin, B., Tanaka, T., Lee, S. Y., Chiappini, C., Liu, X. and Ferrari, M. (2010) 'Size and shape effects in the biodistribution of intravascularly injected particles', *Journal of Controlled Release*. Elsevier, 141(3), pp.

320–327. doi: 10.1016/j.jconrel.2009.10.014.

Donaldson, K., Brown, D., Clouter, A., Duffin, R., MacNee, W., Renwick, L., Tran, L. and Stone, V. (2002) 'The pulmonary toxicology of ultrafine particles', *Journal of Aerosol Medicine*, 15(2), pp. 213–220. doi: 10.1089/089426802320282338.

Donaldson, K., Stone, V., Borm, P. J. A., Jimenez, L. A., Gilmour, P. S., Schins, R. P. F., Knaapen, A. M., Rahman, I., et al (2003) 'Oxidative stress and calcium signaling in the adverse effects of environmental particles (PM10)', *Free Radical Biology and Medicine*. Elsevier, 34(11), pp. 1369–1382. doi: 10.1016/S0891-5849(03)00150-3.

Donaldson, K., Stone, V., Gilmour, P. S., Brown, D. M. and MacNee, W. (2000) 'Ultrafine particles: mechanisms of lung injury', *Philosophical Transactions of the Royal Society A*, 358, pp. 2741–2749. doi: 10.1098/rsta.2000.0681.

Donaldson, K., Wallace, W. A., Elliott, T. and Henry, C. (2017) 'James Craufurd Gregory, 19th century Scottish physicians, and the link between occupation as a coal miner and lung disease', *Journal of the Royal College of Physicians of Edinburgh*, 47(3), pp. 296–302. doi: 10.4997/JRCPE.2017.317.

Driscoll, T., Nelson, D. I., Steenland, K., Leigh, J., Concha-Barrientos, M., Fingerhut, M. and Prüss-Üstün, A. (2005) 'The global burden of non malignant respiratory disease due to occupational airborne exposures', *American Journal of Industrial Medicine*, 48(6), pp. 432–445. doi: 10.1002/AJIM.20210.

Driscoll, T., Steenland, K., Pearce, N., Rushton, L., Hutchings, S. J., Straif, K., Abate, D., Acharya, D., et al (2020) 'Global and regional burden of chronic respiratory disease in 2016 arising from non-infectious airborne occupational exposures: A systematic analysis for the Global Burden of Disease Study 2016', *Occupational and Environmental Medicine*, 77(3), pp. 142–150. doi: 10.1136/oemed-2019-106013.

Elmes, M., Delbem, I., Gasparon, M. and Ciminelli, V. (2020) 'Single-particle analysis of atmospheric particulate matter using automated mineralogy: the potential for monitoring mine-derived emissions', *International Journal of Environmental Science and Technology*. Springer, 17(5), pp. 2743–2754. doi: 10.1007/S13762-020-02660-W/FIGURES/5.

Fandrich, R., Gu, Y., Burrows, D. and Moeller, K. (2007) 'Modern SEM-based mineral liberation analysis', *International Journal of Mineral Processing*, pp. 310–320. doi: 10.1016/j.minpro.2006.07.018.

Finkelman, R. B. (1994) 'Modes of occurance of potentially hazardous elements in coal: levels of confidence', *Fuel Processing Technology*, 39, pp. 21–34. doi: 10.1016/0378-3820(94)90169-4.

Finkelman, R. B., Dai, S. and French, D. (2019) 'The importance of minerals in coal as the hosts of chemical elements: A review', *International Journal of Coal Geology*. Elsevier BV, 212, p. 103251. doi: 10.1016/j.coal.2019.103251.

Finkelman, R. B., Orem, W., Castranova, V., Tatu, C. A., Belkin, H. E., Zheng, B., Lerch, H. E., Maharaj, S., et al (2002) 'Health impacts of coal and coal use: Possible solutions', *International Journal of Coal Geology*. Elsevier, 50, pp. 425–443. doi: 10.1016/S0166-5162(02)00125-8.

Fiordelisi, A., Piscitelli, P., Trimarco, B., Coscioni, E., Iaccarino, G. and Sorriento, D. (2017) 'The mechanisms of air pollution and particulate matter in cardiovascular diseases', *Heart Failure Reviews*. Heart Failure

Reviews, 22(3), pp. 337–347. doi: 10.1007/s10741-017-9606-7.

French, D., Ward, C. and Butcher, A. R. (2008) *QEMSCAN for Characterisation of Coal and Coal Utilisation By-products*.

French, D. and Ward, C. R. (2009) 'The Application of Advanced Mineralogical Techniques to Coal Combustion Product Characterisation', in *2009 World of Coal Ash Conference*. Lexington. Available at: http://www.flyash.info/ (Accessed: 25 July 2018).

Fubini, B. (1997) 'Surface Reactivity in the Pathogenic Response to Particulates', *Environmental Health Perspectives*, 105(5), pp. 1013–1020.

Fubini, B. (1998) 'Surface Chemistry and Quartz Hazard', *Annals of Occupational Hygienene*, 42(8), pp. 521–530. Available at: https://academic.oup.com/annweh/article/42/8/521/148104 (Accessed: 7 November 2022).

Fubini, B., Bolis, V. and Giamello, E. (1987) 'The surface chemistry of crushed quartz dust in relation to its pathogenicity', *Inorganica Chimica Acta*, 138, pp. 193–197.

Fubini, B., Giamello, E., Volante, M. and Bolis, V. (1990) 'Chemical functionalities at the silica surface determining its reactivity when inhaled. Formation and reactivity of surface radicals', *Toxicology and Industrial Health*, 6(6), pp. 571–598. Available at: https://pubmed.ncbi.nlm.nih.gov/1965871/ (Accessed: 22 June 2021).

Fubini, B. and Ivana, F. (2007) 'Toxic Potential of Mineral Dusts', *Elements*, 3(6), pp. 407–414. doi: 10.2113/GSELEMENTS.3.6.407.

Fubini, B. and Otero Areán, C. (1999) 'Chemical aspects of the toxicity of inhaled mineral dusts', *Chemical Society Reviews*, 28, pp. 373–381. doi: 10.1039/a805639k.

Galindo-Prieto, B., Eriksson, L. and Trygg, J. (2014) 'Variable influence on projection (VIP) for orthogonal projections to latent structures (OPLS)', *Journal of Chemometrics*, 28(8), pp. 623–632. doi: 10.1002/cem.2627.

Gatti, E., Rehak, P. and Walton, J. T. (1984) 'Silicon drift chambers - first results and optimum processing of signals', *Nuclear Inst. and Methods in Physics Research, A*, 226(1), pp. 129–141. doi: 10.1016/0168-9002(84)90181-5.

GBD 2016 Occupational Chronic Respiratory Risk Factors Collaborators (2020) 'Global and regional burden of chronic respiratory disease in 2016 arising from non-infectious airborne occupational exposures: A systematic analysis for the Global Burden of Disease Study 2016', *Occupational and Environmental Medicine*, 77(3), pp. 142–150. doi: 10.1136/oemed-2019-106013.

Ghio, A. J., Kennedy, T. P., Whorton, A. R., Crumbliss, A. L., Hatch, G. E. and Hoidal, J. R. (1992) 'Role of surface complexed iron in oxidant generation and lung inflammation induced by silicates', *American Journal of Physiology*, 263, pp. 511–518. doi: 10.1152/ajplung.1992.263.5.l511.

Ghio, A. J. and Quigley, D. R. (1994) 'Complexation of iron by humic-like substances in lung tissue: role in coal workers' pneumoconiosis', *American Journal of Physiology*, 267(2), pp. L173–L179. doi: 10.1152/ajplung.1994.267.2.l173.

Ghose, M. K. and Majee, S. R. (2000a) 'Assessment of dust generation due to opencast coal mining - An Indian case study', *Environmental Monitoring and Assessment*, 61(2), pp. 255–263. doi: 10.1023/A:1006127407401.

Ghose, M. K. and Majee, S. R. (2000b) 'Assessment of the impact on the air environment due to opencast

coal mining - An Indian case study', *Atmospheric Environment*, 34(17), pp. 2791–2796. doi: 10.1016/S1352-2310(99)00302-7.

Ghose, M. K. and Majee, S. R. (2007) 'Characteristics of hazardous airborne dust around an Indian surface coal mining area', *Environmental Monitoring and Assessment*, 130(1–3), pp. 17–25. doi: 10.1007/s10661-006-9448-6.

Gibbs, A. R. (1990) 'Human Pathology of Kaolin and Mica Pneumoconioses', in *Health Related Effects of Phyllosilicates*. Berlin Heidelberg: Springer, pp. 217–226. doi: https://doi.org/10.1007/978-3-642-75124-0_20.

Gómez-Gener, L., Gubau, M., von Schiller, D., Marcé, R. and Obrador, B. (2018) 'Effect of small water retention structures on diffusive CO2 and CH4 emissions along a highly impounded river', *Inland Waters*. Taylor & Francis, 8(4), pp. 449–460. doi: 10.1080/20442041.2018.1457846.

Gonzalez, J., Keles, C., Pokhrel, N., Jaramillo, L. and Sarver, E. (2022a) 'Respirable dust constituents and particle size: a case study in a thin-seam coal mine', *Mining, Metallurgy and Exploration*, 1, pp. 1007–1015. doi: 10.1007/s42461-022-00611-2.

Gonzalez, J., Keles, C. and Sarver, E. (2022b) 'On the Occurrence and Persistence of Coal-Mineral Microagglomerates in Respirable Coal Mine Dust', *Mining, Metallurgy and Exploration*. Springer, 39(2), pp. 271–282. doi: 10.1007/s42461-022-00555-7.

Gormley, I. P., Collings, P., Davis, J. M. G. and Ottery, J. (1979) 'An Investigation into the Cytotoxicity of Respirable Dusts from British Collieries', *British Journal of Experimental Pathology*, 60, pp. 526–536.

Gulumian, M., Borm, P. J. A., Vallyathan, V., Castranova, V., Donaldson, K., Nelson, G. and Murray, J. (2006) 'Mechanistically identified suitable biomarkers of exposure, effect, and susceptibility for silicosis and coal-worker's pneumoconiosis: A comprehensive review', *Journal of Toxicology and Environmental Health - Part B: Critical Reviews*, 9(5), pp. 357–395. doi: 10.1080/15287390500196537.

Haberlah, D., Owen, M., Botha, P. W. S. K. and Gottlieb, P. (2012) 'SEM-EDS-based protocol of subsurface drilling mineral identification and petrological classification', in *Proceedings of the 10th International Congress for Applied Mineralogy (ICAM)*, pp. 265–266. doi: 10.1007/978-3-642-27682-8.

Haddrell, A. E., Davies, J. F. and Reid, J. P. (2015) 'Dynamics of Particle Size on Inhalation of Environmental Aerosol and Impact on Deposition Fraction', *Environmental Science and Technology*, 49(24), pp. 14512–14521. doi: 10.1021/acs.est.5b01930.

Hall, N. B., Blackley, D. J., Halldin, C. N. and Laney, A. S. (2019) 'Continued increase in prevalence of r-type opacities among underground coal miners in the USA', *Occupational and Environmental Medicine*, 76(7), pp. 479–481. doi: 10.1136/oemed-2019-105691.

Harrington, A. D., Hylton, S. and Schoonen, M. A. (2012) 'Pyrite-driven reactive oxygen species formation in simulated lung fluid: implications for coal workers' pneumoconiosis', *Environmental Geochemistry and Health*. Springer, 34(4), pp. 527–538. doi: 10.1007/s10653-011-9438-7.

Harrington, A. D., Smirnov, A., Tsirka, S. E. and Schoonen, M. A. (2015) 'Metal-sulfide mineral ores, Fenton chemistry and disease – Particle induced inflammatory stress response in lung cells', *International Journal of Hygiene and Environmental Health*. Elsevier, 218(1), pp. 19–27. doi: 10.1016/J.IJHEH.2014.07.002.

Harrington, A. D., Tsirka, S. E. and Schoonen, M. A. A. (2013) 'Inflammatory stress response in A549 cells as a result of exposure to coal: Evidence for the role of pyrite in coal workers' pneumoconiosis pathogenesis', *Chemosphere*, 93(6), pp. 1216–1221. doi: 10.1016/j.chemosphere.2013.06.082.

Harrison, J. C., Brower, P. S., Attfield, M. D., Doak, C. B., Keane, M. J., Grayson, R. L. and Wallace, W. E. (1997) 'Surface composition of respirable silica particles in a set of U.S. anthracite and bituminous coal mine dusts', *Journal of Aerosol Science*, 28(4), pp. 689–696. doi: 10.1016/S0021-8502(96)00033-X.

Hassan, M. S. and Lau, R. W. M. (2009) 'Effect of Particle Shape on Dry Particle Inhalation: Study of Flowability, Aerosolization, and Deposition Properties', *AAPS PharmSciTech*, 10(4), pp. 1252–1262. doi: 10.1208/s12249-009-9313-3.

HEI, Health Effects Institute. and IHME, Institute for Health Metrics and Evaluation. (2020) *State of Global Air 2020.Special Report*. Boston.

Hendryx, M., Zullig, K. J. and Luo, J. (2020) 'Impacts of Coal Use on Health', *Annual Review of Public Health*, 41, pp. 397–415. doi: 10.1146/annurev-publhealth.

Heppleston, A. G. (1992) 'Coal workers' pneumoconiosis: a historical perspective on its pathogenesis.', *American Journal Of Industrial Medicine*, 22(6), pp. 905–923.

Hiraiwa, K. and Van Eeden, S. F. (2013) 'Contribution of Lung Macrophages to the Inflammatory Responses Induced by Exposure to Air Pollutants', *Mediators of Inflammation*. Hindawi Publishing Corporation, pp. 1–10. doi: 10.1155/2013/619523.

Hiura, T. S., Kaszubowski, M. P., Li, N. and Nel, A. E. (1999) 'Induce Apoptosis in Macrophages Generate Reactive Oxygen Radicals and Chemicals in Diesel Exhaust Particles', *The Journal of Immunology*, 163, pp. 5582–5591. Available at: http://www.jimmunol.org/content/163/10/http://www.jimmunol.org/content/163/10/5582.full#ref-list-1 (Accessed: 13 February 2019).

Huang, C., Li, J., Zhang, Q. and Huang, X. (2002) 'Role of Bioavailable Iron in Coal Dust-Induced Activation of Activator Protein-1 and Nuclear Factor of Activated T Cells Difference between Pennsylvania and Utah Coal Dusts scale mining', *American Journal of Respiratory Cell and Molecular Biology*, 27, pp. 568–574. doi: 10.1165/rcmb.4821.

Huang, X. and Finkelman, R. B. (2008) 'Understanding the Chemical Properties of Macerals and Minerals in Coal and its Potential Application for Occupational Lung Disease Prevention', *Journal of Toxicology and Environmental Health, Part B*, 11(1), pp. 45–67. doi: 10.1080/10937400701600552.

Huang, X., Gordon, T., Rom, W. N. and Finkelman, R. B. (2006) 'Interaction of Iron and Calcium Minerals in Coals and their Roles in Coal Dust-Induced Health and Environmental Problems', *Reviews in Mineralogy and Geochemistry*, 64(1), pp. 153–178. doi: 10.2138/rmg.2006.64.6.

Huang, X., Li, W., Attfield, M. D., Nádas, A., Frenkel, K. and Finkelman, R. B. (2005) 'Mapping and prediction of coal workers' pneumoconiosis with bioavailable iron content in the bituminous coals.', *Environmental health perspectives*, 113(8), pp. 964–8. doi: 10.1289/ehp.7679.

Huang, X., Zalma, R. and Pezerat, H. (1999) 'Chemical reactivity of the carbon-centered free radicals and

ferrous iron in coals: Role of bioavailable Fe2+ in coal workers' pneumoconiosis', *Free Radical Research*, 30(6), pp. 439–451. doi: 10.1080/10715769900300481.

Huang, X., Zalma, R., Pezerat, H. and Huang, X. (1994) 'Factors That Influence the Formation and Stability of Hydrated Ferrous Sulfate in Coal Dusts. Possible Relation to the Emphysema of Coal Miners', *Chemical Research in Toxicology*, 7(3), pp. 451–457. doi: 10.1021/tx00039a025.

Huertas, J. I., Huertas, M. E., Cervantes, G. and Di´az, J. (2014) 'Assessment of the natural sources of particulate matter on the opencast mines air quality', *Science of the Total Environment*. Elsevier, 493(2000), pp. 1047–1055. doi: 10.1016/j.scitotenv.2014.05.111.

Huertas, J. I., Huertas, M. E., Izquierdo, S. and Gonzalez, E. D. (2012a) 'Air quality impact assessment of multiple open pit coal mines in northern Colombia', *Journal of Environmental Management*. Elsevier, 93(1), pp. 121–129. doi: 10.1016/j.jenvman.2011.08.007.

Huertas, J. I., Huertas, M. E. and Solis-Casados, D. A. (2012b) 'Characterization of airborne particles in an open pit mining region', *Science of the Total Environment*. Elsevier B.V., 423, pp. 39–46. doi: 10.1016/j.scitotenv.2012.01.065.

Humphreys, F. J. and Brough, I. (1999) 'High resolution electron backscatter diffraction with a field emission gun scanning electron microscope.', *Journal of microscopy*, 195(Pt 1), pp. 6–9. Available at: http://www.ncbi.nlm.nih.gov/pubmed/10444296.

Hurley, J. F., Alexander, P., Hazledine, J., Jacobsen, M. and Maclaren, W. M. (1987) 'Exposure to respirable coalmine dust and incidence of progressive massive fibrosis', *British Journal of Industrial Medicine*, 44, pp. 661–672.

Hurley, J. F., Burns, J., Copland, L., Dodgson, J. and Jacobsen, M. (1982) 'Coal workers' simple pneumoconiosis and exposure to dust at 10 British coalmines', *British Journal of Industrial Medicine*, 39, pp. 120–127. doi: 10.1136/oem.39.2.120.

Igathinathane, C., Pordesimo, L. O., Columbus, E. P., Batchelor, W. D. and Methuku, S. R. (2008) 'Shape identification and particles size distribution from basic shape parameters using ImageJ', *Computers and Electronics in Agriculture*. Elsevier, 63(2), pp. 168–182. doi: 10.1016/J.COMPAG.2008.02.007.

Jacobsen, M., Rae, S., Walton, W. H. and Rogan, J. M. (1970) 'New dust standards for British coal mines', *Nature*, 227(5257), pp. 445–447. doi: 10.1038/227445a0.

Jelic, T. M., Estalilla, O. C., Sawyer-Kaplan, P. R., Plata, M. J., Powers, J. T., Emmett, M. and Kuenstner, J. T. (2017) 'Coal Mine Dust Desquamative Chronic Interstitial Pneumonia: A Precursor of Dust-Related Diffuse Fibrosis and of Emphysema', *The International Journal of Occupational and Environmental Medicine*, 8, pp. 153–165. doi: 10.15171/IJOEM.2017.1066.

Johann-Essex, V., Keles, C., Rezaee, M., Scaggs-Witte, M. and Sarver, E. (2017a) 'Respirable coal mine dust characteristics in samples collected in central and northern Appalachia', *International Journal of Coal Geology*. Elsevier, 182(September), pp. 85–93. doi: 10.1016/j.coal.2017.09.010.

Johann-Essex, V., Keles, C. and Sarver, E. (2017b) 'A Computer-Controlled SEM-EDX Routine for Characterizing Respirable Coal Mine Dust', *Minerals*, 7(15), pp. 1–15. doi: 10.3390/min7010015.

Johnson, D., Rollinson, G. K., Arif, A. T., Moreno, T., Pedro Ruiz, T., Lah, R., Lubosik, Z., Pindel, T.,

Gminsk, R. and Williamson, B. J. (2022) 'QEMSCAN® automated mineralogical analysis of PM2.5 and PM4: A preliminary study of underground coal mine dust from Poland and Slovenia', *Frontiers in Earth Science*, 10(September), pp. 1–12. doi: 10.3389/feart.2022.788928.

De Jong, S. (1993) 'SIMPLS: an alternative approach squares regression to partial least', *Chemometrics and Intelligent Labratory Systems*, 18, pp. 251–263.

Kamanzi, C., Becker, M., Von Holdt, J. and Broadhurst, J. (2022) 'Development of a SEM-EDS-XRD Protocol for the Physicochemical and Automated Mineralogical Characterisation of Coal Dust Particles', *Resources*. Multidisciplinary Digital Publishing Institute, 11, p. 114. doi: 10.3390/RESOURCES11120114.

Kaya, E., Hogg, R. and Mutmansky, J. M. (1996) 'Evaluation of procedures for production of dust samples for biomedical research', *Applied Occupational and Environmental Hygiene*, 11(7), pp. 745–750. doi: 10.1080/1047322X.1996.10389964.

Kehrer, J. P. (2000) 'The Haber-Weiss reaction and mechanisms of toxicity', *Toxicology*, 149, pp. 43–50. Available at: www.elsevier.com/locate/toxicol (Accessed: 20 June 2019).

Keles, C., Pokhrel, N. and Sarver, E. (2022) 'A Study of Respirable Silica in Underground Coal Mines: Sources', *Minerals*, 12, p. 1115. doi: 10.3390/min12121555.

Keles, C. and Sarver, E. (2022) 'A Study of Respirable Silica in Underground Coal Mines: Particle Characteristics', *Minerals*. MDPI, 12, p. 1555. doi: 10.3390/MIN12121555/S1.

Kennedy, T., Ghio, A. J., Reed, W., Samet, J., Zagorski, J., Quay, J., Carter, J., Dailey, L., et al (1998) 'Copper-dependent inflammation and nuclear factor-κb activation by particulate air pollution', *American Journal of Respiratory Cell and Molecular Biology*. American Lung Association, 19(3), pp. 366–378. doi: 10.1165/AJRCMB.19.3.3042.

Kodros, J. K., Volckens, J., Jathar, S. H. and Pierce, J. R. (2018) 'Ambient Particulate Matter Size Distributions Drive Regional and Global Variability in Particle Deposition in the Respiratory Tract', *GeoHealth*, 1(10), pp. 298–312. doi: 10.1029/2018GH000145.

Könczöl, M., Ebeling, S., Goldenberg, E., Treude, F., Gminski, R., Gier, R., Grob, B., Rothen-Rutishauser, et al (2011) 'Cytotoxicity and Genotoxicity of Size-Fractionated Iron Oxide (Magnetite) in A549 Human Lung Epithelial Cells: Role of ROS, JNK, and NF-κB', *Chemical Research in Toxicology*, 24(9), pp. 1460–1475. Available at: http://doc.rero.ch (Accessed: 4 March 2020).

Kongsuebchart, W., Praserthdam, P., Panpranot, J., Sirisuk, A., Supphasrirongjaroen, P. and Satayaprasert, C. (2006) 'Effect of crystallite size on the surface defect of nano-TiO2 prepared via solvothermal synthesis', *Journal of Crystal Growth*, 297(1), pp. 234–238. doi: 10.1016/J.JCRYSGRO.2006.09.018.

Kroll, A., Dierker, C., Rommel, C., Hahn, D., Wohlleben, W., Schulze-Isfort, C., Göbbert, C., Voetz, M., et al (2011) 'Cytotoxicity screening of 23 engineered nanomaterials using a test matrix of ten cell lines and three different assays', *Particle and Fibre Toxicology*, 8(9), pp. 1–19. doi: 10.1186/1743-8977-8-9.

Kuempel, E. D., Attfield, M. D., Vallyathan, V., Lapp, N. L., Hale, J. M., Smith, R. J. and Castranova, V. (2003) *Pulmonary inflammation and crystalline silica in respirable coal mine dust: dose-response*, *Journal of Biosciences*.

LaBranche, N., Keles, C., Sarver, E., Johnstone, K. and Cliff, D. (2021) 'Characterization of particulates from Australian underground coal mines', *Minerals*, 11(5), pp. 1–10. doi: 10.3390/min11050447.

LaBranche, N., Teale, K., Wightman, E., Johnstone, K. and Cliff, D. (2022) 'Characterization Analysis of Airborne Particulates from Australian Underground Coal Mines Using the Mineral Liberation Analyser', *Minerals*, 12(796), pp. 1–13.

Landsiedel, R., Ma-Hock, L., Wiench, K., Wohlleben, W. and Sauer, U. G. (2017) 'Safety assessment of nanomaterials using an advanced decision-making framework, the DF4nanoGrouping', *Journal of Nanoparticle Research*, 19(5), p. 171. doi: 10.1007/s11051-017-3850-6.

Laney, A. S. and Weissman, D. N. (2014) 'Respiratory Diseases Caused by Coal Mine Dust', *Journal of Occupational and Environmental Medicine*, 56, pp. 18–22. doi: 10.1097/JOM.0000000000000260.

Laskin, D. L. (2009) 'Macrophages and inflammatory mediators in chemical toxicity: A battle of forces', *Chemical Research in Toxicology*, 22(8), pp. 1376–1385. doi: 10.1021/tx900086v.

Lauweryns, J. and Baert, J. (1977) 'Alveolar Clearance and the Role of the Pulmonary Lymphatics', *American Review of Respiratory Disease*, 115(4), pp. 625–683. Available at: https://www.atsjournals.org/doi/abs/10.1164/arrd.1977.115.4.625?journalCode=arrd (Accessed: 24 October 2022).

Lee, C. Y., Lee, S. L., Sheehan, C. E. and Wang, Y. (1996) *Composition of coal dusts and their cytotoxicity on alveolar macrophages*. Technical report ARCCB-TR-96026. Available at: https://pdfs.semanticscholar.org/8185/85459224e1ac9db8dce8b006c415033ec7d9.pdf (Accessed: 10 May 2019).

Leigh, G. M., Sutherland, D. N. and Gottlieb, P. (1993) 'Confidence limits for liberation measurements', *Minerals Engineering*, 6(2), pp. 155–161. doi: 10.1016/0892-6875(93)90129-B.

Leinardi, R., Pavan, C., Yedavally, H., Tomatis, M., Salvati, A. and Turci, F. (2020) 'Cytotoxicity of fractured quartz on THP-1 human macrophages: role of the membranolytic activity of quartz and phagolysosome destabilization', *Archives of Toxicology*. Springer, 94(9), pp. 2981–2995. doi: 10.1007/s00204-020-02819-x.

León-Mejía, G., Silva, L. F. O., Civeira, M. S., Oliveira, M. L. S., Machado, M., Villela, I. V., Hartmann, A., Premoli, S., et al (2016) 'Cytotoxicity and genotoxicity induced by coal and coal fly ash particles samples in V79 cells', *Environmental Science and Pollution Research*, 23(23), pp. 24019–24031. doi: 10.1007/s11356-016-7623-z.

Leonard, R., Zulfikar, R. and Stansbury, R. (2020) 'Coal mining and lung disease in the 21st century', *Current Opinion in Pulmonary Medicine*, 26(2), pp. 135–141. doi: 10.1097/MCP.0000000000000653.

Leung, C. C., Yu, I. T. S. and Chen, W. (2012) 'Silicosis', *The Lancet*. Elsevier, 379(9830), pp. 2008–2018. doi: 10.1016/S0140-6736(12)60235-9.

Li, M., Wilkinson, D. and Patchigolla, K. (2005) 'Comparison of particle size distributions measured using different techniques', *Particulate Science and Technology*, 23(3), pp. 265–284. doi: 10.1080/02726350590955912.

Linkov, I., Steevens, J., Chappell, M., Merad, M., Tervonen, T. and Figueira, J. R. (2009) 'Classifying Nanomaterial Risk Using Multi-Criteria Decision Analysis', in *Nanomaterials: risks and benefits*. Springer, pp. 179–191. Available at: http://www.nanotechproject.org/inventories/ (Accessed: 12 January 2022).

Lison, D., Cile Lardot, C., Ois Huaux, F., Zanetti, G. and Fubini, B. (1997) 'Influence of particle surface area on the toxicity of insoluble manganese dioxide dusts', *Archives of toxicology*, 71, pp. 725–729. Available at:

https://link.springer.com/content/pdf/10.1007/s002040050453.pdf (Accessed: 6 February 2019).

Little, L. (2016) *The Development and Demonstration of a Practical Methodology for Fine Particle Shape Characterisation in Minerals Processing*. University of Cape Town.

Little, L., Becker, M., Wiese, J. and Mainza, A. N. (2015) 'Auto-SEM particle shape characterisation: Investigating fine grinding of UG2 ore', *Minerals Engineering*. Elsevier Ltd, 82, pp. 92–100. doi: 10.1016/j.mineng.2015.03.021.

Little, L., Becker, M., Wiese, J., Yorath, G., Mainza, A. and Tonzetic, I. (2016a) 'Shape characterisation: Can different devices produce comparable data for particulate samples?', in *Proceedings of the XXVIII th International Mineral Processing Congress*.

Little, L., Mainza, A. N., Becker, M. and Wiese, J. G. (2016b) 'Using mineralogical and particle shape analysis to investigate enhanced mineral liberation through phase boundary fracture', *Powder Technology*. Elsevier, 301, pp. 794–804. doi: 10.1016/J.POWTEC.2016.06.052.

Liu, T. and Liu, S. (2020) 'The impacts of coal dust on miners' health: A review', *Environmental Research*. Elsevier Inc., 190(June), p. 109849. doi: 10.1016/j.envres.2020.109849.

Maanen, J. M. S. Van, Borm, P. J. A., Knaapen, A., Herwijnen, M. Van, Schilderman, P. A., Smith, K. R., Aust, A. E. and Tomatis, M. (1999) 'In vitro effects of coal fly ashes: Hydroxyl Radical Generation, Iron Release , and DNA Damage and Toxicity in Rat Lung Epithelial Cells', *Inhalation Toxicology*, 11, pp. 1123–1141.

Mandal, K., Kumar, A., Tripathi, N., Singh, R. S., Chaulya, S. K., Mishra, P. K. and Bandyopadhyay, L. K. (2012) 'Characterization of different road dusts in opencast coal mining areas of India', *Environmental Monitoring and Assessment*, 184, pp. 3427–3441. doi: 10.1007/s10661-011-2197-1.

Marsalek, R. and Sassikova, M. (2016) 'Characterization of the size distribution of subbituminous coal by laser diffraction', *Instrumentation Science and Technology*, 44(3), pp. 233–240. doi: 10.1080/10739149.2015.1113429.

Mauderly, J. L., Jones, R. K., Griffith, W. C., Henderson, R. F. and Mcclellan, R. O. (1987) 'Diesel exhaust is a pulmonary carcinogen in rats exposed chronically by inhalation', *Toxicological Sciences*, 9(2), pp. 208–221. doi: 10.1093/toxsci/9.2.208.

Maynard, A. D. and Kuempel, E. D. (2005) 'Airborne nanostructured particles and occupational health', *Journal of Nanoparticle Research*, 7(6), pp. 587–614. doi: 10.1007/s11051-005-6770-9.

Mazzoli, A. and Favoni, O. (2012) 'Particle size, size distribution and morphological evaluation of airborne dust particles of diverse woods by Scanning Electron Microscopy and image processing program', *Powder Technology*. Elsevier, 225, pp. 65–71. doi: 10.1016/J.POWTEC.2012.03.033.

McClellan, R. O. (2000) 'Particle Interactions with the respiratory Tract', *Lung Biology in Health and Disease*, 143, pp. 3–56.

Meneghini, R. (1997) 'Iron Homeostasis, Oxidative Stress, and DNA Damage', *Free Radical Biology and Medicine*, 23(5), pp. 783–792. doi: 10.1016/S0891-5849(97)00016-6.

Mevik, B.-H. W. (2022) 'Introduction to the pls Package', *CRAN*. Netherlands, pp. 1–24. Available at: https://cran.r-project.org/web/packages/pls/vignettes/pls-manual.pdf (Accessed: 12 December 2022).

Mevik, B.-H. and Wehrens, R. (2007) 'The pls Package: Principal Component and Partial Least Squares Regression in R', *Journal of Statistical Software*, 18(2), pp. 1–24.

Michael, S., Montag, M. and Dott, W. (2013) 'Pro-inflammatory effects and oxidative stress in lung macrophages and epithelial cells induced by ambient particulate matter', *Environmental Pollution*, 183, pp. 19–29. doi: 10.1016/j.envpol.2013.01.026.

Minov, J. (2021) 'Occupational chronic obstructive pulmonary disorder: prevalence and prevention', *Expert Review of Respiratory Medicine*. doi: 10.1080/17476348.2021.2011722.

Mischler, S. E., Cauda, E. G., Di Giuseppe, M., McWilliams, L. J., St. Croix, C., Sun, M., Franks, J. and Ortiz, L. A. (2016) 'Differential activation of RAW 264.7 macrophages by size-segregated crystalline silica', *Journal of Occupational Medicine and Toxicology*, 11(57), pp. 1–14. doi: 10.1186/S12995-016-0145-2/FIGURES/9.

Mishra, R. K., Pandey, J., Chaudhary, S. K., Khalkho, A. and Singh, V. K. (2012) 'Estimation of air pollution concentration over Jharia coalfield based on satellite imagery of atmospheric aerosol', *International Journal of Geomatics and Geosciences*, 2(3), pp. 723–729.

Moreno, T., Trechera, P., Querol, X., Lah, R., Johnson, D., Wrana, A. and Williamson, B. (2019) 'Trace element fractionation between PM10 and PM2.5 in coal mine dust: Implications for occupational respiratory health', *International Journal of Coal Geology*, 203, pp. 52–59. doi: 10.1016/j.coal.2019.01.006.

Morgan, W., C., K., Burgess, D. B., Jacobson, G., O'Brien, R. J., Pendergrass, E. P., Reger, R. B. and Shoub, E. P. (1973) 'The Prevalence of Coal Workers' Pneumoconiosis in US Coal Miners', *Archives of Environmental Health: An International Journal*. Taylor & Francis Group, 27(4), pp. 221–226. doi: 10.1080/00039896.1973.10666356.

Morrow, P. E. (1988) 'Possible Mechanisms to Explain Dust Overloading of the Lungs', *Fundamental and aplied Toxicology*, 10, pp. 369–384.

Muhle, H., Creutzenberg, O., Bellmann, B., Heinrich, U. and Mermelstein, R. (1990) 'Dust Overloading of Lungs: Investigations of Various Materials, Species Differences, and Irreversibility of Effects', *Journal of Aerosol Medicine*, 3(s1), p. S-111-S-128. doi: 10.1089/jam.1990.3.suppl_1.s-111.

Muhle, H. and Mangelsdorf, I. (2003) 'Inhalation toxicity of mineral particles: Critical appraisal of endpoints and study design', *Toxicology Letters*, 140–141, pp. 223–228. doi: 10.1016/S0378-4274(02)00514-3.

Nel, A., Xia, T., Mädler, L. and Li, N. (2006) 'Toxic Potential of Materials at the Nanolevel', *Science*, 311, pp. 622–627. doi: DOI: 10.1126/science.1114397.

O'Neill, L. A. J. (2008) 'How frustration leads to inflammation', *Science*, 320(5876), pp. 619–620. doi: 10.1126/science.1158398.

Oberdörster, G. (2000) 'Pulmonary effects of inhaled ultrafine particles', *International Archives of Occupational and Environmental Health*, 74(1), pp. 1–8. doi: 10.1007/s004200000185.

Oberdörster, G., Ferin, J. and Lehnert, B. (1994) 'Correlation between Particle Size, In Vivo Particle Persistence, and Lung Injury', *Environmental Health Perspectives*, 102, pp. 173–179. doi: 10.1016/B978-0-12-386454-3.00341-9.

Oberdörster, G., Oberdörster, E. and Oberdörster, J. (2005) 'Nanotoxicology: An emerging discipline

evolving from studies of ultrafine particles', *Environmental Health Perspectives*, 113(7), pp. 823–839. doi: 10.1289/ehp.7339.

Oliveira, M. L. S., Ward, C. R., French, D., Hower, J. C., Querol, X. and Silva, L. F. O. (2012a) 'Mineralogy and leaching characteristics of beneficiated coal products from Santa Catarina, Brazil', *International Journal of Coal Geology*, 94, pp. 314–325. doi: 10.1016/j.coal.2011.10.004.

Oliveira, M. L. S., Ward, C. R., Izquierdo, M., Sampaio, C. H., de Brum, I. A. S., Kautzmann, R. M., Sabedot, S., Querol, X., et al (2012b) 'Chemical composition and minerals in pyrite ash of an abandoned sulphuric acid production plant', *Science of the Total Environment*. Elsevier, 430, pp. 34–47. doi: 10.1016/j.scitotenv.2012.04.046.

Orona, N. S., Astort, F., Maglione, G. A., Saldiva, P. H. N., Yakisich, J. S. and Tasat, D. R. (2014) 'Direct and indirect air particle cytotoxicity in human alveolar epithelial cells', *Toxicology in Vitro*, 28, pp. 796–802. doi: 10.1016/j.tiv.2014.02.011.

Pan, L., Golden, S., Assemi, S., Sime, M. F., Wang, X., Gao, Y. and Miller, J. (2021) 'Characterization of particle size and composition of respirable coal mine dust', *Minerals*, 11(3), pp. 1–12. doi: 10.3390/min11030276.

Patel, S., Sankhyan, S., Boedicker, E. K., Decarlo, P. F., Farmer, D. K., Goldstein, A. H., Katz, E. F., Nazaroff, W. W., et al (2020) 'Indoor Particulate Matter during HOMEChem: Concentrations, Size Distributions, and Exposures', *Environmental Science and Technology*, 54(12), pp. 7107–7116. doi: 10.1021/acs.est.0c00740.

Patra, A. K., Gautam, S. and Kumar, P. (2016) 'Emissions and human health impact of particulate matter from surface mining operation-A review', *Environmental Technology and Innovation*. Elsevier, 5, pp. 233–249. doi: 10.1016/j.eti.2016.04.002.

Pavan, C., Santalucia, R., Leinardi, R., Fabbiani, M., Yakoub, Y., Uwambayinema, F., Ugliengo, P., Tomatis, et al (2020) 'Nearly free surface silanols are the critical molecular moieties that initiate the toxicity of silica particles', *Proceedings of the National Academy of Sciences*. National Academy of Sciences, 117(45), pp. 27836–27846. doi: 10.1073/PNAS.2008006117/SUPPL_FILE/PNAS.2008006117.SAPP.PDF.

Perret, J. L., Plush, B., Lachapelle, P., Hinks, T. S. C., Walter, C., Clarke, P., Irving, L., Brady, P., et al (2017) 'Coal mine dust lung disease in the modern era', *Respirology*, 22(4), pp. 662–670. doi: 10.1111/resp.13034.

Petruk, W. (2000) 'Applied Mineralogy in the Mining Industry', in *Applied Mineralogy in the Mining Industry*. Elsevier, pp. 198–199. doi: 10.1016/b978-0-444-50077-9.x5000-7.

Petruk, W. and Skinner, H. C. W. (1997) 'Characterizing Particles in Airborne Dust by Image Analysis', *Review of Extraction & Processing*, pp. 58–61.

Petsonk, E. L., Rose, C. and Cohen, R. (2013) 'Coal mine dust lung disease: New lessons from an old exposure', *American Journal of Respiratory and Critical Care Medicine*, 187(11), pp. 1178–1185. doi: 10.1164/rccm.201301-0042CI.

Pilcer, G., Vanderbist, F. and Amighi, K. (2008) 'Correlations between cascade impactor analysis and laser diffraction techniques for the determination of the particle size of aerosolised powder formulations', *International Journal of Pharmaceutics*, 358, pp. 75–81. doi: 10.1016/j.ijpharm.2008.02.014.

Pinho, R. A., Bonatto, F., Andrades, M., Ma´rio, M., Frota, L. C., Ritter, C., Klamt, F. F., Dal-Pizzol, F., et al (2004) 'Lung oxidative response after acute coal dust exposure', *Environmental Research*, 96, pp. 290–297. doi:

10.1016/j.envres.2003.10.006.

Pirrie, D. and Rollinson, G. K. (2011) 'Unlocking the applications of automated mineral analysis', *Geology Today*, 27(6), pp. 226–235. doi: 10.1111/j.1365-2451.2011.00818.x.

Van der Plas, L. and Tobi, A. C. (1965) 'A chat for judging the reliability of point counting results', *American Journal of Science*, 263(1), pp. 87–90.

Plumlee, G. S., Morman, S. and Ziegler, T. (2006) 'The Toxicological Geochemistry of Earth Materials: An Overview of Processes and the Interdisciplinary Methods Used to Understand Them', *Reviews in Mineralogy and Geochemistry*, 64(1), pp. 5–57. doi: 10.2138/rmg.2006.64.2.

Plumlee, G. S. and Ziegler, T. L. (2003) *The Medical Geochemistry of Dusts, Soils, and Other Earth Materials*. 9th edn, *Environmental geochemistry*. 9th edn. Elsevier. doi: 10.1016/B0-08-043751-6/09050-2.

Pritchard, R. J., Ghio, A. J., Lehmann, J. R., Winsett, D. W., Tepper, J. S., Park, P., Gilmour, M. I., Dreher, et al (1996) 'Oxidant Generation and Lung Injury after Particulate Air Pollutant Exposure Increase with the Concentrations of Associated Metals', *Inhalation Toxicology*. Taylor & Francis, 8(5), pp. 457–477. doi: 10.3109/08958379609005440.

Ram, S. S., Majumdar, S., Chaudhuri, P., Chanda, S., Santra, S. C., Maiti, P. K., Sudarshan, M. and Chakraborty, A. (2012) 'SEMEDS: An important tool for air pollution bio-monitoring', *Micron*. Elsevier Ltd, 43(2–3), pp. 490–493. doi: 10.1016/j.micron.2011.07.007.

Rana, N. (2015) 'Particle Size and Shape Analysis using Imagej with Customized Tools for Segmentation of Particles', *International Journal of Engineering Research & Technology*, 4(11), pp. 247–250. Available at: www.ijert.org (Accessed: 14 March 2023).

Reisner, M. T. R., Bruch, J., Hilscher, W., Kriegseis, W., Prajsnar, D., Robock, K., Rosmanith, J., Scharmann, et al (1982) 'Specific harmfulness of respirable dusts from west German coal mines VI: Comparison of experimental and epidemiological results', *Annals of Occupational Hygiene*, 26(4), pp. 527–539. doi: 10.1093/annhyg/26.4.527.

Rice-Evans, C. A. (1994) 'Formation of free radicals and mechanisms of action in normal biochemical processes and pathological states', in Burdon, R. . and Rice-Evans, C. A. (eds) *Free Radical Damage and its Control*, pp. 131–153. doi: 10.1016/S0167-7306(08)60441-X.

Roesslein, M., Hirsch, C., Kaiser, J.-P., Krug, H. F. and Wick, P. (2013) 'Comparability of in Vitro Tests for Bioactive Nanoparticles: A Common Assay to Detect Reactive Oxygen Species as an Example', *International Journal of Molecular Sciences*, 14, pp. 24320–24337. doi: 10.3390/ijms141224320.

Rosmanith, J., Reisner, M. T. R., Prajsnar, D., Breiningj, H., Ehm, W. and Germany, W. (1982) 'Specific harmfulness of respirable dusts from west German coal mines II: Results of intratracheal tests on rats', *Annals of Occupational Hygiene*, 26, pp. 481–490.

Ross, H. F., King, E. J., Yoganathan, M. and Nagelschmidt, G. (1962) 'Inhalation experiments with coal dust containing 5 per cent, 10 per cent, 20 per cent and 40 per cent quartz: Tissue reactions in the lungs of rats', *Annals of Occupational Hygiene*, 5(3), pp. 149–161. doi: 10.1093/annhyg/5.3.149.

Ross, M. H. and Murray, J. (2004) 'Occupational respiratory disease in mining', *Occupational Medicine*, 54(5), pp. 304–310. doi: 10.1093/occmed/kqh073.

RStudio Team (2020) 'RStudio: Integrated Development Environment for R'. Boston: RStudio, PBC. Available at: http://www.rstudio.com/.

Ruby, M. V., Schoof, R., Brattin, W., Goldade, M., Post, G., Harnois, M., Mosby, E., Casteel, S. W., et al (1999) 'Advances in evaluating the oral bioavailability of inorganics in soil for use in human health risk assessment', *Environmental Science and Technology*, 33(21), pp. 3697–3705. doi: 10.1021/es990479z.

Sarver, E., Keleş, Ç. and Afrouz, S. G. (2021) 'Particle size and mineralogy distributions in respirable dust samples from 25 US underground coal mines', *International Journal of Coal Geology*, 247, p. 103851. doi: 10.1016/j.coal.2021.103851.

Sarver, E., Keles, C. and Rezaee, M. (2019) 'Beyond conventional metrics: Comprehensive characterization of respirable coal mine dust', *International Journal of Coal Geology*. Elsevier, 207, pp. 84–95. doi: 10.1016/j.coal.2019.03.015.

Schins, R. P. F. and Borm, P. J. A. (1999) 'Mechanisms and Mediators in Coal Dust Induced Toxicity: A Review', *Annals of Occupational Hygiene*, 43, pp. 7–33. Available at: https://academic.oup.com/annweh/article-abstract/43/1/7/162163 (Accessed: 5 June 2019).

Schoonen, M. A., Harrington, A. D., Laffers, R. and Strongin, D. R. (2010) 'Role of hydrogen peroxide and hydroxyl radical in pyrite oxidation by molecular oxygen', *Geochimica et Cosmochimica Acta*, 74, pp. 4971–4987. doi: 10.1016/j.gca.2010.05.028.

Schoonen, M. A., Roemer, E. J. and Simon, S. (2006) 'Mineral-Induced Formation of Reactive Oxygen Species', *Reviews in Mineralogy and Geochemistry*, 64, pp. 179–222. doi: 10.2138/rmg.2006.64.7.

Schulz, B., Sandmann, D. and Gilbricht, S. (2020) 'Sem-based automated mineralogy and its application in geo-and material sciences', *Minerals*, 10(11), pp. 1–26. doi: 10.3390/min10111004.

Schulz, H., Brand, P. and Heyder, J. (2000) 'Particle Deposition in the Respiratory Tract', in Gehr, P. and Heyder, J. (eds) *Particle-Lung Interactions*. New York, pp. 229–290.

Scrivener, K. L., Füllmann, T., Gallucci, E., Walenta, G. and Bermejo, E. (2004) 'Quantitative study of Portland cement hydration by X-ray diffraction/Rietveld analysis and independent methods', *Cement and Concrete Research*. Pergamon, 34(9), pp. 1541–1547. doi: 10.1016/J.CEMCONRES.2004.04.014.

Sellaro, R., Sarver, E. and Baxter, D. (2015) 'A standard characterization methodology for respirable coal mine dust using SEM-EDX', *Resources*, 4, pp. 939–957. doi: 10.3390/resources4040939.

Semsari, P. P., Parian, M. and Rosenkranz, J. (2020) 'Breakage process of mineral processing comminution machines – An approach to liberation', *Advanced Powder Technology*. Society of Powder Technology Japan, 31(9), pp. 3669–3685. doi: 10.1016/j.apt.2020.08.005.

Shangguan, Y., Zhuang, X., Querol, X., Li, B., Moreno, N., Trechera, P., Sola, P. C., Uzu, G. and Li, J. (2022) 'Characterization of deposited dust and its respirable fractions in underground coal mines: Implications for oxidative potential-driving species and source apportionment', *International Journal of Coal Geology*, 258, p. 104017. doi: 10.1016/j.coal.2022.104017.

Sherekar, P., Jain, R., Pingle, S. and Suke, S. (2022) 'Role of Pyrite in Aggravating Coal Worker's Pneumoconiosis', in Randive, K., Pingle, S., and Agnihotri, A. (eds) *Medical Geology in Mining*. Springer G.

Springer, pp. 15–47. doi: 10.1007/978-3-030-99495-2_2/COVER.

Shi, P., Xing, X., Xi, S., Jing, H., Yuan, J., Fu, Z. and Zhao, H. (2020) 'Trends in global, regional and national incidence of pneumoconiosis caused by different aetiologies: An analysis from the Global Burden of Disease Study 2017', *Occupational and Environmental Medicine*, 77(6), pp. 407–414. doi: 10.1136/oemed-2019-106321.

Slade, R., Stead, A. G., Graham, J. A. and Hatch, G. E. (1985) 'Comparison of lung antioxidant levels in humans and laboratory animals', *The American review of respiratory disease*, 131, pp. 742–746. doi: 10.1164/arrd.1985.131.5.742.

Song, Y., Southam, K., Basil, B., Zosky, G. R., Graeme Zosky, C. R., Bardin, P. and Reynolds, P. (2022) 'Effects of chemical composition on the lung cell response to coal particles: Implications for coal workers' pneumoconiosis', *Respirology*, 12, pp. 447–454. doi: 10.1111/resp.14246.

Soutar, C. A., Hurley, J. F., Miller, B. G., Cowie, H. A. and Buchanan, D. (2004) 'Dust concentrations and respiratory risks in coalminers: Key risk estimates from the British Pneumoconiosis Field Research', *Occupational and Environmental Medicine*, 61(6), pp. 477–481. doi: 10.1136/oem.2002.006726.

Stoeger, T., Reinhard, C., Takenaka, S., Schroeppel, A., Karg, E., Ritter, B., Heyder, J. and Schulz, H. (2006) 'Instillation of six different ultrafine carbon particles indicates a surface area threshold dose for acute lung inflammation in mice', *Environmental Health Perspectives*, 114(3), pp. 328–333. doi: 10.1289/ehp.8266.

Straszheim, W. E., Younkin, K. A., Greer, R. T., Markuszewski, R. and Younkinl, K. A. (1988) 'Mounting Materials for Automated Image Analysis of Coals Using Backscattered Electron Imaging', *Scanning Microscopy International*. AMF O'Hare, 2(3), pp. 1257–1264.

Sun, Y., Kinsela, A. S., Cen, X., Sun, S., Collins, R. N., Cliff, D. I., Wu, Y. and Waite, T. D. (2021) 'Impact of reactive iron in coal mine dust on oxidant generation and epithelial lung cell viability', *Science of the Total Environment*. Elsevier B.V., 810, p. 152277. doi: 10.1016/j.scitotenv.2021.152277.

Sun, Y., Kinsela, A. S. and Waite, T. D. (2022) 'Elucidation of alveolar macrophage cell response to coal dusts: Role of ferroptosis in pathogenesis of coal workers' pneumoconiosis', *Science of the Total Environment*. Elsevier B.V., 823, p. 153727. doi: 10.1016/j.scitotenv.2022.153727.

Tambwe, O., Kotsiopoulos, A. and Harrison, S. T. L. (2020) 'Desulphurising high sulphur coal discards using an accelerated heap leach approach', *Hydrometallurgy*. Elsevier, 197(May), p. 105472. doi: 10.1016/j.hydromet.2020.105472.

Tomašek, I., Horwell, C. J., Damby, D. E., Barošová, H., Geers, C., Petri-Fink, A., Rothen-Rutishauser, B. and Clift, M. J. D. (2016) 'Combined exposure of diesel exhaust particles and respirable Soufrière Hills volcanic ash causes a (pro-)inflammatory response in an in vitro multicellular epithelial tissue barrier model', *Particle and Fibre Toxicology*, 13(1), pp. 1–14. doi: 10.1186/s12989-016-0178-9.

Tourmann, J.-L. and Kaufmann, R. (1994) 'Laser Microprobe Mass Spectrometric (LAMMS) Study of Quartz-Related and Non-Quartz-Related Factors of the Specific Harmfulness of Coal Mine Dusts', *The Annals of Occupational Hygiene*, 38, pp. 455–467. doi: 10.1093/ANNHYG/38.INHALED_PARTICLES_VII.455.

Tran, C. L., Buchanan, D., Cullen, R. T., Searl, A., Jones, A. D. and Donaldson, K. (2000) 'Inhalation of poorly soluble particles. Influence of particle surface area on Inflammation and Clearance', *Inhalation Toxicology*,

12, pp. 1113–1126.

Trechera, P., Moreno, T., Córdoba, P., Moreno, N., Amato, F., Cortés, J., Zhuang, X., Li, B., et al (2021a) 'Geochemistry and oxidative potential of the respirable fraction of powdered mined Chinese coals', *Science of The Total Environment*. Elsevier, 800, p. 149486. doi: 10.1016/J.SCITOTENV.2021.149486.

Trechera, P., Moreno, T., Córdoba, P., Moreno, N., Zhuang, X., Li, B., Li, J., Shangguan, Y., et al (2021b) 'Comprehensive evaluation of potential coal mine dust emissions in an open-pit coal mine in Northwest China', *International Journal of Coal Geology*. Elsevier, 235, p. 103677. doi: 10.1016/J.COAL.2021.103677.

Trechera, P., Moreno, T., Córdoba, P., Moreno, N., Zhuang, X., Li, B., Li, J., Shangguan, Y., et al (2020) 'Mineralogy, geochemistry and toxicity of size-segregated respirable deposited dust in underground coal mines', *Journal of Hazardous Materials*. Elsevier, 399, p. 122935. doi: 10.1016/j.jhazmat.2020.122935.

Turci, F., Pavan, C., Leinardi, R., Tomatis, M., Pastero, L., Garry, D., Anguissola, S., Lison, D., et al (2016) 'Revisiting the paradigm of silica pathogenicity with synthetic quartz crystals: the role of crystallinity and surface disorder', *Particle and Fibre Toxicology*. doi: 10.1186/s12989-016-0136-6.

Vallyathan, V. (1994) 'Generation of Oxygen Radicals by Minerals and Its Correlation to Cytotoxicity', *Environmental Health Perspectives*, 102, pp. 111–115.

Vallyathan, V., Castranova, V., Pack, D., Leonard, S., Shumaker, J., Hubbs, A. F., Shoemaker, D. A., Ramsey, D. M., et al (1995) 'Freshly fractured quartz inhalation leads to enhanced lung injury and inflammation: Potential role of free radicals', *American Journal of Respiratory and Critical Care Medicine*, 152(3), pp. 1003–1009. doi: 10.1164/ajrccm.152.3.7663775.

Vallyathan, V., Schwegler, D., Reasor, M., Stettler, L., Clere, J. and Green, F. H. Y. (1988a) 'Comparative in vitro cytotoxicity and relative pathogenicity of mineral dusts', *Annals of Occupational Hygiene*, 32(inhaled_particles_VI), pp. 279–289. doi: 10.1093/annhyg/32.inhaled_particles_VI.279.

Vallyathan, V., Shi, X. and Castranova, V. (1998) 'Reactive Oxygen Species: Their Relation to Pneumoconiosis and Carcinogenesis', *Environmental Health Perspectives*, 106, pp. 1151–1155.

Vallyathan, V., Shi, X., Dalal, N. S., Irr, W. and Castranova, V. (1988b) 'Generation of free radicals from freshly fractured silica dust. Potential role in acute silica-induced lung injury', *American Review of Respiratory Disease*, 138(5), pp. 1213–1219. doi: 10.1164/ajrccm/138.5.1213.

Vanka, K. S., Shukla, S., Gomez, H. M., James, C., Palanisami, T., Williams, K., Chambers, D. C., Britton, W. J., et al (2022) 'Understanding the pathogenesis of occupational coal and silica dust-associated lung disease', *European Respiratory Review*, 31(165). doi: 10.1183/16000617.0250-2021.

Vickery, K. and Eckardt, F. (2021) 'A closer look at mineral aerosol emissions from the Makgadikgadi Pans, Botswana, using automated SEM-EDS (QEMSCAN®)', *South African Geographical Journal*. Routledge, 103(1), pp. 7–21. doi: 10.1080/03736245.2020.1824805.

Wallace, W. E., Harrison, J. C., Grayson, R. L., Keane, M. J., Bolsaitis, P., Kennedy, R. D., Wearden, A. Q. and Attfield, M. D. (1994) 'Aluminosilicate surface contamination of respirable quartz particles from coal mines dust and from clay works dusts', *Annals of Occupational Hygiene*, 38, pp. 439–445.

Wallenborn, J. G., Mcgee, J. K., Schladweiler, M. C., Ledbetter, A. D. and Kodavanti, U. P. (2007) 'Systemic

Translocation of Particulate Matter-Associated Metals Following a Single Intratracheal Instillation in Rats', *Toxicological science*, 98(1), pp. 231–239. doi: 10.1093/toxsci/kfm088.

Wanner, A., Salathe, M. and O'Riordan, T. G. (1996) 'Mucociliary clearance in the airways.', *American journal of respiratory and critical care medicine*, 154(6), pp. 1868–1902. doi: 10.1164/AJRCCM.154.6.8970383.

Ward, C. R. (2016) 'Analysis, origin and significance of mineral matter in coal: An updated review', *International Journal of Coal Geology*. Elsevier, 165, pp. 1–27. doi: 10.1016/j.coal.2016.07.014.

Ward, C. R., Spears, D. A., Booth, C. A., Staton, I. and Gurba, L. W. (1999) 'Mineral matter and trace elements in coals of the Gunnedah Basin, New South Wales, Australia', *International Journal of Coal Geology*, 40(4), pp. 281–308. doi: 10.1016/S0166-5162(99)00006-3.

Warheit, D. B., Hansen, J. F., Yuen, I. S., Kelly, D. P., Snajdr, S. I. and Hartsky, M. A. (1997) 'Inhalation of High Concentrations of Low Toxicity Dusts in Rats Results in Impaired Pulmonary Clearance Mechanisms and Persistent Inflammation', *Toxicology and Applied Pharmacology*, 145(1), pp. 10–22. doi: 10.1006/TAAP.1997.8102.

Warr, L. N. and Nieto, F. (1998) 'Crystallite thickness and defect density of phyllosilicates in low-temperature metamorphic pelites: A TEM and XRD study of clay-mineral crystallinity-index standards', *Canadian Mineralogist*, 36(6), pp. 1453–1474.

Wastiaux, A. and Daniel, H. (1990) 'Pulmonary Toxicity of Kaolin in Rats Exposed by Inhalation', *Health Related Effects of Phyllosilicates*. Springer, pp. 405–414. doi: 10.1007/978-3-642-75124-0_36.

Weaver, C. E. (1976) 'The Nature of TiO2 in Kaolinite', *Clays and Clay Minerals*. Springer, 24(5), pp. 215–218. doi: 10.1346/CCMN.1976.0240501.

Williamson, B. J., Rollinson, G. and Pirrie, D. (2013) 'Automated mineralogical analysis of PM10: New parameters for assessing PM toxicity', *Environmental Science and Technology*, 47(11), pp. 5570–5577. doi: 10.1021/es305025e.

Winterbourn, C. C. (1995) 'Toxicity of iron and hydrogen peroxide: the Fenton reaction', *Toxicology Letters*, 82(83), pp. 969–974. doi: 10.1016/0378-4274(95)03532-X.

Wittmaack, K. (2007) 'In search of the most relevant parameter for quantifying lung inflammatory response to nanoparticle exposure: Particle number, surface area, or what?', *Environmental Health Perspectives*, 115(2), pp. 187–194. doi: 10.1289/ehp.9254.

Yadav, A. K. and Jamal, A. (2018) 'Impact of mining on human health in and around mines', *Environmental Quality Management*, 28(1), pp. 83–87. doi: 10.1002/tqem.21568.

Yang, H., Liu, C., Yang, D., Zhang, H. and Xi, Z. (2009) 'Comparative study of cytotoxicity, oxidative stress and genotoxicity induced by four typical nanomaterials: the role of particle size, shape and composition Comparative study of cytotoxicity, oxidative stress and genotoxicity', *Journal of Applied Toxicology*, 29, pp. 69–78. doi: 10.1002/jat.1385.

Yeh, H. C., Phalen, R. F. and Raabe, O. G. (1976) 'Factors influencing the deposition of inhaled particles', *Environmental Health Perspectives*, Vol.15(June), pp. 147–156. doi: 10.1289/ehp.7615147.

Zazouli, M. A., Dehbandi, R., Mohammadyan, M., Aarabi, M., Dominguez, A. O., Kelly, F. J., Khodabakhshloo, N., Rahman, M. M., et al (2021) 'Physico-chemical properties and reactive oxygen species

generation by respirable coal dust : Implication for human health risk assessment', *Journal of Hazardous Materials*. Elsevier, 405, p. 124185. doi: 10.1016/j.jhazmat.2020.124185.

Zhang, P., Huang, W., Ji, Z., Zhou, C. and Yuan, S. (2018) 'Mechanisms of hydroxyl radicals production from pyrite oxidation by hydrogen peroxide: Surface versus aqueous reactions', *Geochimica et Cosmochimica Acta*, 238, pp. 394–410. doi: 10.1016/j.gca.2018.07.018.

Zhang, Q., Dai, J., Ali, A., Chen, L. and Huang, X. (2002) 'Roles of bioavailable iron and calcium in coal dust-induced oxidative stress: Possible implications in coal workers lung disease', *Free Radical Research*, 36(3), pp. 285–294. doi: 10.1080/10715760290019309.

Zhang, Q. and Huang, X. (2002) 'Induction of Ferritin and Lipid Peroxidation by Coal Samples With Different Prevalence of Coal Workers' Pneumoconiosis: Role of Iron in the Coals', *American Journal of Industrial Medicine*, 42, pp. 171–179. doi: 10.1002/ajim.10101.

Zosky, G. R., Bennett, E. J., Pavez, M. and Beamish, B. B. (2021) 'No association between pyrite content and lung cell responses to coal particles', *Scientific Reports*, 11(1), p. 8193. doi: 10.1038/s41598-021-87517-z.

Zschech, E., Löffler, M., Krüger, P., Gluch, J., Kutukova, K., Zgłobicka, I., Silomon, J., Rosenkranz, R., et al (2018) 'Laboratory computed x-ray tomography - A nondestructive technique for 3D microstructure analyis of materials', *Practical Metallography*, 55(8), pp. 539–555. doi: 10.3139/147.110537.

# APPENDICES

## List of appendix figures

## List of appendix tables

# Appendix A LINKS TO FULL DATASETS

- Characterisation of dust-sized coal particulates: Major element analysis using X-ray Fluorescence (XRF):

  https://figshare.com/s/a2b7cc3446ec3f931fc5

- Characterisation of dust-sized coal particulates: X-ray Diffraction analysis, crystallite size calculation and reformatting of mineralogical data:

  https://figshare.com/s/6cddaa67781bf94dcc8f

- Characterisation of dust-sized coal particulates: Malvern particle size analysis:

  https://figshare.com/s/7ce62738a517ad24336d

- Characterisation of dust-sized coal particulates: Brunauer-Emmett-Teller (BET) specific surface area measurements:

  https://figshare.com/s/b736671f18460c77503f

- Characterisation of dust-sized coal particulates: Full physicochemical, mineralogical, and textural dataset extracted from QEMSCAN analysis:

  https://figshare.com/s/cbb80039b66277057e0b

- Results reporting the immunological responses of THP-1 cells exposed to coal dust in vitro:

  https://figshare.com/s/9b9de0653f5f72cb1c06

# Appendix B SUPPLEMENTARY INFORMATION FOR CHAPTER 4

Table B-1 General classification of coal composition across coal rank, based on work described in Rasheed et al, (2015).

| Rank | Sub-bituminous | Bituminous |
|---|---|---|
| % Carbon | 72-76 | 76-90 |
| % Hydrogen | ~4-3 | ~3-2 |
| %Nitrogen | ~1-2 | ~1-2 |
| %Oxygen | ~20-10 | ~10-1 |
| %Sulfur | ~0-4 | ~4-0 |

Table B-2 Elemental composition of the different descriptions of carbonaceous matter outlined for this study.

| Elements | Bituminous coal CM: Dull coal (%) | CM: Bright coal (%) | CM: Sub-bituminous coal (%) |
|---|---|---|---|
| C | 82 | 90 | 74 |
| H | 3 | 2 | 3 |
| N | 2 | 2 | 2 |
| O | 12 | 6 | 19 |
| S | 2 | 1 | 2 |

Table B-3 Composition of minerals classified for the QEMSCAN measurement reports, extracted from Deer et al, (1992) and Barthelmy, (1997).

| Mineral Name | Mineral group | Composition (% element) |
|---|---|---|
| Kaolinite | Silicate | Al 20.90, H 1.56, O 55.78, Si 21.76 |
| Quartz | Silicate | Si 46.74, O 53.26 |
| Muscovite | Silicate | Al 20.30, F 0.95, H 0.46, K 9.81, O 47.35, Si 21.13 |
| Zircon | Silicate | Zr 43.14, Hf 4.69, La 3.78, Si 14.76, O 33.63 |
| Illite | Silicate | Al 9.01, Fe 1.43, H 1.35, K 6.03, Mg 1.87, O 55.06, Si 25.25 |
| Talc | Silicate | Mg 19.23, H 0.53, O 50.62, Si 29.62 |
| Szomolnokite | Sulfate | Fe 32.87, H 1.19, O 47.07, S 18.87 |
| Rhomboclase | Sulfate | Fe 17.40, H 2.83, O 59.80, S 19.97 |
| Alunogen | Sulfate | Al 8.32, H 5.29, O 71.55, S 14.84 |
| Coquimbite | Sulfate | Fe 19.87, H 3.23, O 59.78, S 17.12 |
| Voltaite | Sulfate | Al 1.33, Fe 22.02, H 1.79, K 3.85, O 52.04, S 18.96 |
| Hydronium-jarosite | Sulfate | Fe 34.85, H 1.89, O 49.92, S 13.34 |
| Jarosite | Sulfate | Fe 33.45, H1.21, K 7.81, O 44.72, S 12.81 |
| Gypsum | Sulfate | Ca 23.28, H 2.34, O 55.76, S 18.62 |
| Dolomite | Carbonate | Ca 21.73, Mg 13.18, C 13.03, O 52.06 |
| Siderite | Carbonate | Fe 48.20, C 10.37, O 41.43 |
| Ankerite | Carbonate | Ca 19.42, Fe 16.24, Mg 3.53, Mn 2.66, C 11.64, O 46.51 |
| Calcite | Carbonate | Ca 40.04, C 12.00, O 47.96 |
| Apatite | Phosphate | Ca 39.36, Cl 2.32, F 1.24, H 0.07, O 38.76, P 18.25 |
| Pyrite | Sulfide | Fe 46.55, S 53.45 |
| Pyrrhotite | Sulfide | Fe 62.33, S 37.67 |
| Barite | Sulfide | Ba 58.84, O 27.42, S 13.74 |
| Galena | Sulfide | Pb 86.60, S 13.40 |
| Sphalerite | Sulfide | Fe 2.88, S 33.06, Zn 64.06 |
| Chalcopyrite | Sulfide | Cu 34.63, Fe 30.43, S 34.94 |
| Molybdenite | Sulfide | Mo 59.94, S 40.06 |
| Bornite | Sulfide | Cu 63.31, Fe 11.13, S 25.56 |
| Rutile | Oxide | Ti 59.94, O 40.06 |
| Spinel | Oxide | Al 37.93, Mg 17.08, O 44.98 |
| Hematite | Oxide | Fe 69.94, O 30.06 |
| Goethite | Hydroxide | Fe 62.85, H 1.13, O 36.01 |
| Gibbsite | Hydroxide | Al 34.59, H 3.88, O 61.53 |

## B.1. Wax block preparation: general casting methodology

As a standard methodology for block preparation, this study employed the following procedure: 100 g of dry Carnauba wax was weighed in a glass beaker and placed in a microwave to melt. Subsequently, 0.2 g of sample (coal dust particles) was weighed and placed in a 25 mm mould, after which ~ 8.5 g of the hot wax was added to the mould. Conventionally at this stage, powdered graphite would be used to aid in the deagglomeration of particles, however, due to the similarity in composition between graphite and the carbonaceous matter in coal, this step could not be done. To further assist in particle deagglomeration, a period of continuous stirring in a "figure of eight" motion was applied to provide thorough mixing before the block was allowed to cure in the oven at 60˚C for approximately 40 minutes. Following this, the moulds were cooled and re-set under vacuum in a 30 mm mould with epoxy resin. After the resin has set, a three-stage polishing process was employed using employing three different types of silica sandpaper, where water was used as the polishing lubricant (stage 1: 1200 grit pad, stage 2: 2000 grit pad and stage 3: 4000 grit pad, all conducted for 10 second at 300 rpm). A final hand polishing stage using a special woven polishing pad and aluminium silicate is used as the lubricant is employed to finish the surface of the block. During each stage the blocks are checked under an optical microscope to inspect the consistency of the exposed surface due to the softness of the wax. After surface inspection, the blocks were then carbon coated and kept in a vacuum cupboard for at least two days to allow for the removal of any volatiles prior to loading them in the QEMSCAN.

## B.2. Ash methodology

Approximately 1 g (weighed to the nearest 0.1 mg) of the thoroughly mixed sample was transferred to a weighed capsule. After weighing the capsules were placed in a cold furnace and gradually heated so that the temperature reaches $500 \pm 10°C$ at the end of 1 h. Continue heating the sample until the temperature rises from $500 \pm 10°C$ to $750 \pm 15°C$ at the end of another 1 hour. After this period continue to heat the capsules at the final temperature (750°C or 950°C) for an additional 2 h. After this point the furnace is turned off and allowed to cool for 3 hours without opening the door. Subsequently, the capsules were removed from the muffle furnace and placed in a desiccator overnight to cool.

The two-stage ashing procedure allows pyritic sulfur to be oxidized and expelled before most metal carbonates are decomposed. An ample supply of air in the muffle furnace, "two to four volume changes per minute," must be assured at all times to ensure complete oxidation of the pyritic sulfur and to remove the $SO_2$ formed.

To calculate the ash percent in the analysis sample as follows:

Ash % in sample=[(A-B)/C]×100                                              (A-1)

$A$ = weight of capsule, cover, and ash residue, g,

$B$ = weight of empty capsule and cover, g, and

$C$ = weight of analysis sample used, g.

## B.3. XRF analysis information

The samples were crushed to a fine powder (particle size < 70 µm) with a jaw crusher and milled in a tungsten-carbide ring mill prior to the preparation of a fused disc for major and trace elements analysis. The jaw crusher and mill were cleaned with clean uncontaminated quartz between samples to avoid cross contamination. Glass disks were prepared for XRF analysis using 7 g of high purity trace element and Rare Earth Element-free flux ($LiBO_2$ = 32.83%, $Li_2B_4O_7$ = 66.67%, $LiI$ = 0.50%) mixed with 0.7g of the powder sample. A mixture of sample and flux were fused in platinum crucibles with a Claisse M4 gas fluxer at temp between $1100^{O}C$ -$1200^{O}C$. Whole-rock major element compositions were determined by XRF spectrometry on a PANalytical Axios Wavelength Dispersive spectrometer at the Central Analytical Facilities, Stellenbosch University, South Africa. The spectrometer is fitted with an Rh tube and with the following analyzing crystals: LIF200, LIF220, PE 002, Ge 111 and PX1. The instrument is fitted with a gas-flow proportional counter and a scintillation detector. The gas-flow proportional counter uses a 90% Argon-10% methane mixture of gas. Major elements were analyzed on a fused glass disk using a 2.4kW Rhodium tube. Matrix effects in the samples were corrected for by applying theoretical alpha factors and measured line overlap factors to the raw intensities measured with the SuperQ PANalytical software. The concentration of the control standards that were used in the calibration procedures for major element analyses fit the range of concentration of the samples. Amongst these standards were NIM-G (Granite from the Council for Mineral Technology, South Africa) and BE-N (Basalt from the International Working Group).

# Appendix C SUPPLEMENTARY INFORMATION CHAPTER 4

## SECTION 2

Table C-1 Mineral distribution defined for each sample determined by XRD analysis.

| Sample | CM | Qz | Kln | Ilt | Pl | Py | Cal | Dol | Gp | Szo | Rt | Rbc |
|---|---|---|---|---|---|---|---|---|---|---|---|---|
| Br-Dsulf | 11.5 | 19.9 | 35.9 | 22.4 | 2.6 | 1.2 | - | - | 4.4 | - | - | - |
| Br-Dis | 16.9 | 16.5 | 27.8 | 24.3 | 2.4 | 4.7 | 1.5 | - | 1.7 | - | 1.8 | - |
| Br-Tail | 21.4 | 33.4 | 25.7 | 4.9 | - | 7.6 | - | - | 5.7 | - | 1.2 | - |
| Br-MDT | 32.5 | 8.9 | 28.4 | 20.5 | 2.7 | 0.8 | 1.1 | - | 2.2 | - | - | 1.3 |
| SA-UF1 | 44.1 | 21.7 | 18.8 | 3.9 | - | 0.4 | 2.4 | 5.5 | 1.6 | - | 0.6 | - |
| SA-Dis2 | 34.4 | 16.8 | 25.2 | 8.5 | - | 5.6 | 2.9 | - | 3.3 | - | 2.2 | - |
| SA-MDT | 43.8 | 19.4 | 29.9 | 2.7 | - | 1.6 | - | - | - | - | 2.0 | - |
| SA-UF2 | 55.2 | 8.3 | 27.4 | 4.8 | - | 0.5 | - | - | 1.4 | - | 2.3 | - |
| Br-PyC | 33.3 | 6.3 | 5.8 | - | - | 24.0 | 0.2 | - | 0.7 | 6.6 | - | 19.3 |
| Mz-ROM1 | 76.0 | 5.2 | 8.8 | 5.5 | - | 0.2 | 0.8 | 0.5 | 0.1 | 1.4 | - | - |
| Mz-ROM2 | 75.2 | 5.2 | 8.7 | 5.6 | - | 0.3 | 1.4 | 0.4 | 1.0 | 1.8 | 0.1 | - |
| *US-ROM | - | - | - | - | - | - | - | - | - | - | - | - |
| SA-ROM2 | 89.7 | 2.3 | 6.9 | 0.8 | - | - | - | 0.4 | 0.3 | 0.2 | - | - |
| SA-ROM3 | 64.5 | 5.0 | 25.8 | - | - | - | 0.1 | 0.3 | 0.1 | 1.9 | - | - |
| SA-UF3 | 73.6 | 4.3 | 12.3 | 2.8 | - | 0.4 | 3.4 | 1.5 | 0.5 | - | 1.4 | - |
| SA-UF4 | 74.4 | 3.5 | 13.7 | 3.2 | - | 0.4 | 1.7 | 1.1 | 0.7 | - | 1.3 | - |
| SA-Dis1 | 61.5 | 14.8 | 17.0 | - | - | 2.2 | - | - | 2.3 | - | 0.7 | 0.7 |

*For sample US-ROM the amorphous content was too high to perform the XRD refinement.

CM-carbonaceous matter, Qz-quartz ($SiO_2$), Kln-kaolinite ($Al_2Si_2O_5(OH)_4$),
Ilt-illite ($K_{0.6}(H_3O)_{0.4}Al_{1.3}Mg_{0.3}Fe^{2+}_{0.1}Si_{3.5}O_{10}(OH)_2 \cdot (H2O)$), Pl-plagioclase ($Na_{0.5}Ca_{0.5}Si_3AlO_8$), Py-pyrite ($FeS_2$), Cal-Calcite ($CaCO_3$), Dol-dolomite ($CaMg(CO_3)_2$), Gp-gypsum ($Ca(SO_4) \cdot 2(H_2O)$), Szo-szomolnokite ($Fe^{2+}(SO_4) \cdot (H_2O)$), Rt-rutile ($TiO_2$), and Rbc-rhomboclase ($HFe^{3+}(SO_4)_2 \cdot 4(H_2O)$)

Table C-2 Mineral distribution defined for each sample determined by QEMSCAN analysis for major and minor phases.

| Sample | CM | Clys | Qz | Py | Cal | Sulfates |
|---|---|---|---|---|---|---|
| Br-Dsulf | 14.1 | 56.7 | 22.8 | 3.5 | 0.9 | 0.7 |
| Br-Dis | 10.1 | 62.7 | 17.8 | 6.2 | 0.9 | 0.4 |
| Br-Tail | 22.4 | 51.5 | 15.1 | 8.0 | 0.7 | 1.3 |
| Br-MDT | 26.0 | 55.7 | 14.2 | 1.0 | 1.7 | 0.2 |
| SA-UF1 | 41.1 | 18.2 | 25.9 | 0.8 | 5.6 | 2.3 |
| SA-Dis2 | 43.6 | 30.8 | 12.1 | 9.8 | 1.0 | 1.6 |
| SA-MDT | 34.7 | 44.5 | 16.6 | 1.8 | - | 0.0 |
| SA-UF2 | 50.9 | 36.3 | 8.3 | 1.0 | 0.3 | 0.5 |
| Br-PyC | 32.8 | 3.1 | 7.3 | 29.8 | 0.1 | 26.1 |
| Mz-ROM1 | 73.8 | 14.0 | 7.5 | 0.7 | 2.0 | 0.6 |
| Mz-ROM2 | 73.8 | 13.1 | 8.0 | 1.8 | 0.5 | 0.6 |
| US-ROM | 92.3 | 2.3 | 0.8 | 2.6 | 0.7 | 0.9 |
| SA-ROM2 | 88.4 | 4.9 | 1.9 | 1.4 | 1.7 | 0.6 |
| SA-ROM3 | 62.6 | 22.9 | 8.6 | 0.8 | 1.8 | 0.9 |
| SA-UF3 | 68.3 | 14.3 | 4.6 | 1.5 | 3.9 | 1.4 |
| SA-UF4 | 67.3 | 15.0 | 6.3 | 1.4 | 3.2 | 0.7 |
| SA-Dis1 | 61.4 | 24.0 | 6.4 | 4.8 | 0.2 | 1.4 |

CM-carbonaceous matter, Clys-clays, Qz-quartz, Py-pyrite, Cal-calcite

Table C-3 Mineral distribution defined for each sample determined by QEMSCAN analysis for trace phases.

| Sample | FeOx | Rt | Dol | Sd |
|--------|------|------|------|------|
| Br-Dsulf | 0.01 | 1.12 | - | 0.08 |
| Br-Dis | 0.05 | 1.14 | 0.01 | 0.25 |
| Br-Tail | 0.05 | 0.41 | - | 0.10 |
| Br-MDT | 0.01 | 0.42 | 0.07 | 0.12 |
| SA-UF1 | 0.43 | 0.08 | 1.93 | 2.30 |
| SA-Dis2 | 0.02 | 0.30 | 0.14 | 0.31 |
| SA-MDT | 0.02 | 1.85 | - | 0.10 |
| SA-UF2 | 0.36 | 0.62 | 0.01 | 1.25 |
| Br-PyC | 0.02 | 0.18 | - | 0.05 |
| Mz-ROM1 | 0.01 | - | 0.87 | 0.30 |
| Mz-ROM2 | 0.07 | 0.48 | 0.61 | 0.49 |
| US-ROM | - | 0.04 | 0.01 | 0.06 |
| SA-ROM2 | 0.06 | 0.01 | - | 0.41 |
| SA-ROM3 | 0.21 | 0.35 | 0.59 | 0.68 |
| SA-UF3 | - | 0.25 | 4.96 | 0.09 |
| SA-UF4 | 0.03 | 0.38 | 4.25 | 0.81 |
| SA-Dis1 | 0.03 | 0.43 | - | 0.47 |

FeOx-iron oxides, Rt-rutile, Dol-dolomite, Sd-siderite ($Fe^{2+}(CO3)$)

Table C-4 Pearson correlation between the mineral back-calculated chemistry based on XRD and QS and the measured chemistry from XRF analysis.

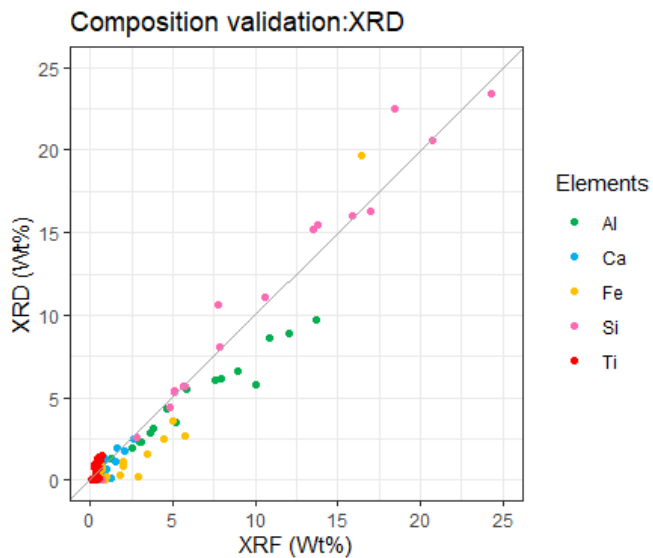| Element | XRD-XRF | QS-XRF |
|---------|---------|--------|
| Al | 0.96 | 0.96 |
| Si | 0.97 | 0.98 |
| Fe | 093 | 0.95 |
| Ca | 062 | 0.76 |
| Ti | 0.51 | 0.59 |

Figure C-1 Composition validation by a parity assessment between the major elements defined by XRF and back calculated by XRD.
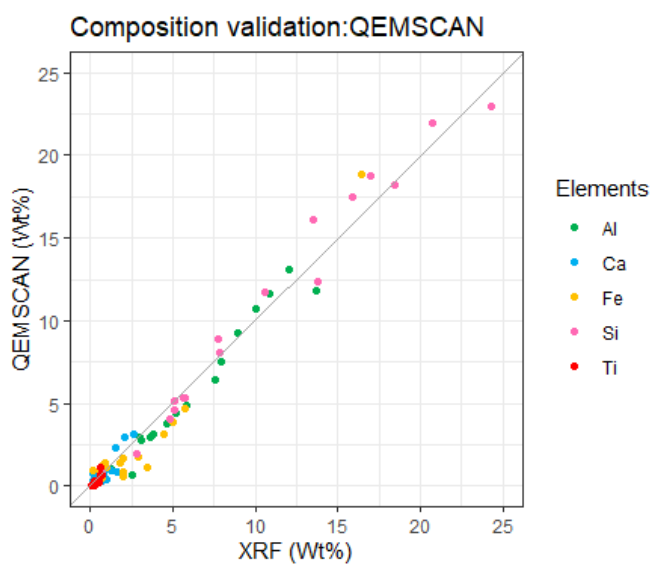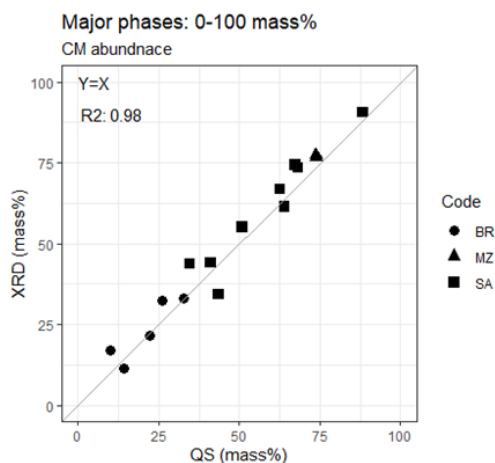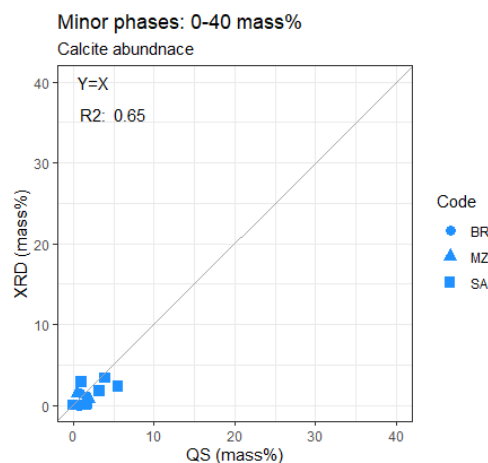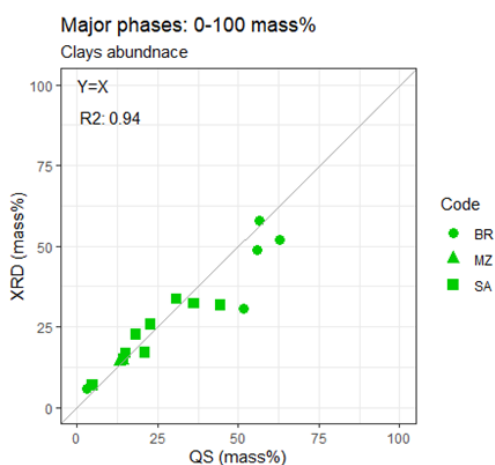


Figure C-2 Composition validation by a parity assessment between the major elements defined by XRF and back calculated by QEMSCAN.
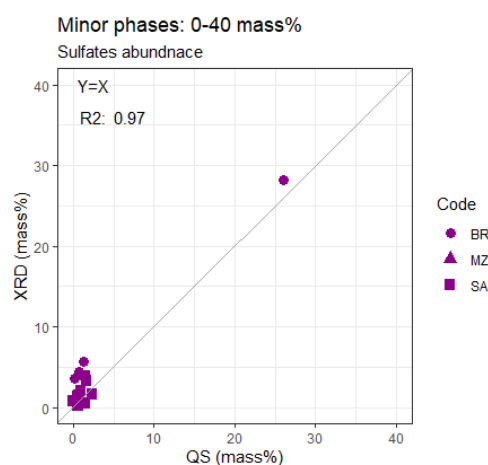
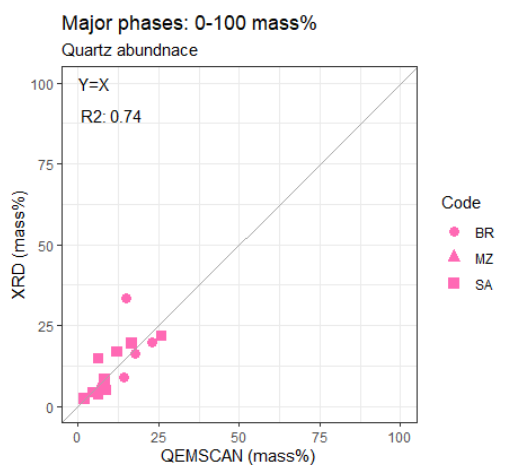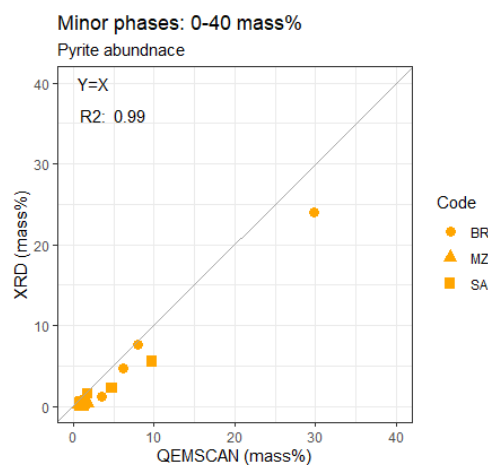Figure C-3 Variation between the mineral abundances defined by XRD and QEMSCAN. Figures a, b, and c represent the comparison of the major phases ranging between 0-100 mass % abundance respectively. Figures d, e, and f represent the comparison of the minor phases ranging between 0-40 mass % abundance respectively.

Table C-5 Description of the mineral formulae for the minerals analysed.

| Mineral Name | Mineral group | Composition (% element) |
| --- | --- | --- |
| Kaolinite | Silicate | Al 20.90, H 1.56, O 55.78, Si 21.76 |
| Quartz | Silicate | Si 46.74, O 53.26 |
| Muscovite | Silicate | Al 20.30, F 0.95, H 0.46, K 9.81, O 47.35, Si 21.13 |
| Zircon | Silicate | Zr 43.14, Hf 4.69, La 3.78, Si 14.76, O 33.63 |
| Illite | Silicate | Al 9.01, Fe 1.43, H 1.35, K 6.03, Mg 1.87, O 55.06, Si 25.25 |
| Talc | Silicate | Mg 19.23, H 0.53, O 50.62, Si 29.62 |
| Szomolnokite | Sulfate | Fe 32.87, H 1.19, O 47.07, S 18.87 |
| Rhomboclase | Sulfate | Fe 17.40, H 2.83, O 59.80, S 19.97 |
| Alunogen | Sulfate | Al 8.32, H 5.29, O 71.55, S 14.84 |
| Coquimbite | Sulfate | Fe 19.87, H 3.23, O 59.78, S 17.12 |
| Voltaite | Sulfate | Al 1.33, Fe 22.02, H 1.79, K 3.85, O 52.04, S 18.96 |
| Hydronium-jarosite | Sulfate | Fe 34.85, H 1.89, O 49.92, S 13.34 |
| Jarosite | Sulfate | Fe 33.45, H1.21, K 7.81, O 44.72, S 12.81 |
| Gypsum | Sulfate | Ca 23.28, H 2.34, O 55.76, S 18.62 |
| Dolomite | Carbonate | Ca 21.73, Mg 13.18, C 13.03, O 52.06 |
| Siderite | Carbonate | Fe 48.20, C 10.37, O 41.43 |
| Ankerite | Carbonate | Ca 19.42, Fe 16.24, Mg 3.53, Mn 2.66, C 11.64, O 46.51 |
| Calcite | Carbonate | Ca 40.04, C 12.00, O 47.96 |
| Apatite | Phosphate | Ca 39.36, Cl 2.32, F 1.24, H 0.07, O 38.76, P 18.25 |
| Pyrite | Sulfide | Fe 46.55, S 53.45 |
| Pyrrhotite | Sulfide | Fe 62.33, S 37.67 |
| Barite | Sulfide | Ba 58.84, O 27.42, S 13.74 |
| Galena | Sulfide | Pb 86.60, S 13.40 |
| Sphalerite | Sulfide | Fe 2.88, S 33.06, Zn 64.06 |
| Chalcopyrite | Sulfide | Cu 34.63, Fe 30.43, S 34.94 |
| Molybdenite | Sulfide | Mo 59.94, S 40.06 |
| Bornite | Sulfide | Cu 63.31, Fe 11.13, S 25.56 |
| Rutile | Oxide | Ti 59.94, O 40.06 |
| Spinel | Oxide | Al 37.93, Mg 17.08, O 44.98 |
| Hematite | Oxide | Fe 69.94, O 30.06 |
| Goethite | Hydroxide | Fe 62.85, H 1.13, O 36.01 |
| Gibbsite | Hydroxide | Al 34.59, H 3.88, O 61.53 |

# Appendix D SUPPLEMENTARY INFORMATION FOR CHAPTER 5

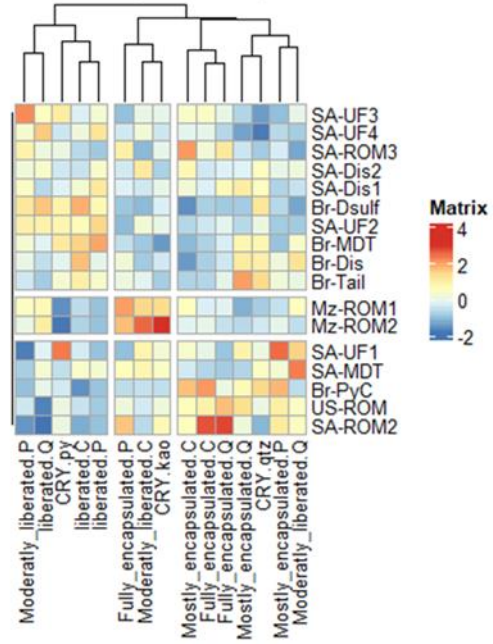## D.1. Physicochemical particle characterisation
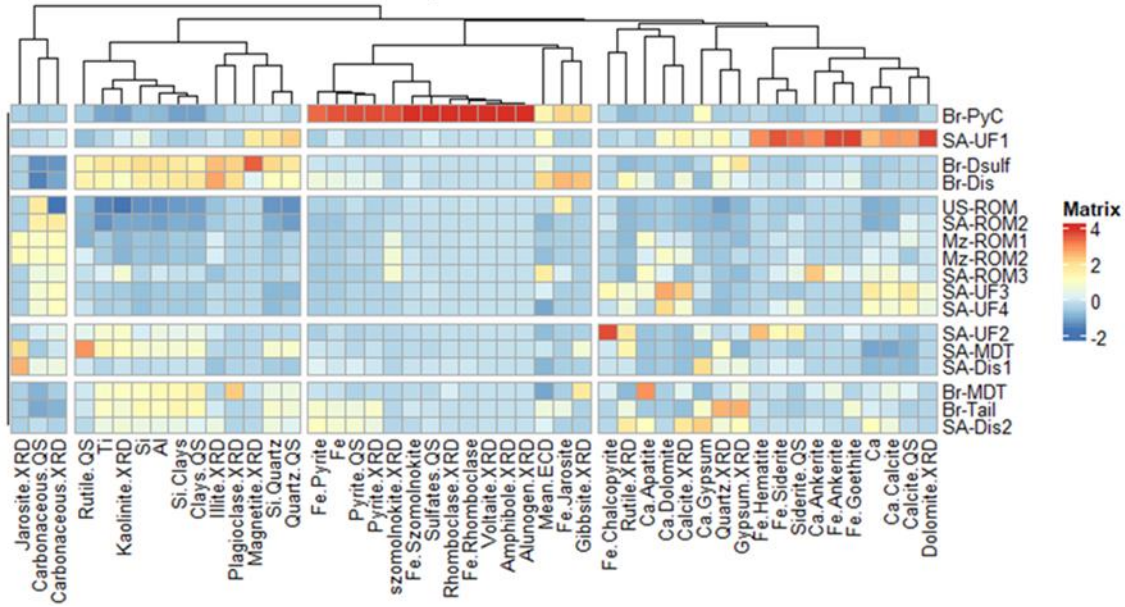


(a)
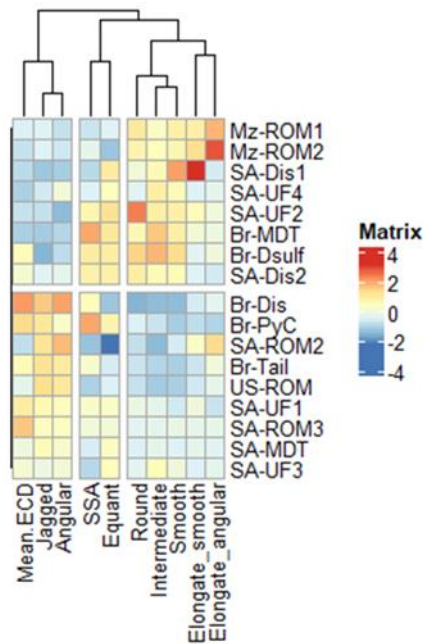


(b)



(c)

Figure D-1 Clustered heatmap showing sample associations between the standardised parameters. The variables are standardised to allow for comparison between parameters (mean and standard deviation of each column are 0 and 1 respectively). Figures a-c represent the mineral and element, general and mineral specific data classes respectively.

## D.2. Dose response modelling of cell viability

Table D-1 Outputs from the linear regression applied to model the dose-response relationships per sample. The goodness of fit was determined by the adjusted R2, coefficient representing the gradient of the straight line, standard error defining the uncertainty in the model, and the strength of the relationship defined by the p-value (p <0.05 statistically significant, p <0.01 highly significant).

| Sample | Adjusted $R^2$ | Coefficient | Standard error | p-value |
|---|---|---|---|---|
| Br-Dsulf | 0.99 | 0.085 | 0.006 | 0.004 |
| Br-Dis | 0.87 | 0.057 | 0.012 | 0.044 |
| *Br-Tail | 0.80 | 0.037 | 0.010 | 0.067 |
| Br-PyC | 1.00 | 0.088 | 0.004 | 0.002 |
| Br-MDT | 0.99 | 0.071 | 0.003 | 0.002 |
| Mz-ROM1 | 0.99 | 0.031 | 0.001 | 0.002 |
| Mz-ROM2 | 0.98 | 0.038 | 0.003 | 0.008 |
| US-ROM | 0.92 | 0.025 | 0.004 | 0.027 |
| SA-ROM2 | 0.84 | 0.025 | 0.006 | 0.056 |
| SA-ROM3 | 0.98 | 0.049 | 0.004 | 0.005 |
| SA-Dis1 | 0.98 | 0.097 | 0.009 | 0.008 |
| SA-UF2 | 0.91 | 0.052 | 0.010 | 0.032 |
| SA-Dis2 | 0.99 | 0.073 | 0.005 | 0.005 |
| SA-UF3 | 0.92 | 0.040 | 0.007 | 0.026 |
| SA-MDT | 0.92 | 0.056 | 0.009 | 0.027 |
| SA-UF2 | 0.98 | 0.067 | 0.005 | 0.005 |
| SA-UF4 | 0.91 | 0.040 | 0.007 | 0.032 |

*Coefficient was still considered irrespective of the p-value (0.067) as the gradient was still considered reasonable compared to a sample with an overlapping fit (Br-Dis)
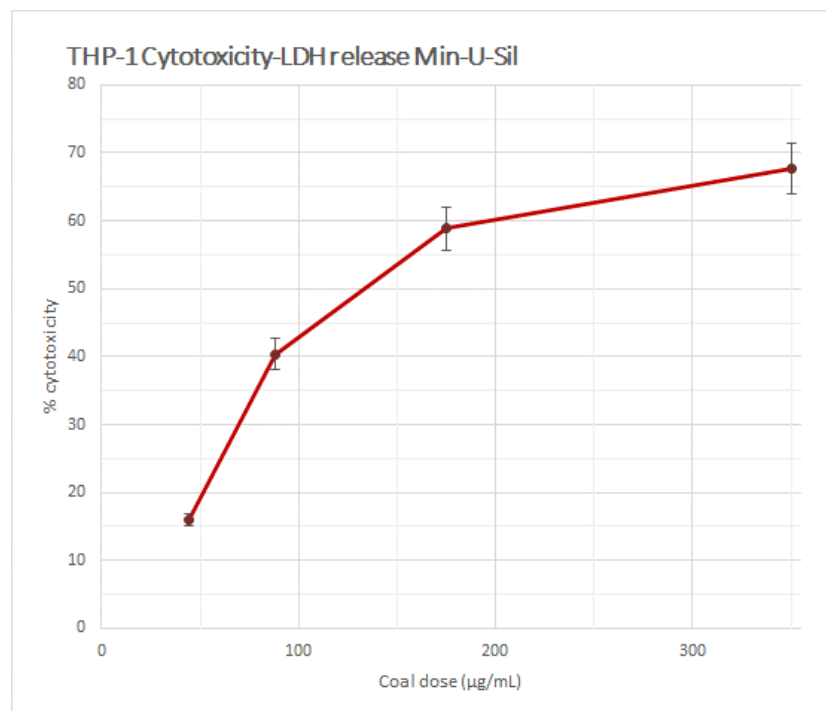


Figure D-2 dose-response relationship between the different coal particle samples at the 72-hour timepoint (exposure concentrations 350, 175, 88, 44 µg/mL | 218,8; 109,4; 55; 27,5 µg/cm²).Model validation and optimisation

Table D-2 A summary of the LDH and MDA model validation parameters, describing the results of cross-validation (10 random segments), explained variance along the X and Y direction, strength of model (model estimation) and model uncertainty.

| | | Cross-validation results | | % Explained variability | | Model estimation | Model uncertainty | |
|---|---|---|---|---|---|---|---|---|
| | n Comps | RMSEP (CV) | RMSEP (adjCV) | Explanatory variable (X) | Response variable (Y) | $R^2$ (Predictions vs Observations) | RMSE (Lower bound) | MAE (Upper bound) |
| LDH | 1 | 0.8489 | 0.8240 | 19.94 | 71.49 | 0.86 | - | - |
| | 2 | 0.8305 | 0.7997 | 32.33 | 85.70 | 0.95 | - | - |
| | **3** | **0.8147** | **0.7811** | **46.69** | **91.18** | **0.95** | **0.2882** | **0.2269** |
| MDA | 1 | 0.9921 | 0.9361 | 21.86 | 79.56 | 0.88 | - | - |
| | 2 | 0.898 | 0.842 | 36.95 | 93.28 | 0.96 | - | - |
| | 3 | 0.8257 | 0.7718 | 52.93 | 97.08 | 0.97 | - | - |
| | **4** | **0.7736** | **0.7236** | **63.71** | **98.26** | **0.99** | **0.1267** | **0.0817** |

RMSEP- Root mean squared error of prediction
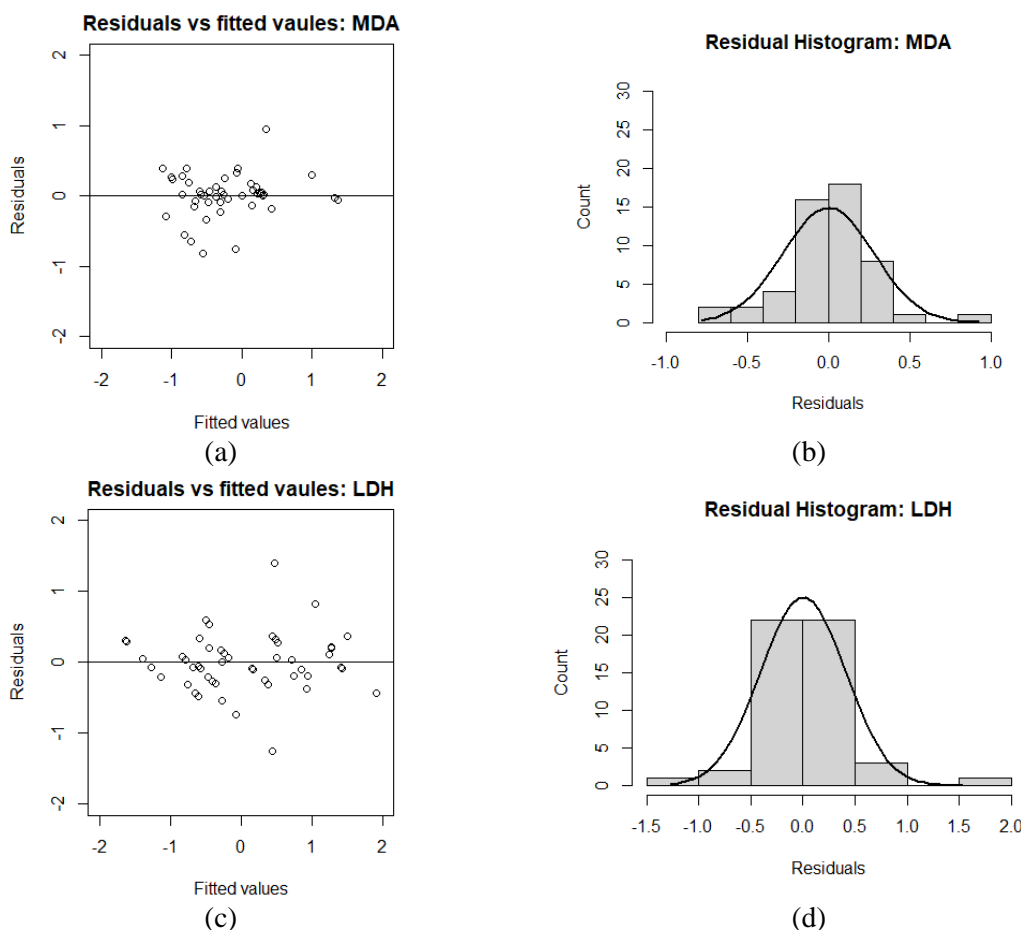MAE- Mean absolute error



(a)  (b)  (c)  (d)

Figure D-3 Assessment of model performance based on the distribution of residual errors. Figures a and b show the respective graphs defining the orientation of the errors in the MDA-based model as the residuals relative to the fitted/predicted values centred around zero, and the distribution of the errors in a histogram format. Figures c and d show the respective graphs defining the orientation of the errors in the LDH-based model as the residuals relative to the fitted/predicted values centred around zero, and the distribution of the errors in a histogram format.
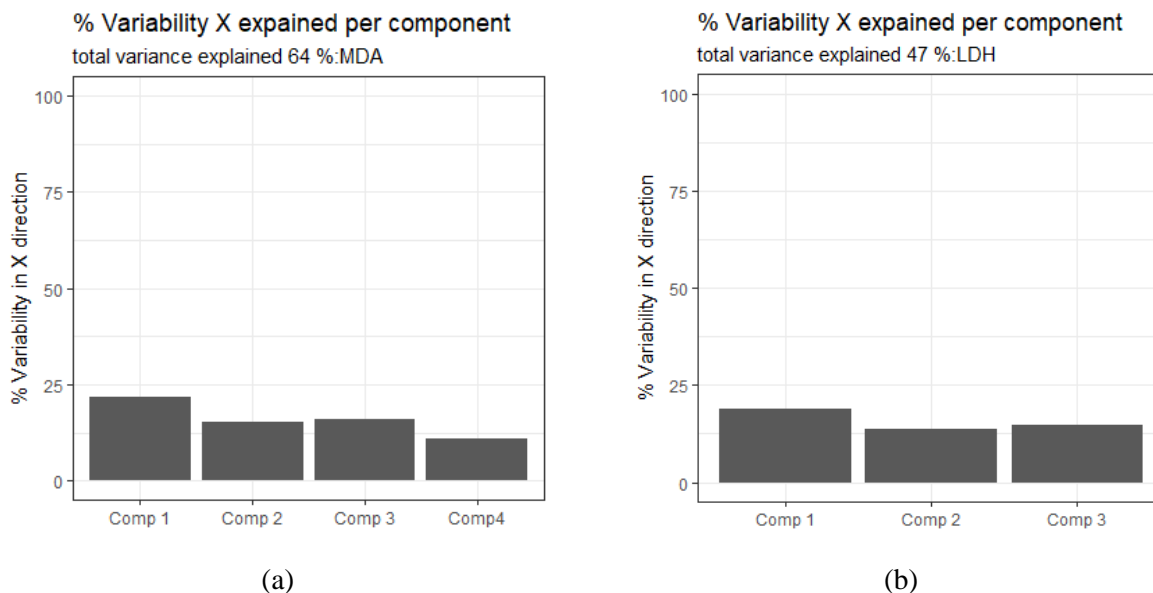
(a)                                          (b)

Figure D-4 Percentage of the variability explained by the model components for the X (explanatory variables). (a) represents the percentage variability explained in the x direction per component for the MDA model (comp1=21.86 %, comp2=15.09 %, comp3=15.98 %, comp4=10.78 %). (b) represents the percentage variability explained in the x direction per component for the LDH model (comp1=19.94 %, comp2=12.39%, comp3=14.36 %).
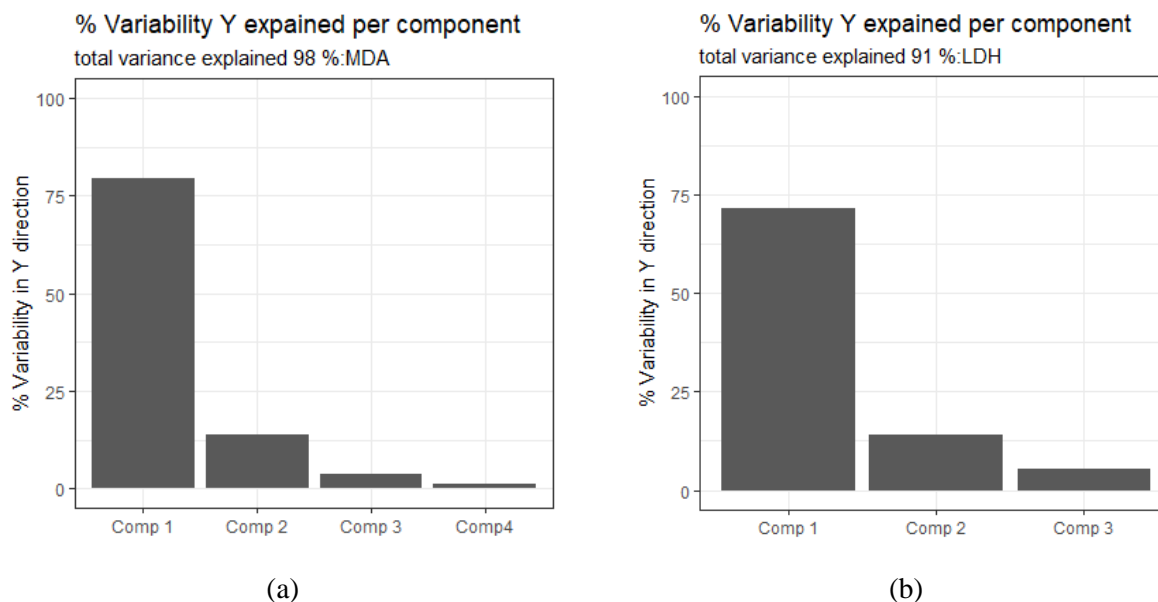


(a)                                          (b)

Figure D-5 Percentage of the variability explained by the model components for the Y (response variable). (a) represents the percentage variability explained in the y direction per component for the MDA model (comp1=79.56 %, comp2=13.72 %, comp3=3.8 %, comp4=1.18 %). (b) represents the percentage variability explained in the y direction per component for the LDH model (comp1=71.49 %, comp2=14.21 %, comp3=5.48 %).

# Appendix E SUPPLEMENTARY INFORMATION FOR CHAPTER 6

Table E-1 List of variables screened by relevance to the model (based on their VIP score) and ranked by importance to the LDH response based on Eq. 6-1.

| Variable relative positive importance to cytotoxicity | | |
|---|---|---|
| Characterisation class | Variables | Coefficient rank |
| General | Elongate smooth | 5.31 |
| Chemical | Ca Gypsum | 4.74 |
| General | Smooth | 4.64 |
| General | Equant | 4.12 |
| Mineralogical | Jarosite XRD | 3.71 |
| General | Intermediate | 2.69 |
| Mineral specific | Liberated P (pyrite) | 2.32 |
| Mineral specific | CRY qtz | 2.18 |
| Mineralogical | Kaolinite XRD | 1.91 |
| Chemical | Fe Pyrite | 1.78 |
| Chemical | Fe | 1.59 |
| Mineralogical | Rhomboclase XRD | 1.54 |
| Mineralogical | Pyrite QS | 1.53 |
| Chemical | Fe Rhomboclase | 1.44 |
| Mineralogical | Sulfates QS | 1.41 |
| General | SSA | 1.39 |
| Chemical | Si Quartz | 1.36 |
| Mineralogical | Amphibole XRD | 1.26 |
| Mineralogical | Alunogen XRD | 1.26 |
| Mineralogical | Voltaite XRD | 1.26 |
| Chemical | Fe Szomolnokite | 1.22 |
| Chemical | Al | 1.04 |
| Chemical | Si | 0.95 |
| Mineralogical | Pyrite XRD | 0.83 |
| Chemical | Ti | 0.67 |
| Mineralogical | Clays QS | 0.44 |
| Chemical | Si Clays | 0.32 |
| Variable relative negative importance to cytotoxicity | | |
| Characterisation class | Variables | Coefficient rank |
| General | Jagged | 3.80 |
| General | Elongate angular | 3.36 |
| General | Angular | 3.35 |
| Mineral specific | Fully encapsulated P (pyrite) | 2.74 |
| Mineral specific | CRY kao (kaolinite crystallite size) | 1.25 |
| Mineralogical | Carbonaceous QS | 1.24 |

QS- shorthand for the QEMSCAN

Table E-2 List of variables screened by relevance to the model (based on their VIP score) and ranked by importance to the MDA response based on Eq. 6-1.

| Variable relative positive importance to lipid peroxidation | | |
|---|---|---|
| Characterisation class | Variables | Coefficient rank |
| General | Elongate smooth | 3.88 |
| Chemical | Ca Gypsum | 3.86 |
| Mineral specific | CRY qtz (quartz crystallite size) | 3.80 |
| General | Smooth | 2.44 |
| Chemical | Fe Pyrite | 2.30 |
| General | Equant | 2.24 |
| Mineralogical | Rhomboclase XRD | 2.17 |
| Mineralogical | Pyrite QS | 2.15 |
| Chemical | Fe | 2.09 |
| Mineralogical | Sulfates QS | 2.08 |
| Chemical | Fe Rhomboclase | 2.03 |
| Mineralogical | Pyrite XRD | 1.96 |
| Mineralogical | Amphibole XRD | 1.93 |
| Mineralogical | Alunogen XRD | 1.93 |
| Mineralogical | Voltaite XRD | 1.93 |
| Chemical | Fe Szomolnokite | 1.75 |
| Mineralogical | Szomolnokite XRD | 1.63 |
| General | SSA (specific surface area) | 1.32 |
| Variable relative negative importance to lipid peroxidation | | |
| Characterisation class | Variables | Coefficient rank |
| Chemical | Ca Dolomite | 3.41 |
| General | Angular | 3.00 |
| Mineralogical | Calcite QS | 2.40 |
| Chemical | Ca Calcite | 1.73 |
| Chemical | Fe Jarosite | 0.97 |

QS- shorthand for the QEMSCAN

Table E-3 Description of the characteristic groups used in the k means cluster differentiation analysis.

| Characteristic group | Group breakdown |
|---|---|
| Silicate chemistry | Si distribution in quartz and clays; the elemental content of Al, Si and Ti |
| Silicate abundance | The abundance of silicate minerals such as amphibole and kaolinite, as well as the clay content |
| Fe.sulfate chemistry | Fe distributed in rhomboclase, szomolnokite and jarosite |
| Fe.sulfate abundance | The abundance of rhomboclase, alunogen, voltaite, szomolnokite, and jarosite |
| Ca.sulfate abundance | Gypsum abundance |
| Sulfate abundance | The abundance of rhomboclase, alunogen, voltaite, szomolnokite, jarosite and the QEMSCAN-based sulfate group which contains gypsum |
| Fe.sulfide chemistry | Fe distributed in pyrite |
| Fe.sulfide abundance | Pyrite abundance |
| Carbonate chemistry | Ca distribution in calcite and dolomite |
| Carbonate abundance | Calcite abundance |
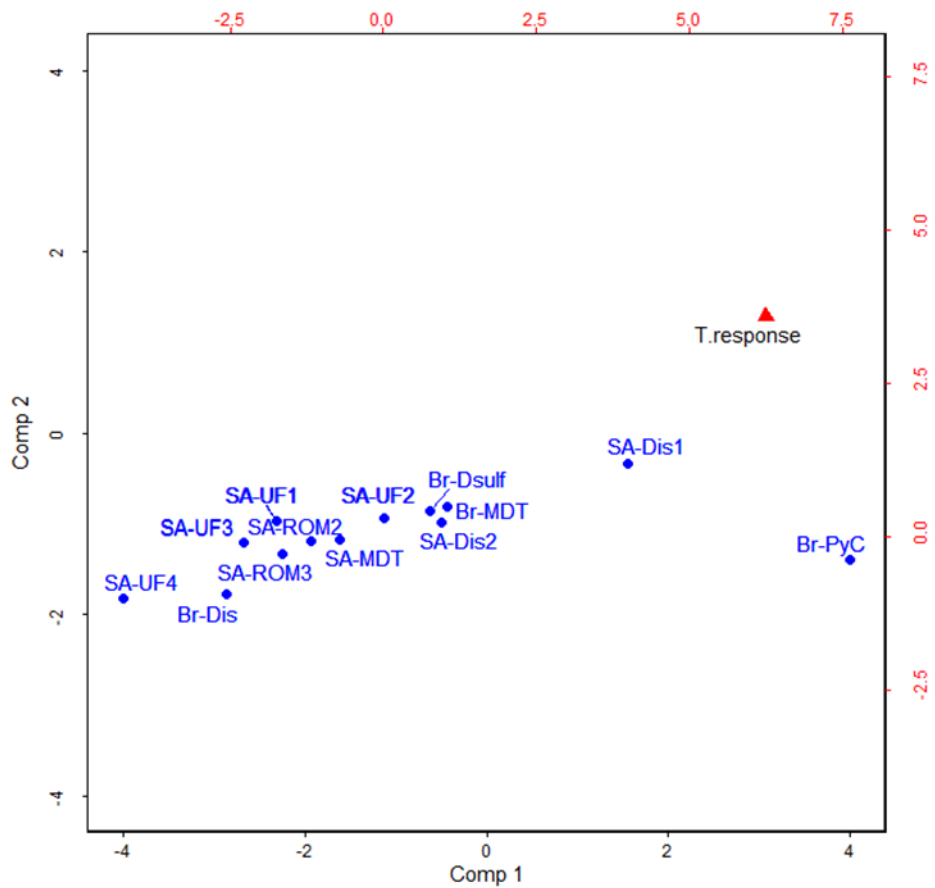
Figure E-1 MDA biplot representing the scores in blue as the samples and the loadings (red triangle) as the MDA response vector (% variability explained by comp1= 79.56 %, comp2= 13.73 %).
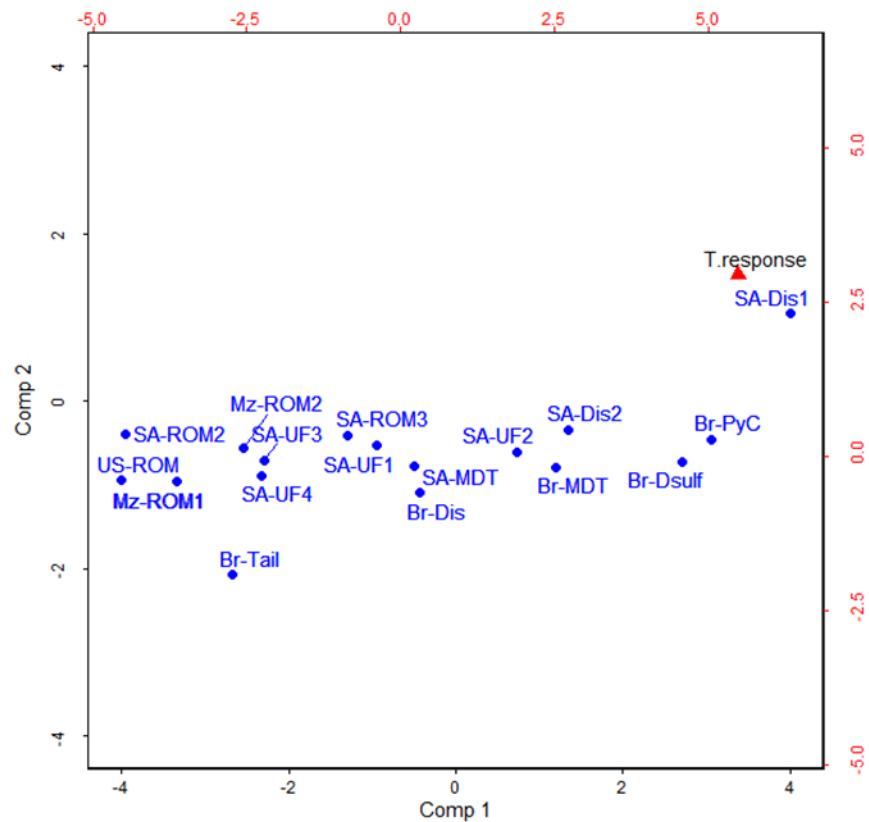
Figure E-2 LDH biplot representing the scores in blue as the samples and the loadings (red triangle) as the LDH response vector (% variability explained by comp1= 71.49 %, comp2= 14.21 %).